Dosimetry of small x-ray beams for stereotactic radiotherapy

Carolyn McKerracher

PhD

The University of Edinburgh

2003

EX BIBL. UNIV. EDINBURGH

I declare that this thesis has been composed by myself and that the work contained in it is my own.

Carolyn McKerracher

November 2003

For Joshua

Abstract

The dosimetry of small (=<40mm width) x-ray beams, such as those used in stereotactic radiotherapy, is much more complex than that of those used in routine clinical treatments. A thorough understanding of the properties of both small beams and small detectors is necessary to determine the optimum detector to use in each measurement situation. Accurate and reproducible experimental methods must also be developed to measure absolute and relative doses, obtain precise beam data and subsequently verify the delivered treatment dose.

This work is an investigation of the above aspects of small beam dosimetry, with particular reference to the types of small fields used for stereotactic radiotherapy in the Edinburgh Cancer Centre. These are fields formed by circular stereotactic collimators (12.5 to 40mm diameter), used in conjunction with arc therapy for the treatment of small brain lesions.

Several detectors were compared in the measurement of percentage depth doses, tissue maximum ratios, off axis ratios, head scatter and relative output factors, on a 6MV linac. This included the testing of three new, commercially available detectors. Clinical beam data were obtained via detector comparison and recommendations made as to the best methodology for each measurement parameter. The most accurate and reproducible technique for head scatter factors was extended to smaller stereotactic collimators (5 to 10mm diameter) and square fields with widths 10 to 20mm. These were shaped with both the movable linac collimators and the multileaf collimator and the results will be applied to the measurement of the small sub-fields used in intensity modulated radiotherapy (IMRT).

A verification phantom was designed to be compatible with the stereotactic head frame and the properties of various small detectors were investigated for use in the phantom to measure point doses in both single arcs and multiple non-coplanar plans.

The recommendations on beam data acquisition and dose verification were applied to two additional linacs. On all machines, the dose to the isocentre was verified in several typical treatment plans to within 2% of the calculated dose, for all clinical collimators. The results confirm the accuracy of the measurement processes used. The verification technique also provides the basis for a proposed audit of dosimetry in all stereotactic centres in the UK.

Acknowledgements

I am indebted to Dr David Thwaites for his supervision and invaluable suggestions at crucial stages of the work and for tirelessly reading and re-reading the thesis. I am also grateful to my second supervisor, Dr Tony Redpath, for his comments, especially with regard to the head scatter work. Thanks to the Mechanical Workshop section of Oncology Physics, in particular Mr Dave Colburn and Mr Bryan Doig for manufacturing the phantoms and build-up materials perfectly -even at 5pm on a Friday! Thanks to Mr Ronnie Robertson, for the excellent photographs presented in this work, to Miss Amanda Stewart in Mammography for her excellent x-rays of the detectors and to Mr Martin Connell in Medical Physics for reading and processing the images. Many thanks to all colleagues within the ECC, particularly in Oncology Physics, for their support throughout this PhD.

At the University of Edinburgh I am grateful to Dr Sara Erridge for her comments on the clinical section and to Dr Pete Hoskins for advice on thesis writing. Also to Mrs Kathleen Fiddes for organisation of some of the PhD administration. Thanks also to Dr Jon Turner for organisation of the University's excellent Transferable Skills Programme, which offers a number of invaluable courses to PhD students.

I am grateful to Dr John Byrne, Newcastle General Hospital, for several discussions on the head scatter work and on curve fitting. Also to Dr Mania Aspradakis for commenting on sections, providing the Greek translations and above all listening to every heartache throughout the five years. Thanks too to Mrs Anne McCurrach, Western Infirmary, Glasgow for the PhD-encouragement sessions shared in Edinburgh.

I am grateful to Qados and Scanditronix for the loan of a stereotactic diode and to PTW for the loan of a PinPoint chamber. Also to the Queen Elizabeth Hospital, Birmingham for the loan of a diamond detector, in particular to Dr Richard Hugtenburg for advice with regard to its use and for other discussions on scatter. All of these detectors were subsequently purchased. I am also grateful to Radionics for the loan of the small stereotactic collimators.

I acknowledge the financial support I received from Oncology Physics, the Department of Clinical Oncology Endowment Fund and the University Department of Clinical Oncology. The diamond detector was purchased with money from a Small Project Grant (C/2000/09). I also acknowledge copyright permission from both the Institute of Physics publishing and Elsevier Science for the reproduction of the papers in appendices 9 and 10 and permission from my co-author, Dr David Thwaites.

Many thanks too to my examiners, Mr Jim Warrington, Head of Radiotherapy Physics at the Royal Marsden (Sutton) and Mr Jerry Williams, Head of Diagnostic Physics at the Edinburgh Royal Infirmary, for agreeing to undertake this arduous task and doing so in a shorter timescale than required. Their comments on the thesis and suggestions for small changes were both helpful and challenging!

Finally, thanks to all colleagues, friends and family for putting up with years of trauma. Life can now begin again.

Contents

List of Figures

List of Tables

List of Appendices

Abbreviations

A	atomic weight
AN	acoustic neuroma
AVM	Arterio-venous malformation
BDAS	beam data acquisition system
BEV	Beam's eye view
BFF	beam flattening filter
BJR	British Journal of Radiology
BSF	backscatter factor
CAL	calibration factor for each detector
CAX	central axis
CF	correction factor for directional dependence
coeff. of var.	coefficient of variation
CoP	Code of Practice
D_c	calculated dose to isocentre
D_m	measured dose to isocentre
ECC	Edinburgh Cancer Centre
EE	electronic equilibrium
EFD	electron field detector
EQSQ	equivalent square
FAD	Focus to Axis (isocentre) distance
FSD	Focus to Surface Distance
FWHM	full width half maximum
Fx	traceable calibration factor
GTC	Gill Thomas Cosman
IC	ionisation chamber
IMRT	Intensity modulated radiotherapy
ISL	inverse square law
LEE	lateral electronic equilibrium
LIC	liquid ionisation chamber
LIC	liquid ionisation chamber
M	ISL correction
MC	Monte Carlo
MLC	multileaf collimator
mMLC	micro MLC
MOSFET	metal-oxide-semiconductor field effect transistor
MU	monitor unit
NPSF	normalised peak scatter factor
OAR	off axis ratio
PDD	percentage depth dose
PFD	photon field detector
PMT	photomultiplier tube
PP-IC	parallel-plate ion chamber
PSF	peak scatter factor
QI	quality index
RMI	solid water
s.d.	standard deviation
S_c	head scatter factor
S_{cp}	total scatter factor
SFD	stereotactic field detector
S_p	phantom scatter factor
SRT	Stereotactic radiotherapy
TLD	thermoluminescent dosimeter
TMR	tissue maximum ratio
TP	Temperature and pressure correction
TPR	tissue phantom ratio
TPS	treatment planning system
WT1	solid water
Z	Atomic number

Chapter 1

Introduction

1.1 Foreword

Stereotactic radiotherapy (SRT) has been in use in the UK since 1985, when the first Gamma Knife unit was installed in Sheffield (Walton et al, 1987). Today there are three Gamma Knife units and several linear accelerator (linac) based systems across the country, bringing the total number of stereotactic centres to around 10 (Hampshire and Walton, 2003). This is approximately 15% of the total number of radiotherapy departments in the UK. Stereotactic radiotherapy therefore remains a somewhat specialised technique, available in a relatively small number of centres.

Specialised techniques generally require specialised technology. Radiotherapy technology is advancing rapidly, in terms of hardware, imaging modalities and dedicated software. However, it would appear that the implementation of this new technology into routine clinical practice is generally much slower. In 1998, an audit of 3D planning facilities in the UK showed that although approximately 62% of centres had the facilities to carry out complex non-coplanar planning, only 20% actually did so on a regular basis (McNee et al, 1998). Although this percentage is likely to have increased over the last five years, it is apparent that the availability of equipment alone is not sufficient to make a new technique a reality in the clinic, as staffing, resources, training and cost-benefit analyses will all also have an effect. However, one other problem is related to the increasing complexity of the measurements required, because although these new techniques might bring new dosimetric tools (new detectors, film, scanning systems etc), the tools themselves require verification. Indeed, although stereotactic radiotherapy has been available in the UK for almost twenty years, the dosimetry of small fields is an ongoing problem. A recent article states that:

> *"The measurement of small-field data for treatment planning SRT remains an enduring challenge for the radiotherapy physicist, particularly for small irregular fields or field segments" (Warrington, 2003)*

Measurements in stereotactic fields and small field segments such as those used in intensity modulated radiotherapy (IMRT), are particularly complex. This is due to the specific properties of small fields and the availability of suitable detectors to both measure and verify the dose. The implementation of either technique requires a detailed comparison of several detectors and/or experimental techniques.

The investigation of the dosimetry of stereotactic fields began in the Edinburgh Cancer Centre (ECC) in 1994 and has been on-going ever since, as new detectors have become available and as the methodology has improved. During this time a greater understanding of the measurement complexities has been developed and in recent years other types of small fields have been investigated. Preliminary measurements have been carried out in small open, conventionally collimated fields and those formed by the multileaf collimator (MLC), to determine common beam properties and the most suitable detectors and methods. These results are being used as the basis of part of the dosimetric commissioning of IMRT.

This thesis is an account of the measurements made, conclusions reached and knowledge gained in an eight year investigation of small field dosimetry, with particular reference to the comparison of small detectors in various experimental situations. This chapter introduces some basic radiotherapy concepts for the non-specialist and describes the development of stereotaxy and its use in radiotherapy. As measurement problems in small fields are related to the general properties of megavoltage x-ray beams, these properties are reviewed and the relevant terminology summarised. Detector types and properties are also considered with particular reference to the small field situation.

1.2 Overview of radiotherapy

1.2.1 Definition

Radiotherapy is the use of ionising radiation to treat or control disease. Most commonly the disease is cancer, but a range of non-malignant conditions can also benefit. Although x-rays, gamma-rays, electrons, protons, α or β particles and neutrons etc can all be used to treat particular conditions, this thesis is concerned only with x-rays produced by a linac.

The main aim of radiotherapy is to deliver a maximum dose to the target volume, whilst minimising the dose to surrounding normal tissues. In particular, care is taken to avoid radiation sensitive structures, such as the eyes, brainstem, spinal cord, rectum etc as the prescribed radiation dose to the tumour is limited by the severity of the side effects. New

techniques are constantly being developed to improve the conformity of the dose to the target volume and further minimise the dose to healthy tissue.

1.2.2 Treatment techniques

Static beam therapy

The most common types of linac based treatments are delivered via multiple static beams of x-rays, in which the direction of each beam is chosen both to optimise coverage of the target volume and avoid sensitive structures. Most fields are directed coplanarly, such that the central axis (CAX) lies in the same plane as the transverse cross-section of the target. However, both the use of CT to acquire anatomical information and the advent of computerised 3D planning systems, have led to an increase in the use of multiple non-coplanar fields. These offer more degrees of freedom in which to place a beam, which in turn helps to avoid sensitive structures.

Conformal therapy

Takahashi (1965) defined "conformation therapy" as the method whereby the radiation beam is made to fit, or conform to, the actual treatment volume. This is achieved by shaping the cross-section of each beam to match that of the target volume. The "beam's eye view" (BEV) can be shaped using conformal blocks, which have, until recently, been the most popular method of implementing conformal therapy. Although almost any shape of conformal block can be poured from molten alloy, there are some disadvantages. Significant staff-time is required in the manufacturing process and the resulting blocks are heavy and have to be attached manually to the linac at each treatment session.

An alternative to conformal blocks, is the MLC. Webb (1993) described the development of the modern MLC from its inception in 1906 to the motorised version commonly available today. The MLC is nowadays based on two opposing banks of leaves with individual leaf widths of between 5 and 10mm at isocentre. The position of each leaf is computer controlled and although many shapes can be created, the direction and width of each leaf limits the total number of possibilities. The MLC is generally an integral part of the linac head, but its position within the head is manufacturer dependent. On a Varian linac it is located below the lower collimators and on the Elekta and Siemens linacs it replaces the upper and lower collimators respectively. Small MLCs, known as either as micro or miniature MLCs (mMLC) have recently become available as an add-on facility. The leaf

widths are generally 2.5-4mm at isocentre and can be used to conform fields of up to 100mm width (Schlegel et al, 1992; Cosgrove et al, 1999).

Intensity modulated radiotherapy

Further improvements in conformal therapy have been achieved through the use of intensity modulated radiotherapy (IMRT). This technique is based on the delivery of a beam portal via the addition of multiple small field segments. These can be produced using an MLC either in dynamic mode (Convery and Rosenbloom, 1992) or using multiple static MLC segments, known as "step and shoot" (Bortfeld et al, 1994). The use of IMRT can improve the conformity and homogeneity of dose to a larger number of lesion shapes, including concave and can also improve the protection of sensitive structures. The widespread availability of IMRT compatible MLC systems and the existence of IMRT specific machines such as the Tomotherapy unit (Mackie et al, 1993), the MIMiC (Carol et al, 1996) and the Cyberknife (Alder and Cox, 1995), mean that IMRT has the potential to expand quickly into wider clinical use.

Rotational beam therapy

An alternative to multiple static-beam therapy is rotational (arc) therapy, in which x-rays are delivered whilst the gantry is moving. This technique reduces the skin dose and spreads the dose to normal tissues over a larger volume, thereby reducing the risk of complications. A single 360° rotation produces a cylindrical volume, with the maximum dose located at the isocentre. A partial rotation displaces the high dose region towards the bisector of the arc and, if multiple, non-coplanar partial arcs are used, the treatment volume can be shaped in three dimensions. Gravity orientated blocks can also be used to conform the beam shape, produce concave dose distributions and protect sensitive structures (Proimos, 1960).

1.3 Stereotactic radiotherapy

1.3.1 Introduction

Definition

The word "stereotactic" stems from two ancient words; the Greek word "stereos" (στερεο), which means three-dimensional and either the Greek word "taxic" (τάξη), which means system, or more likely, the Latin word "tactus" which means to touch (Galloway and Maciunas, 1990).

Horsley and Clark (1908) developed a 3D stereo system for functional neurosurgery, based on a rigid head frame. This was pinned invasively to the skull and used as a basis for a 3D co-ordinate system. Although any arbitrary co-ordinate system can be defined, the Brown-Roberts-Wells (BRW) system is one of the most common (Galloway and Maciunas, 1990).

Gamma Knife

Leksell (1951) used the stereotactic system to develop a precise radiotherapy technique for the treatment of small, inoperable brain lesions. This involved the design of a dedicated cobalt-60 unit, known as the "Gamma Knife", now manufactured commercially by Elekta. This unit contains 201 small sources, distributed evenly over a hemispherical region and finely collimated such that all 201 beams converge at the isocentre. Secondary collimation is provided by a helmet which contains 201 holes, each of which can be blocked or left open according to the treatment requirements. The invasive frame is pinned surgically to the skull and attached to the helmet such that the target volume is positioned at the isocentre. Treatment is in one single session (fraction). The system is very accurate with coincidence of the radiation and mechanical isocentres reported as +/-0.3mm (Lunsford et al, 1989).

Radiosurgery

Treatment in a single fraction relies on the late effect of radiation necrosis, in which the tissue within the target volume is completely obliterated. As this is similar to a surgical outcome, single fraction stereotactic radiotherapy is commonly known as "radiosurgery". A high degree of accuracy is essential to ensure that only the target volume is necrosed.

Linac based radiosurgery

Betti and Derechinsky (1984) and Heifelz et al (1984) introduced the idea of using multiple, non-coplanar arcs to extend the stereotactic technique to a linac. Originally the small fields were defined by the movable linac collimators (Colombo et al, 1985), but additional, circular stereotactic cones with diameters <40mm were soon developed (Hartmann et al, 1985) to remove the uncertainties in the field size settings for small fields. Although "dynamic radiosurgery", involving the rotation of both the couch and the gantry was soon to follow (Podgorsak et al, 1988), this technique is less popular than the conventional technique, perhaps due to the engineering modifications necessary (Gillies et al, 1993). A recent study by the American Society for Therapeutic Radiology and Oncology (ASTRO) (Larson et al, 1993) found that only 3 out of 69 linac based stereotactic facilities used the dynamic technique.

Relocatable frames

A fixed frame requires all planning and treatment processes to be carried out on the same day. To allow more flexibility and to include fractionated treatments, Gill et al (1991) developed a relocatable "Gill-Thomas" (GT) frame, based on impressions of the occiput and upper dentition. Extensive quality assurance (QA) is carried out on a relocatable frame to ensure that uncertainties are minimised. It has been shown that the GT frame, and its commercial counterpart, the Gill-Thomas-Cosman (GTC) frame, can be relocated to within 1mm, at 1 s.d. (Graham et al, 1991; Warrington et al 1994; Rosenberg et al, 1999).

The GT frame has been adapted for paediatric use by reducing the weight and allowing access for anaesthesia (Adams et al, 2001). Other types of frame are available, also based on a mouthbite and occiput impression (Theodorou et al, 1998; Theodorou, 1999), or on a dental impression and a thermoplastic mask (Scott et al, 1997). Frames have been developed for head and neck treatments (Karger et al, 2001; Fairclough-Tompa et al, 2001) and to extend the stereotactic technique to the torso (Lax et al, 1994; Wulf et al, 2000).

The use of a stereotactic frame at all stages of the planning and treatment processes, reduces the uncertainties associated with patient movement. As a result, the treatment planning margins can be reduced and more normal tissues spared.

Frameless stereotaxy has been investigated in a few centres to eliminate the need for high precision frames which are often uncomfortable for the patient. Although thermoplastic masks are often used in the "frameless" technique, the accuracy of the patient position relies primarily on the identification of markers either on or in the patient's head, either by a camera system, or an imaging technique. Jones et al (1993) used three gold wires implanted in the scalp to verify the patient position (in a thermoplastic mask) on treatment using beam localisation films. Repeat films were taken until the movements required to obtain agreement with the CT position were <1mm. The authors found that the positions of the markers were not stable in about 25% of patients and now screw markers into the cranium. Bova et al (1997) used six LED markers on a bite plate and located them with an infrared camera system. Again this "frameless" technique also used a thermoplastic mask to stabilise the patient's head. The re-positioning error was found to be 0.5 +/-0.3mm (1s.d.).

Beam shaping

Stereotactic treatments on a linac can be administered via non-coplanar arcs or multiple static beams. Beam shaping with multiple non-coplanar arcs can be further improved

through the use of simultaneous couch rotation, as discussed previously. Static beams can be shaped with either small conformal blocks (Bourland and McCollough, 1994; Perks et al, 1999), a standard MLC (Adams et al, 1999), the mMLC (Schlegel et al, 1992; Cosgrove et al, 1999), or using IMRT (Cardinale et al, 1998). The mMLC has also been used in conjunction with arc therapy, whereby the beam portal is shaped at every increment of gantry angle (Solberg et al, 2001).

1.3.2 Clinical indications

Arterio-venous malformations

An arterio-venous malformation (AVM) is a non-malignant vascular condition which has an annual risk of bleeding of approximately 4% (Ondra et al, 1990). Three treatment options are available; surgery, radiological embolisation with coils or glue and radiosurgery. Radiosurgery is usually reserved for those patients for whom surgery or embolisation are not technically possible, or for whom embolisation has been unsuccessful.

The Gamma-Knife has been used to treat AVMs for more than three decades. A recent report (Flickenger, 2002) showed an obliteration rate of 76% at 3 years. Linac based radiosurgery has also been used to treat AVMs and early results suggest that it produces equivalent results (Touboul et al 1998; Friedman, 1995).

Brain metastases

Stereotactic radiotherapy, usually in conjunction with whole brain radiotherapy, is becoming more common for the treatment of patients with solitary brain metastases. The RTOG 95-08 study compared the results of whole brain radiotherapy alone or with a stereotactic boost and showed a survival benefit for lung cancer patients under 50 and with good performance status (Sperduto, 2002). Fractionated stereotactic treatment has also been used without whole brain treatment, with median survival of 21 months for patients without extracranial tumours (Tokuuye et al 1998).

Vestibular schwannoma

A vestibular schwannoma is also known as an acoustic neuroma (AN), although this latter term is clinically imprecise. It is a slow growing non-malignant tumour of the hearing nerve which is usually surgically removed. However, there are common side-effects such as ipsilateral deafness and damage to the facial nerves, which can result in permanent facial

palsy. Radiosurgery has shown good results (Pollock et al, 1995), but the proximity of the lesion to the brainstem and the risk of damage to the facial nerve makes a fractionated regime preferable. Two approaches exist; standard fractionation schedules (Fuss, 2000) or hypofractionated schedules (Lederman, 1998). Early results from these studies suggest surgically equivalent local control rates of 91-100%.

Other lesions

Many other types of lesion such as pituitary adenomas (Mitsumori et al, 1998) and cranial chordoma (Corn et al, 1996) have also been treated with multiple fractions. It is apparent from the literature that both single and multiple fraction stereotactic treatments are important in the management of patients with many types of small brain lesions.

1.4 Beam dosimetry

1.4.1 Introduction

Dosimetry is the measurement of radiation dose, either in relative, or absolute terms. The various beam properties which may affect the measurement of dose are outlined in this section along with an explanation of the types of measurement commonly carried out. The range of detectors used and their corresponding properties are also discussed.

1.4.2 Production of x-rays

X-rays are produced in a linear accelerator through the interaction between high energy electrons and the nuclei of atoms in a target material. The electrons are decelerated in the vicinity of the nuclei and the loss of energy is accounted for in the production of bremsstrahlung x-rays. Although x-rays are produced in all directions, at megavoltage energies the distribution is mainly forward and the spectrum is comprised of a range of x-ray energies, up to, and including, the maximum accelerating potential of the electrons.

1.4.3 Beam properties

Fluence

Photon interactions in the head of the linac and in the air, produce electrons which contaminate the beam (electron contamination). The resultant beam at the surface of a phantom is therefore a combination of both photons and electrons. The number of photons and/or electrons per unit area is known as the fluence and the total energy of all particles

within the same area is known as the energy fluence. The fluence varies with the field size and is inversely dependent on the square of the distance from the source i.e. fluence follows the inverse square law (ISL).

Kerma and absorbed dose

In a photon beam, energy is transferred from a photon to the medium in two-stages. The first stage is the interaction between the photon and an electron in the absorbing material, whereby the photon transfers some of its energy to the electron, in the form of kinetic energy. The kinetic energy per unit mass is known as "kerma" and is measured in Gy, which is the energy (in joules) transferred per unit mass (in kg). In the second stage the electron gives up its energy to the absorbing material through a series of multiple, coulomb interactions with electrons in the medium. This deposition of energy results in temperature increases, chemical changes and the breaking of molecular bonds and is known as the "absorbed dose". The absorbed dose is a measure of the energy (in joules) absorbed in a material, per unit mass (in kg) and is also measured in Gy.

Electron range and stopping power

The electron path through a medium is not linear, due to multiple scattering. The "electron range" is the total distance travelled by an electron, along its tortuous path. The mean effective distance travelled by all electrons is known as the "mean projected range", the magnitude of which is dependent on the mean energy of all electrons. The amount of energy lost by the electron, per unit length along its track, is known as the "linear stopping power". An electron will lose its energy in a shorter distance in a material with a higher atomic number (Z) than water i.e. the linear stopping power is greater in a high Z material.

Electronic equilibrium

Electronic equilibrium (EE) occurs when the number of electrons created within a volume is equal to the number of electrons brought to a halt within that same volume. In the forward direction, this occurs within a depth equal to the mean projected range of the electrons. Although a 6MV beam will produce secondary electrons with a maximum range in water of approximately 30mm, electronic equilibrium occurs at a shallower depth (approximately 15mm) because the electron path is tortuous and non-linear and because the secondary electrons will have a whole range of energies. This depth is the depth of maximum dose (dmax). If photon attenuation is ignored (over a small distance), then electronic equilibrium exists beyond dmax where kerma and dose are approximately equivalent (ignoring the

minimal effects of bremsstrahlung). The region between the surface and dmax is known as the "build-up region". It is a region of electronic disequilibrium where kerma > dose as more electrons are set in motion than are stopped.

Lateral electronic equilibrium (LEE) occurs within a beam radius which is less than the depth of dmax (Dutreix, 1964), due to the fact that most of the electrons will be scattered in the forward direction rather than at, or near, 90°. Electronic equilibrium does not therefore exist in very small beams. The exact field size at which electronic equilibrium fails to exist is a matter of debate, but Li et al (1995) used Monte Carlo to calculate some values. At 6MV, electronic equilibrium will fail to occur in fields with radii <15mm, which is approximately the equilibrium depth in the forward direction.

Primary and scatter

The dose at a point can be split into two constituent parts; primary dose and scatter dose. Physically, the two cannot be separated, but the concept is useful in mathematical terms, particularly for the calculation of dose in irregularly shaped fields. For MLC, blocked or asymmetric fields, the dose must either be measured in each individual shape, or calculated using a model which incorporates the separation of primary and scatter dose.

Primary dose is something of an abstract concept, the definition of which varies in the literature. Khan (Chapter 10, 1994) defines it as the dose resulting from the "original photons emitted from the source", whilst Mohan (1985) defines it as the dose deposited by a hypothetical zero area beam. The primary dose varies with depth and the distance between the source and the point of measurement.

The scatter dose is easier to define and, at its simplest, is the dose due to all scattered photons (Khan et al 1984). These scattered photons can be further split into head and phantom scattered photons. Head scattered photons are defined as those which have been scattered in the various components of the treatment head, such as the flattening filter, ion chamber, collimators etc. and have interacted in the phantom only once (Nizin and Kase 1988). The greatest source of head scatter is the flattening filter (Kase and Svensson, 1986) and the amount of head scatter measured at a point is dependent on the amount of the flattening filter visible from the measurement point. In open fields, this area is dependent on the field size setting on the movable collimators. It is for this reason that head scatter is sometimes known as "collimator scatter", although the term can cause confusion. The

amount of head scatter detected is also dependent on the backscatter into the monitor unit (MU) chamber which will affect the dose/MU.

Phantom scattered photons are composed of those which have interacted in the medium more than once and those which have resulted from bremsstrahlung in the phantom (Nizin and Kase 1988). In high-energy beams, phantom scatter also includes annihilation radiation which occurs as a result of pair production. The relative amount of phantom scatter is dependent only on the beam area at the surface of the phantom. This is defined by the collimation system, which can be the movable collimators, the MLC, beam blocks or stereotactic collimators, for example.

Dose rate

Although the dose rate of a beam is strictly the number of Gy/minute at a point, the term is more commonly used to describe the number of Gy delivered per MU setting on a linac. The dose/MU decreases with depth and with increasing distance from the source. In addition, the dose/MU at the surface of a phantom (or in-air) in a large field is smallest on the central axis (CAX) of the beam and increases with off axis distance. This is due to the differential absorption of more photons at the centre of a beam, through the thickest part of the flattening filter.

Quality

The quality of a beam is a measure of its penetrating capabilities. A single parameter to specify the penetrating capabilities is useful to compare beams of different quality. Nominal accelerating potential is often used, but this defines only the maximum energy of photons within the overall beam spectrum. Linacs with the same accelerating potential will usually have different beam qualities, unless they are specifically matched. The depth of the 80% isodose has also been used to quantify quality and Supplement 25 of the British Journal of Radiology (BJR) lists these depths for each nominal potential (Jordan, 1996). However, the tissue phantom ratio (TPR) is more commonly used to specify beam quality. This is a ratio of the dose at a depth d_1 to the dose at a depth d_2 with the measurement made at the isocentre in the same field size. This measurement is known as a tissue phantom ratio (TPR, see Chapter 8) and the quality index (QI) is defined as the TPR measured at d_1 = 100mm and d_2 = 200mm, for a field size of 100x100mm^2 and can be referred to as the TPR(200,100).

1.4.4 Beam measurements

Beam commissioning: types of measurements

An absolute dose measurement for beam calibration is generally carried out in one field size, depth and source (focus) to phantom surface distance (FSD) only, according to national protocols. In the UK, the Code of Practice (CoP) for high energy photons (IPSM, 1990) requires that the absolute dose is measured in a 100x100mm^2 field at 50mm depth for beams =<10MV, 70mm for beams between 11 and 25MV and 100mm for 26-35MV. The MU chamber is then adjusted to deliver 1Gy to a reference point. Historically this has been chosen to be dmax in a 100x100mm^2 field at 1000mm FSD, but some formalisms are based on the delivery of 1Gy to a point deeper than dmax, either at 1000mm FSD or with the reference point at 1000mm focus to isocentre (axis) distance (FAD).

Numerous relative dose measurements are generally carried out both as input to a treatment planning system (TPS), or to verify the output from the TPS. Typical measurements such as percentage depth dose (PDD), tissue maximum ratio (TMR), off axis ratio (OAR), relative output and head scatter measurements are generally required. Each of these will be discussed in full in subsequent chapters.

PDDs and TMRs are measured for a range of field sizes and normalised to dmax; either the individual dmax positions for each field size, or the dmax value for the 100x100mm^2 field. OARs are measured at various depths and normalised to dose on the central axis (CAX) at the same depth. Relative outputs are commonly measured at dmax and normalised to the reference field. However, formalisms based on a reference depth beyond that reached by contaminant electrons are becoming more popular. A reference point of 50mm has been recommended for energies up to 8MV and 100mm either for higher energies, or also including the lower energies (van Gasteren et al, 1991, Dutreix et al 1997, NCS, Report 12, 1998). It is important to ensure that the normalisation between data sets is internally consistent, whichever type of formalism is used.

1. 5 Detectors

1.5.1 Introduction

An ideal detector should be water equivalent and have a response which is independent of energy, dose-rate and direction. Unfortunately, no such detector exists. It is important therefore to understand the properties of all detectors under investigation, in order to

determine which are the most appropriate in which situations. Selected detector properties and types are outlined below.

1.5.2 Detector properties

Composition

As most beam measurements are carried out in water, or in a water-equivalent material, an ideal detector should also be water-equivalent, with effective atomic number close to 7.4. In non-water-equivalent detectors, the electron range will change according to $\rho Z/A$. As a result, electronic equilibrium will exist in a shorter distance in a higher density material compared with water. The composition (density and material) of a detector will primarily affect measurements in regions of electronic disequilibrium.

Directional dependence

The directional dependence of a detector is important when measuring the dose at off-axis positions, and at a point in a phantom when beams are directed from different directions. However it may also affect the response to scatter incident from the sides, or from behind the detector. If a detector has a directional dependence, the magnitude of the variation in response may need to be measured and accounted for.

Energy dependence

An ideal detector should have a constant response over a range of energies. The mean energy of the beam decreases with depth, due to the increase in scatter and decreases with off axis distance (off axis softening) as fewer low energy photons are removed in the flattening filter. As a result, detectors which show an energy dependence may over or under-estimate the dose at depth or off axis.

Dose rate dependence

Dose-rate independence is important mainly because the dose rate will vary with depth and off axis position. A detector's dose rate dependence is a result of the ion, or charged particle, recombination speed, which is dependent on the concentration of particles and the electric field strength. As the concentration of particles is much higher in a solid than in air, recombination effects are generally greater in solid state detectors.

Size

In any measurement with a finite sized detector, the dose is an average of the signal over the entire sensitive volume. This is sometimes known as volume averaging. Volume averaging is not a problem in regions of constant dose, but will affect the results in regions of rapid dose gradient, such as at the edge of a beam. In very small beams (<12.5mm width) the region of constant dose is only of the order of a few (1-4)mm and therefore it is important to either use a small detector, or apply a correction factor to account for the size.

Effective point of measurement

For solid state detectors, the effective point of measurement is the physical centre of the sensitive volume and is documented by the manufacturer. For ion chambers, the measurement volume is usually an air cavity and when used in conventional orientation, the effective point of measurement is generally taken to be upstream, at half the internal radius of the chamber. For air-filled parallel plate chambers, the inside of the front window of the detector is usually chosen. The effective point of measurement should be taken into account in all beam data measurements.

1.5.3 Types of detectors

Air filled ion chambers

The most common detector used in dosimetry is the air ionisation chamber (IC). The two main designs are cylindrical and parallel-plate, the sensitive volume in either case being an air-filled cavity (effective Z=7.4). The response of an ionisation chamber is dependent on the mass of gas contained within the sensitive volume. A larger chamber is obviously more sensitive than a small volume chamber. However, a consequence of this is that a greater amount of volume averaging will occur in a large volume chamber, which again is a problem in regions of rapidly changing dose gradient.

Relatively large (0.6cc) ICs are commonly used in beam calibration. Relative output measurements in fields of width 400-40mm are usually carried with ICs of between 0.1 to 0.6cc. For relative dose measurements in a water tank, a 0.1cc IC is useful to minimise the volume averaging effects at the edge of the beam. Much smaller chambers are also available, such as the 0.015cc PinPoint chamber from PTW. One disadvantage of this chamber is that it has a steel electrode, which causes it to over-respond to low energy photons (Martens et al, 2000). Other types and sizes of small ICs exist, such as the ultra-micro-cylindrical IC (UCIC) which has dual sensitive volumes of 0.008cc air and 0.0023cc

borosilicate (Vahc et al, 2001). Although air filled ICs are not independent of energy and dose/pulse, the changes are small and are generally ignored. Cylindrical chambers are also directionally independent.

To improve the resolution of an ion chamber, liquid filled cylindrical and parallel plate ion chambers (LICs) have recently been developed. The replacement of the air volume with a dielectric liquid increases the chamber sensitivity by approximately 300 times and as a result, smaller detectors can be produced. Although air filled cylindrical chambers have been shown to be energy and directionally independent, LICs have been shown to exhibit small directional and energy dependencies (Wickman et al, 1998, Dasu et al, 1998, Westermark et al, 2000).

Diodes

Diodes are solid-state semiconductor detectors. The sensitive volume generally has a width of 2-3mm and is composed of silicon (Z=14). As $\rho Z/A$ is higher for silicon than water, electrons will lose their energy over a shorter distance. For example, electrons with energies in the 1-6MeV range, will be stopped in silicon in half the distance compared to water. One drawback of diodes is that silicon is more sensitive to low energy photons. This is due to the photoelectric effect, which is dependent on Z^3 and therefore they will over-respond in regions with more relative scatter.

The outer shape of the dosimetry diodes manufactured by Scanditronix is cylindrical. The silicon chip is square in cross-section (2.5mm width) and is approximately 0.1mm thick. The width of the chip is orientated as symmetrically as possible, across the diameter of the cylindrical casing and positioned just below (0.4-0.6mm) the detector surface. The chip is embedded in an epoxy resin material and the outer casing is metallic. The "unshielded diode" contains no additional materials and is generally used in electron beams. In megavoltage photon beams it overestimates the dose at large depths and field sizes, due to the increased sensitivity to low-energy photons. Scanditronix have named this diode an "electron field detector", abbreviated to EFD.

Energy compensated diodes have been developed for use in photon beams. These have been empirically modified to absorb some of the low energy scatter through the addition of a layer of high atomic number material (tungsten) immediately behind the chip (Gager et al, 1977; Rikner and Grusell, 1985). This matches the response more closely to that of an

ionisation chamber and hence the term "photon diode". Scanditronix have labelled this diode, a "photon field detector" (PFD).

Most commercial diodes are manufactured from p-type silicon as these have been shown to be relatively dose-rate independent (Rikner, 1985) when compared with n-type. However, some p-type diodes have been shown to exhibit large increases in response as the dose rate increases (Van Dam et al, 1990; Hoban et al, 1994). Van Dam (1990) showed that the dose rate response increased with cumulative dose, as did Wilkins et al (1997), who also found that this was dependent on the doping levels. Scanditronix diodes manufactured since 1993, have higher doping levels than previous types, to minimise dose rate effects. Diode sensitivity decreases with cumulative dose and therefore it must be calibrated regularly against an ion chamber for absolute dose determination and ensure that the dose-rate effects are still acceptable.

The conventional orientation for the above types of diodes is with the long axis of the casing parallel to the beam CAX. However, the resolution can be increased by orientating the diode with the long axis of the casing perpendicular to the beam CAX, such that the dose is averaged over the 0.1mm chip thickness. However, when diodes are irradiated in this orientation, the response decreases. Scanditronix unshielded and shielded diodes show reductions in response of approximately 5 and 15% respectively (Rikner and Grusell, 1985) with the larger decrease in the shielded diode due to the tungsten shielding.

Diamonds

Although a diamond is an insulator, conductivity is induced when radiation is incident on it. This is caused by a decrease in the resistivity (Burgemeister, 1981) and means that it can be used as a solid state detector (Hoban et al, 1994). Commercial diamond detectors incorporate naturally grown crystals, of volume $<6mm^3$, embedded in a thin layer of epoxy, surrounded by polystyrene (Mobit and Sandison, 1999). A diamond detector is relatively tissue equivalent (Z=6) and directionally independent, but the response decreases with increasing dose rate (Planskoy, 1980). This decrease in response is a feature of radiation-induced conductivity in an insulator and is due to the short electron-hole recombination time, which decreases as the dose rate increases (Hoban et al, 1994).

Thermoluminescent dosimeters

Thermoluminescent dosimeters (TLDs) are based on the luminescent phenomena of phosphorescence, which is a delayed response to radiation. TLDs are materials which, on

heating, give out light in proportion to the radiation previously incident on them. Lithium fluoride is a common TLD material and can be processed into various forms, such as small square ($3x3mm^2$) or circular (4.5mm diameter) chips, 6mm rods and $1mm^3$ micro-cubes. Lithium Fluoride has an effective atomic number of 8.1 and Lithium Borate = 7.4 (Mayles et al, 2000). TLDs are dose rate and directionally independent, but their sensitivity is highly dependent on the read-out and annealing processes.

Semiconductor transistors

A metal-oxide-semiconductor field effect transistor (MOSFET) is a semiconductor transistor with a sensitive volume of p-type silicon in contact with an insulating oxide layer. It is unique in that it can be used to measure both dose rate and cumulative dose simultaneously (Gladstone and Chin, 1991). The active volume is $0.4x0.5x0.1mm^3$ inside an overall outer casing diameter of 2.5mm. Measurements with MOSFETs in in-vivo dosimetry have shown the to compare favourably with TLD (Ramani et al, 1997).

Scintillators

Scintillator detectors are luminescent devices, but are based on fluorescence. Flashes of light are emitted almost immediately ($\sim 10^{-10}$s) in response to incident radiation. This light can be measured at the time of exposure and counted in situ by connection to a photomultiplier-tube (PMT). Plastic scintillators are almost tissue equivalent and have been found to be resistant to radiation damage. They are also more energy independent than many other detectors used in radiotherapy (Beddar et al, 1992a). Their response is linear with dose and independent of dose rate (Beddar et al, 1992b).

Radiographic Film

Radiographic film is useful primarily for the measurement of relative dose distributions. On irradiation, crystals of silver bromide or halide turn to pure silver (Z=45) and appear as a dark region on the developed film. As the photoelectric effect is proportional to Z^3, film tends to over-respond to photon energies <200KeV. The number of these low energy photons increases with depth, due to scatter and therefore the sensitivity of film also increases with depth (Khan, Chapter8: 1994).

The sensitivity of film is very dependent on the calibration and processing conditions (Williamson et al 1981) and on the size and density of the silver crystals, which are extremely variable, both film-film and across each film (Cheng and Das, 1996). The

resolution is however, mainly determined by the densitometer on which it is read out. Point densitometers should have an aperture no larger than $1x1mm^2$, but higher resolution can be obtained through the use of a scanning densitometer.

A slow film, such as Kodak X-Omat V (XV film) is commonly used in dosimetry, where a dose of approximately 0.3Gy produces an optical density of 1. However, the film saturates at doses comparable to those used in patient treatment fractions. Care must be taken to ensure that air pockets are expelled from the film envelopes, by piercing them prior to use and gaps between the film and the phantom should be eliminated. In addition, some authors apply a gantry angle of approximately 2° to ensure that the film is not irradiated entirely along its edge (Suchowerska et al, 2001).

Recently, slower films such as CEA (Cheng and Das, 1996) and Kodak EDR (Chetty and Charland, 2002) have been produced. These films have a higher dose range (linear up to approximately 5Gy) and contain smaller, more uniform silver crystals. These attributes make the film more reproducible and useful for measurements in more typical clinical treatment situations.

Radiochromic film

An alternative to radiographic film is radiochromic film, sold under the brand name of GafChromic™. It is unique in that it is insensitive to daylight and turns a blue colour on exposure to x-rays (Saylor et al, 1988, McLaughlin et al, 1991). An AAPM report (Niroomand-Rad et al, 1998) recommended techniques for the calibration, exposure and analysis of radiochromic film. The first type of film (DM-1260) required doses in excess of 50Gy to obtain +/-2% precision, but the commonly used MD-55 is sensitive to doses down to 3Gy. However, this still implies that doses higher than those used in a typical treatment fraction may be necessary to achieve the required precision. Recently, a more senstive type of Gafchromic film (HS) has been released onto the market (Das and Cheng, 2001; Ashburn et al, 2001). Radiochromic film must be read out on a spectrophotometer or a scanning densitometer with a helium-neon laser. However, a document scanner has also been shown to be useful (Stevens et al, 1996).

Radiosensitive gel

Radiochromic gels such as BANG (Maryanski et al, 1996) and other chemicals such as ferrous sulphate (Chan et al, 1995) can be mixed and inserted in any shape of phantom. The phantom is irradiated and MR scanned appropriately. As the MR signal is approximately

proportional to the dose, relative dose distributions can be obtained. Although gels offer full 3D information, the techniques are expensive, time-consuming and messy.

1.6 Dose modeling

1.6.1 Introduction

The forward attenuation and lateral spread of dose in a phantom can be calculated most simply using beam models based almost entirely on measured data (Milan & Bently, 1970). The accuracy of the dose calculation can be improved by using semi-empirical methods based on the separation of primary and scatter and range from the simplest involving tissue air ratios (Sontag and Cunningham, 1978) to the more complex. The main drawback with these techniques is their inability to model electron transport at interface regions. Algorithms which attempt to do this are based on convolution and superposition techniques, or Monte Carlo but the incorporation of these algorithms into routine planning systems is limited by the calculation time.

1.6.2 Convolution / superposition

Convolution is a mathematical technique used to determine the resulting effect of the multiplicative combination of two functions. In some dose calculation models, the photon fluence at the surface of a phantom can be convolved with kernels which describe the energy spread around a point (Mackie et al, 1985) or along a pencil beam (Mohan et al, 1986). Superposition places each kernel at the appropriate position within the phantom in order to carry out the convolution. Both the fluence and the pencil beam kernels can either be calculated from measured profiles or by using Monte Carlo data. Convolution /superposition is a more accurate approach to dose modelling than models based wholly on measured data, as it can account for electronic disequilibrium.

1.6.3 Monte Carlo

The Monte Carlo (MC) technique can be used to simulate radiation transport. It is the most accurate method for calculating the dose in a phantom as it models the real physical processes. The probability that a single photon, or electron will interact with a particular particle at a particular time and position can be calculated and subsequently used to determine the dose deposited at a point. By considering millions of such interactions, a complete dose distribution can be calculated in a phantom. Any MC code is only part of the

overall beam model and must be attached to a user-code, which contains information on the specific linac used.

MC calculations are outwith the scope of this thesis. However, in several publications concerned with small field data, measurements with detectors are compared against MC. Although several MC algorithms exist, the Electron Gamma Shower (EGS) 4 (Nelson et al, 1985) program is the only one referenced in small field publications to date. EGS4 is the most commonly used MC code in radiotherapy dose calculations (Verhaegen, 2001) and is generally attached to the BEAM user-code (Rogers et al, 1995). BEAM includes files into which the user must input specific linac parameters such as the dimensions and composition of all critical parts of the head.

MC calculations are generally benchmarked against dose measurements and parameters are adjusted within the code until satisfactory agreement has been achieved. However, in situations where measurements are problematic, such as at interfaces between two mediums, or in very small fields, MC has been used to test the accuracy of the actual dose measurements. The flaw in this process is that the accuracy of MC itself depends very much on the accuracy of the data input by the user and the calculation algorithm used.

The main strength of these complex algorithms lies in their ability to model the dose in regions of electronic disequilibrium. This is particularly important at tissue interfaces, where there is a build-up and build-down effect, at beam edges and in very small fields.

1.7 The small field situation

1.7.1 Definition

Standard tables of beam data in megavoltage photon beams, such as those in BJR Supplement 25 (Jordan, 1996), exist for square beams between 400 and 40mm width. A small field is therefore defined in this work as anything with a beam width <40mm.

1.7.2 Small field problems

As discussed in section 1.4.3, the exact width at which lateral electronic equilibrium is achieved at 6MV is debatable, but must be less than a radius of 15mm, as the scatter is mainly in the forward direction. This suggests that some small fields will exist under electronic disequilibrium. As measurements are subject to more uncertainties in regions of electronic disequilibrium, small field measurements are therefore more complex.

The spectrum in a small beam defined by stereotactic collimators is different from that in a larger beam defined by the movable collimators. The stereotactic collimators firstly harden the beam by limiting it mainly to those photons which have passed through the thickest part of the beam flattening filter. However, the beam is also softened by the secondary photons and pair production produced in the stereotactic collimators. The resulting beam spectrum is therefore very different from that of a larger field (Sanchez-Doblado et al, 2003).

The measurement of beam parameters is also much more complex in small fields than for more conventional field sizes, most obviously because the size of many detectors used in conventional fields is physically too large to be used in small field measurements. In addition, the high dose region is likely to be smaller than or comparable with, the size of the detector, which will also lead to additional measurement uncertainties.

1.7.3 Small field detectors

Podgorsak (1992) recommends that several different detectors be used in each small beam measurement situation. Ionisation chambers, diodes, TLD and film are commonly available in most departments and, where appropriate, these should form the basis of a measurement comparison. Other, more stereotactic-specific detectors require investigation as and when they become available. These should be tested with a view to determining whether or not they offer any advantages over other, more conventional detectors. In addition, it is important to consider that although larger detectors can be corrected for their size, it is preferable, where possible, to use a detector which does not require a correction.

Paskalev et al (2002) pointed out that the two most important features of a detector used to measure the dose in small fields, were the detector resolution and material and recommended that both properties should be corrected for. The authors corrected for the size of a small (2mm sensitive width) parallel-plate IC though a series of complex calculations involving the physical dimensions of internal components and the direction of the electric field. The detector material was corrected for using Monte Carlo simulations of the air cavity and the fluence in the beam. However, these extensive calculations were carried out only for very small beams of 5 and 1.5mm diameter, where the differences were likely to be greatest.

1.8 Accuracy and precision

1.8.1 Definition

The measurement of beam data and the delivery of a patient's treatment require high degrees of both accuracy and precision. Accuracy refers to how close a measurement is to the "true" value and precision refers to the reproducibility of the measurement. Beam data measurements must primarily be accurate, in that the correct quantity must be measured with the most appropriate detector and measurement set-up. Measurements must also be precise, in that they must be reproducible. Dose delivery must be accurate, in that the calculated dose should be delivered to the prescription point and must be precise, in that the same dose should be delivered on repeat occasions. Importantly, the geometric set-up of the patient must also be accurate (isocentre located correctly) and precise (day to day). This must be achieved to the highest degree in stereotactic treatments.

The dose delivered to the target in conventional treatments should be within +/-5% of the prescribed dose (ICRU 24, 1976), but later recommendations suggest that an accuracy of +/-3% at 1 s.d. is achievable (Mijnheer et al, 1987; Brahme et al 1988). As this is a clinical requirement for a group of patients, better accuracy, of the order of 2% should be achievable in a phantom. The agreement between the measured and calculated dose distribution should be within +/-2mm in regions of high dose gradient and +/-2% elsewhere (ICRU 42, 1987). The geometrical accuracy of the patient set-up (positioning of field edges, blocks, patient movement, linac tolerances etc) should be within 4-5mm at 1 s.d. (IPEM 81, 1999).

Although there are no specific recommendations for the accuracy of stereotactic dose delivery, the above limits should be adhered too and improved on where possible. Stereotactic beam data should therefore be measured with an accuracy of better than +/-1% and the dose to the isocentre in a phantom to within +/-2% of the expected dose. The main problem with achieving these aims is that the "true" value of the beam data is unknown. Whereas in conventional fields the performance of detectors such as ionisation chambers and diodes is well understood, their behaviour in small fields is not.

1.8.2 Verification

In addition to accurate measurement of beam parameters, the introduction of any new radiotherapy technique to a department also requires a robust method of verification. Conventional clinical treatments can be verified using a detector positioned at a known point within a phantom. This phantom is CT scanned, planned and then "treated" on the linac. The method can be used to check the accuracy and precision of the entire planning

and treatment process within a department, but also used in inter-departmental audit (Thwaites et al, 1992, 1997, 2003).

Verification is of increased importance in stereotactic treatments because of the higher degree of accuracy required, but is more complicated both because of the need for a dedicated phantom (attachable to the stereotactic frame) and the use of multiple non-coplanar beams. A small, water-equivalent, energy and directionally independent detector, which can also be calibrated following current dosimetry protocols, is also required.

1.9 Small beams at The Edinburgh Cancer Centre

Stereotactic radiotherapy has been carried out at the Edinburgh Cancer Centre (ECC) since October 1995, originally on a 6MV BBC CH6 linac and currently on a 6MV Varian 600CD linac. The stereotactic system from Radionics incorporates an add-on collimator system, a couch mount, the GTC relocatable head frame and the XKnife treatment planning system. The add-on collimation systems consists of a collimator housing which is screwed to the base-plate of the head and twelve divergent collimators with diameters between 40 and 12.5mm at isocentre.

At the time of commissioning (1994), there were very little published data on small field dosimetry. Publications in which small field results were presented, often included only one detector, or a prototype detector. In 1994, only standard detectors were available in the ECC and optimum detectors and experimental methods were determined through a comparison of measurements. When new, more stereotactic specific detectors became available, these were tested against the standard detectors and recommendations made as to whether or not they presented any advantages.

Currently the department is beginning a programme to commission IMRT on a newly installed Varian Clinac 2100 multimode with Millennium MLC (5mm width at isocentre). It is anticipated that the use of dynamic step and shoot may involve very small beam segments. Initially the relative output and beam profiles will be measured in these segments, through static step and shoot. The results from this work will therefore form a basis for the commissioning of IMRT.

1.10 Aim

The main aim of this work was to study the absolute and relative dosimetry of small x-ray beams to determine the optimum detector(s) and method(s) for a variety of experimental situations. The immediate application of this was to the measurements required for stereotactic radiotherapy in the ECC and to a verification technique. Beam data should be measured with an accuracy of +/-1% and the dose to the isocentre verified to within +/-2%. The secondary application of the results was to provide a framework for similar measurements in other small fields. These included small collimators between 10 and 5mm diameter and small square fields between 40x40 and 10x10mm^2 formed by both the movable linac collimators and the MLC. The framework will also be applied to measurements in IMRT fields in the near future. The above aims were fulfilled, where appropriate, by an investigation of the following:

- Optimum detectors and methods for the measurement of beam parameters.
- The factors influencing head scatter, in small fields.
- The design of a phantom for the verification of a typical stereotactic treatment plan and the comparison of appropriate detectors.

Each of the above was considered with respect to practical measurements within a clinical department. Only commercially available detectors, available at the time within the ECC, were initially considered and, where possible, were considered against other commercially available, stereotactic-specific, detectors, with a view to determining whether these offered any significant advantages. Some of the results have been published (McKerracher and Thwaites, 1999; 2002), but they have also been expanded upon since those dates.

1.11 Outline of chapters

The thesis has been split into this introductory chapter, a general materials and methods chapter, seven beam measurement chapters and an overall conclusion. The type of measurement is defined at the start of each chapter. The relevant literature to date is critically reviewed to determine the small field knowledge available at the time of each investigation and to note the overall progress which has been made in recent years. The materials used and measurement methods employed are then also described in each chapter and the results presented and discussed. All detectors available within the ECC are compared in each measurement situation, as appropriate. Where possible, recommendations are made regarding the most appropriate detectors and measurement methods.

Chapter 2 describes the materials and methods which are common to more than one chapter. The dose calculation algorithm is outlined and the types of detectors used are described.

Chapter 3 examines the detector comparison in the measurement of PDDs in stereotactic beams between 40 and 12.5mm diameter. Extrapolated and measured data for collimators between 10 and 5mm diameter are also compared.

Detectors are compared in the measurement of in-water beam profiles in stereotactic beams between 40 and 12.5mm diameter, in Chapter 4. In-air and in-water profiles are also examined for collimators of 10-5mm diameter and small square fields. This information is used to assess the effects of volume averaging in Chapters 5 and 6.

Detectors are compared in the measurement of total scatter factors (40 to 12.5mm diameter), in Chapter 5. Results for smaller collimators (10-5mm) and small square fields are presented and are used in the calculation of phantom scatter factors in Chapter 7.

Chapter 6 examines both the detector and phantom comparison in the measurement of head scatter factors in stereotactic collimators between 40 and 12.5mm diameter. Measurements were also carried out in smaller collimators (10-5mm) and small square fields with the appropriate detector, to be used in the calculation of phantom scatter factors in Chapter 7.

Phantom scatter factors are calculated in Chapter 7, for each beam defining system separately and the results compared. The possibility of a common table of phantom scatter factors for small fields is discussed.

TMRs are calculated in Chapter 8 from the PDD data in Chapter 3 and the phantom scatter factors in Chapter 7 and are compared with measured TMRs.

A new verification technique is described in Chapter 9, for use in typical stereotactic plans used at the ECC.

The overall conclusions with respect to optimum detectors and measurement methods are presented in Chapter 10, along with some suggestions for future work.

Chapter 2

General Materials and Methods

2.1 Materials

2.1.1 Linacs

The BBC (Brown Bovari Corporation, Baden, Switzerland) CH6 linac is a single energy (6MV) linac and the CH20 is a multi-mode, with two photon energies (6 and 16MV) and five electron energies (5-20MV). Both linacs have a 270° bending magnet and a motorised 60° wedge, but no MLC. The Varian (Palo Alto, USA) 600CD is a single energy (6MV) linac with a straight through waveguide and includes the enhanced dynamic wedge (EDW) and Millennium (120 leaf) MLC (5mm leaf width at isocentre). Figure 2.1 shows a schematic diagram of the 600CD collimating system.

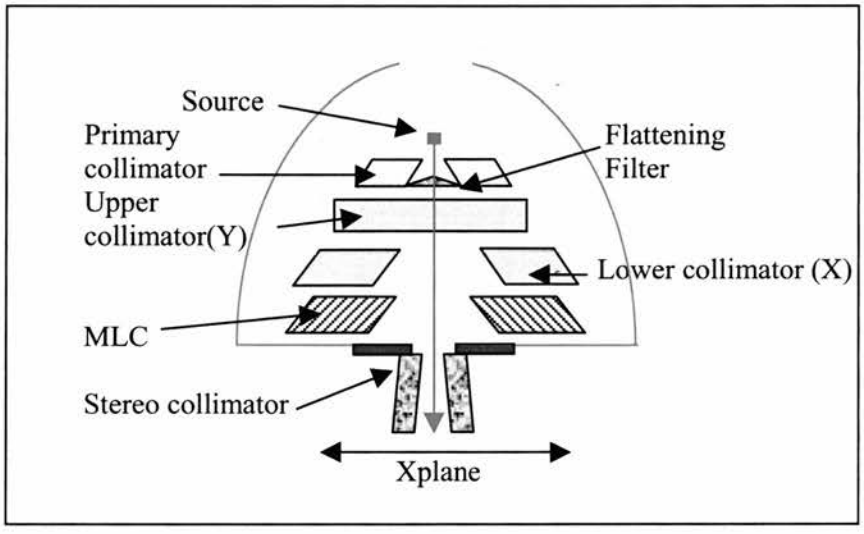

Figure 2.1 Schematic diagram of the collimating system within the head of the 600CD.

On all three linacs, the upper movable collimators are known as Y, and the lower as X. When the linac head (collimator) is at 0°, the direction of movement of the Y jaws is known here as Inplane (into the gantry) and the direction of the X jaws as Crossplane (Xplane - across the gantry). The 600CD MLC is located below the movable X collimators and the

leaves travel in the Xplane direction. The stereotactic housing is attached to the face-plate of the linac, below the X movable collimators (BBC linacs) or below the MLC (600CD).

Linac co-ordinate system

The IEC (1996) co-ordinate system is adhered to on all linacs in the ECC. The orientation of the gantry and floor co-ordinate systems are shown in Figure 2.2.

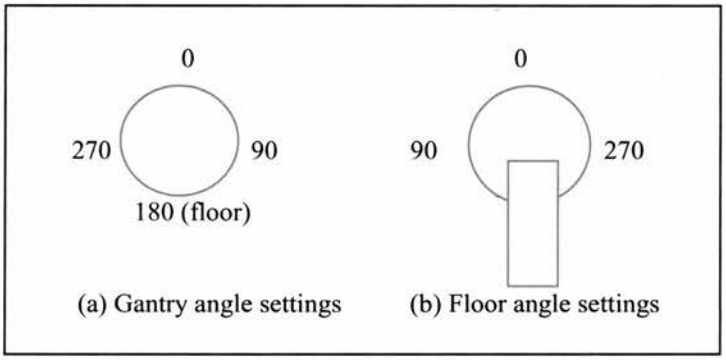

Figure 2.2. The orientation of the (a) gantry co-ordinate system, viewed towards the gantry and (b) the floor co-ordinate system, viewed from above.

Figure 2.2 shows that when the gantry is at 0°, the beam is directed downwards and when the floor is at 0°, the patient's head is towards the gantry.

Beam quality

The nominal energy of the beams used for stereotactic treatments on each of the three linacs is 6MV. The corresponding quality index values (QI), as measured by the TPR (200/100), are shown in Table 2.1.

Linac	QI
CH6	.678
CH20	.692
600CD	.663

Table 2.1. The quality index (TPR 200/100) for each of the three linacs investigated.

The highest energy beam is therefore that on the CH20 and the lowest is on the 600CD.

2.2.2 Stereotactic hardware

Stereotactic hardware

The stereotactic hardware from Radionics RSA Inc. (Boston, USA) is comprised of two stainless steel tertiary collimator housings, one of which is common to both BBC linacs and the other which is unique to the 600CD. The housing is bolted to the face-plate of the linac and used to hold each of twelve lead alloy collimators, which are coated in stainless steel. These have been drilled with divergent holes to produce circular fields of between 40 and 12.5 mm diameter at isocentre. The collimator diameters were chosen by clinicians to be of most use for the lesions of interest within the ECC. Three smaller collimators of 10, 7.5 and 5mm diameter were obtained on loan from Radionics to investigate beam parameters as the field size tends towards zero. Figure 2.3 shows a photograph of the head of the 600CD with the collimator housing attached to the face-plate of the linac. The 20mm collimator has been inserted in the housing.

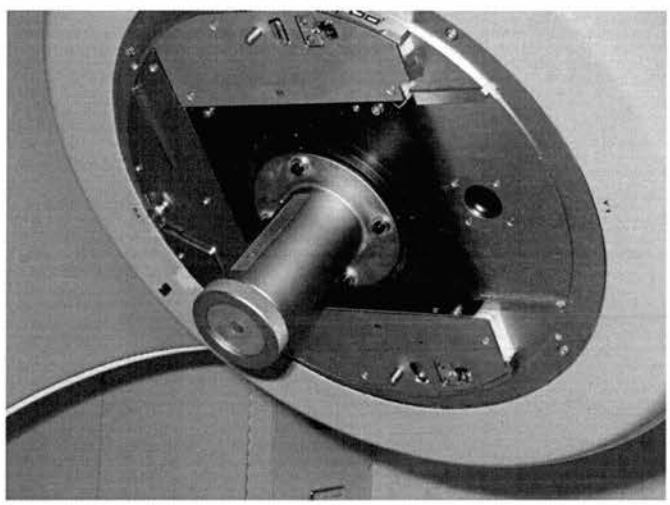

Figure 2.3. Photograph of the stereotactic housing attached to linac head, with the 20mm collimator inserted.

2.2.3 Detectors

The detectors used and their most important properties are summarised in Table 2.2. Abbr. indicates the detector abbreviation used in this thesis. Each detector has been colour coded and the same colour is used in all graphs and diagrams. For all detectors, other than the PP-IC, the colour has been chosen to correspond, as much as possible, to the actual colour of the detector, either the outer casing (diodes and diamonds), or the cable (cylindrical ICs) or the colour of developed film.

Abbr.	Detector Type	Manufacturer	Model	Volume /cc	Active size/mm	Physical size/mm	P (eff) / mm
PFD	shielded diode	Scanditronix-Medical AB	DEB010	29E(-5)	2.5	7	+0.6†
EFD	unshielded diode	Scanditronix-Medical AB	DEB000	29E(-5)	2.5	7	+0.4†
SFD	stereotactic diode	Scanditronix-Medical AB	DEB050	1.7E(-5)	0.6	5	+0.5†
Diam	diamond	PTW-Frieburg	60003	1.8E(-3)	2.2	7.3	+1
0.125cc IC	cylindrical ion chamber	PTW-Frieburg	233642	0.125	d = 5.5 l = 6.5	d = 7 l = 7.25	-1.4 † +4.5‡
0.015cc IC	cylindrical ion chamber	PTW-Frieburg	PinPoint 31006	0.015	d = 2 l = 5	d = 3.7 l = 6.95	-0.5 † +3.4‡
PP-IC	Parallel plate ion chamber	PTW-Frieburg	Markus M233-3	0.05	5	30	+0.03†
Film	radiographic film	Kodak	X-Omat V	N/A	-	-	-

Table 2.2. Summary of detectors used and their most important properties.

The volume is the active volume quoted by the manufacturer. The active size is the width of the sensitive volume in conventional orientation (see section 2.3.1). For the cylindrical ICs, d indicates the active (internal) diameter and l indicates the active (internal) length. The physical size is the width of the outer casing. P(eff) is the effective point of measurement (conventional orientation) and † indicates distance along beam CAX, away from the source. It is positive (downstream) for all solid state detectors and negative (upstream) for all cylindrical ICs. For the PP-IC it is downstream, just inside the front window of the detector. ‡ indicates the distance from the outer tip of each cylindrical IC along its own axis.

Solid state detectors

All solid state detectors are shown in Figure 2.4 and discussed in detail individually.

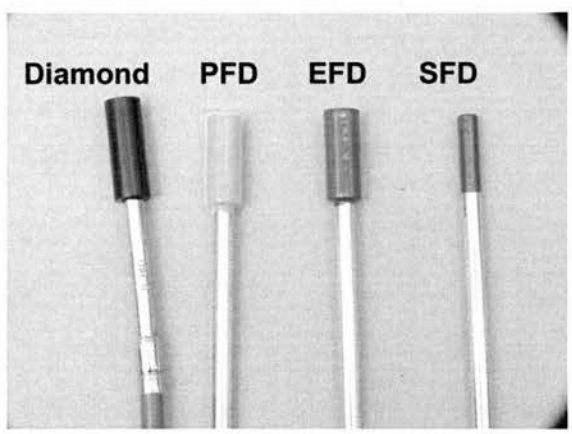

Figure 2.4. Solid state detectors, from left to right; Diamond, PFD, EFD, SFD.

Diamond

The diamond detector incorporates a naturally grown crystal, which is sliced to form a square diamond "plate". The size of the diamond plate is different in each detector, within the range o 3-15mm^2 area and thickness of 0.2-0.4mm. The specification sheet from the manufacturer for the diamond used in this work suggests a square chip of side 2.2mm and a thickness of 0.3mm. Although the PTW instruction manual contains a schematic diagram of the detector, the exact composition of each component is not described, nor the parts labelled. The detector has however been described in a few publications (Heydarian et al, 1993; Vatnitsky and Jarvinen, 1993; Rustgi, 1995; Mobit and Sandison, 1999; Westermark et al, 2000;) and this information is used to label parts in Figure 2.5 (a).

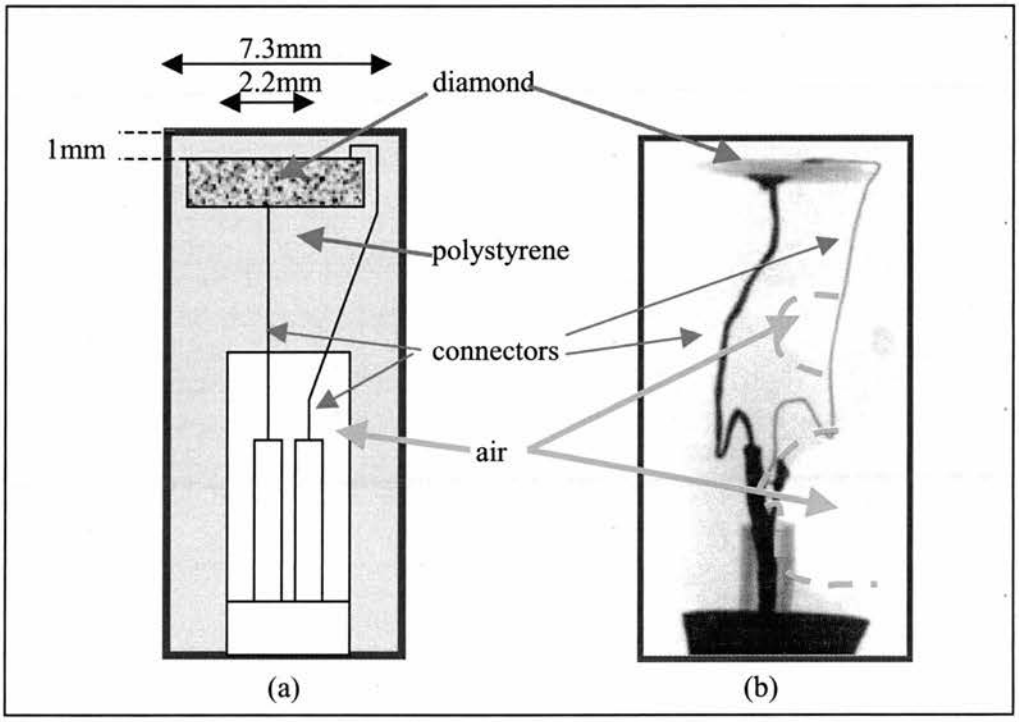

Figure 2.5 (a) Schematic diagram and (b) x-ray of diamond detector

Gold contacts connect the silvered copper wire to the diamond plate, all of which is contained within a polystyrene housing (Heydarian et al, 1993). Although the detector is manufactured such that the centre of the sensitive volume is assumed to be located at the centre of the detector width, the accuracy of this alignment is unspecified. It is interesting that only Mobit and Sandison (1999) describe an air-filled cavity as shown in Figure 2.5(a). An x-ray of the detector used in this work is shown in Figure 2.5 (b). Adjustment of the grey scale to obtain optimal resolution of the diamond plate and connectors, loses the position of the outer canning. However, the position of the canning is indicated by the solid blue lines added to the x-ray. The diamond plate measures approximately 3.8mm-4.7mm

wide, depending on the estimate of the edges. This is much larger than the width defined on the specification sheet (2.2mm) and the reason for this is unclear. The width viewed on the x-ray could be the diagonal width (calculated to be 3.1mm), or simply be a result of the greyscale selected as this changes the visible dimensions. Alternatively, the specification sheet could be inaccurate. The thickness of the plate is however, as expected (0.4mm). In this work, a square width of 2.2mm is assumed. Finally, it is interesting to note that air is visible in pockets only, not as a block in the centre of the detector and may be a phenomena of the manufacturing process.

EFD

The electron field diode (EFD) is an unshielded p-type silicon detector designed primarily for use in electron beams, or in fields with minimal scatter. Scanditronix no longer provide diagrams of any of the dosimetry diodes in their information sheets. However, a diagram of the EFD is contained in an older brochure (undated) and in Heydarian et al (1993). This is reproduced in Figure 2.6 (a).

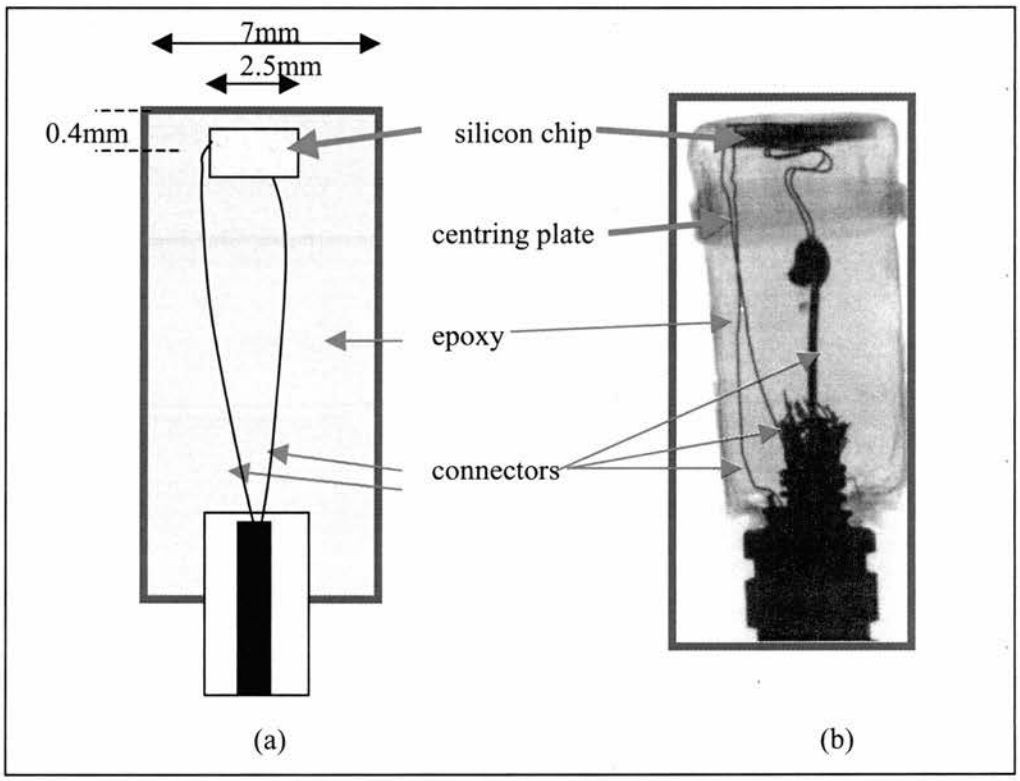

Figure 2.6 (a) Schematic diagram and (b) x-ray of EFD detector

The silicon chip is quoted by the manufacturers as a square of 2.5mm width and 0.5mm thickness. The connectors are aluminium foil. The width of the chip is therefore just over

one third of the overall outer diameter of the detector (Scanditronix brochure, Heydarian et al, 1993). However, an x-ray of the EFD used in this work (Figure 2.6 (b)) shows the silicon to be much wider than this, at approximately 4.8mm, but of the expected thickness (0.5mm). Again, this could be because the diagonal of the chip is presented to the beam, or the greyscale selected is distorting the image. However, an alternative explanation might be that the silicon chip is actually wider than the sensitive area. Although the greatest part of the chip is p-type silicon, the sensitive area is only that region surrounding the p-n junction. It may be that the width of the p-n junction (depletion layer) is narrower than the overall width of the chip, as described by Gager et al (1977) for a non-commercial diode. There is no information in the literature regarding this problem and no answer has been forthcoming from the manufacturers. Consequently, in this work, the silicon is assumed to be a square of 2.5mm width. The lighter coloured disc below the silicon chip is a mechanical structure composed of PVC and used for centring the silicon.

PFD

The photon field diode (PFD) is an energy compensated diode ("photon diode") with tungsten (wolfram) added behind the chip, in the form of tungsten powder mixed with epoxy, to absorb low energy scatter. Scanditronix do not provide any information on the structure of this diode, nor are there any useful diagrams in the literature. However, the basic structure can be assumed to be similar to that of the EFD, as shown in Figure 2.7 (a).

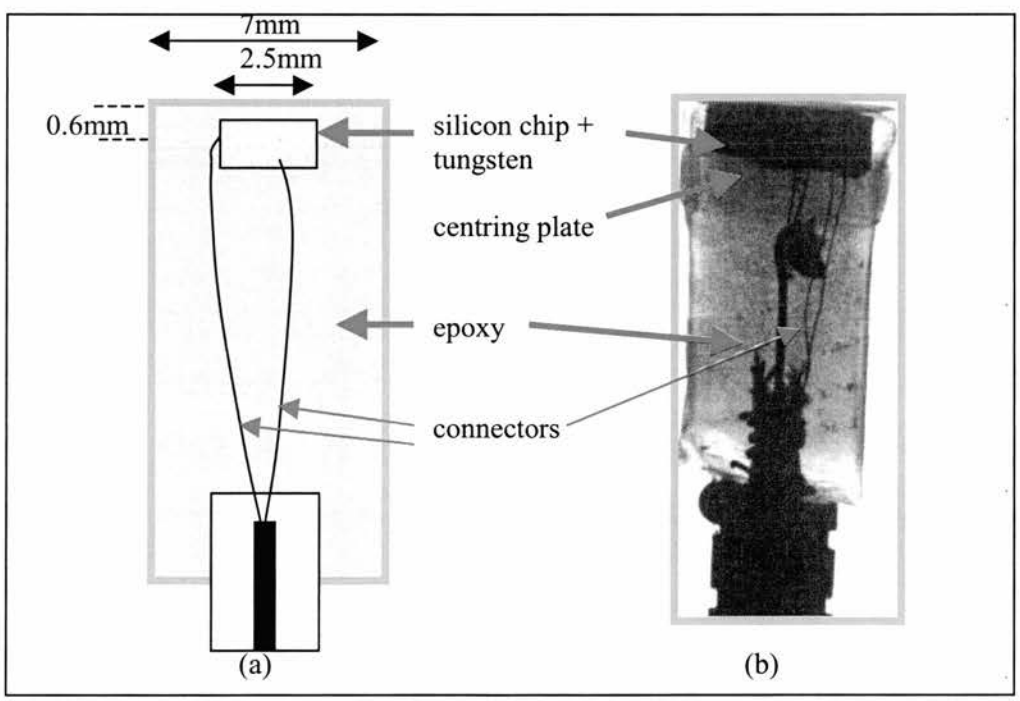

Figure 2.7 (a) Schematic diagram and (b) x-ray of PFD detector

An x-ray of the PFD used in this work is shown in Figure 2.7 (b). It is obvious that the high density region is much larger (approximately 5.3mm wide and 2mm thick) and darker than the corresponding region in the EFD. This is due to a combination of the tungsten energy compensating material and the silicon chip.

SFD

The stereotactic field diode (SFD) is also an unshielded diode, but has a smaller sensitive area than the EFD. It is designed specifically for measurements in stereotactic beams. Again, there are no useful diagrams of the detector in the literature, but if the basic design of the EFD is assumed, the SFD is likely to be constructed as shown in Figure 2.8 (a).

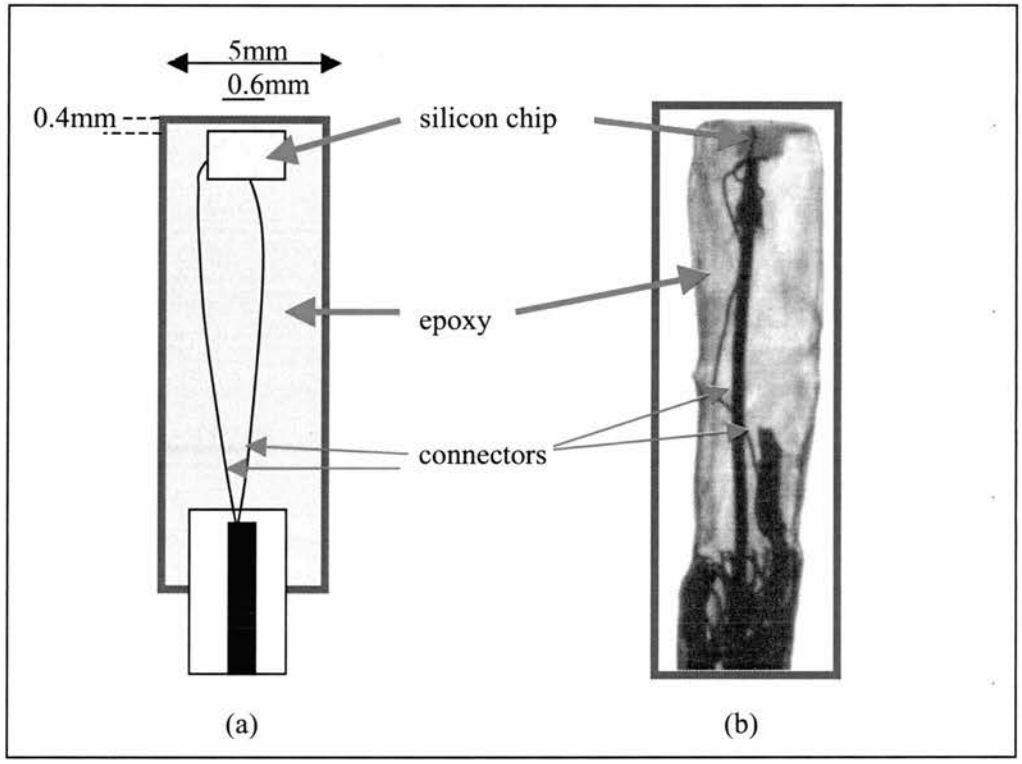

Figure 2.8 (a) Schematic diagram and (b) x-ray of SFD detector

An x-ray of the SFD used in this work is shown in Figure 2.8 (b). It is obvious that the silicon chip is much smaller than that in the EFD, but the size of the connectors are approximately the same. However, the width of the silicon is approximately 0.8mm, which is comparable with the expected width (0.6mm). This is interesting, particularly as it is for the SFD that the comment has been made that the depletion layer is formed as a cylinder within the chip (Westermark et al, 2000).

It is apparent that information in the literature on the construction of each of the above detectors is limited. Indeed the manufacturers, although helpful, have been reluctant to allow the publication of any more information than that already in the public domain. Further information would be necessary to model the detectors and this would presumably be available under a non-disclosure agreement. However, for the purposes of this work, the manufacturers published specifications are taken at face value. The possible discrepancies (sizes of diamond, silicon and depletion areas) will be considered as part of future work.

Ion chambers

The 0.125cc and the 0.015cc ICs are both waterproof, vented, cylindrical ion chambers. The 0.015cc (PinPoint) IC has a small volume and cross-sectional diameter and has been specifically designed for stereotactic beams. The (Markus) PP-IC is a vented IC with an active diameter of 5mm. Additional non-water equivalent materials, mainly PMMA, surround the air cavity and extend the overall physical dimension to 30mm. All of the detectors can be calibrated against the secondary standard according to the IPSM Code of Practice (1990) and are shown in Figure 2.9.

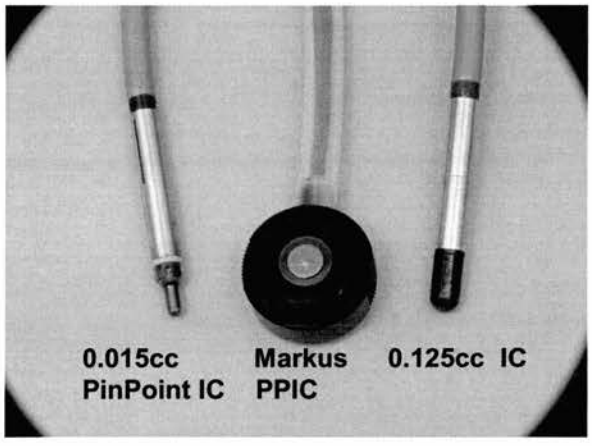

Figure 2.9. ICs, from left to right; 0.015cc PinPoint, Markus PPIC, 0.125cc PTW.

Film

Kodak X-Omat V film is a slow film, on which approximately 30cGy produces an optical density (O.D.) of 1.0. The film was developed in a Kodak processor operated and maintained by the Breast Unit at the ECC. This unit has a high film throughput and a strict QA programme is adhered to.

2.2.4 Phantoms

Water tank

The RFA 300+ water tank and software (version 5.3), with main control unit (MCU) electrometer are manufactured by Scanditronix AB. In all square field measurements, the reference signal is measured with an unshielded diode which is attached to the face-plate of the linac and positioned within the field. For measurements in the stereotactic collimators, the position of the reference detector is linac dependent. As the housing is flush with the face-plate on the BBC linacs, the reference diode must be placed in the beam, below the stereotactic collimators, but ensuring that perturbation of the beam is minimised. A 10mm gap between the housing and the Mylar window on the face-plate of the 600CD allows the reference diode to be placed above the stereotactic collimators, within the field defined by the movable collimators, but outside the circular field.

Solid water

Two types of commercial water equivalent materials are used for absolute and relative dose measurements in this work and both are based on the work of White (1978). Slabs of solid water (RMI 450 and 457) with thicknesses between 1 and 60mm and square cross-sections of 300x300mm^2 were purchased from Gammex-RMI (Middleton, WI). A few of these slabs and smaller blocks were drilled to enable each of the appropriate detectors to be irradiated in their conventional geometric orientation. The mini-phantoms and build-up caps and tops described in Chapter 6 and the head-like phantom described in Chapter 9 were all manufactured from solid water (WT1) purchased from the Tissue Substitutes Materials section of the Clinical Physics group at St Bartholomew's Hospital in London. Photographs are shown in the relevant chapters. All epoxy-resin water-substitute materials were tested for water equivalence for measurements in 6MV beams in the ECC (Allahverdi et al, 1999).

2.2.5 Measurement devices

Electrometers

Several different types of electrometer were used in conjunction with a range of detectors. The diamond was connected to a Unidos (PTW) electrometer and a bias of 100V set. Prior to each measurement session, the diamond was pre-irradiated with approximately 10Gy, according to the manufacturer's instructions. The diodes were connected to a single channel on a DPD6 monitor from Scanditronix and the sensitivity maximised. The PP-IC and 0.125cc ICs were connected to an NE 2620 electrometer (NE Technology, Berkshire), with

a bias of 300V. The 0.015cc (PinPoint) IC was connected to a PTW Unidos electrometer and a bias of 100V set.

Densitometers

The Tobias manual point densitometer (Tobias Associates Inc, PA), with 1mm spot size, was originally the only densitometer available in the ECC. The Vidar VX12 automatic film digitiser (Vidar Systems Corporation, VA) was purchased at a later date and is based on a one-dimensional charge coupled device (CCD). It was calibrated as a scanning densitometer using the RFA scanner software, with maximum resolution setting of 300dpi.

2.3 Methods

2.3.1 Measurements

Overview

The methods used to compare detectors in the measurement of PDDs, TMRs, OARs and relative scatter factors are described fully in each corresponding chapter. The original detector comparisons were initially carried out on the BBC CH6 6MV linac, with a range of detectors available at the time. These results were then applied to measurements on the 6MV beam of the BBC CH20 linac. Both of these linacs have since been decommissioned. Measurements were also carried out on the Varian 600CD linac using a more limited number of the most suitable detectors and the results compared with those from the other two linacs. The examination of small square fields and very small collimators (10-5mm diameter) was only carried out on the 600CD.

Detector orientation

The orientation of each detector discussed in this work will be defined with respect to the long axis of the housing, in all measurements and also in each author's work in the literature review. Examples are shown in Figure 2.10.

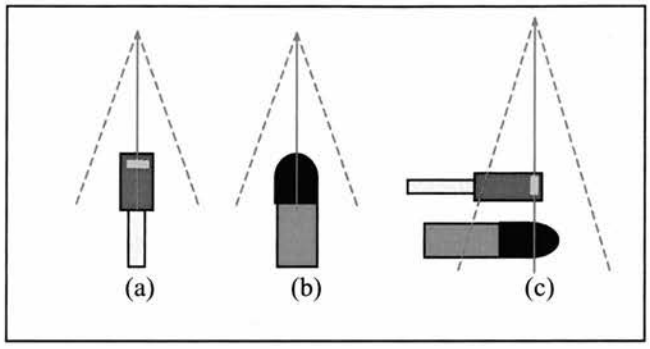

Figure 2.10. Detectors with (a) and (b) long axes parallel to beam CAX and (c) long axes perpendicular to beam CAX.

Diagrams (a) and (b) of Figure 2.6 show a diode (or diamond) and cylindrical IC orientated with long axes parallel to the beam central axis. (a) is the conventional orientation for both diodes and diamonds and (b) maximises the resolution for cylindrical ICs. Note that for diodes and diamonds, the sensitive crystals (drawn in yellow) have long axes which are orientated perpendicularly to the long axes of the detectors. Part (c) shows a diode (or diamond) and IC orientated with long axes perpendicular to the beam CAX. This is the conventional orientation for cylindrical ICs. This orientation maximises the resolution for the solid state detectors.

Tank measurements

The position of zero depth for each detector was always defined without accounting for the effective point of measurement. All solid state detectors were used in conventional orientation and positioned at the water level such that the front surface of each detector touched its own reflection, when viewed from below the water level. The ICs were also used in conventional orientation and were set up with the geometrical centre of their cross-sections positioned at the surface of the water, such that they formed a perfect circle with their reflection, as viewed from below the water level and shown in Figure 2.11.

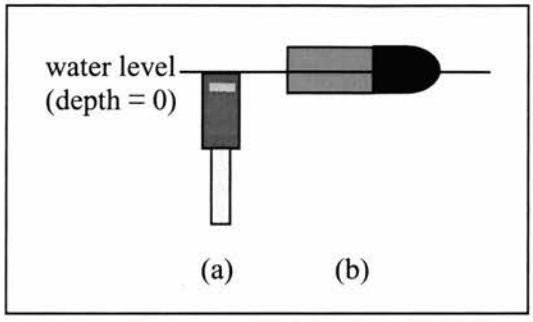

Figure 2.11. Set-up of zero depth in water tank, viewed in line with the water surface.

The true depth was then accounted for by shifting the depth dose curve by the appropriate amount, taken from Table 2.2 and as discussed more fully in Chapter 3.

Detectors were only used in the tank in conventional orientation because of problems securing each to a holder attached to the tank mechanism. Movements of up to 3mm were found to occur in the Inplane/Xplane direction as the depth increased in PDD measurements. This was due to inadequate detector immobilisation and although new holders could have been manufactured, this was only considered necessary if the other methods proved to be unsatisfactory.

The zero position for Inplane/Xplane co-ordinates was set by aligning the geometric centre of the front surface of each solid state detector with the crosswires. The crosswires were also aligned with the effective point of measurement of each IC, along its length, as described by the manufacturers and shown in Figure 2.12.

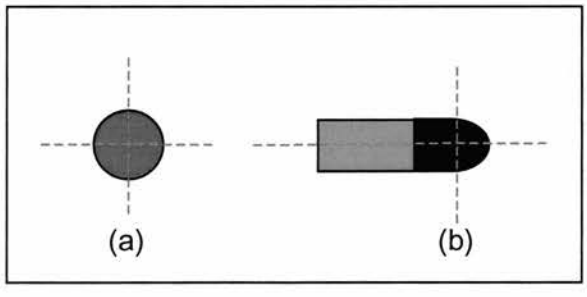

Figure 2.12. Set-up of Inplane/Crossplane zero co-ordinates, viewed looking down into the tank.

Solid water

Slabs of RMI were drilled such that the effective point of measurement of each solid state detector could be placed at a known depth. The ion chambers were positioned with the centre of their geometric cross-section also placed at a known depth. The true depth could then be calculated.

Reference field

All linacs in the ECC are calibrated to deliver a dose of 1Gy at the reference point, for 100 MU. The reference point is dmax in a 100x100mm^2 field, at 1000mm FSD. All PDDs and TMRs were normalised to dmax in the reference field.

Field terminology

Beam areas defined by the stereotactic collimators are referred to in this work as "stereotactic fields". In all measurements in stereotactic fields, the movable collimators of the linac were set to a constant 50x50mm^2. In all relative output measurements, the results were normalised initially to the largest (40mm) collimator. Beam areas defined solely by the movable collimators of the linac are referred to as "open fields". In all relative output measurements, the results were normalised initially to an open 50x50mm^2 field. Beam areas defined by the MLC are referred to as "MLC fields". In all relative output measurements, the results were normalised initially to an open 50x50mm^2 field.

2.3.2 XKnife calculation

XKnife stereotactic planning system

The XKnife stereotactic treatment planning system from Radionics is based solely on measured data and requires the input of the absolute dose at a reference point, relative outputs (S_{cp}), TMRs and OARs. It uses a simple, isocentric calculation and no account is taken of inhomogeneities i.e. the dose is calculated in water.

OARs are measured by placing the detector at 1000mm focus to axis (isocentre) distance (FAD) at a depth of 50mm only, for each collimator. S_{cp} values are measured at dmax, 1000mm FAD and normalised to a 100x100mm^2 field at the same FAD. A factor M is used to relate these relative outputs to the reference field (1000mm FSD).

The dose (D), per MU, to a point with (x,y,z) co-ordinates, at a depth d in a field size s (beam radius r_{iso}) at the isocentre, is given by:

$$D(d,s,x,y,z) = M \times S_{cp}(s) \times TMR(d,s) \times OAR(r_{iso}(x,y,z)) \times \frac{FAD^2}{(FAD-z)^2} \qquad (2.1)$$

Using the inverse square law (ISL), M = 1.030 cGy/MU for an FAD/FSD of 1000mm and a dmax depth of 15mm.

The geometry and BRW(x,y,z) co-ordinate system are shown in Figure 2.13, where x and y lie in the plane perpendicular to the beam CAX, with (0,0) at the CAX. z increases along the CAX in the positive direction, towards the source.

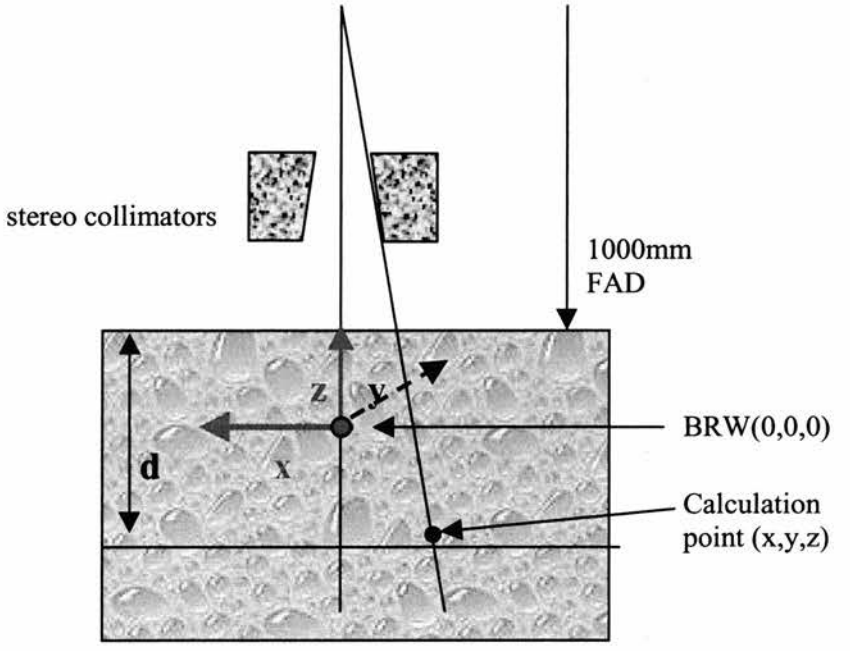

Figure 2.13. The geometry of the XKnife dose calculation at a point.

Chapter 3

Percentage depth doses

3.1 Introduction

3.1.1 Definitions

Inverse Square Law

The fall off in beam intensity with distance from a point source in air or a vacuum, is characterised by the inverse square law (ISL), such that the dose-rate D_2 at distance f_2 is related to the dose-rate D_1 at distance f_1 by:

$$D_2 = (f_1/f_2)^2 \; D_1 \qquad (3.1)$$

Percentage depth dose

The fall off in intensity with depth along the beam central axis (CAX) in a phantom, is characterised by the percentage depth dose (PDD). This is the ratio of the dose rate (D) at depth d to the dose rate at a reference depth d_0, for the same beam focus to surface distance (FSD) and field size setting (s) and is expressed as a percentage:

$$PDD(d, s, FSD) = D(d)/D(d_0) \times 100\ \% \qquad (3.2)$$

The PDD varies with beam energy (attenuation), FSD (ISL) and scatter.

Attenuation of the primary

PDDs for a zero-area beam, with the effect of ISL removed, represent the attenuation of the primary beam in water. The attenuation of the primary is of the form:

$$e^{-\mu d} \qquad (3.3)$$

where μ is the linear attenuation coefficient in units of mm^{-1} and d is the depth in water, in mm. The linear attenuation coefficient can be measured using narrow beam geometry, or

calculated from a log-linear plot of zero-area PDDs, with the ISL removed, against depth, where μ is the gradient of the straight line.

Equivalent square

For routine, megavoltage photon beam commissioning, PDDs are generally only measured for square fields. PDDs for regular rectangular and circular fields can be calculated from square fields with equivalent scatter. Tables of equivalent squares (EQSQs) for rectangular and circular fields are listed in BJR Supplement 25 (Day and Aird, 1996). These figures are based on measured data i.e. the equivalent square fields have the same measured PDDs and relative outputs. As an approximation, EQSQs of regular rectangular fields can be calculated from the ratio of the area to the perimeter:

$$EQSQ = 2ab/(a+b) \qquad (3.3)$$

The lengths of the sides of the rectangle are represented by a and b. Calculated EQSQs match the tabulated values for all fields other than for elongated beams with one side less than approximately 40mm, where differences of up to 9% exist. For these types of beams, an elongation factor can be applied, also described in Supplement 25. The rule of thumb for the EQSQ of a circular field is 0.9 x d, where d is the beam diameter.

3.1.2 Properties of PDDs

Depth of dmax

The depth of the maximum dose (dmax) along the CAX is mainly determined by the number and energy of contaminant and scattered electrons present within the beam. As these vary with field size, energy and FSD, dmax will also vary with these parameters. The depth of dmax decreases with increasing field size due to the increase in contaminant and scattered electrons which pull the maximum dose towards the surface. Sixel and Podgorsak (1994) found in routine field sizes, in any beam energy, the maximum depth of dmax occurs in a 50x50mm^2 field and decreases as the field size increases. The shift in dmax at smaller field sizes will be discussed in section 3.1.5. The depth of dmax increases with FSD as fewer contaminant electrons reach the surface of the phantom, due to absorption in the air. The depth of dmax also increases with energy due to an increase in the mean projected range of secondary electrons. On all three 6MV beams used in this work, dmax in a 100x100mm^2 field, at 1000mm FSD, is 15 +/-0.5mm.

Reference depth

The reference depth (d_0) in equation 3.2 is historically most often chosen to be dmax. The PDDs for all field sizes can be normalised to the dose at dmax in a 100x100mm^2 field, or to the dose at the individual dmax positions in each field size. Alternatively, PDDs can be normalised to a depth beyond the range of contaminant electrons. The selection of normalisation depth is dependent on the requirements of the treatment planning system (TPS) and on the formalism adopted within individual departments. It is important to ensure that there is consistency between all beam data sets (PDDs, OARs, Sc_p etc.), whichever normalisation method is used. It should be noted that the normalisation method used may affect the perceived relative response of two detectors. For example, a PDD curve measured with detector 'a' may be higher than that measured with detector 'b', when both curves are normalised to dmax. This could show that detector 'a' over-responds at depth. However, if the PDDs were renormalised to a depth of 100mm, detector 'b' would appear to over-respond at dmax, or detector 'a' appear to under-respond. Comparisons in terms of absolute detector response cannot therefore be extracted from PDD measurements alone and care should be taken when assessing such conclusions in the literature.

PDD variation

The PDD at a depth, increases with field size, energy and FSD. The increase in PDD with field size is primarily due to increases in phantom scatter. The increase in PDD at a depth with FSD is due primarily to the effect of the ISL, as shown in equation (1) of Appendix B, BJR Supplement 25 (Burns, 1996) which describes the conversion of PDDs from one FSD to another. However, it is also due to the decrease in the relative dose at dmax caused by the reduction in contaminant electrons. The increase in PDD with energy is simply due to the increased penetration of the beam.

In some instances, the PDD at a depth can actually decrease with field size, as reported in BJR Supplement 17 (Greene and Williams, 1983). The decrease with field size could be due to an increase in the absolute dose at dmax caused by the increase in contaminant electrons with field size. As contaminant electrons only contribute to the absolute dose at dmax, the relative dose at depth decreases. On some designs of linac, this effect could counterbalance the increase in PDD with field size. BJR Supplement 25 (Jordan, 1996) contains tables of PDDs for a range of beam qualities, produced from measured data averaged over a large number of beams from different machine designs and departments. These tables show an overall increase in PDD with field size, which is typical of most energies and designs.

3.1.3 Measurement of PDDs

Phantoms

PDDs are most efficiently measured in a water scanning tank equipped with computer control of the detector position. This is commonly known as a Beam Data Acquisition System (BDAS). Queues of beam measurements can be set up using the BDAS to acquire data for a whole range of field sizes automatically. An individual depth dose can be measured within 2 or 3 minutes of beam-on time, dependent on the parameters set within the software. The variation in beam output within this time must be monitored and accounted for. The most accurate way to do this is to take the signal from the linac MU chamber directly to the tank software. Alternatively, a reference detector can be placed in air, between the surface of the water and the collimating system, ensuring that it is within the field but does not obscure or affect (perturb) the measurement. The use of the signal from the MU chamber monitors variations across the whole beam (depending on the design of the MU chamber), whereas the use of a reference chamber monitors changes at one point only. Although it is difficult to assess what effect these differences might have on the measurement of PDDs, they are assumed to be small.

PDDs should be measured in both the downward and upward directions, to account for any uncertainties caused by the motion of the depth controller. PDDs in the build-up region may be subject to uncertainties caused by the ripple of the meniscus. When PDDs are measured from the surface downwards, the meniscus may be pulled down with the detector for a few millimetres, resulting in semi "in-air" measurements at small depths >0. In the opposite direction, the meniscus is pushed up, such that "in-water" measurements are made at small depths <0. The magnitude of these uncertainties is dependent on the speed of movement and the size and shape of the detector and for greatest accuracy, a slow acquisition speed and a small step size should be used.

PDDs can also be measured in a solid water phantom, if the water-equivalence has been verified at the energy used. This process is more time consuming and the resolution is dependent on the thickness of slabs available. To ensure that the FSD remains the same, the slabs must be "shuffled" to obtain the correct depth for each measurement point. This technique, in conjunction with a parallel-plate IC (PP-IC) and thin slab thicknesses, is useful to determine accurate data in the build-up region.

Detectors used

An ion chamber is the most accurate detector to use for depth dose measurements, although the resultant curve will be a depth ionisation curve. This can be converted to a depth dose curve via the use of replacement factors which account for the air cavity, chamber wall thickness and effective point of measurement. In photon beam calculations, the replacement factor is small as the mean energy of electrons stopped within the cavity is fairly constant with depth. Experimentally based corrections for the effective point of measurement can also be used to account for the above. In megavoltage photon beams, the depth ionisation curves are generally shifted upstream by 0.5r, where r is the internal radius of the IC. The use of depth shifted ionisation curves assumes that quality dependent correction factors to convert ionisation to dose are constant with depth. The use of the ratio of two detector readings to obtain depth dose curves in all field sizes, also assumes that the correction factors to convert ionisation to dose are constant with field size.

For parallel plate chambers the effective point of measurement is generally taken to be inside the front surface of the detector and additional corrections are only necessary in the build-up region (Gerbi and Khan, 1990).

Diamonds and diodes can also be used to measure depth dose curves. Although a correction for the effective point of measurement is required, this needs only to account for the position of the centre of the measurement volume within the detector. Depth dose curves measured without corrections should be shifted downstream by this distance (approximately 0.5-1.0mm). Alternatively, the correction can be input to the BDAS software.

As discussed in Chapter 1, diamonds and diodes have been shown to exhibit dose rate dependencies, such that their responses are decreased and increased respectively, with increasing dose rate. This has led to PDDs which are approximately 2% too high and 1% too low for the diamond and diode respectively at 300mm deep when compared with an IC, in a 200x200mm^2 beam, normalised to dmax (Hoban et al 1994). However, Westermark et al (2000) found that a small diode and a diamond both underestimated the relative dose at dmax by 0.5-0.8% compared with an IC in a 100x100mm^2 field when the results were normalised to 100mm deep. It is interesting to note however, that if the data were re-normalised to dmax, the PDDs would be too high for both detectors.

The energy dependence of diodes, such that they over-respond to scatter, is also a problem in the measurement of PDDs, resulting in curves which are too high, when compared with those measured with an IC. Shielded diodes, which incorporate some high Z material

behind the silicon chip, are designed to absorb some of this scatter and ensure that PDDs measured with a diode match those of an IC, particularly in a 100x100mm^2 field.

Film, orientated parallel to the beam CAX, is a fast method for obtaining both PDD and isodose information in a single beam exposure. However, Williamson et al (1981) found that this orientation resulted in PDDs (normalised to dmax) which were higher than IC measurements by 30% in a cobalt-60 beam and 5% at 25MV, due to the over-response of film to photons <200keV. The problem was reduced to random differences of up to only 2.5% at 10MV, by using different calibration curves at different depths.

3.1.4 Small field problems

Standard PDD tables, such as those in Supplement 25, do not exist for field sizes <40x40mm^2 field and until fairly recently, there was no demand for such data. As discussed in the introduction, measurements in small fields are more complex than those in routine fields and require a more careful consideration of the methodology. This is due to the lack of lateral electronic equilibrium, changes in scatter effects and the sizes and responses of available detectors. As no single detector appears to be appropriate, a careful comparison of a range of small detectors must be carried out for all measurements.

If small field measurements are carried out using a BDAS, care must be taken to ensure that if a reference detector is used, it does not perturb the beam. Perturbation of the beam would primarily affect the measurements near dmax and result in PDDs (normalised to dmax) which were incorrect. The centre of the detector sensitive volume and the depth control direction on the tank must also be accurately aligned with the beam CAX, to ensure that the detector does not move out of the high dose region in the off axis direction as the depth is increased. This would cause the PDDs to be underestimated (when normalised to dmax). Ideally, the detector should be positioned at the centre of the 50% isodose regions, measured via profiles at more than one depth.

Volume averaging over the detector sensitive volume is also a problem. Not only will the measured dose be underestimated, but the amount of under-response will change with depth. The effect will be maximised at dmax and decrease as the beam diverges with depth, such that the PDDs will be over-estimated at depths >dmax. For ICs, the effect can be minimised by using the chamber "end-on" with long axis parallel to the beam CAX. The position of the effective point of measurement must be determined in this orientation by matching depth dose curves between the two orientations, in a larger field size. Stabilising the IC in this

orientation can sometimes be a problem and any movement or twist in the chamber as the depth is increased will lead to errors in the measurements.

As discussed previously, the conversion of the ratio of two detector readings to a ratio of dose assumes that the correction factors are independent of field size. This may not be the case in very small fields, where there is a lack of lateral electronic equilibrium (LEE) and the beam spectrum is very different. However, Verhaegen et al (1998) showed that the stopping power ratios for air, graphite and TLD, varied by only =<0.2% in 50 and 15mm diameter collimators, for depths between dmax and 50mm. Andreo and Brahme (1986) showed that the maximum difference in stopping power ratios for air to water was 1% in a 5mm diameter collimator. Sanchez-Doblado et al (2003) found that the same stopping power ratios in 10 and 3mm diameter collimators differed from those in the $100x100mm^2$ reference field by only 0.1% and advised that the same correction factors could be used for ion chamber measurements in large and small fields.

3.1.5 Small field PDDs in the literature

Variation of dmax with field size

As discussed in section 3.1.2, the depth of dmax decreases with increasing field size in fields $>50x50mm^2$, due mainly to the effects of contaminant electrons. In contrast with this, Arcovito et al (1985) found that the depth of dmax decreases with decreasing field size, in fields smaller than $50x50mm^2$. Although only fields down to $30x30mm^2$ field were possible with the linac used, smaller fields (down to $10x10mm^2$) were generated by placing additional lead collimators, inside the linac collimators. To investigate the reason for the effect, the authors tried to eliminate electrons from the beam by placing an aluminium plate in the head, behind the movable collimators. The same decrease in dmax with decreasing field size was found, which suggested that contaminant electrons, were not responsible for the shift in dmax. However, it should be noted that the aluminium plate is itself a source of electron contamination, although this is assumed to be constant. In reality it is very difficult to eliminate contaminant electrons from a clinical photon beam. The authors suggested that the shift in dmax is due to a reduction in the mean energy of the beam caused by additional head scattered photons at dmax.

The stereotactic field situation could be different from the small open field situation as the linac collimators are generally set to a constant field size setting, in all stereotactic beams. However, Kubsad et al (1990) investigated the shift in dmax for measurements in stereotactic collimators and also reported a decrease in the depth of dmax as the collimator

diameter decreased. The authors did not explain whether or not the linac collimators were set to a constant field size. They suggested that the shift in dmax was caused by a decrease in the contribution of lateral scatter to the depth dose, but did not expand on this hypothesis.

Serago et al (1992) found the same shift in dmax for TMR measurements in stereotactic collimators, with the linac collimators set to a constant 50x50mm^2. The authors suggested that this was because electrons which are scattered out of the beam and are not counter-balanced by a corresponding fraction scattered into the beam.

Sixel and Podgorsak (1994) explain the effect most thoroughly. They investigated the shift in dmax in stereotactic fields, with the linac collimators set to a constant 40x40mm^2 field size. Using Monte Carlo (MC) they showed that in very small fields, the depth dose is almost entirely due to the dose deposited by the primary. As the field size increases, Compton scattered electrons (i.e. not contaminant electrons) arise at the edges of the beam and deposit some dose on the CAX, thus increasing the depth of dmax. Although this effect will increase with field size, it will saturate at a field size in which the electrons at the beam edges are no longer able to reach the CAX. Beyond this field size, contaminant electrons and collimator scattered photons begin to deposit dose in the build up region and pull the depth of dmax back towards the surface.

Verhaegen et al (1998) calculated the depth of dmax on a 6MV Varian Clinac-600SR in stereotactic collimators between 5 and 50mm diameter, with BEAM (EGS4). The depth of dmax increased from 9mm in the 5mm collimator, to a maximum of 16.5mm in a 30mm collimator and then decreased again to 14.5mm in the 50mm diameter collimator.

Measurement of PDDs

At the time of the original commissioning of the stereotactic system on the CH6 (1994), only two publications existed on the measurement of PDDs in small fields. Unless stated otherwise, all of the following PDD results have been normalised to dmax.

Arcovito et al (1985) measured PDDs in open fields down to 30x30mm^2 (linac minimum field size), using a 0.22cc IC. Smaller fields were generated by placing custom-made lead collimators inside (i.e. towards the CAX) the movable collimators of the linac. TLDs (3x3x1mm^3) were verified against the IC in a 40x40mm^2 and found to agree to within +/- 3%. TLDs were then used to measure PDDs in smaller fields, but could not be compared against any other detector.

Kubsad et al (1990) stated that the purpose of their work was to verify the accuracy of film and diode PDD measurements in small (40-5mm diameter) fields, using Monte Carlo (EGS4) and convolution (Mackie et al, 1985). A small RK ion chamber was also used, although the dimensions of neither it, nor the diode, were specified. PDDs generated via MC and the convolution algorithm agreed beyond dmax but differed in the build-up region. According to the authors, this was because the low energy scatter from the stereotactic collimating system was not accounted for in the convolution algorithm. The IC and small diode both agreed with MC and convolution in fields >=30mm diameter. In the 20mm collimator the IC was too large and consequently produced results which were 2% (PDD) higher than the diode at a depth of 120mm. The convolution results were higher than MC by less than 1% (PDD) at the same depth and the diode results lay in between. The authors concluded that MC and convolution were good methods for calculating the dose in small fields, but the validity of the detector measurements was not discussed.

Neither of the above papers made any firm conclusions regarding the most appropriate detector to use for PDDs. Although the small diode appeared to be useful, its dimensions were unspecified. Neither was it compared with a more routine size of detector. As a result, in the absence of access to MC or convolution, several small detectors available within the ECC in 1994 were compared as part of the original commissioning process, in order to determine the most appropriate detector for the measurement of PDDs in small fields.

Prior to the publication of the small fields work from this project at the ECC (McKerracher and Thwaites, 1999), several additional papers were published on the subject of the measurement of PDDs in small fields. Heydarian et al (1996) measured PDDs in stereotactic collimator fields between 41 and 8.9mm diameter, with an RK83-05 IC, a PTW-Riga diamond and a Scanditronix (2.5mm width) photon diode and compared the results against Monte Carlo (EGS4). The photon diode and diamond produced PDDs which were too low and too high respectively, by approximately 0.7% (PDD) compared with the IC, at a depth of 200mm, in a 30x30mm^2 field. This was thought to be due to the dose-rate under and over response of the diode and diamond respectively. The IC measured PDDs which were too high by approximately 5% (PDD) with respect to MC in a 5x5mm^2 field, due to the partial volume effect. The diode measured PDDs which were too low by more than 2% (PDD) and the diamond appeared to match MC. However, the authors did not discuss the responses of the diode and diamond at this field size. It should also be noted that although it appears that stereotactic collimators were used, the terminology throughout the paper is not consistent and it is unclear whether the beam areas quoted are at the isocentre.

Dasu et al (1998) measured PDDs at 900mm FSD and normalised the results to a depth of 100mm. Measurements were carried out with a photon and an electron diode (2.5mm sensitive width) and a prototype parallel-plate liquid ionisation chamber (LIC, 3mm diameter). Only the results for an 8mm diameter collimator were presented, in which all detectors agreed, other than in the region around dmax. The authors noted that the relative responses of the diodes were approximately 3% higher than those of the LIC, due to the dose-rate response of diodes. The response of the EFD was the highest, which was thought to be due to an over-response to electron contamination. However, it is not clear why this should have affected the electron more than the photon diode, unless the authors meant that the tungsten shielding absorbed some of the contaminant electrons, which led to a reduction in dose at dmax. It is interesting to note that if all of the above results were renormalised to dmax, the diode curves would be lower than those of the LIC. This is the opposite effect to that normally obtained with diodes compared to an air-filled IC. However, the authors did not note this, nor consider the possibility that the LIC may have been too large in the 8mm collimator. This would have resulted in an under-response in the LIC at dmax, compared with depth and although the authors recommended the LIC because of its dose-rate independence, the results did not conclusively shown it to be the most appropriate detector.

Francescon et al (1998) compared MC (BEAM) with measurements made with Gafchromic film and a prototype parallel plate micro-chamber (PPMC) in beam diameters between 19 and 4.4mm. Although all three agreed to within 1.5% (PDD) at a depth of 150mm, the Gafchromic film was noisy and repeat measurements were required to average the data.

Verhaegen et al (1998) used BEAM (EGS4) to calculate PDDs in stereotactic fields on a 6MV Varian Clinac-600SR. Calculated PDDs were compared with measurements carried out with a diamond of 3mm sensitive width, in collimators of 40 and 15mm width and agreement beyond dmax was found to be "excellent". Electron contamination was thought to have caused differences in the build-up region.

As a result, by the time of the publication of the ECC results (1999), there was still no firm recommendation for an optimum, commercial, detector for use in the measurement of PDDs. Although a "small diode" had been tested (Kubsad et al, 1990), its dimensions were unspecified. In addition, it was not compared with a more routinely available diode and therefore the necessity of a stereotactic-specific detector was not addressed. McKerracher and Thwaites (1999) published results from this work for PDDs measured in collimators between 40 and 12.5mm diameter, with a shielded, unshielded and stereotactic diode,

0.125cc and 0.015cc ICs and film placed parallel to the beam CAX. These measurements will be discussed in full, in the results section.

More recently, Westermark et al (2000) reported on PDD comparisons in a 100x100mm^2 field and an 8mm diameter collimator using a small diode, double chip diode, scintillator, diamond and LIC. Although both diodes had sensitive diameters of 0.6mm, the sensitive diameter of the diamond appeared to be 3.8mm (volume 4.2mm^3, 0.29mm thick), which is relatively large for a diamond. The sensitive diameters of the non-commercial scintillator and LIC were 1.0 and 1.5mm respectively. A 4mm diameter RK chamber was used in the 100x100mm^2 field only and all results were normalised to 100mm depth. In the 100x100mm^2 field, the authors noted that all detectors under-estimated the dose at dmax compared to the IC, by between 1 and 1.5% (PDD). The IC was not used in the 8mm diameter collimator, but the same relative responses were noted for all other detectors.

Westermark et al (2000) and Dasu et al (1998) all found that PDDs measured with diodes were higher at dmax (results normalised to 100mm) than those measured with an LIC. Westermark et al explained that this was due to an under-response of the LIC, whereas Dasu et al explained that it was due to an over-response in diodes. This highlights the importance of distinguishing between measurements of absolute and relative detector response and is an example of how similar results can be used to "prove" different effects.

Although Yin et al (2002) presented some PDD results for stereotactic collimators, it is unclear which detectors were used. In contrast, measurements were also carried out in a 6x6mm^2 mMLC field with an IC (sensitive diameter 2mm, length 4mm) and a small diode (0.6mm sensitive width). The IC (conventional orientation) PDDs were higher than the diode by approximately 3% PDD, between 50 and 250mm deep. This was thought to be due to the partial volume effect, which led to PDDs which were too high. When the IC was used with its long axis parallel to the beam CAX, the results agreed with the diode, which is perhaps surprising in such a small field, for two very different detectors.

Paskalev et al (2002) used a micro PP-IC (mPP-IC) with inner cavity of 2mm diameter and HS Gafchromic film to measure PDDs in beams of 5 and 1.5mm diameter on the 10MV beam of a Varian Clinac-18. The mPP-IC measurements were corrected to account for the size, construction and material of the detector. All measurements agreed well with EGS/BEAM calculations in the 5mm diameter collimator, but the measured data appeared to be approximately 8% (local dose) higher than the MC calculations at 120mm deep in the

1.5mm diameter collimator. However, it was difficult to extract numbers from the graph and the authors do not comment on the agreement and disagreement.

Sanchez-Doblado et al (2003) calculated PDDs in small stereotactic collimators (10.5 and 3mm diameter) on the 6MV beam of an Elekta SL-18 using EGS4 (BEAM). Unshielded diode measurements (2.5mm sensitive width) were in "good agreement" with MC.

Comparison of results

As discussed in the introduction, BJR Supplement 25 (Jordan, 1996) contains tables of PDDs for a range of energies (2-50MV), averaged over several linac designs and qualities. These tables are useful, both as a baseline against which to compare a department's own measured data and as examples of measurements in beam energies which may not be available within a department. The minimum field size tabulated is 40x40mm^2 and until recently there has been no requirement for smaller field sizes.

In a 400x400mm^2 field, the spread in PDD over energies between 4 and 12MV, at a depth of 100mm, is approximately 8%(PDD). This increases to approximately 12% in a 100x100mm^2 field and 15%(PDD) in a 40x40mm^2 field. In a small field the scatter is mainly determined by the energy, but in a large field it is mainly determined by the field size. It is expected therefore, that in field sizes <40x40mm^2, the spread over the same range of energies is likely to be >=15%. Figure 3.1 shows a plot of the PDDs in a 40x40mm^2 field for energies between 6 and 10MV, taken from Supplement 25.

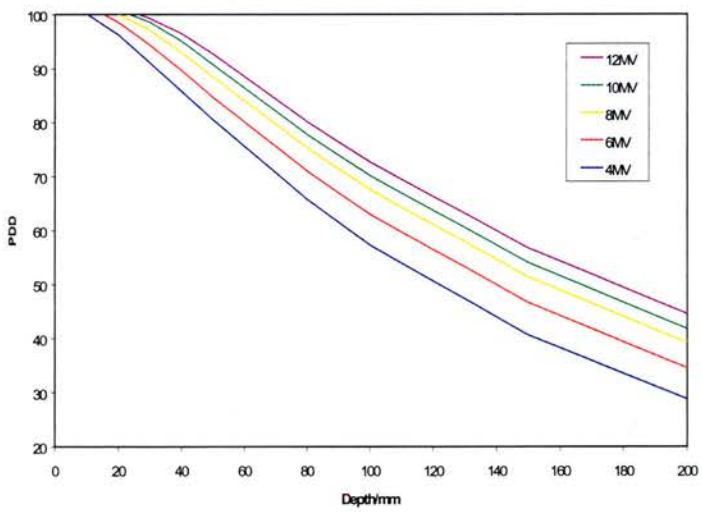

Figure 3.1 BJR Supplement 25 PDDs in a 40x40mm^2 field, for energies between 4 and 12MV.

To compare the small field results in the publications previously discussed, PDDs (normalised to dmax only) for either the recommended detector, or the smallest detector have been extracted , as summarised in Table 3.1.

Author	Year	Energy (MV)	Linac	Field type	Measurement system
Arcovito et al	1985	9	Neptune CGR	□	TLD 0.3mm wide
Dasu et al	2002	6	Clinac 2300 CD	○	LIC
Francescon et al	1998	6	Siemens Mevatron	○	MC BEAM
Heydarian et al	1996	6	Siemens Mevatron KD-2	○	EGS4
Houdek et al	1983	10	LMR-13 Toshiba	□	TLD ribbons
Kubsad et al	1990	6	?	○	EGS4
McKerracher & Thwaites	1999	6	BBC CH6	○	EFD
Paskalev et al	2001	10	Clinac 1800	○	MC
Sanchez-Doblado et al	2003	6	Elekta SL-18	○	MC
Verhaegen et al	1998	6	Clinac 600SR	○	MC
Westermark et al	2000	6	Varian Clinac 2100C	○	small diode
Yin et al	2002	6	Varian Clinac	○	?

Table 3.1 A summary of PDD data extracted from the literature review, for circular (○) and square (□) fields.

The above table contains a broad spectrum of energies and measurement methods. The linac manufacturer is not stated in Kubsad et al and Yin et al do not explain which detector was used. As most authors only report the results in the smallest fields, only the PDDs for fields of approximately 10mm width have been plotted in Figure 3.2.

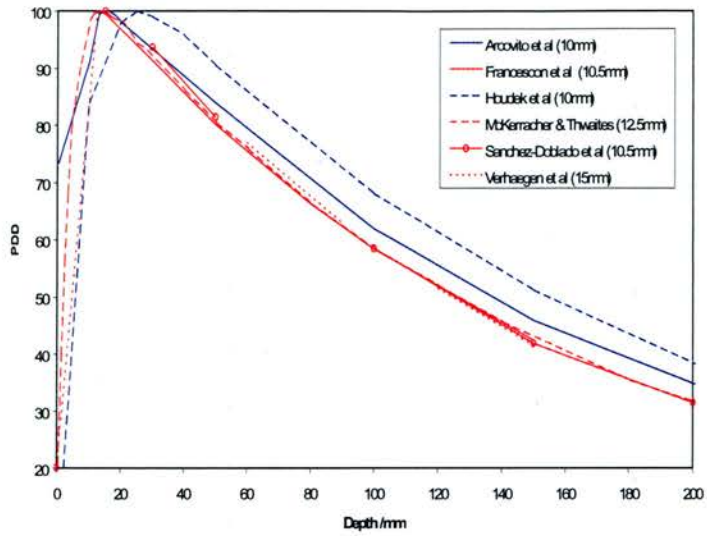

Figure 3.2. Plot of data from Table 3.1, for fields close to 10mm width.

Supplement 25 suggests a 7% spread in PDD at 100mm deep in a 40x40mm^2 field and the spread in Figure 3.2 is approximately 10% PDD at 100mm deep, which is comparable for energies between 6 and 10MV. However, the difference between the results of Arcovito et al (9MV) and Houdek et al (10MV) is >5%. Although Arcovito et al measured dmax in a 100x100mm^2 field to be 20mm, they reported a shift to 16mm in a 10x10mm^2 field. Houdek found dmax to be 25mm in all field sizes measured. This difference in the depth of dmax may explain the differences in PDD. The results for the 6MV beams are almost identical and independent of the methodology. Although the linacs are of different designs and qualities, the agreement gives some credence to the measured data. Figure 3.3 shows a comparison of very small beams, all at 6MV.

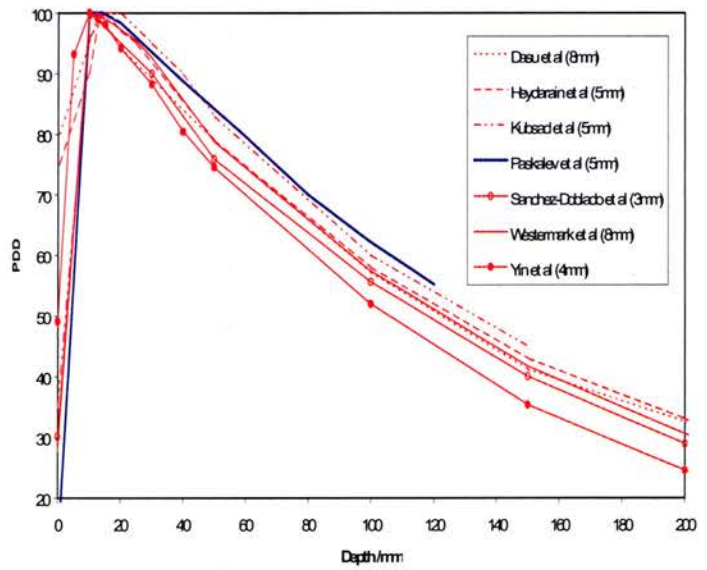

Figure 3.3. Plot of data from Table 3.1, for fields of width <10mm.

Although all beam energies (other than in Paskalev et al) are nominally 6MV, the spread over all beams at100mm deep is approximately 10% and the results reported in Yin et al are much lower than expected.

Zero area PDDs

A zero area PDD shows the decrease in primary with depth and can be obtained either through extrapolation or from a measured linear attenuation coefficient (Arcovito et al, 1985; Houdek et al, 1983). A zero area PDD can be used to interpolate PDDs for field sizes smaller than those available. Figure 3.4 shows zero area PDDs in the literature.

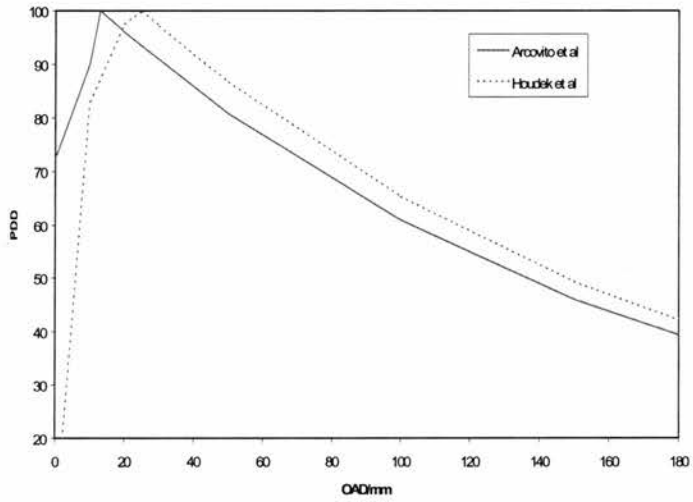

Figure 3.4 Zero area PDDs from the literature.

Again the differences reflect the differences in dmax position, as shown in Figure 3.2.

Summary

The diversity in all of the above results shows the extent of the problem in small field measurements. The magnitude of the spread in PDD over all publications is not only a reflection of the beam energies, but is a result of the measurement methods used. These differences increase as the beam diameter decreases and show that extreme care must be taken in measuring small field PDDs. In addition, it is clear that in the absence any recommendations for detectors and methods, the production of standard PDD tables for very small field sizes is unlikely for some significant time.

3.1.6 Aim

The primary aim of this work was to compare different detectors in the measurement of small field PDDs in collimators between 40 and 12.5mm diameter, in order to determine an optimum commercial detector(s), from those available to the ECC. In particular, the performance of more stereotactic specific detectors such as a small diode or IC was compared against that for their more routine counterparts. The optimum detector was then used for measurements on all linacs. Zero area PDDs were also extrapolated from measured data and used to interpolate PDDs for collimators in the 10-5mm diameter range. These results were compared against measurements in these collimator sizes.

3.2 Materials and Methods

3.2.1 Materials

All diodes (PFD, EFD, SFD), both cylindrical ICs (0.125cc, 0.015cc) and the PPIC were compared in the water tank. Film was used in solid water. A diamond was originally unavailable and was later found to be unsuitable for measurements in the Scanditronix tank due to the design and weight of the 'M' connector, as shown in Figure 3.5, which made it physically unstable in the detector holder.

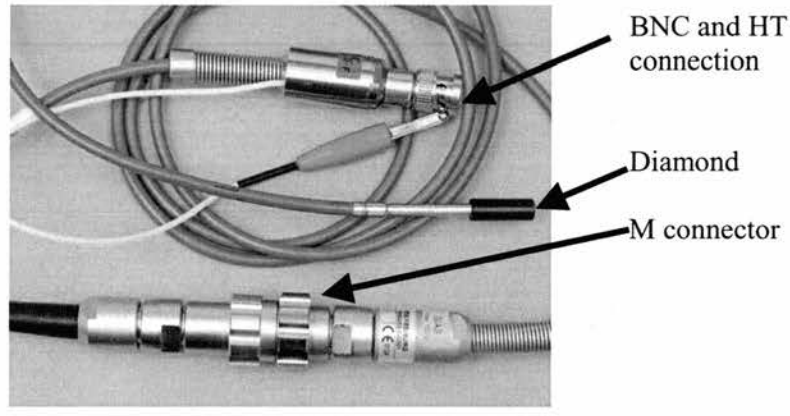

Figure 3.5. Diamond with 'M' connector.

3.2.2 Methods

Detectors

All detectors were initially compared in the 40 and 12.5mm diameter collimators on the BBC CH6, to determine the optimum detector. This was then used to measure PDDs in intermediate collimators and all collimators on the 600CD. PDDs measured on the 600CD

were extrapolated to zero field size and the calculated data in 10 and 5mm collimators compared against data measured with the SFD.

Tank measurements

PDDs were measured in the water tank at 1000mm FSD. Neither of the linacs used, nor the Scanditronix tank, provided the means to take a reference signal from the MU chamber and input it directly to the electrometer attached to the tank, unless extensive in-house modifications were made. On the CH6, the reference detector (unshielded diode) was placed inside the field, between the surface of the water and the end of the stereotactic collimator, because the tertiary collimator housing was mounted flush with the face-plate of the linac. However, on the 600CD, the reference detector was placed above the stereotactic collimator, inside the $50x50mm^2$ field, but outwith the stereotactic field, because the housing was mounted with a 5mm gap. Measurements were made in both the upward and downward directions, along the CAX.

The cylindrical ICs were orientated conventionally, with long axes perpendicular to the beam CAX. This was because there were physical problems in fixing the chambers to the detector holder in any other orientation, making their position very unstable. The diodes were used conventionally, with long axes parallel to the beam CAX. Film was used parallel to the beam, in solid water only.

The centre of the sensitive volume of each detector was aligned with the beam CAX by scanning beam profiles at both dmax and 100mm deep. The Inplane/Xplane zero co-ordinates were then set at the centre of the 50% dose regions, averaged over both depths. Measurements were carried out in precision mode, in 0.5mm depth steps.

Solid water measurements

Both the PPIC and film were used in solid water (RMI). Film was positioned parallel to the beam and calibrated at dmax using film positioned normal to the beam CAX. Although this method was not recommended by Williamson et al (1981) in conventional field sizes, the situation was investigated in small fields. The film envelope was pierced prior to use and then sandwiched tightly between blocks of RMI. The PFD and EFD were also used in RMI at a few depths as an independent check of the tank data. The dose in the build-up region was measured using each detector in RMI and this was combined with the tank data.

Data smoothing and extrapolation

PDDs were smoothed by plotting PDD against collimator diameter at selected depths and obtaining best fit lines to the data. In this way data for fields <12.5mm diameter could be extrapolated and the effects of noise smoothed. The extrapolated data was necessary for the conversion of PDDs to TMRs (Chapter 8).

3.3 Results and discussion

3.3.1 CH6 measurements

Reproducibility

Measurements were made with each detector in the tank, in both directions, on different days, in order to determine the reproducibility. The noise in the measurements increased with decreasing collimator diameter. On the BBC linacs this was primarily because the reference detector was positioned at the very edge of the field, in the region of high dose gradient. The reproducibility of repeat tank measurements in both directions, at depths beyond dmax, is +/-0.5% PDD. The largest uncertainties are in the region around dmax, as the effect of the reference detector position is largest and the push and pull of the meniscus has the greatest effect. The EFD measurements in the 12.5mm collimator are shown in Figure 3.6. Measurements in RMI averaged over two occasions are also included.

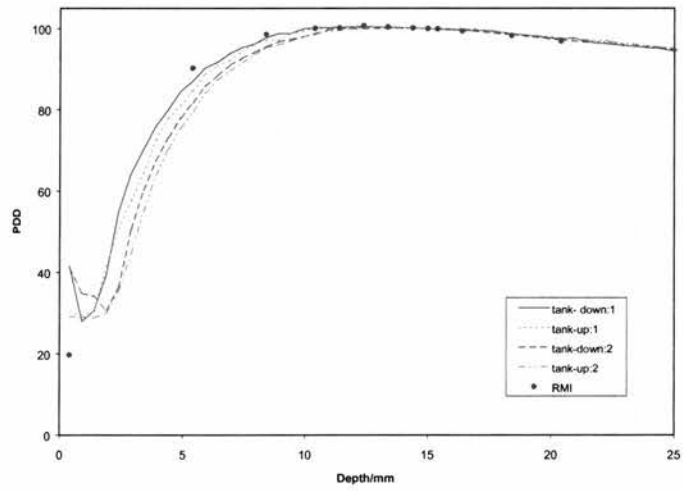

Figure 3.6. Repeat PDDs in the 12.5mm collimator, measured with the EFD.

The spread over repeat tank measurements is 1mm (i.e. +/-0.5mm) due to differences in the set-up of the tank zero co-ordinate, the FSD and the movement of the meniscus. The RMI measurements are approximately 0.5mm nearer the surface than the highest tank

measurements. This could be a real effect caused by a systematic error in the set-up of either the tank or the RMI, or due to the water-equivalent material. The magnitude of the uncertainties is similar for all other detectors.

Dmax shift

The position of dmax decreases from approximately 15.6mm for the 40mm collimator, to 13.8mm for the 12.5mm collimator, averaged over all detectors. The standard dmax in the reference field (100x100mm^2) is 15mm. These results agree with those of other authors as discussed in the literature review. Although the noise associated with each detector causes the measured dmax to vary by up to +/- 1mm, the field size dependence is still apparent. A constant normalisation depth of 15mm, is used in all further measurements, in accordance with other authors (Serago 1992, Das 1996, Fan 1997). As a result, PDDs will be >100% at depths <15mm, in the smaller collimators.

Surface dose

Nominal surface dose was measured in RMI with all detectors other than the ICs. True surface dose could only be measured with the PP-IC. Although the surface dose varied between 10 and 20%, noise in the measurements was too large to extract any field size dependence, in accordance with other authors (Sixel and Podgorsak, 1993 and Das, 1996).

Detector comparison

Figure 3.7 shows a plot of PDD against depth, in the 40mm collimator, on the CH6.

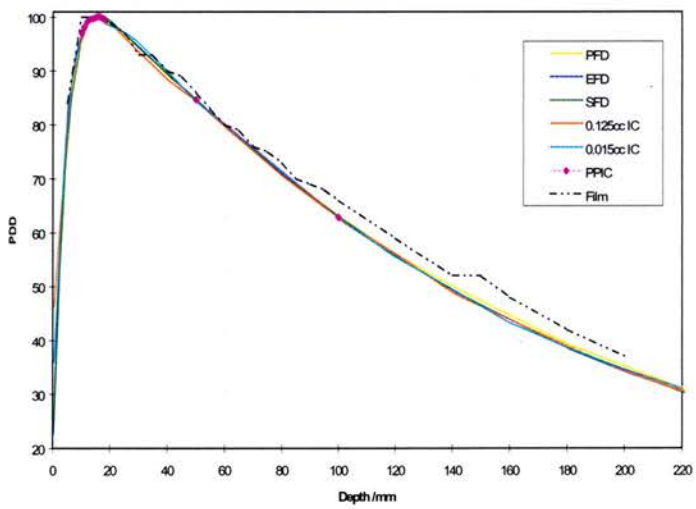

Figure 3.7. Comparison of detectors in the measurement of PDDs in the 40mm diameter collimator on the CH6.

The maximum spread over all detectors, other than film, at 100mm deep is <0.5% PDD (i.e. <0.8% local dose), with a minimal increase as the depth increases. Film PDD is >2% (>5% local dose) higher than the mean of the other detectors at the same depth. This could be due to the over-response of film to low energy photons and suggests that phantom scatter still has an effect at this field size. However, air pockets and gaps between slabs of RMI may not have been entirely eliminated and could have introduced some additional experimental uncertainties, accounting for the more irregular appearance of the film depth dose curve.

The unshielded diodes might also be expected to over-respond to scatter at depth. However, it is the PFD which is higher than the others, but only by approximately 1% PDD at 200mm deep. This suggests that phantom scatter is not a problem for the unshielded diode at this field size and that the energy compensation in the PFD has caused an under-response at dmax, perhaps due to the absorption of too many contaminant electrons. This apparent contradiction regarding phantom scatter effects in the diodes compared with film is due to the difference in atomic number between silver and silicon i.e. phantom scatter will have a larger effect on film, due to the higher atomic number of silver.

An alternative way to consider differences between PDDs measured with a variety of detectors, is to normalise to a depth other than dmax. This method can highlight small differences between curves as the differences are shifted to the high dose region around dmax. Figure 3.8 shows the PDDs for the 40mm collimator, normalised to 100mm deep.

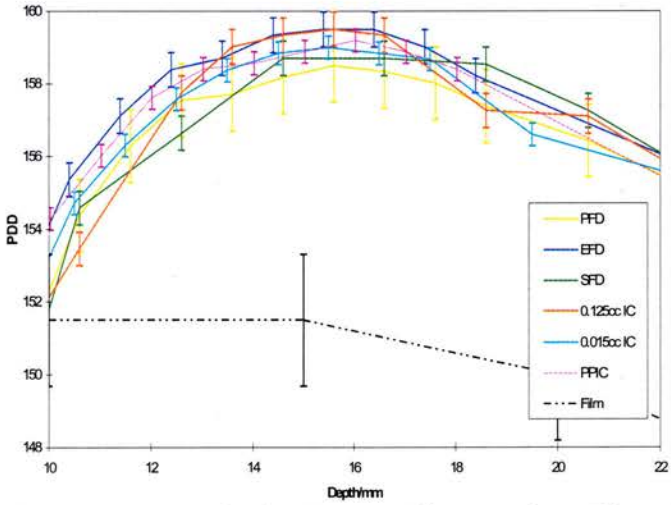

Figure 3.8. PDDs around dmax in the 40mm collimator, from Figure 7.7, renormalised to 100mm deep.

The relative response of film at dmax is approximately 8% PDD (>5% local dose) lower than the other detectors. This could suggest an under-response at dmax, rather than an over-response at depth, although the latter seems more likely. The responses of the diodes match that of the 0.125cc IC. Figure 3.9 shows the corresponding results in the 12.5mm collimator, normalised to dmax.

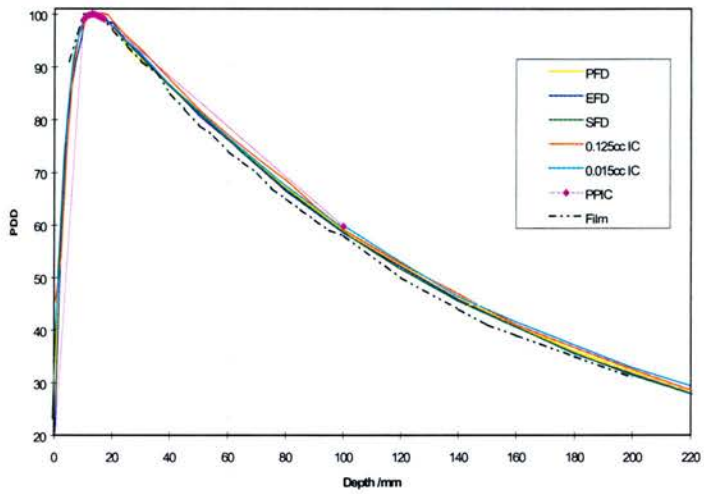

Figure 3.9 Comparison of detectors in the measurement of PDDs in the 12.5mm diameter collimator on the CH6.

The spread over all detectors, other than film, is larger than in the 40mm and is approximately 1.5% PDD (2.5% local dose) at 100mm deep. Figure 3.10 shows the region around 100mm deep only.

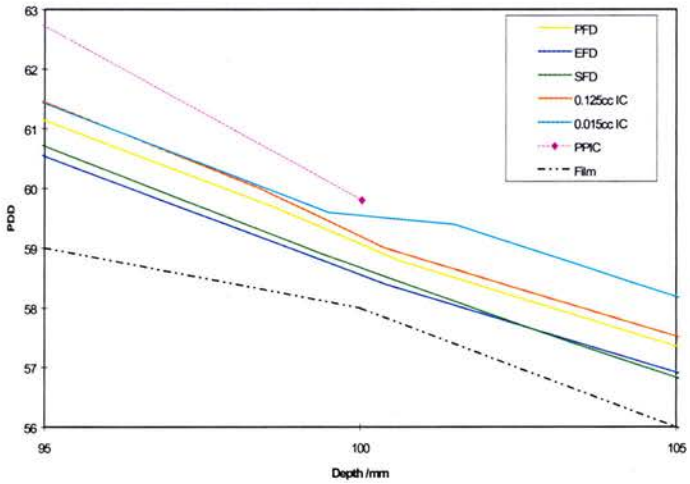

Figure 3.10. PDD region near 100mm deep in the 12.5mm collimator (from Figure 3.9.)

The maximum depth measured with the PPIC measurements was 100mm. The 0.015cc IC measurements appear to have a discontinuity around 100mm, likely to be due to movement

between the detector and/or the tank mechanism. The PFD is closely matched to the 0.125cc IC and both are <0.5% PDD higher than the two unshielded diodes, which themselves are almost indistinguishable. The film results are approximately 0.6% PDD (1% local dose) lower than the unshielded diodes. The differences between detectors in this field could be due to differences in the effects of scatter, or due to the partial volume effect, which would cause the IC PDDs to be too high, as found. The decrease in the over-response of film could also be a result of the reduction in phantom scatter. The change in the response of the PFD could be due to the lack of contaminant electrons in the smallest field size. Figure 3.11 shows the results normalised to 100mm deep.

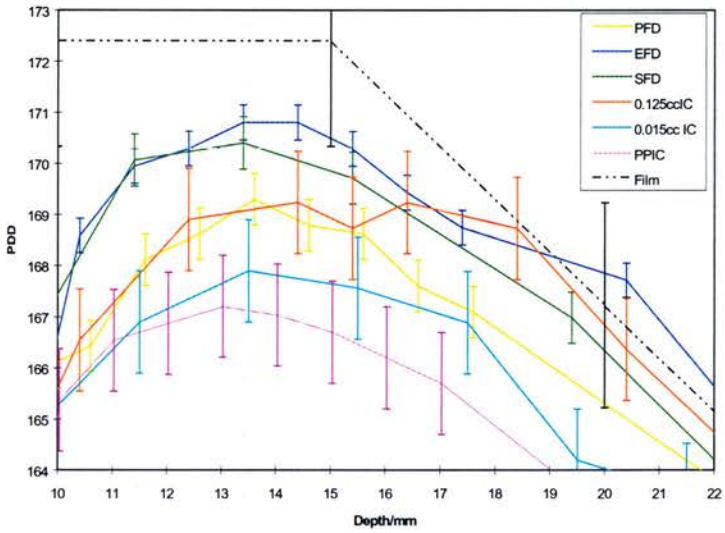

Figure 3.11 PDDs in the dmax region, from Figure 3.9, renormalised to 100mm deep.

Film and the unshielded diodes appear to be over-responding with respect to the ICs in the 12.5mm collimator, although again this is more likely due to due to an under-response in the ICs caused by the partial volume effect. Although the PFD matches the 0.125cc IC, this does not necessarily imply that both are correct. As stated, the IC could be under-responding at dmax due to the partial volume effect.

Optimum detector

It is important to be aware that differences between curves could be due to detector under or over-response at dmax or depth, irrespective of the normalisation. Conclusions regarding the absolute detector response cannot be made from relative measurements alone. MC could be used to determine absolute response, but this is outwith the scope of this work.

The match of the unshielded diodes to the ICs in the 40mm collimator shows that scatter effects are minimal, in terms of their effect on the response in silicon. In the 12.5mm

collimator, both cylindrical ICs are likely to be too large and produce PDDs which are too high, when normalised to dmax. A PFD measures PDDs which are also too high, possibly due to the absorption of too many contaminant electrons in the tungsten shielding at dmax. The unshielded diodes are therefore the most appropriate detectors to use in all collimators measured. Differences between the two types (EFD and SFD) are inconclusive at this stage, but the SFD has the lowest signal and therefore a slower acquisition speed must be used to improve the signal to noise ratio.

3.3.2 Measurements on the 600CD

Reproducibility

BDAS measurements in the 40 and 12.5mm collimators were repeated on three separate occasions, in both directions. The mean, standard deviation and coefficient of variation of the relative dose at each depth were then calculated from the six sets of data for each collimator. Beyond dmax, the mean variation in local dose between repeat measurements was 0.4%. As the uncertainty is largest in the build-up region and in the 12.5mm collimator, these results are shown in Figure 3.12, with the mean of all results shown in red.

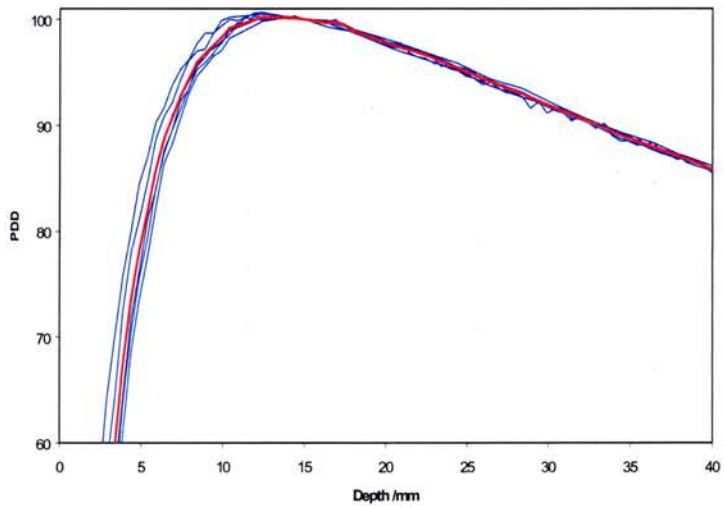

Figure 3.12. Reproducibility of measurements with the EFD in the 12.5mm collimator.

In the build-up region the spread in depth, over all measurements at 5mm deep, is approximately 1.3mm, again comparable with the CH6 results although more repeats were carried out on the 600CD. This shows that the largest uncertainties are associated with the doses in the build-up region.

Data measurements and smoothing

PDDs were measured on the 600CD with the EFD in all collimators between 40 and 12.5mm diameter. The curves were smoothed by plotting PDD against collimator diameter and fitting a straight line at each depth of interest. An example of the data, extrapolated to zero field size using the linear fits, is shown in Figure 3.13. The extrapolation assumes a linear fit down to zero field size, which is not actually physically correct.

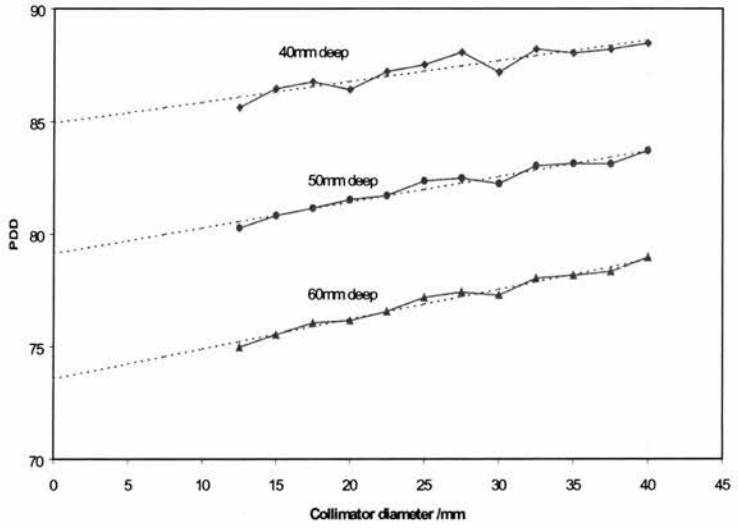

Figure 3.13. An example of some crossplots of PDD data against collimator diameter for three depths, with best fit lines superimposed.

The R^2 value for straight line fits to the PDD data for depths beyond 50mm was >0.95. However, at shallower depths R^2 decreased rapidly to 0.25 at 20mm deep and 0.1 at 10mm deep. Figure 3.14 shows examples for depths of 10 and 13mm.

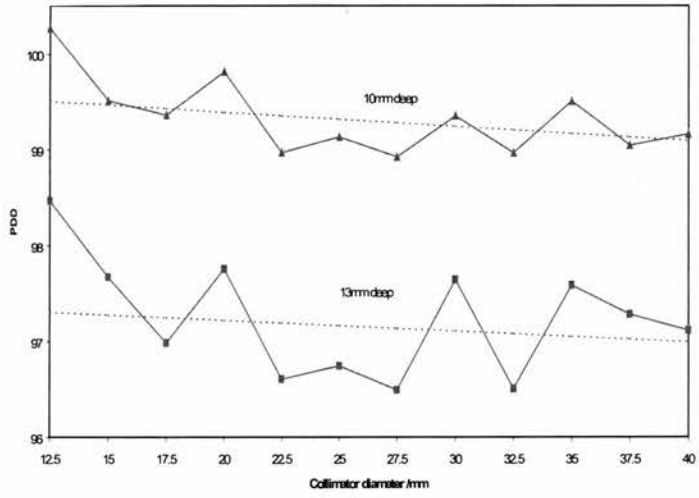

Figure 3.14. PDDs against collimator diameter at both 10 and 13mm deep, with straight line fits.

This highlights the problems of extrapolation at shallow depths. Figure 3.15 shows the smoothed data for all collimator diameters and extrapolated data for 10mm diameter and zero area.

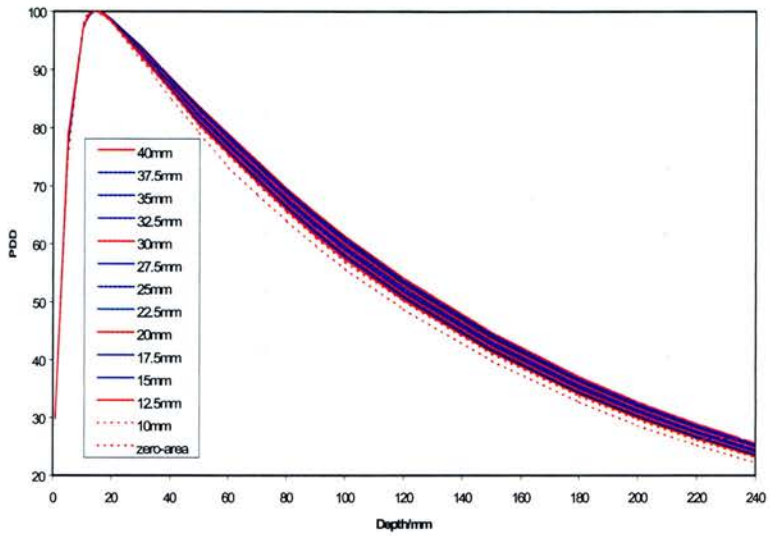

Figure 3.15. Final smoothed PDD data on 600CD measured with the EFD and extrapolated data for 10mm diameter and zero-area.

Zero area PDDs

Figure 3.16 shows a log-linear plot of the extrapolated zero-area PDDs, with ISL removed, against depth.

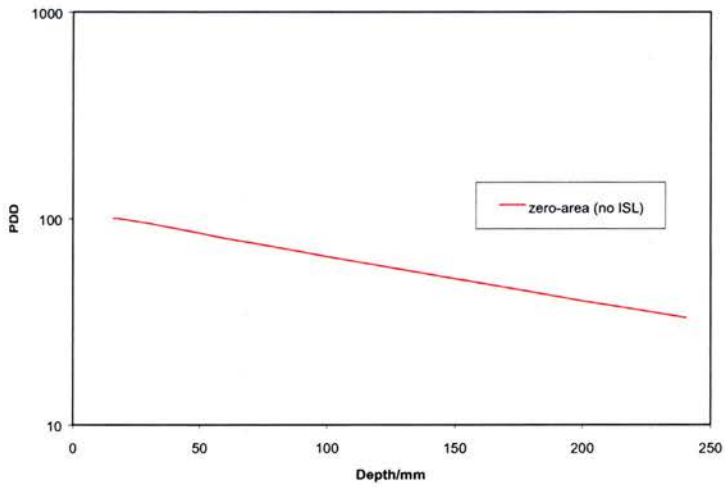

Figure 3.16. Zero-area PDDs, with ISL removed, plotted on a log-linear graph.

The linear attenuation coeffiecient calculated from the gradient of the above curve, was 0.00496mm^{-1}. On the 600CD, μ had previously been measured in a 30x30mm^2 field and found to be 0.00484mm^{-1}. The difference of 2.5% is likely to be a result of differences in

extrapolation. The extrapolated zero-area PDDs are compared against those calculated using the measured linear attenuation coefficient in Figure 3.17.

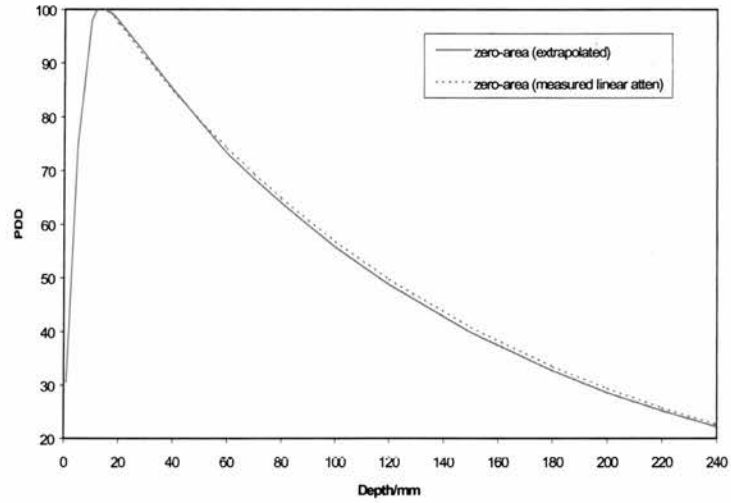

Figure 3.17. Extrapolated zero-area PDDs comapred with those calculated from a measured linear attenuation coefficient.

The difference between these two curves reflects the differences in extrapolation between a conventional field size and a small one, as shown in Figure 3.18, where the open square field data has been plotted against equivalent circle.

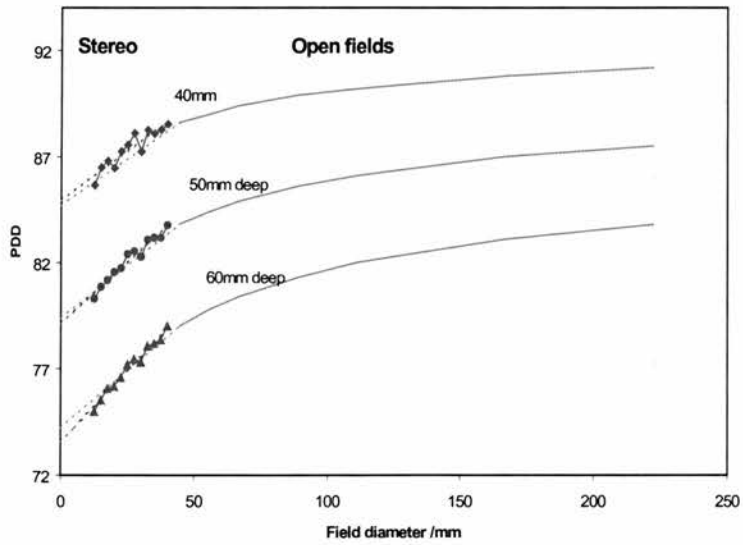

Figure 3.18. Comparison of PDDs at three depths extrapolated from conventional open field measurements and extrapolated from stereotactic field measurements.

As the depth increases, the PDDs extrapolated from the conventional open field data are higher than those extrapolated from the stereotactic data. This is because the slope of the curve increases as the field size decreases. It should be noted that below a 12.5mm

collimator the slope is likely to increase further and shows that extrapolation is a flawed technique.

Measurements in very small collimators

Smaller collimators (<12.5mm diameter) became available at the time of the commissioning of the 600CD. Raw measurements in the 40 and 12.5mm collimators with both the EFD and SFD are shown in Figure 3.19.

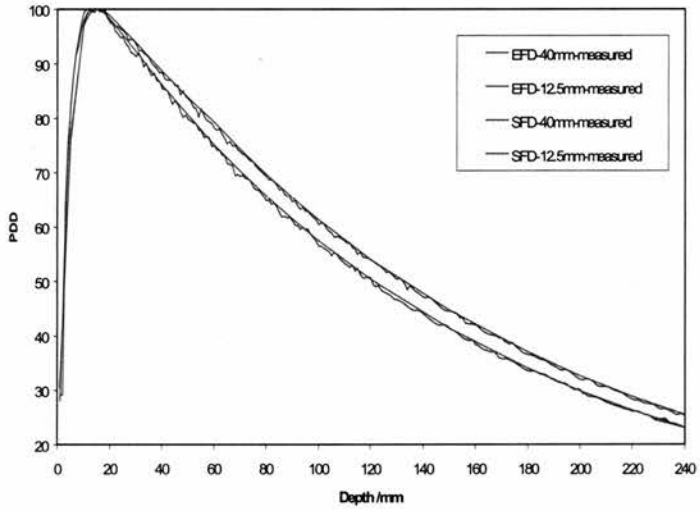

Figure 3.19. Comparison of the EFD and SFD in the 40 and 12.5mm collimators.

The two detectors are virtually indistinguishable in both collimators. However, as the use of the EFD could result in volume averaging effects in smaller collimators and as it was desirable to use only one detector to minimise the number of measurements, only the SFD was used in collimators <12.5mm diameter. The PDDs measured in the 10mm collimator are compared against the extrapolated data in Figure 3.20, with the 40mm (measured) and zero-area (extrapolated) data included for comparison.

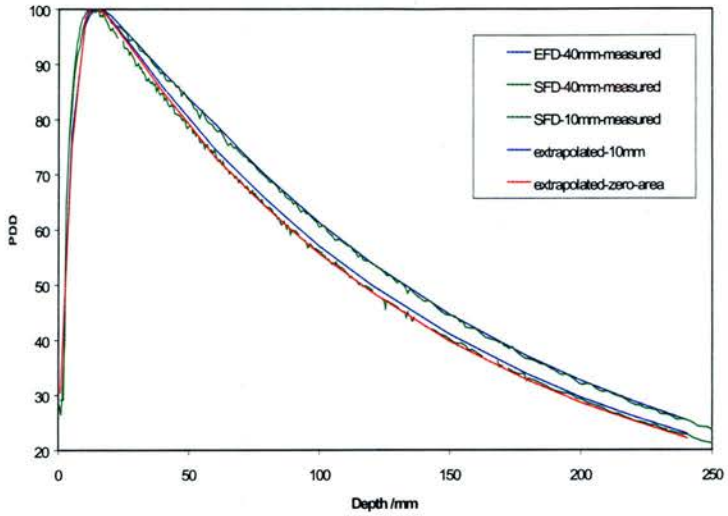

Figure 3.20. Comparison of (EFD) extrapolated data and (SFD) measured data, in the 10mm collimator. 40mm and zero-area data included for comparison.

At 100mm deep in the 10mm collimator, the extrapolated data is approximately 1% PDD (1.8% local dose) higher than the measured data. Larger differences are apparent in the build-up region and in the region between dmax and 50mm deep. These differences could be due to the extrapolation of data in this region, as discussed previously, but could also be due to a systematic error in the positioning of the SFD. The measured depth of dmax is approximately 13mm. Comparable results for the 5mm collimator are shown in Figure 3.21.

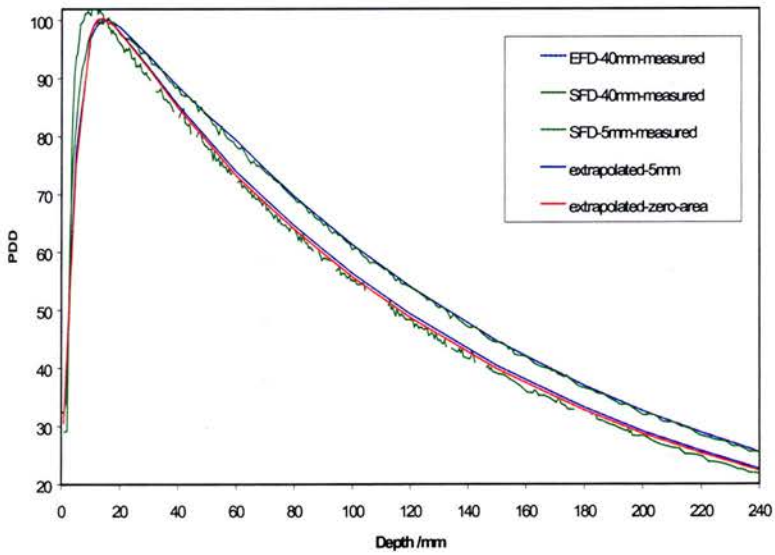

Figure 3.21. Comparison of (EFD) extrapolated data and (SFD) measured data, in the 5mm collimator. 40mm and zero-area data included for comparison.

The differences between the extrapolated and measured data are comparable with those for the 10mm collimator. The depth of dmax appears to have shifted to <11mm, which is in approximate agreement with Verhaegen et al (1998) who calculated dmax to be approximately 9mm in a 5mm diameter collimator. This relatively large shift in dmax would not have been accounted for in the extrapolation and this could be the reason for some of the differences. However, there are other experimental uncertainties which could account for the differences. At very small field sizes, the accuracy of the set-up becomes more critical. If the detector axis and the movement of the depth controller are not exactly aligned with the beam CAX, the detector will not measure the same off axis dose at each depth. In addition, the relatively high signal on the reference detector, compared with the very small signal on the SFD, particularly in the 5mm collimator, could mean that small variations in linac output are not compensated for in the SFD measurements.

3.3.3 Comparison with CH6

Final PDDs on both the CH6 and the 600CD, measured with the EFD, in the 40 and 12.5mm collimators are shown in Figure 3.22.

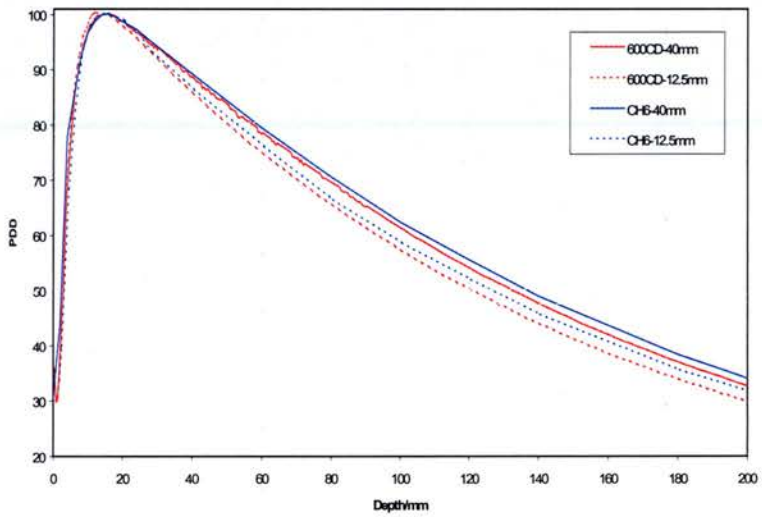

Figure 3.22. A comparison of PDDs in the 40 and 12.5mm collimators, on both the 600CD and the CH6.

In both collimators, the PDDs on the CH6 are higher than those on the 600CD, due to the higher beam quality (QI= 0.678, compared with 0.663). The approximate 1.5% increase in PDD at 100mm deep corresponds to that measured in the standard field sizes.

3.3.4 XKnife requirements

The XKnife planning system requires the input of TMRs, rather than PDDs. TMRs are calculated from PDDs using equation 2(a) in BJR Supplement 25 (Burns, 1996), in Chapter 8. TMRs calculated in collimators between 40 and 12.5mm diameter require PDDs down to a 10mm collimator. At the time of this original work, the very small collimators were not available and therefore extrapolated data down to a 10mm collimator was used. The final PDD data set used for TMR calculation on the 600CD is shown in Appendix 1.

3.4 Conclusion

From the detectors tested, an unshielded diode has been shown to be the most suitable for the measurement of PDDs in collimators between 40-12.5mm. The EFD is more practical than the SFD in this range because of the higher signal to noise ratio. However, the use of the term "electron diode" (EFD) to describe the unshielded diode is somewhat confusing as it suggests that the diode has been designed specifically for use in electron beams. This is not the case. The only difference between the "electron" and "photon" diodes is the inclusion of energy compensating material in the "photon" diode. This is used to compensate for the over-response of a diode to low energy scatter. The results outlined in this chapter have shown that phantom scatter is minimal in small fields and therefore the diode over-response is practically eliminated. Indeed the photon diode could be a disadvantage in small fields as too many contaminant electrons may be absorbed in the energy compensating shield. This would cause the PDDs to be under-estimated in larger small fields, when normalised to dmax. Because of its small size, the SFD should be the most appropriate detector to use in very small fields. However, there is some uncertainty over the differences between measured PDDs and those extrapolated from the EFD measurements. This requires further examination, perhaps with repeat measurements, a longer sampling time and the reference signal taken directly from the MU chamber. MC calculations would be extremely useful to determine the accuracy of the measured data at these field sizes. However, it would appear that PDDs for fields smaller than 12.5mm diameter can be extrapolated with an uncertainty of approximately =<1% (PDD) in a 5mm collimator, at 100mm deep.

PDDs should be measured with the reference signal ideally taken from the linac MU chamber, or placed above the tertiary collimator system, within the open field, but outwith the stereotactic field. In addition, the detector should be carefully aligned with the beam CAX by scanning the beam profile at a minimum of two depths and aligning the Inplane/Xplane zero co-ordinate with the centre of the 50% regions.

Chapter 4

Profiles

4.1 Introduction

4.1.1 Definitions

Profile

The change in the x-ray dose distribution along a defined line in a plane perpendicular to the beam CAX is characterised by the beam profile, the shape of which is dependent on both the geometric and dosimetric properties of the beam. Although a megavoltage x-ray source produces photons in all directions, the beam has a forward peak which is reduced by the inclusion of a beam flattening filter (BFF), downstream of the target. The BFF is conical in shape and is comprised of a mixture of metals. On the 600CD these are predominantly lead and tin. The shape of the BFF is designed to remove more photons from the centre of the beam than the edges and thus flatten the overall profile, making it more useful for clinical treatments. IEC (1989) states that the flatness within the central 80% of the beam width, at a depth of 100mm in water, 1000mm FAD, should be within +/-3% of the dose on the CAX.

Field size

Although IEC (1989) states that the field size should be defined as the width of the 50% isodose at the isocentre, 100mm deep, it is almost invariably set up to be the width of the 50% at the phantom surface. The field size is determined by the collimating system, such as the movable collimators of the linac, MLC, blocks or stereotactic collimators.

Penumbra

If scatter and transmission effects are ignored and a point source is considered, the dose outside the geometrical edge of a beam is zero. However, the finite size of the source, the transmission through the collimators, the in-air and in-phantom photon scattering and the secondary electron transport, all result in a dose gradient, known as the penumbra. The penumbra is a region of electronic disequilibrium, where electrons are predominantly scattered out of the main beam. Figure 4.1 shows a schematic diagram of the situation.

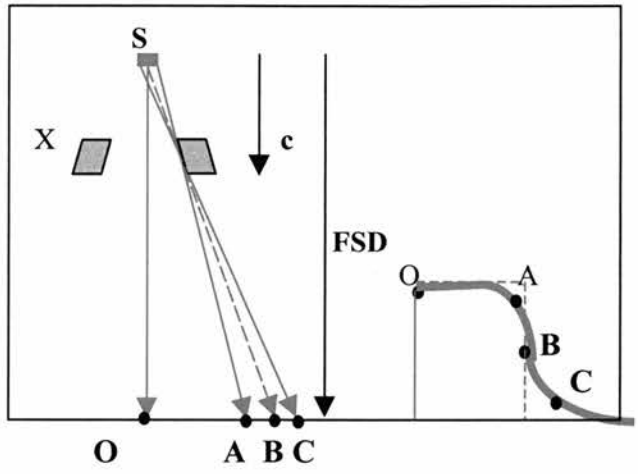

Figure 4.1 Schematic diagram of the penumbra.

The left-hand diagram in Figure 4.1 shows a finite source, s and a beam defined by the collimation system at X. The line SB represents the geometrical edge of a beam from a theoretical point source at S and the region ABC represents the penumbra (p) in the real beam. The distance between the source and the lower edge of the linac collimators is represented by c and the FSD is the distance to the phantom surface. The broken line in the right hand diagram represents the theoretical beam, the intensity of which drops to zero at B. The broad line represents the true situation, where ABC again represents the penumbra.

The true dose in the shoulder region at A is less than that in the theoretical situation because electrons are predominantly scattered out of the beam. Conversely, the dose in the tail at C is greater than that in the theoretical situation, because although it lies entirely outside the geometric edge of the beam, some of the source can still be "seen" at that point. In addition, photons and electrons are scattered to that point from inside the beam and some dose is deposited as a result of transmission through the collimators.

The width of the penumbra can be characterised either as the distance between the 20 and 80% or between the 10 and 90% regions. IEC (1989) recommends that penumbra is measured at 100mm deep, 1000mm FAD in a 100x100mm^2 field. Although IEC do not state a recommended penumbra width under these conditions, on a linac the 20-80% distance is approximately 10mm (Almond and Horton, 2000).

The width of the penumbra changes with field size, FSD, depth and energy, due to geometry and changes in scatter. The width of the penumbra decreases as the field size decreases, due to geometrical effects and differences in transmission through the movable collimators.

These can be minimised by mounting the linac collimators on an arc such that the inner surface of each collimator remains parallel to the edge of the beam as the field size is adjusted (Khan, Chapter 4, 1994). All linac manufacturers design the movable collimators in this manner. However, the only linac on which this also applies to the MLC is the Siemens Primus. On the Varian 600CD the MLC leaves travel only in the plane perpendicular to the beam CAX. However, the rounded ends of the MLC leaves have been designed to try to ensure that transmission effects are constant for all field sizes.

The width of the penumbra increases with depth, due to geometrical effects and the increase in scatter with depth. The relationship between the penumbra and FSD can be expressed analytically (Bomford, 2003):

$$p = s(FSD - c) / c \qquad (4.1)$$

It is apparent that p increases as the FSD and spot size (s) increases. It is also apparent that p can be minimised by increasing the distance c, between the source and the lower edge of the collimating system i.e. by decreasing the distance between the end of the collimation system and the isocentre.

Off axis ratio

The ratio of the dose at any off axis distance (OAD) to that on the CAX at the same depth and FSD, is known as the off axis ratio (OAR).

$$OAR = D(r, d) / D(r_0, d) \qquad (4.2)$$

where r is the distance off axis from the CAX to the point of measurement, at a depth d and r_0 is the CAX (i.e. r = 0).

Planning systems based predominantly on measured data generally require the input of OARs at several fixed depths and field sizes. Profiles at intermediate depths and field sizes are calculated by interpolation. Alternatively, some planning systems require only profile information in the largest field size, at several depths. The penumbra is extracted from the profile and convolved with pencil beams or point spread functions to obtain the profile in any field size.

Apparent profile

Although the geometric and dosimetric properties of the beam determine the *actual* profile, the properties of the measurement device will have an affect on the *apparent* profile. The composition, directional response, energy, dose rate dependence and, most importantly, size of the detector will all affect the apparent profile (Heydarian et al, 1996).

4.1.2 Measurement of profiles

Phantoms

OARs are most efficiently measured in a water tank using a field detector and a reference detector. Measurements should be made over both beam axes and compared. Although the shape of the profile is dependent on the axis (Inplane/Xplane), profiles in both directions are generally considered to be sufficiently similar that profiles in only one direction are input to the TPS. Measurements should only be carried out in beams which are sufficiently symmetrical to allow the profiles to be averaged over both sides of the CAX.

It should be noted that the scan direction for an ion chamber used in conventional orientation (long axis perpendicular to beam CAX) must be perpendicular to the long axis of the chamber, to optimise the resolution and avoid potential asymmetry in the measurements.

OARs can also be measured in a solid water phantom using a point detector. However, the process is time consuming and the couch lateral co-ordinate must be adjusted to obtain measurements at off axis positions. If solid water is used, it is more common to use it in conjunction with film, with which 2D information can be obtained in a single exposure.

Detectors

The finite size of any detector will affect the resolution of measurements in regions of significant dose gradient, as the dose will be averaged over the entire detector volume (volume averaging). For large detectors, such as ion chambers, this will result in a broadening of the penumbra caused by a decrease in dose in the shoulders and an increase in dose in the tails. However, it has been shown that correction factors can be calculated to account for the size of the chamber. Dawson et al (1986) extrapolated detector size to zero by measuring the same profile with several cylindrical ICs of different diameters. The authors concluded that IC penumbra measurements could be adjusted by increasing and decreasing the distance from the CAX in the high and low dose regions respectively, in

proportion to the radius of the IC. This correction did however, still underestimate the profile width in a 100x100mm^2 field compared with film, by up to 1.5mm.

Sibata et al (1991) defined a similar correction, based on a quadratic fit to the data, but the 80-20% penumbra regions in a half beam blocked 50x70mm^2 field were still approximately 1mm wider than those measured with film.

Diodes can be used to improve the resolution when measuring profiles. However, although the sensitive volume is small (approximately 2.5mm width), volume averaging will still occur when the detector is used with its long axis parallel to the beam CAX. This has led some investigators to orientate the detector with long axis perpendicular to the beam CAX. The thickness of the silicon chip will then be presented to the beam and as this is generally of the order of 0.2mm, the resolution is greatly increased. However, the asymmetric construction of the detector in this orientation may produce an asymmetrical response.

The non-tissue-equivalence of silicon will also have an effect on the apparent penumbra. In some of the literature discussed in the next section this is considered to be a positive feature. $\rho Z/A$ is higher in silicon than in water or air and as a result, the electron range in silicon is shorter than in water or air. This is important in regions of electronic disequilibrium, such as the penumbra. The stopping power (MeVcm^2/g) multiplied by the physical density (g/cm^2) shows that an electron of the same energy will be stopped in silicon in approximately half the distance required in water. In penumbral measurements the effect of this would be to reduce the number of electrons scattered out of the beam, increase the dose in the shoulder region and consequently sharpen the penumbra. Volume averaging and electron range are conflicting effects, but the magnitude of each still requires further investigation.

The energy, dose rate and directional response of diodes may also cause problems in the measurement of OARs. For example, at off axis distances, the directional response of diodes could lead to an underestimation of the dose. The decrease in the mean energy and the increase in dose rate at off axis distances might also cause the diode to over-respond.

It is interesting to note that Dawson et al (1984) claimed to be the first to describe two types of distribution in the penumbra. These were the photon-fluence distribution (head scatter) and the dose distribution. The authors stated that an ionisation chamber is an electron detector and consequently measures the dose distribution. A diode is however a photon detector and therefore measures the photon fluence associated with the geometry of the linac

head. The net result of this is that a diode measures a sharper profile than an IC and underestimates the width of the penumbra, by an amount that increases with beam energy. At 6MV the difference between the 10-90% penumbra measured with a very small diode (0.13mm sensitive width) and an IC with 3.5mm inner diameter, in a 100x100mm^2 field at an unspecified depth in water, was 0.4mm. The authors advised that the true penumbra lay in between these two measured penumbras.

Film is a useful detector for the measurement of profiles as 2D information can be obtained quickly, at one depth, for a single exposure. Although film is energy dependent and its over-response to low energy photons could affect off axis doses, Sibata et al (1991) found that the variation in beam spectra across a beam profile had no significant effect on the energy response of film. As the resolution of film measurements is only dependent on the resolution of the densitometer, film would appear to be the ideal detector for use in profile measurements.

4.1.3 Small field situation

Penumbra

A narrow penumbra is particularly desirable in stereotactic fields, where a small target volume may be located close to a sensitive structure. Tertiary collimators, matched to the geometric divergence of the beam, reduce the overall penumbra by sharpening the geometric penumbra, reducing collimator transmission and minimising the effects of scatter in the head and in the air. Both of these effects can be maximised by positioning the tertiary collimators nearer to the patient (increasing c). However, this has to be weighed against increasing the distance between the isocentre and the end of the tertiary collimators, to maximise the number of possible approaches for each beam. Serago et al (1992) found that increasing the distance between the source and the ends of the collimators from 585mm to 760mm, decreased the penumbra in a 30mm diameter collimator by less than 0.4mm and in smaller collimators by only 0.1mm. The Radionics system used in the ECC employs a distance of 770mm between the source and the end of the collimators.

Although the 20-80% distance is most often quoted for the penumbra in larger fields, the 10-90% is more clinically significant in stereotactic fields as the target volume is generally covered by the 90% isodose and the requirement is for the dose to fall off quickly outside this region. Many authors discuss uncertainties in penumbra width of the order of 0.5mm. Although this should be put in the context of the overall uncertainty of both localisation and

treatment, small uncertainties in various measurements may add to increase the overall uncertainty.

High dose region and detectors

Accurate determination of the width of the 90% isodose is probably more important than accurate determination of the penumbra width, as this determines the size of collimator chosen for treatment. The use of a collimator which is too large (underestimation of the 90% width) will lead to the unnecessary irradiation of excess normal tissue. The use of a collimator which is too small (over-estimation of the 90% width) will lead to the under-dosage of the target volume.

As the field size is described by the width of the 50% isodose, the full width half maximum (FWHM) is often quoted as an important parameter. However, in stereotactic fields, the fall off in dose is much sharper than in conventional fields and the width of the 50% becomes a much less useful parameter, particularly with reference to the size of detector used. A detector must ideally fit within the very high dose region, such as the 99%, to be used in stereotactic field measurements, without the need for a correction for detector size.

Volume averaging

If a detector is too large for measurements in small fields, volume averaging will occur. This can be accounted for by extrapolating the detector size to zero, as previously discussed. However, it is also important to note that when measuring the penumbra in small circular fields, the width of the sensitive area is important not only in the scan direction, but also in the perpendicular direction, as shown in Figure 4.2.

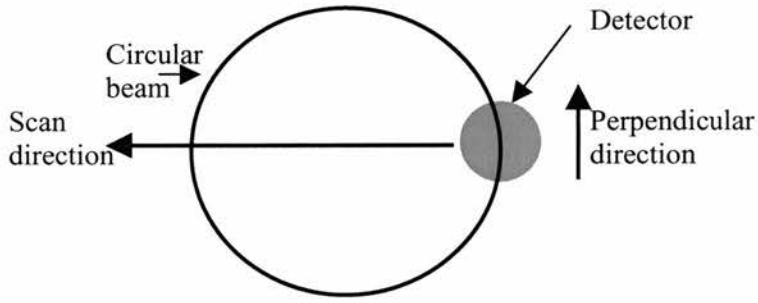

Figure 4.2. Example of scan direction for measurements in circular collimators.

Averaging of the dose occurs over the steep dose gradient in the penumbra and also over the curvature of the field edge. Ideally, both changes should be accounted for.

4.1.4 Small field profiles in the literature

At the time of the original commissioning of the stereotactic system on the CH6 linac (1994), only three publications existed on the measurement of OARs in small fields.

Rice et al (1987) used ICs of different diameter and extrapolated the results to zero detector size to determine the profile width at 75mm deep in a 17.5mm diameter collimator. The extrapolated results were within 0.3mm of measurements with film and 0.9mm TLD ribbons. Measurements were also made at other depths and in-air with an IC and a brass build-up cap. No significant change in penumbra with depth in water was reported and the authors concluded that the profile shape was independent of depth in small beams. Although the in-air profile in the 30 and 12.5mm diameter collimators showed a sharper penumbra and a wider high dose region, this was not discussed by the authors.

Haworth and Perry (1993) used a photon diode (2.5mm sensitive width) orientated with long axis perpendicular to the beam, to measure profiles at 50mm deep, at three FSDs. The authors found that the 50% width determined by the diode, matched that measured on film to within 0.25mm, in collimators down to 7mm diameter. However, their measurements were painstakingly made in a solid water phantom, only half of each profile was measured and the results were not compared against a diode in conventional orientation. Although the penumbra was measured at different FSDs, no results were presented.

Beddar et al (1994) compared a photon and an electron diode (both 2.5mm sensitive width) in both orientations to measure profiles at an unspecified depth in a 10mm diameter collimator. Maximum spatial resolution was achieved when each diode was orientated with long axis perpendicular to the beam CAX i.e. the thickness of the measurement volume was presented to the beam. This decreased the measured penumbra by approximately 0.6mm compared with that measured in conventional orientation. However, the perpendicular orientation also led to an asymmetrical beam profile, thought to be due to the difference in density between the materials in front of and behind the detectors. In front of the sensitive volume of each diode is epoxy (in the detector) and water (in the tank). Behind the sensitive volume there is epoxy, cable connections and the detector stems. The measured dose, in the penumbra in particular, is therefore dependent on the direction of scan. The measured asymmetry was greatest with the photon diode due to the additional tungsten shielding. A

symmetrical profile can however be obtained by turning the diode around at the CAX and measuring the two halves of the profile separately. However, for simplicity and greater accuracy, the authors recommended the use of an electron diode, orientated with long axis parallel to the beam. Although the size of the sensitive area was larger in this orientation, the authors suggested that the decreased electron range in silicon cancelled out the effect of volume averaging. The maximum error introduced by using an electron diode parallel to the beam CAX was thought to be =<0.5mm, based on film measurements in materials of different density. Haworth and Perry (1993) did not report any asymmetry, but this was probably because only half of each beam profile was measured.

At the start of the stereotactic commissioning in the ECC (1994), an electron diode (parallel to the beam CAX), or film, appeared to be the most useful detectors. These detectors were selected for use, but were also compared against a PFD and 0.125cc IC.

Prior to the publication of the small detectors work at the ECC (McKerracher and Thwaites, 1999), several additional papers were published on the subject of the measurement of OARs in small fields. Higgens et al (1995) used deconvolution of (3.5mm internal diameter) IC size to correct small beam profiles. Although measurements were carried out at both 15 and 105mm deep, the results were only presented for one, unspecified depth. In the 12.5 and 10mm collimators, the deconvolved IC results were up to 1.0mm wider than those measured with film. The authors made the interesting point that if the detector was too large, the dose on the CAX could have been underestimated. This would have led to incorrect normalisation and a corresponding increase in the penumbra. Consequently, they recommended that the maximum inner diameter of any detector should be less than half the full width half maximum (FWHM) of the smallest beam in order to use deconvolution.

Rustgi (1995) compared a photon diode (2.2mm sensitive width), a diamond (2.7mm sensitive width) and a 0.14cc IC, in elongated fields (10x200, 30x200mm^2) at dmax. The diode and diamond were orientated with long axes perpendicular to the beam CAX to maximise the resolution. As only half of the beam profile was presented, there was no evidence of skew. This would be expected when a photon diode is used in this orientation. The authors recommended the use of the photon diode as this measured penumbras which were 0.4 and 0.8mm narrower than those measured with the diamond in small fields.

Das et al (1996) measured profiles at dmax, 50 and 100mm, using a diamond (2.7mm sensitive width) with long axis parallel to the beam. The results were found to be identical with those in both Kodak XV and CEA film in all collimators between 40 and 12.5mm

diameter. This suggested that the resolution of a diode in this orientation was satisfactory. The authors also noted that the OARs were relatively independent of depth, when measured isocentrically. This suggested that phantom scatter had little effect on the penumbra.

Fan et al (1997) used Kodak XV-2 film to measure profiles at 50mm deep in collimators between 40 and 5mm diameter, but did not compare it with any other detector.

Gotoh et al (1996) compared profiles measured at 50mm deep with a micro IC (0.009cc) and film in collimators with diameters between 31.4 and 11.6mm. The IC and film results agreed to within 3.5% in the low dose region, but the profiles measured with the IC were 0.5mm wider than those measured with film.

Heydarian et al (1996) measured profiles at 60mm deep in collimators between 41.0 and 8.9mm diameter with a photon diode (2.5mm sensitive width) parallel to the CAX, a diamond (0.25mm thickness) perpendicular to the CAX and film. The penumbra measured with the diamond was <0.2mm narrower in the smallest collimator than that calculated with EGS4 MC and the diode and film measured penumbras were too large by approximately 0.5mm. The authors suggested that the effects of the diode size (volume averaging) and composition (reduced electron range in silicon) could cancel. However, they also suggested that directional response could have an effect off axis. The maximum off axis distance presented was 50mm in the 23mm diameter collimator. At an FAD of 1000mm, this represents an angle of approximately 1.4°, which is unlikely to have any effect on the directional response. However, the authors could be referring to scatter into the detector volume from different directions, as this could have an effect on the directional response. The broadening of the penumbra by film was thought to be due to the low energy components in the beam off axis, which would cause an over-response off axis.

Dasu et al (1998) used both a photon and an electron diode (both 2.5mm sensitive width) and a prototype LIC (sensitive diameter 3mm, thickness 0.3mm) in both orientations, to measure profiles at 100mm deep in collimators with diameters between 44 and 8mm. Both types of diode matched when used parallel to the beam CAX, but asymmetrical profiles were measured when they were used perpendicularly. The smallest penumbra was measured with the long axis of the LIC perpendicular to the beam CAX, due to the 0.3mm thickness of the sensitive volume. The largest penumbra was measured with the LIC parallel to the beam CAX. The difference between the two orientations was 0.8mm in the 8mm collimator. The authors recommended the LIC for profile measurements.

Francescon et al (1998) used both radiographic and radiochromic film to measure profiles at an unspecified depth, in collimators between 19 and 4.4mm diameter. Although the results from both types of film were in agreement, there was more noise with the radiochromic film and repeat measurements had to be carried out and the results averaged and smoothed.

Norrgard (1998) used a PFD and EFD (2.5mm sensitive width), a 0.1cc IC (4mm inner diameter) and film to measure profiles at 50mm deep in collimators between 45 and 15mm diameter. In the 15mm collimator the 20-80% penumbra measured with the IC was approximately 2mm broader than that measured with film. The profiles measured with both the PFD and EFD were 0.2mm broader than those measured with film.

Radiochromic film has been used to measure off axis ratios and dose distributions for stereotactic fields on the Gamma Knife unit (Sanders 1992, McLaughlin 1994, Somigliana 1999) and on a linac (Guan 1993, Somigliana 1999). However, the results have all been comparable with those for radiographic film. The advantage of radiochromic film appears to be in terms of its use practically, rather than a dosimetric advantage.

Verhaegen et al (1998) used BEAM (EGS4) to calculate OARs in stereotactic fields on a 6MV Varian Clinac-600SR. Calculated OARs were compared with measurements carried out with a diamond of 3mm sensitive width, in collimators of 40 and 20mm width. The calculated profiles reproduced the measurements "very well" but over-estimated the dose in the tails due to an over-estimation of photon scatter in the stereotactic collimators.

McKerracher and Thwaites (1999) compared standard detectors used in the commissioning process (PFD, EFD, 0.125cc IC, film) with two new detectors which had not yet been tested for profile measurements. One was a small (0.6mm sensitive width) stereotactic diode manufactured by Scanditronix and the other the PTW PinPoint IC (0.015cc, 2 and 5mm sensitive diameter and length). These measurements will be discussed in the results section.

Since 1999, four other publications have reported on the measurement of small field profiles. Westermark et al (2000) measured profiles at 100mm deep in collimators between 18 and 4mm diameter, with a diamond (3.8mm sensitive width) and a prototype LIC (1.5mm sensitive diameter, 0.6mm thick), both orientated perpendicular to the beam and two small (0.6mm sensitive width) diodes. One incorporated a single chip (SFD) and the other a prototype double chip (DD). Both diodes were orientated parallel to the beam and the measurements compared with MC calculations. The diamond produced an asymmetric profile and a radiograph showed a larger electrode below the diamond than above it, which

could have led to the problem. The corrected LIC measurements were found to match MC and although the SFD was also closely matched, the DD significantly underestimated the penumbra. The authors noted that the size and shape of the penumbra was not only a feature of the detector size, but was also affected by the detector composition and dose-rate dependence. In addition, deconvolution of detector size should only be applied to detectors which are water-equivalent. Although the diodes showed a sharper penumbra, the authors suggested that this was in fact too sharp and was caused by a reduction in the electron range in silicon. This effect is enhanced in the double chip diode. MC agreed primarily with LIC and a scintillator corrected for detector size. In-air profiles (Pb build-up cap) were also measured, although the detectors used were not specified. The in-air penumbras were found to be constant with field size, whereas the in-water penumbras increased with field size, due to increases in phantom scatter. In-air profiles were not presented graphically.

Paskalev et al (2002) used a micro PP-IC (mPP-IC) with inner cavity of 2mm diameter and HS Gafchromic film to measure OARs in beams of 5 and 1.5mm diameter on the 10MV beam of a Varian Clinac-18. The mPP-IC measurements were corrected to account for the size, construction and material of the detector. All measurements agreed well with EGS/BEAM calculations to within +/-3% of the dose on the CAX. Differences were due to slight differences in the alignment of the collimators.

Laub and Wong (2003) used extrapolation of detector size to zero to reconstruct profiles measured with a 0.3cc, 0.125 and 0.015cc IC, both parallel and perpendicular to the beam CAX, a Markus PP-IC and a linear chamber array (LCA). The corrected profiles agreed with those measured with a diamond at dmax in a $20x20mm^2$ field. The authors recommended this technique in preference to film because of its over-response to low energy photons, but it should be noted that they did not actually use film.

Sanchez-Doblado et al (2003) calculated OARs in small stereotactic collimators (10.5 and 3mm diameter) on the 6MV beam of an Elekta SL-18 using EGS4 (BEAM). Measurements with Kodak X-Omat V film were in "good agreement" with MC.

Comparison of results

A direct comparison of results between authors is not possible for profile measurements simply because the data is difficult to extract from the figures in each publication. Table 4.1 summarises the range of detectors described in each publication and emphasises the amount of work carried out to date.

Author	Year	Film	EFD	PFD	SFD	IC*	LIC	Diam	MC	TLD
Rice et al	1987	✔				✔				✔
Haworth & Perry	1993	✔		✔						
Beddar et al	1994		✔	✔						
Rustgi et al	1995			✔		✔		✔		
Das et al	1996	✔						✔		
Fan et al	1996	✔								
Gotoh et al	1996	✔				✔				
Francescon et al	1998	✔								
Norrgard	1998	✔	✔	✔		✔				
Verhaegen et al	1998							✔	✔	
Heydarian et al	1999	✔		✔				✔	✔	
McKerracher & Thwaites	1999	✔	✔	✔	✔	✔				
Westermark et al	2000				✔		✔	✔	✔	
Paskalev et al	2001	✔				✔			✔	
Dasu et al	2002		✔	✔			✔			
Laub & Wong	2003					✔				
Sanchez-Doblado et al	2003	✔							✔	

Table 4.1. Summary of detectors used in small field publications. IC* encompasses measurements with one or many ICs, deconvolution of detector size and measurements with very small ICs.

The number of publications summarised above shows that the measurement of small field profiles has been investigated quite extensively. However, it should be noted that most of the comparisons were carried out in the last five years and that the paper by McKerracher and Thwaites (1999) was published at the same time as the main bulk of the work. Film or a diode (particularly an unshielded diode) appear to be the most useful of the commercially available detectors. However, it has not yet been established exactly how much of an effect the silicon has on the measured penumbra.

4.1.5 Aim

An EFD and film have been recommended in several publications as the detectors of choice in the measurement of beam profiles. The primary aim of this work was to determine whether either of two previously unpublished detectors (pre 1999) had any advantages over these detectors in the measurement of profiles in collimators between 40 and 12.5mm diameter. These were a small stereotactic diode (0.6mm sensitive width) and a small (0.015cc) IC. The detectors were compared using penumbra widths and the width of the 99% region.

The second aim was to measure the width of the 99% high dose region in all stereotactic collimators and small open and MLC fields between 50x50 and 10x10mm^2. This information was used to remove the effects of volume averaging and determine the most suitable detector to use in the measurement of S_{cp} and S_c in Chapters 5 and 6. Measurements were therefore carried out in-air and in-phantom at dmax and 50mm.

4.2 Materials and Methods

4.2.1 Materials

All diodes, both cylindrical ICs and the PPIC were compared in the water tank. Film was used in solid water. The diamond was unavailable at the time of the original measurements and later found to be unsuitable for measurements in the Scanditronix tank due to the design and weight of the 'M' connector, which made it physically unstable in the detector holder. Although modifications could have been made to accommodate the detector, this was only considered necessary if the measurements with other detectors proved to be unsatisfactory.

4.2.2 Methods

Tank measurements

All detectors were initially compared on the CH6, in-water at 50mm deep, 1000mm FAD, in collimators between 40 and 12.5mm diameter. The reference detector was positioned in the same manner as for PDD measurements; within each stereotactic field on the CH6 and above the stereotactic collimators, within the open field, on the 600CD. On the CH6, care was taken to ensure that the reference detector was not positioned along the scan direction.

In-air and in-water profiles at dmax and 50mm, all 1000mm FAD, were measured with the most appropriate detector, in the above collimators and in the smaller collimators (10-5mm diameter) and in square fields between 50x50 and 10x10mm^2, formed by the movable collimators and the MLC. These results will be used to determine the effects of detector volume in Chapters 5 and 6. In-air measurements were made using a small RMI build-up cap without side scatter (build-up top), to minimise the phantom scatter. The diameter of the build-up top was equal to the diameter of the detector housing. The merit of this type of build-up will be discussed more fully in Chapter 6.

The cylindrical ICs were orientated with long axes perpendicular to the beam CAX. The diodes were only orientated with long axes parallel to the beam CAX, due to problems in attaching each detector to the detector holder. New attachments would have been designed if the resolution of the diodes in conventional orientation proved to be unacceptable. The centre of the sensitive volume of each detector was aligned with the beam CAX by repeatedly scanning beam profiles until the profiles along both axes were symmetrically aligned with the Inplane/Xplane zero co-ordinate.

Film measurements

Film orientated perpendicular to the beam was used in RMI, at 50mm deep only, 1000mm FAD. Originally the point densitometer (Tobias) was used to analyse the film results, but at a later date, a scanning densitometer (Vidar) was purchased. The maximum resolution on the Vidar is 300dpi. However, after scanning in the film, 1D profile information can only be extracted by selecting scan parameters. Although a step size of 0.2mm was selected for all scans, the smallest area over which the dose is averaged without introducing an unacceptable level of noise, is a square of side 1mm. As a result, the film acts as a detector with a 1mm sensitive width when read on either densitometer.

Data smoothing

OARs were measured on only one occasion. Where appropriate, the data was firstly averaged over both Inplane and Xplane axes and then averaged around the CAX. No smoothing was carried out, other than to ensure that the normalisation point on the CAX was representative of the maximum dose i.e. care was taken to ensure that the curves were not normalised to a "spike" caused simply by noise.

4.3 Results and Discussion

4.3.1 CH6 Measurements

Detector comparison

The Inplane and Xplane profiles were symmetrical and identical, within the experimental uncertainty, in all measured profiles in all stereotactic collimators. The profiles were therefore averaged over both axes and around the CAX. Figure 4.3 shows a plot of OAR against OAD in a 40mm collimator, with all detectors.

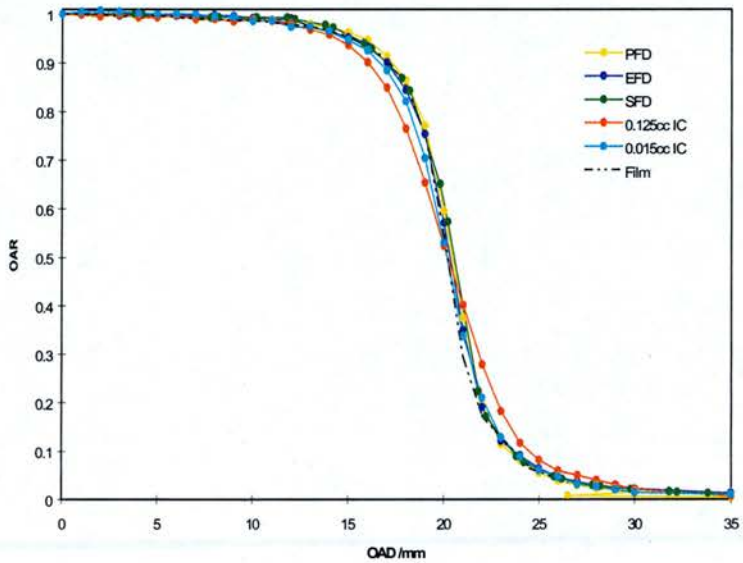

Figure 4.3. OARs measured on CH6 at 50mm deep, 1000mm FAD with a variety of detectors in the 40mm collimator.

All diodes and film measure the 10-90% penumbra to be 6.4mm. The 0.015cc IC measures 6.8mm and the 0.125cc IC 7.9mm. As expected, the ICs broaden the apparent penumbra. Although the 0.015cc IC improves the resolution, the dose is still slightly underestimated in the shoulder region compared with film. The distance between the 90% regions on the IC and film curves is of the order of 0.5r, where r is the internal radius of the chamber. Although it would therefore be appropriate to make the correction advised by Dawson et al (1986), film and the three diodes would seem to be the more practical detectors to use. The corresponding measurements in the 12.5mm collimator are shown in Figure 4.4.

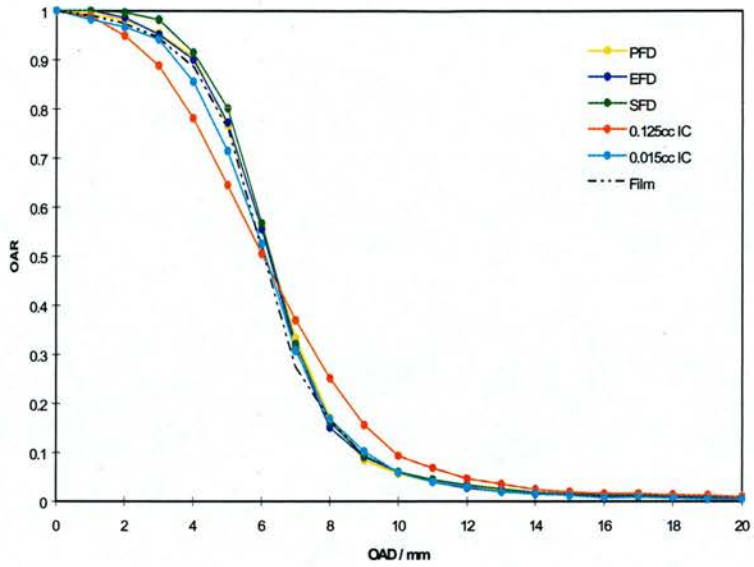

Figure 4.4. OARs measured on CH6 at 50mm deep, 1000mm FAD with a variety of detectors in the 12.5mm collimator

The 10-90% penumbra measured with all diodes and film is approximately 5.0mm. The 0.015 and 0.125cc ICs measured 5.5 and 7.0mm respectively. Again, the ICs are too large and broaden the penumbra and although corrections could be made, it is apparent that these detectors are not particularly useful for the measurement of small field profiles. The PFD, EFD and film are again well matched, although the SFD measures a slightly higher dose in the shoulder region. The most obvious reason for this is that the SFD has the smallest sensitive width, noting that film is acting as a 1mm detector. However, Westermark et al (2000) suggested that the silicon in diodes causes the penumbra to be underestimated.

In both collimators, the 90% regions were underestimated by approximately 3.5 and 1.5mm when measured with the 0.125 and 0.015cc ICs respectively. These differences are clinically significant in terms of choosing the appropriate collimator diameter for treatment.

In all of the above BDAS measurements, the resolution was sub-optimal, at 1mm. All subsequent measurements were carried out with a much smaller step size of 0.2mm. Although there were no differences between the profiles measured with the PFD and the EFD, the EFD was chosen for comparison with the SFD. This was also for consistency, as the EFD was shown to be better than the PFD in the measurement of PDDs (Chapter 3).

Small collimators

Towards the end of the use of the CH6, small collimators (10-5mm diameter) were obtained on loan from Radionics. A film scanner was also purchased at this time. Profiles were measured in the new collimators with the EFD, SFD and film. Profiles in the 12.5mm collimator were re-measured with a 0.2mm step size for comparison. The shape of the profiles both Inplane and Xplane were identical, within the experimental uncertainty and therefore all profiles were averaged across both axes and across both sides of the CAX. Figure 4.5 shows the results, including the original measurements with the EFD.

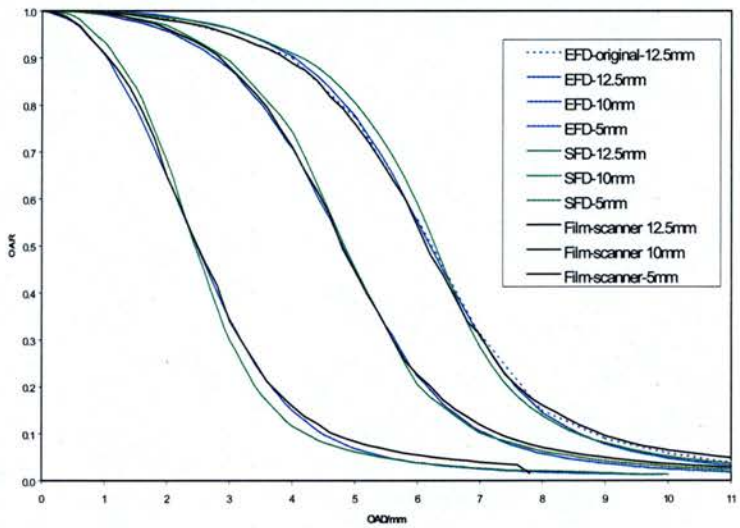

Figure 4.5. Profiles at 50mm deep in the 12.5, 10 and 5mm diameter collimators, measured with the EFD, SFD and Film.

Figure 4.5 shows firstly that, other than differences in resolution, there are no significant differences between the profile in the 12.5mm collimator measured at the time of the original detector comparison and that measured above. This is an indication of the reproducibility of the measurements. The use of the film scanner shows that the dose in the tails measured with film, matches that measured with the diodes. In all collimators the SFD produces the sharpest penumbra. This was also reported by Westermark et al (2000) and thought to be due to the enhanced response in silicon. Although this effect would also occur (to a larger extent) in the EFD, the authors found that the volume averaging in the larger diode cancelled out the enhanced response. The maximum difference between the 90% regions measured with the SFD and film or EFD is of the order of 0.3mm, which is not clinically significant within the overall experimental and patient set-up uncertainties.

The profiles measured with film are less sharp than those measured with the SFD because of the differences in effective sensitive width; 1mm for film and 0.6mm for the SFD. The

maximum spread in penumbra widths is <0.5mm in the 5mm collimator. Figure 4.6 shows Figure 4.5 zoomed in on the high dose region.

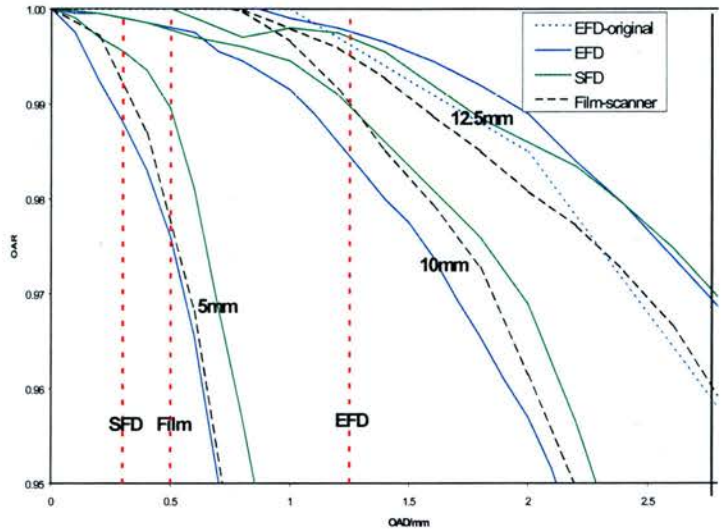

Figure 4.6. High dose regions in the 12.5, 10 and 5mm collimators extracted from Figure 4.5.

Superimposed on the curves in Figure 4.6 are red lines which represent half of the width of the sensitive area of the EFD (1.25mm), the SFD (0.3mm) and film (0.5mm). It is apparent that volume averaging should be insignificant for all detectors in the 12.5mm collimator. In the 10mm collimator, the EFD will be subject to a very small amount of volume averaging as it fits within the 99% isodose. In the 5mm collimator, film fits within the 99% isodose and the SFD within the 99.6%. As a result, the SFD and film could be used for measurements in any of the collimators, with a maximum under-response of less than 1%. The EFD could under-estimate the dose in the 10mm collimator by 1% and by up to 10% in the 5mm collimator, but will have a very minimal under-response in the 12.5mm collimator. The widths of the 10-90% penumbras, the 99% and 50% regions, measured with the SFD have been extracted from the results in Figure 4.5 and are shown in Table 4.2.

Collimator diameter /mm	10-90% /mm	20-80% /mm	99% /mm	50% /mm
40.0	6.5	3.5	21.0	40.2
12.5	4.4	2.4	3.4	12.6
10	4.2	2.4	2.4	9.6
5	3.0	1.8	1.0	4.8

Table 4.2. Penumbra widths and isodose widths extracted from Figure 4.5.

The precision in all measurements is +/-0.2mm. As expected, the penumbra width decreases with collimator diameter, due mainly to geometric penumbra. The width of the 99% high dose region again confirms that a small amount of volume averaging may occur with the

EFD in the 10mm collimator, but will definitely occur in the 5mm collimator. The SFD is suitable for measurements in all collimator diameters.

Although the measured diameter of the 5mm collimator is smaller than expected, this is likely to be due to positioning errors, in the direction perpendicular to the measurement direction. A misalignment of the centre of the detector sensitive area and the beam CAX will result in scans which are not across the main axes of the collimators. For example, a 0.2mm error in position will reduce the measured width of the 5mm collimator by 0.3mm. Although the detector origin was found by repeatedly scanning profiles in both directions, the uncertainty in the position is of the order of 0.2-0.3mm.

4.3.2 600CD detector comparison

Comparison with CH6

The EFD was used to measure all profiles in the standard collimators (40-12.5mm diameter). Figure 4.7 shows a comparison of profiles in the 40 and 12.5mm collimators measured on both the CH6 and 600CD, with the EFD at 50mm deep, 1000mm FAD.

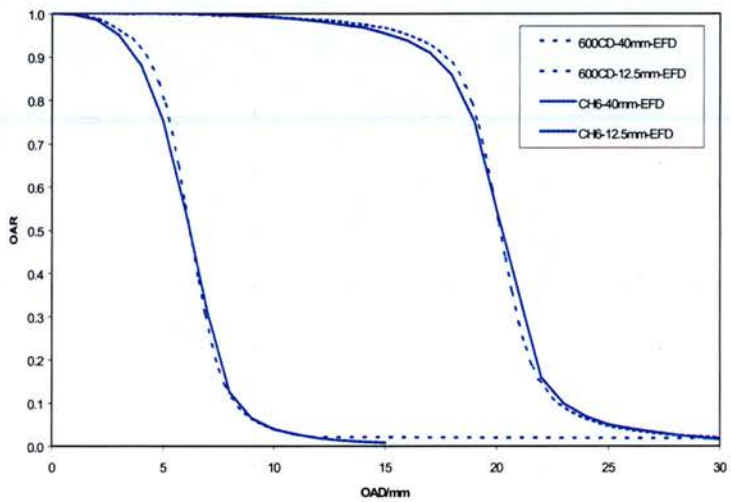

Figure 4.7. Profiles measured in the 40 and 12.5mm collimators on both the CH6 and 600CD, with the EFD at 50mm deep, 1000mm FAD

Although the penumbra appears smallest on the 600CD, the difference is <1.0mm and could be due to experimental uncertainties, or differences in focal spots. In theory the spot size should be smaller on the CH6 due to the 270° bending magnet, but this may not be the case.

Small collimators

Profiles were measured in the smallest collimators with the EFD, SFD and film. At this time, the performance of the detector movement mechanism in the original BDAS system began to deteriorate and differences were noted between the Inplane and Xplane profiles in the smallest collimators. Figure 4.8 shows an example for the 5mm collimator at dmax.

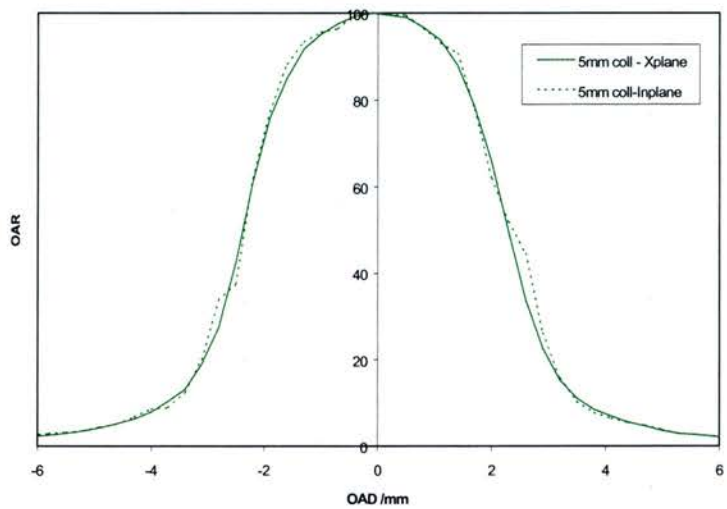

Figure 4.8. Inplane and Xplane profiles in the 5mm collimator, measured with the SFD at dmax, 1000mm FAD.

The difference in noise in the Xplane direction is due to the movement and mounting of the field detector. In the Inplane direction, the detector is driven along rails running parallel to the measurement axis, via a belt. This is a relatively smooth movement. In the Xplane direction, the detector remains stationary and the whole mounting mechanism is driven across the tank. This movement is slightly more "jumpy". The corresponding increase in noise in the Xplane direction only becomes noticeable in the smallest field sizes. As a result, only the Inplane profiles were considered in detail, for the smallest collimators.

Figure 4.9 shows the Inplane profiles at 50mm deep, 1000mm FAD in the 10 and 5mm diameter collimators, on the 600CD. Profiles in the 12.5mm were re-measured with a 0.2mm step size for comparison with the original measurements.

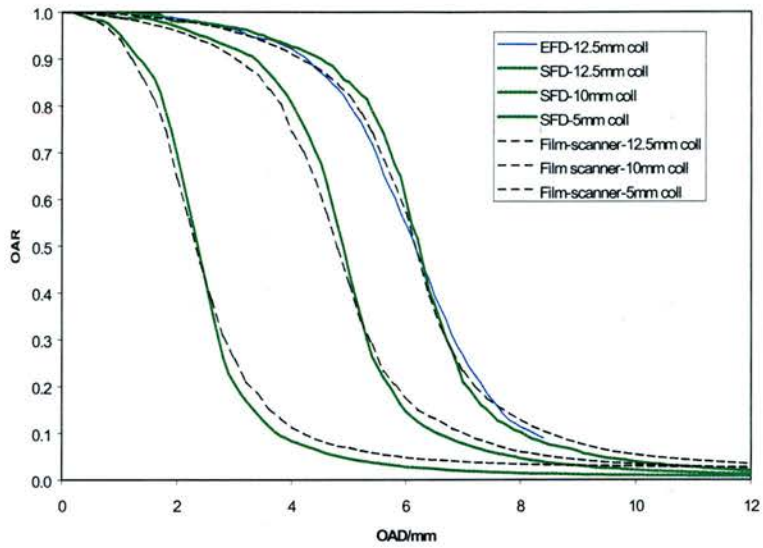

Figure 4.9. Profiles at 50mm deep, 1000mm FAD in the 12.5, 10 and 5mm diameter collimators, on the 600CD

The SFD again measures the sharpest penumbra. Table 4.3 shows the widths of the penumbras and the 99 and 50% regions, in the 40, 12.5, 10 and 5mm diameter collimators and compared with the CH6.

	Penumbra widths /mm				Isodose widths /mm			
Coll. /mm	600CD 10-90%	c.f. CH6 /mm	600CD 20-80%	c.f. CH6 /mm	600CD 99%	c.f. CH6 /mm	600CD 50%	c.f. CH6 /mm
40	5.2	-1.3	2.7	-0.8	21.6	+0.6	40.3	+0.1
12.5	3.5	-0.9	1.7	-0.7	3.4	0	12.4	-0.2
10	3.2	-1.0	1.7	-0.7	2.5	+0.1	9.6	0
5	2.4	-0.6	1.3	-0.5	1.0	+0.1	4.6	-0.2

Table 4.3 Penumbra and isodose widths extracted for a selection of collimators measured on the 600CD, at dmax and compared with the CH6.

All differences in penumbral width between the two machines are of the order of 0.5-1.0mm and as they appear to be consistent, it suggests that the effect is real.

4.3.3 In-air / in-phantom profiles

Overview

The width of the 99% high dose region measured at dmax and 50mm is important to determine the maximum detector diameter for S_{cp} measurements at the two depths, in Chapter 5. The shape of in-air profiles in small fields has only previously been presented by

Rice et al (1987), but was not discussed. The width of the 99% high dose region in-air will determine the maximum detector diameter for use in the measurement of S_c in Chapter 6.

The SFD was used in all measurements to limit the amount of volume averaging. Although the use of a diode has been thought to underestimate the penumbra, the effect is likely to be minimal for the 0.6mm silicon chip. A small RMI build-up top, without side scatter, was attached to the SFD for measurements in-air. The merit of this build-up is discussed in Chapter 6. In-air and in-phantom measurements were carried out in all stereotactic collimators and small open and MLC fields between 50x50 and 10x10mm^2.

Stereotactic collimators

As the Inplane profiles were less noisy than the Xplane, only Inplane profiles were averaged over both sides of the CAX. Figure 4.10 shows the mean in-air and in-phantom profiles at dmax and 50mm deep in the 20 10 and 5mm collimators.

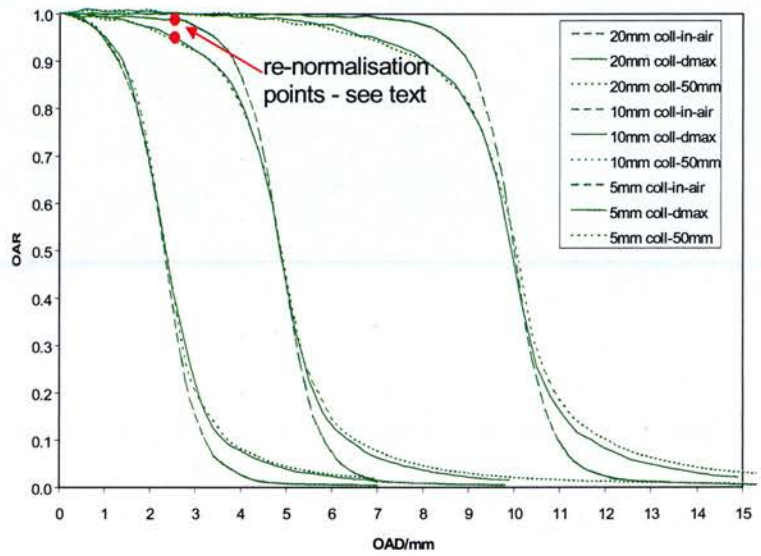

Figure 4.10. In-air and in phantom profiles at dmax and 50mm deep.

The difference in profile shape between the in-air and in-phantom profiles in the 20mm collimator is immediately apparent. The penumbra is sharper and the width of the high dose region is wider, as also shown by Rice et al (1987), but not discussed. Although changes in phantom scatter have no significant effect on the width of the penumbra as the depth is increased, lack of phantom scatter in an in-air measurement will reduce the penumbra. The effect is not apparent in the 5mm diameter collimator due to differences in normalisation. For example, if the penumbra in the 10mm collimator is shifted to the beam CAX and

renormalised at the position of the red dots in Figure 4.10, the wider high dose region in the in-air profile effectively disappears, as shown in Figure 4.11.

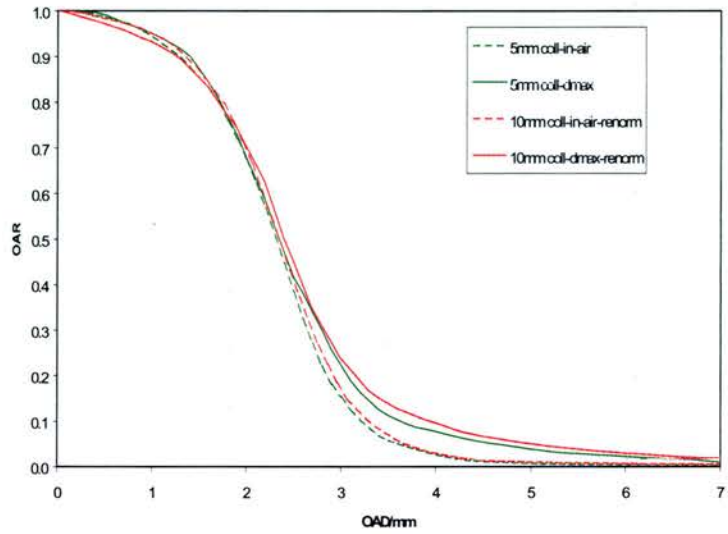

Figure 4.11. Comparison of measured in-air and dmax in-water profiles in the 5mm collimator, with profiles extracted from the 10mm collimator penumbra.

The 10mm renormalised profiles match those in the 5mm collimator, allowing for the actual differences in penumbra (<0.5mm) between the two collimator diameters. Table 4.4 summarises the penumbra, 99 and 50% widths for the in-air and in-phantom profiles.

Collimator diameter /mm	Profile type	10-90% /mm	20-80% /mm	99% /mm	50% /mm
20	in-air	2.0	1.2	14.4	20.2
	dmax	3.7	1.8	8.8	20.0
	50mm	4.1	1.9	9.4	20.0
12.5	in-air	2.0	1.2	6.6	12.4
	dmax	3.5	1.7	3.4	12.4
	50mm	3.5	1.7	3.5	12.4
10	in-air	2.0	1.2	4.1	9.6
	dmax	3.2	1.7	2.5	9.6
	50mm	3.1	1.5	1.7	9.6
5	in-air	1.8	1.1	0.8	4.6
	dmax	2.3	1.4	1.0	4.6
	50mm	2.4	1.3	0.7	4.6

Table 4.4. Penumbra and the widths of the 99 and 50% isodoses, in-air and in-phantom at dmax and 50mm, extracted from Figure 4.9.

The in-phantom penumbra decreases with collimator diameter, but does not increase with depth. There is a small increase in phantom scatter in the tails at 50mm deep, of the order of

2% in the 20mm collimator, also found by Rice et al (1987). This effect is not apparent in the 5mm collimator, as the phantom scatter is less significant in smaller diameters.

Open fields

In all open field measurements with the BDAS, the reference detector had to be placed within the field. To minimise perturbation of the beam at the phantom surface the reference was attached to the face plate of the linac head and positioned in the corner of the field to minimise the effect on measurements across both axes. Figure 4.12 shows the in-phantom Inplane and Xplane profiles measured at dmax only in the 20x20 and 10x10mm^2 fields. The results have been meaned across both sides of the CAX.

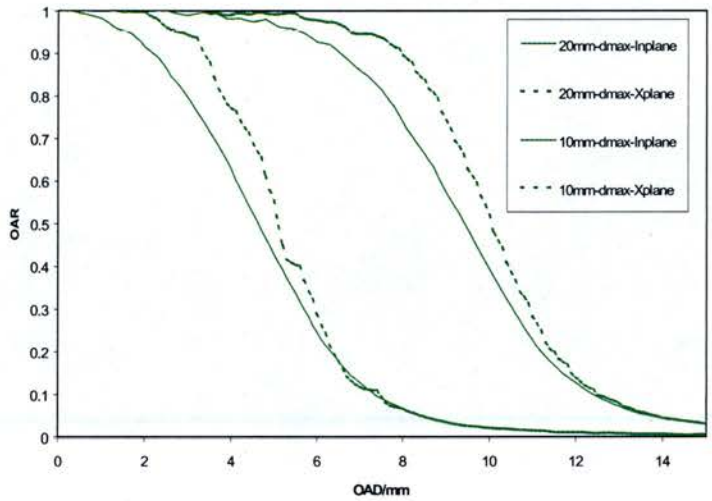

Figure 4.12. The Inplane and Xplane profiles measured at dmax in the 20x20 and 10x10mm^2 fields

Once again the Xplane profiles are noisier than the Inplane, due to the control of the BDAS movement. On reflection, the linac head could have been rotated through 90° to measure Xplane profiles without the effect of the BDAS positional uncertainties. The Inplane penumbra is wider than the Xplane, by approximately 1mm, because of the increased geometric penumbra in the direction of the upper, Y movable collimators. Although the field width in the Xplane direction is approximately 1mm wider than that inplane, the field size settings are within the Varian specification (+/- 2mm). Film tests of the settings on the movable collimators showed the reproducibility to be +/-1.0mm. Figure 4.13 shows Inplane profiles in-air and in-phantom at dmax and 50mm.

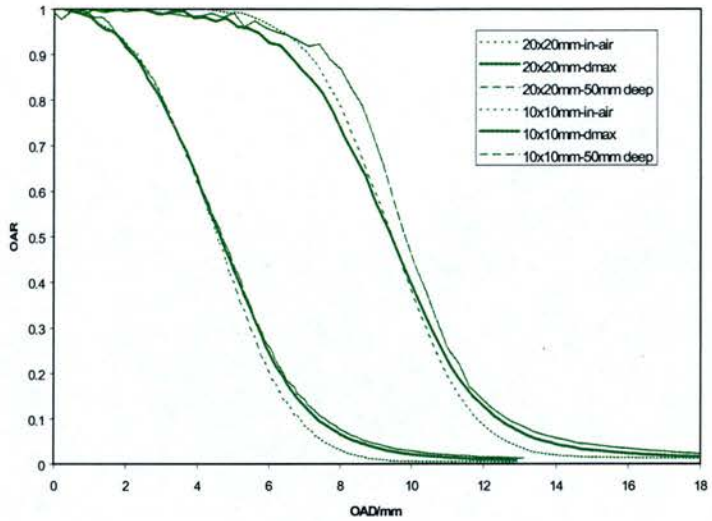

Figure 4.13. Inplane profiles in-air and in-phantom at dmax and 50mm

Although the width of the 20x20mm^2 Inplane profile in Figure 4.13 is approximately 1mm wider at 50mm deep than at dmax, each profile was measured at a different time, with the same nominal field size setting. This was because, for isocentric measurements, it was easier to measure all field sizes at dmax, followed by all field sizes at 50mm and all field sizes in-air, rather than change the tank FSD in between measurements. As a result, the difference in field widths represents differences in field size setting. The widths of the penumbras, 99 and 50% regions are summarised in Table 4.5.

Field size/mm^2	Scan direction	Profile type	10-90% /mm	20-80% /mm	99% /mm	50% /mm
20x20	Inplane	in-air	5.2	3.0	10.6	18.9
		dmax	5.3	3.9	5.9	18.9
		50mm	5.0	3.7	6.1	19.9
	Xplane	in-air	3.4	2.3	13.6	20.4
		dmax	4.6	2.7	10.9	20.1
		50mm	5.1	2.9	10.3	19.8
10x10	Inplane	in-air	4.6	3.0	1.7	9.1
		dmax	5.2	3.6	1.4	9.3
		50mm	5.4	3.4	1.9	9.4
	Xplane	in-air	3.5	2.3	4.6	10.4
		dmax	3.9	2.6	4.2	10.2
		50mm	4.3	2.6	4.1	10.3

Table 4.5. Summary of the widths of the penumbras and the 50% regions in open fields.

The penumbra in the 10x10mm^2 field is larger than that measured in the 10mm diameter collimator, by between 0.5 and 1.0mm in the Xplane direction and 1.5 and 2.0mm Inplane. This is indicative of the improvement in penumbra produced by the tertiary collimators.

The high dose regions are also wider in the open fields compared with the stereotactic fields. The 99% region is wider in-air in the 20x20mm^2 field, but not in the 10x10mm^2 field, again because of normalisation within the penumbra. In-air measurements in the 20x20mm^2 field can therefore be carried out using a larger detector than in in-water measurements.

MLC fields

The reference detector again had to be placed within the beam for all MLC measurements with the BDAS. Figure 4.14 shows the Inplane and Xplane profiles measured at dmax in the 20x20 and 10x10mm^2 fields.

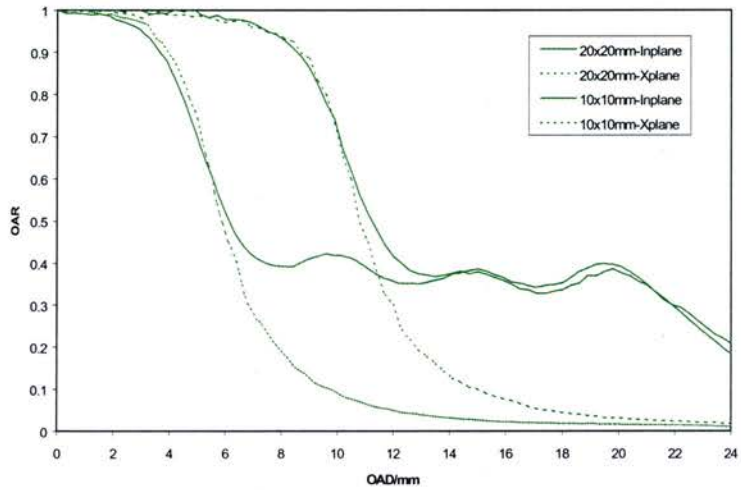

Figure 4.14. Inplane and Xplane MLC profiles measured only at dmax in the 20x20 and 10x10mm^2 fields

It is immediately obvious that the dose is very much higher in the ostensibly low dose region in the inplane direction. This is because the Inplane profiles have been measured through the opposing leaf ends, which have a gap of 0.2 mm between them when in the "closed" position. In addition, the rounded design of the leaf ends will cause some additional transmission and also increase the dose in this region. This will not normally occur in the clinical situation, as the movable collimators will be set close to the MLC field size, whereas in the above measurements, the movable collimators have been set to a constant 50x50mm^2. However, it is important to note that this will need to be accounted for in IMRT fields as the field size will be set to the largest portal defined by the MLC.

The noise is once again higher in the Xplane direction, for the same reasons as before. The width of the high dose region is again narrower in the inplane direction. Inplane scans for the 20x20 and 10x10mm^2 MLC fields are displayed in-air, dmax and 50mm in Figure 4.15.

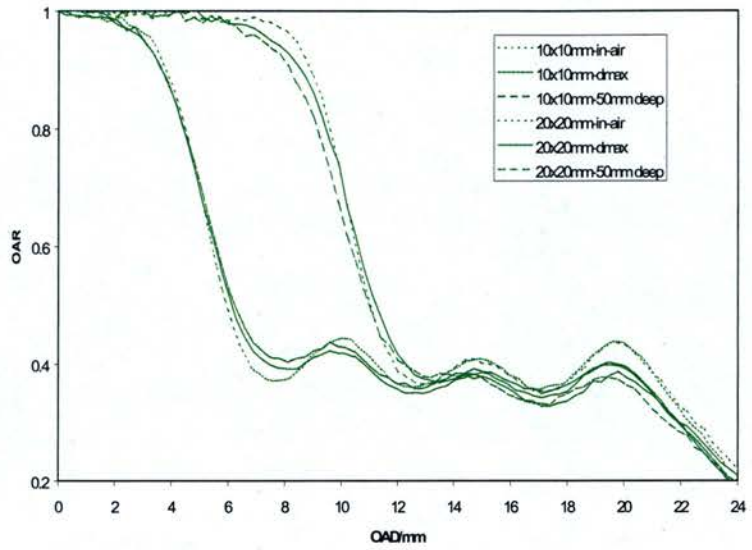

Figure 4.15. Inplane scans for the 20x20 and 10x10mm^2 MLC fields measured in-air, dmax and 50mm.

Table 4.6 summarises the widths of the penumbras and the 50% regions.

Field size/mm^2	Scan direction	Profile type	90-10% /mm	80-20% /mm	99% /mm	50% /mm
20x20	Inplane	in-air	-	-	14.8	21.9
		dmax	-	-	10.0	22.0
		50mm	-	-	10.0	22.1
	Xplane	in-air	4.6	2.5	14.8	21.8
		dmax	6.5	3.5	6.8	21.6
		50mm	6.8	3.8	7.6	21.9
10x10	Inplane	in-air	-	-	4.7	11.9
		dmax	-	-	3.8	12.3
		50mm	-	-	3.4	12.5
	Xplane	in-air	4.5	2.6	3.5	11.8
		dmax	5.9	3.2	3.1	11.7
		50mm	6.3	3.3	3.6	12.0

Table 4.6. Summary of the widths of the penumbras and the 50% regions measured in MLC fields.

Compared with open field profiles in the crossplane direction, the crossplane MLC penumbra is wider. Although the geometry (MLC is closer to the phantom) suggests that the crossplane penumbra should be smaller than that for open fields, the rounded ends of the MLC leaves broaden the penumbra, due to transmission and scatter, particularly in the low dose region. The widths of the 50% regions are between 1.6 and 1.9mm wider than the field size settings, due to the transmission through the leaf ends (Wang et al, 1996). The widths of the high dose regions will be examined more closely in Chapters 5 and 6.

Comparison of beam defining systems

The high dose regions in the Inplane direction of fields of 10mm width defined by each beam defining system are shown in Figure 4.16.

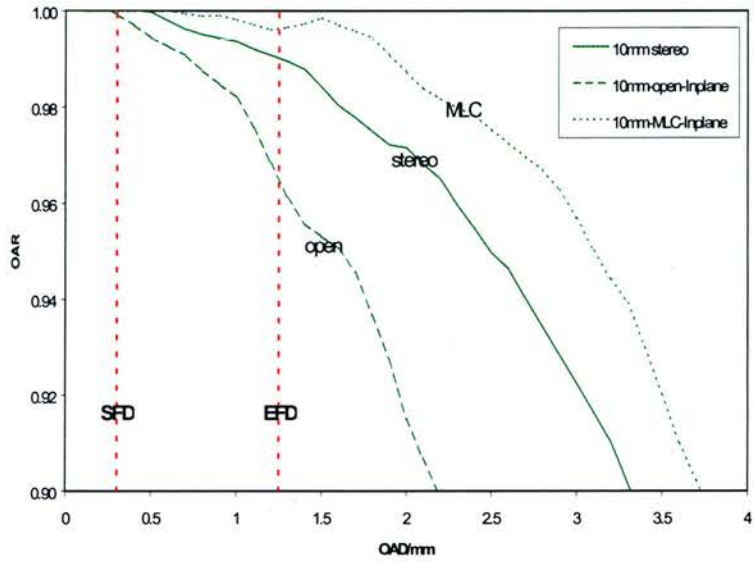

Figure 4.16. Profiles at dmax in a 10mm stereotactic collimator and Inplane profiles in open and MLC fields of 10mm width.

The red lines represent half of the width of the EFD and SFD. It is apparent that the high dose region is widest in the MLC field and narrowest in the open field. This is because the MLC 10x10mm^2 field is wider than the open field and because of geometric and scatter effects caused by the increased distance of the MLC from the source. It is also apparent that although the EFD may not under-respond in either the open or stereotactic 10mm width fields (sensitive width intersects 99-100% regions), it will under-respond in the open field (sensitive width intersects the 96% region approximately). Figure 4.17 shows the corresponding results in the Xplane direction.

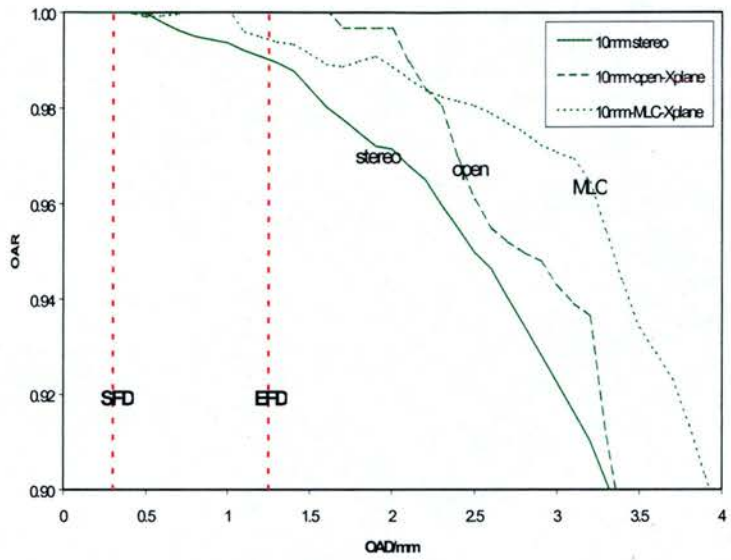

Figure 4.17. Profiles at dmax in a 10mm stereotactic collimator and Xplane profiles in open and MLC fields of 10mm width.

In the Xplane direction, the high dose region is wider in the open and MLC fields and all detectors should fit within the high dose regions. The difference between the widths of the high dose regions in the Inplane and Xplane directions is caused by the effects of geometric penumbra and changes in scatter due to the fact that the Y collimators (Inplane) are nearer the source than the X collimators (Xplane).

4.3.4 XKnife data

The data required for input to the XKnife TPS was measured with the EFD on each linac, in collimators between 40 and 12.5mm diameter. XKnife requires the input of only one profile at a depth of 50mm, 1000mm FAD. The profile at any other depth is obtained by scaling the off axis distance at the point of interest, to an equivalent distance at the isocentre. In effect, XKnife assumes that the change in profile with depth is only dependent on the geometric divergence and not on changes in scatter, as shown by Rice et al (1987) and in the work described above. The final data for the 600CD is presented in Appendix 2.

4.4 Conclusion

The PFD, EFD, SFD and film have all been shown to be suitable detectors for measuring the profiles in collimators with diameters >12.5mm. The SFD has been shown to resolve the penumbra slightly better than the other detectors in the 12.5mm collimator. The largest

difference is in the high dose region, where the SFD measures isodoses which are wider by approximately 0.3mm at the 90% level. However, as this difference is not significant for clinical stereotactic treatments in collimators between 40 and 12.5mm diameter, it can be concluded that any of these four detectors can be used to measure the beam profiles in these collimators. Film is the simplest detector to use and it avoids the problem of aligning the detector with the beam CAX. However, it should be read out on a scanning densitometer. The SFD is the most suitable detector for measuring profiles in fields <12.5mm diameter as the PFD and EFD will broaden the penumbra due to volume averaging, but by <0.5mm. Although film was also shown to broaden the penumbra, the use of a different scanner, processor, or type of film, could allow the dose to be averaged over a smaller area.

The penumbra has been shown to be narrower and the high dose regions wider, for in-air measurements in all stereotactic collimators >=10mm diameter and all square fields other than an open $10x10mm^2$. It is apparent therefore that a larger detector could be used in the in-air measurements compared with in-phantom measurements, due to the wider high dose region. Data extracted from the in-air profiles will be used in the measurement of head scatter factors in Chapter 6. In-water profiles are identical, within the experimental uncertainty, at both dmax and 50mm, which confirms that changes in phantom scatter do not significantly affect the beam profile at different depths. In-water profiles will be used to determine optimal detector width in the measurement of total scatter factors in Chapter 5.

Chapter 5

Relative output factors

5.1 Introduction

5.1.1 Definition

The dose at a depth in any given field size, can be related to the dose in the reference field, at the same depth and FSD, using a relative output factor. This is frequently known as a total scatter factor and denoted by S_{cp}. S_{cp} is defined as the ratio of the dose (D) in the field size of interest (s) to the dose (D_{ref}) in the reference field size (s_{ref}), for both measurements made at depth (d) and distance (f), in a full scatter phantom for the same number of MU.

$$S_{cp}(s) = \frac{D(f, s, d)}{D_{ref}(f, s_{ref}, d)} \qquad (5.1)$$

Historically, the most common formalism employs relative outputs measured at dmax and normalised to a 100x100mm^2 field at 1000mm FSD. This is the formalism currently adopted in the ECC. Some formalisms, based on a reference depth other than dmax, require S_{cp} values which are measured at a greater depth. Commonly, this can be 50, 80 or 100mm. S_{cp} is depth dependent and therefore the chosen measurement depth must be consistent with the rest of the formalism and data used. Formalisms based on isocentric geometry may require S_{cp} to be measured at 1000mm FAD. Again, this must be internally consistent with the rest of the planning data.

5.1.2 Measurement of S_{cp}

Regular fields

Relative output factors are measured for a range of square and rectangular fields for entry into the TPS, tabulation and use in a MU check program. If the response of the detector used is the same in the field size of interest and in the reference field, the correction factors required to convert the detector readings to dose, cancel out. As a result, the ratio of readings can be used. This assumption is generally taken to hold within the experimental uncertainty, for the normal range of field sizes.

Relative output factors should be measured at a selection of FSDs to determine whether the ISL is preserved. This will depend on the linac head design. If the ISL is not preserved, then tables of S_{cp} at different FSDs will be necessary. Relative outputs in field shapes which are non-square, or non-rectangular, are equal to the relative output measured in the EQSQ. Collimator exchange effects are generally minimal for most routine treatments, but for elongated fields, the output in a field with the long axis defined by the X collimators should be compared against that defined by the Y collimators. If significant differences exist (>2%), then independent sets of output tables may be necessary.

Irregular fields

The calculation of relative output is more complex for irregular fields, such as those which are asymmetric, or incorporate blocks, MLC etc. Although the primary dose is constant at a given depth, the head scatter dose is dependent on the machine design and beam defining system. The phantom scatter dose is generally assumed to be dependent only on the irradiated volume, as widely confirmed by measurements in the normal range of field sizes.

One method of calculating the dose in an irregular field is to separate out the head and phantom scatter doses. Holt et al (1970) achieved this by defining a collimator (head) scatter factor (S_c) and a phantom scatter factor (S_p), such that:

$$S_{cp} = S_c \times S_p \qquad (5.2)$$

S_c is dependent primarily on the setting on the movable collimators, but also on the beam defining system, whereas S_p is dependent only on the beam area at the surface.

Another approach, also discussed by Holt (1970), is to use dose, rather than relative output, as described in equation 5.3.

$$\text{Dose} = P_o + \sigma(c) + \sigma(p) \qquad (5.3)$$

P_o is the primary dose, $\sigma(c)$ is the head scattered dose and $\sigma(p)$ is the phantom scattered dose. More complex methods, such as convolution (Mackie et al, 1985; Mohan et al, 1986) can also be used. The most common approach (equation 5.2) is adhered to in this work.

Detectors

An IC is the detector of choice for measurements of relative output in the normal field size range. Although a 0.6cc cylindrical chamber is most commonly used to measure data in

conventional field sizes, the minimum field size in which this can be used without significant volume averaging occurring, is a 40x40mm^2 field.

For simplicity and reproducibility, relative outputs are generally measured in solid water, although water equivalence should be checked at each beam energy. If relative outputs are measured in water, then the 0.6cc IC, if used, must be enclosed in a waterproof sleeve.

Diodes have also been investigated for the measurement of relative outputs. Karlsson et al (1997) compared an unshielded and shielded diode with a 0.5cc IC in the measurement of relative outputs at dmax and 100mm deep in beams of between 4 and 50MV. All results were normalised to a 100x100mm^2 field. The unshielded diode overestimated the relative output in a 400x400mm^2 field by approximately 7.5% at 100mm deep and 2.8% at dmax in beams between 4 and 6MV. The use of the energy compensated diode reduced the overestimation to 2.4 and 0.7% respectively. In fields < 100x100mm^2 the results were virtually indistinguishable, but the spread over all detectors in the 40x40mm^2 appeared to be of the order of 0.7%. The IC was lower than the two diodes, due to volume averaging.

5.1.3 Small field problems

Volume averaging

One of the main problems with the measurement of S_{cp} in small fields is that a 0.6cc IC is generally too large to use in fields <40x40mm^2 as the effect of volume averaging will obviously become more significant as the field size is reduced. In order to determine whether or not a particular detector is suitable for measurements in that field size, the beam profile should be scanned in similar conditions (depth, FSD, phantom) and the width of the high dose region determined. An ideal detector should have a sensitive width which lies within this high dose region, suggested to be the 99% region in Chapter 4. Although Karlsson et al (1997) have shown that diodes are more suitable than an IC in a 40x40mm^2 field, the use of diodes in smaller fields requires further investigation.

Lack of LEE

Lack of LEE will affect small field measurements in non-water equivalent materials, due to changes in the electron range. If LEE does not exist at a particular point in water, the use of a high density material may actually cause LEE to be achieved. Conversely, the use of a low density material will increase the electronic disequilibrium. This will primarily affect measurements carried out with silicon diodes and ion chambers.

Spectral changes

As discussed in Chapter 1, an x-ray beam is composed of a range of photon and electron energies. As the field size decreases, the number of low energy particles will decrease and the beam will be composed primarily of photons which have been filtered through the thickest part of the flattening filter. However, if stereotactic collimators are used, there will be additional low energy photons within the beam (Sanchez-Doblado et al, 2003). These differences may affect measurements with an energy dependent detector. However, if the measurements with the energy dependent detector are normalised to the largest small field size (e.g. 40mm collimator), the effects will be minimised. The results can then be normalised to the reference field ($100x100mm^2$) using a larger, energy independent detector.

In addition, the assumption that the ratio of detector readings is equivalent to the ratio of doses may begin to fall down at small field sizes. The correction factors necessary to convert the readings to dose may not be the same in both the field size of interest and the reference field, due to spectral changes. Although some dosimetric data has been shown to be the same in small and large fields for measurements carried out in ICs (Verhaegen et al, 1998; Sanchez-Doblado et al, 2003), it has not be shown for measurements with other detectors, such as diodes. This problem can however be minimised by normalising all small field measurements to the largest small field, then separately normalising the results to the reference field.

Rapid fall off

As will be shown in the literature review, S_{cp} drops rapidly at very small field sizes. The magnitude of this drop may be dependent on the detector used, or the type of linac investigated. Care must be taken to ensure that the measured outputs are a reflection of the true scatter conditions in each field size and not a result of the measurement technique used.

5.1.4 Small field S_{cp} in the literature

Literature overview

Unless otherwise stated, all of the following references report on S_{cp} measured at dmax, 1000mm FAD, relative to a $100x100mm^2$ field. Most measurements have been carried out at 1000mm FAD, primarily because many small field planning systems are based on an isocentric formalism, particularly if designed for arc therapy.

At the time of the commissioning of the stereotactic system on the CH6 linac (1994), only a few papers were available in which detectors had been compared in the measurement of S_{cp}.

Houdek et al (1983) used only TLD-100 ribbons for square fields between 30 and 10mm width on a 10MV Toshiba-LMR and found a 24% drop in S_{cp} at the smallest field. Arcovito et al (1985) also used only TLDs to measure S_{cp} at dmax on a 9MV CGR-Neptune, and noted a total drop in S_{cp} of 16% between the 100x100 and 10x10mm^2 fields.

Rice et al (1987) were the first to measure S_{cp} with ICs of different volumes and compare the effects of volume averaging. Measurements were carried out in collimators between 40 and 12.5mm diameter, on a 6MV Varian Clinac 2500. Volume averaging was accounted for by extrapolating the S_{cp} measurements to zero detector size. The corrected results were within 0.5% of MC (EGS4) calculations and showed a 12% drop in S_{cp} between a 100x100mm^2 field and the 12.5mm diameter collimator.

Serago et al (1992) also compared several ICs, a diode (type unspecified) of 2mm sensitive diameter, 3mm wide TLD chips and Kodak XV-2 film on a 6MV Varian Clinac 2500. The ICs were found to be too large in the smallest fields, but the diode, TLDs and film agreed to within 3% in an 8mm diameter collimator, where the total drop in S_{cp} was almost 30%.

As a result, at the start of the commissioning (1994), the only detectors which had been tested for small field outputs, were several ICs, which required a correction for detector size, TLD, film and an unspecified type of diode. TLDs and film had generally been used because of their small size, but the reproducibility was not reported on by any authors. As a result, several ion chambers and three types of diode were tested in this work as part of the commissioning process.

Gotoh et al (1996) used a 0.009cc micro-IC and Kodak X-Omat V2 film to measure S_{cp} in circular collimators down to 3.3mm diameter, on a 10MV Varian Clinac 2100. The agreement was within 2.2% for fields down to 8.3mm diameter, where the total drop in S_{cp} was just over 50%. Only film was used in the 3.3mm diameter field, in which the total drop in S_{cp} was 65%. No statistical uncertainty was given for the film. The authors recommended that a diode or diamond should also be tested.

Fan et al (1997) compared 0.6 and 0.1cc ICs, Kodak X-Omat XV-2 film, TLD chips (3mm diameter, 0.4mm thickness) and TLD rods (1mm diameter, 3mm long), on a 6MV Varian Clinac 1800. Although the ICs were too large in fields <15mm diameter, film and TLD agreed to within 2.5% in all fields down to 5mm diameter, where the total drop in S_{cp} was just over 30%. The standard deviation on the TLD chips was +/-3%, but no reproducibility

was given for the film. Indeed, it is unclear which detector results were presented as the final table of S_{cp} values.

Dasu et al (1998) compared several different detectors at a depth of 100mm, on a 6MV Varian Clinac 2300C/D. These were, a prototype parallel plate LIC (sensitive diameter = 3mm), a prototype parallel-plate air-filled IC (PPIC, sensitive diameter = 20mm) and both a photon and an electron diode (sensitive diameters = 2.5mm). Although the PPIC proved to be too large in small square fields, the spread over all other detectors was only 3% in the $5x5mm^2$ field, where the total drop in S_{cp} was of the order of 50%. The highest value of S_{cp} was measured with the photon diode, which the authors attributed to a change in the beam spectrum caused by the tungsten shield, resulting in an over-response in the diode. The LIC and electron diode were in good agreement. As the LIC is energy independent, the match with the electron diode suggests that it too is energy independent in small fields.

Francescon et al (1998) compared radiographic and radiochromic film, a 1.6mm diameter parallel plate micro-chamber (PP-MC), 0.5mm diameter MOSFET, TLD-800 microcubes and MC BEAM, in field diameters between 19 and 4.4mm. Measurements were carried out on a 6MV Siemens Mevatron. A correction factor (F), was calculated for each detector using MC BEAM, to account for detector size and composition and these factors were applied to each set of results. The reproducibility at 2 s.d. was 2-3% for both types of film, 2-4% for TLD, up to 4% for MOSFETs, up to 1% for the ICs and <0.5% for MC. Both types of film and the TLDs agreed with BEAM, which showed just over a 50% drop in S_{cp} in the 4.4mm diameter collimator. The PPMC was found to underestimate S_{cp} due to volume averaging and the MOSFET over-estimated. The authors stated that this was due to an increase in the fraction of scattered electrons from the silicon as the field size decreases.

Verhaegen et al (1998) used BEAM (EGS4) to calculate Scp at both dmax and 50mm deep in stereotactic fields on a 6MV Varian Clinac-600SR. The calculations were normalised to the 40mm diameter collimator. The total drop in S_{cp} between the 40mm diameter collimator and the 5mm, was almost 30% at dmax and 34% at 50mm deep.

As a result, by the time of the publication of the ECC results (1999), several types of detectors had been tested, as outlined above. However, accurate results could only be obtained using ICs with corrections based on volume averaging, or using film or TLD, with a rigorous calibration method. McKerracher and Thwaites (1999) reported on a comparison between commonly available detectors (0.125cc cylindrical ICs, a 5mm diameter PPIC, photon and electron diodes of 2.5mm sensitive diameter) and two new detectors which had

not yet been published. These were a small (0.6mm sensitive width) unshielded diode and a 0.015cc IC. Measurements were carried out on a 6MV BBC CH6 in collimators between 40 and 12.5mm diameter. These measurements will be presented in the results section.

Wierzbicki & Bissonnette (1999) used only a 2.5mm diameter photon diode in collimators between 40 and 10mm diameter and reported a 16% fall off in S_{cp} in a 10mm diameter collimator. Measurements were carried out on a Philips SL75 and although the energy was unspecified, this was likely to have been 5MV.

Westermark et al (2000) were the first to test the 0.004cc diamond to measure S_{cp} in small fields, between 18 and 4mm diameter. Measurements were carried out on 6 and 18MV beams of a Varian Clinac 2100C. The diamond was compared with two 0.6mm diameter unshielded diodes, one with a single chip and one prototype with a double chip, a 1mm diameter plastic scintillator and a prototype 1.5mm diameter LIC, all at 100mm deep. In the 4mm collimator, in the 6 and 18MV beams, the spreads over all detectors were 7 and 5% respectively, with total fall offs of approximately 45 and 30% respectively. The highest values of S_{cp} were measured with the double chip diode and the smallest with the diamond. The authors explained that unshielded diodes suffered from two counter-balancing effects in small fields; the over-response to scatter in field sizes >40x40mm^2 (Rikner 1985) and the over-response in small fields due to the higher atomic number of silicon. As the over-response to scatter is greater in a 100x100mm^2 field compared with a 40x40mm^2 field, this will cause the resulting value of S_{cp} to be too low (if normalised to the 100x100mm^2 field). The over-response due to the high-Z will be greater in a small field without LEE, because LEE may be preserved. This will result in a value of S_{cp} which is too high. The diamond was found to underestimate S_{cp} in the smallest fields, due to volume averaging effects. The size of this diamond, manufactured by Riga, appears to be particularly large. The thickness is quoted as 0.29mm, which implies that the width of the sensitive volume is approximately 4mm. The LIC and scintillator agreed to within 2%. The authors recommended that to minimise the errors caused by the different responses of each detector in larger fields, small field measurements should be normalised to the largest circular field rather than the reference 100x100mm^2 field.

Zhu et al (2000) measured S_{cp} in collimators down to 5mm, using two types of unshielded diode, on a 6MV Varian Clinac 2300CD. Although one incorporated a 2mm diameter chip and the other a 1mm chip, there was a maximum difference of only 1% in all collimators down to 5mm diameter, where the total fall off was approximately 35%. The authors explained that although the 2mm diode is physically too large in the smallest field, it has a

higher than expected response due to the preservation of LEE in silicon. Conversely, although a smaller diode is more likely to be positioned correctly within the high dose region, the precisional advantage is reduced because LEE is not preserved, resulting in a lower response than expected. It was somewhat fortuitous therefore that both diodes produced similar results.

Martens et al (2000) examined the use of the PTW PinPoint (0.015cc) IC to measure beam parameters in IMRT field segments, on 6 and 18MV beams of an Elekta Sli-plus. When compared with the diamond (long-axis perpendicular to beam CAX), in the water tank, the PinPoint (long axis parallel to beam CAX) produced values of Scp which were too low by almost 2% in a 100x10mm^2 field formed by the MLC. This was thought to be due to the over-response of the chamber to low energy photons and caused by the steel electrode. As there is more scatter in the normalisation field (100x100mm^2), the resulting relative output will be too low. The relative output measured with the PinPoint parallel to the beam, was less than 1% higher than when used in perpendicular orientation. Interestingly, the authors also compared the results with a Markus parallel plate IC (PP-IC) used perpendicular to its conventional direction. The relative output was found to be 1% lower than the PinPoint.

Haryanto et al (2002) compared several detectors with the results of BEAM/EGS4 in fields down to 10x10mm^2, on a 6MV, Elekta Sli-plus. The detectors used were a 0.125cc IC, diode (1mm^2 sensitive area), diamond (5.6mm^2 sensitive area), PinPoint IC (0.015cc) and all results were normalised to a 50x50mm^2 field at 100mm deep. All detectors agreed to within 3% in the 20x20mm^2 field and matched MC, but in the 10x10mm^2 there was a 35% difference between the diode and the 0.125cc IC. These authors noted that both the size of the detector and the non-water equivalence will have an effect on the measured dose. For the ion chamber, as the size of the detector increases, the under-estimation will also increase, due to volume averaging. In addition, the electron range in air will be increased, which will further increase the disequilibrium and lead to outputs which are under-estimated. Although there will be some volume averaging in a diode, the measured dose may be over-estimated due to the decreased electron range in silicon. However, in a 1mm^2 silicon chip, this effect is likely to be minimal. Although the diamond is the most water-equivalent of the detectors, it is quite large and the authors do not appear to consider that the 8% difference between the diode and the diamond might be the result of the size of the diamond. However, the diamond results matched those of MC, whereas the diode results only matched when the calculation material was silicon. Finally, the authors commented that the sharp drop in S_{cp} was caused by the size of the electron source, but did not comment any further on this.

Lee et al (2002) compared a new type of PPMC (0.002cc) against a shielded and an unshielded diode (dimensions unspecified), on a 6MV Varian 2100C. From the description given these appeared to be in-vivo patient dosimetry diodes (Sun Nuclear diodes) which are not generally used for the acquisition of beam data. The shielded diode is cylindrical in construction and designed to be directionally independent. It contains inherent build-up in the form of a metallic ring which, according to the authors, caused the diode to act as a kerma detector. It is unclear what the authors meant by this as kerma is not measured by any type of detector. It is however likely that they mean that the inherent build-up causes electronic equilibrium to be achieved at all depths i.e. the manufacturers deliberately create EE by surrounding the silicon with a high density material. The unshielded diode does not contain build-up and is a flat, 12mm diameter, diode with a silicon chip of 3.3mm diameter. Between the 40 and 12.5mm diameter collimators, S_{cp} fell by 2, 6 and 12% as measured with the shielded and unshielded diodes and the PPMC respectively. MC calculations confirmed the results of the unshielded diode, which suggests that the results measured with the shielded diode were too high. According to the authors, the shielded diode over-responded in fields without LEE (<26mm diameter) as kerma and dose are non-equivalent, but this is not explained further. The authors recommended the use of the small, unshielded, diode for measurements in small fields.

Yin et al (2002) used a mini IC with width of 2mm and length of 3.6mm, both parallel and perpendicular to the beam CAX, in addition to a 0.6mm diameter unshielded diode, on a 6MV Varian Clinac. In the 4mm diameter collimator, there was a 20% spread over all measurements, with the unshielded diode highest and the IC, orientated perpendicularly to the beam CAX, lowest. The unshielded diode was higher than the IC orientated parallel to the beam CAX, by approximately 3%. The total fall off from a $100x100mm^2$ field was approximately 50%.

Laub and Wong (2003) investigated the volume effect by comparing 0.6, 0.125 and 0.015cc ICs with a diamond and a $1mm^2$ sensitive area diode in a $10x10mm^2$ field, on two Elekta Sli-plus linacs with energies of 6, 15 and 18MV. The profile of the $10x10mm^2$ field was scanned using the diode and used to calculate a three-dimensional Gaussian function which was then used to account for volume averaging in the geometry of each detector. The results were normalised at zero detector size to the results calculated by EGS4/BEAM. Although the uncorrected results were spread over almost 45%, the corrected results were spread over just less than 15%. However, the ICs, in particular the 0.6cc, still underestimated the output and this was thought to be because lateral electronic disequilibrium increases with increasing detector volume i.e. volume averaging cannot

account entirely for the problem. The authors concluded that an IC should be corrected for both spatial resolution (volume averaging) and water equivalence (electronic disequilibrium). It is interesting to note that the corrected diode result (normalised to MC) is actually smaller than the measured value, by approximately 4%. According to the authors, the increase in importance of secondary electrons in small fields, in silicon and in the materials surrounding it, leads to an over-estimation of outputs.

Comparison of results

Although a large fall off in S_{cp} is reported in most of the above work, it is not clear, whether this fall off is real, or a result of the detectors used. To visualise the extent of the problem, S_{cp} values measured at dmax and normalised to an open 100x100mm^2 field are compared in different publications. Values of S_{cp} in small square and circular stereotactic fields, have been measured by several authors using a variety of detectors. Most S_{cp} data has been measured isocentrically at dmax, 1000mm FAD and normalised to an open 100x100mm^2 field at the same FAD, as this is the most common formalism used. A few authors have measured S_{cp} at 100mm deep, in accordance with a depth-based formalism and therefore these results cannot be compared directly against those measured at dmax. In addition, a few authors have presented results normalised only to the largest small field tested. These results cannot be compared directly against the other results as they require further normalisation to a reference field. The single detector or calculation method recommended in each relevant publication and used to compare the results in the different publications is summarised in Table 5.1.

Author	Energy /MV	Linac	Field type (coll. /mm^2)	FSD /FAD	Detector or measurement system
Arcovito et al (1985)	9	CGR Neptune	Open	FSD	TLD 0.3mm wide
Bucciolini et al (2002)	5	Elekta SL75-5	mMLC (100x100)	FAD	0.6mm diameter diode
Fan et al (1997)	6	Clinac 1800	stereo (60x60)	FAD	Radiographic film
Francescon et al (1998)	6	Siemens Mevatron	stereo (60x60)	FAD	MC BEAM
Gotoh et al (1996)	10	Clinac 2100	stereo (50x50)	FAD	Radiographic film
Houdek et al (1983)	10	LMR-13 Toshiba	Open	FSD	TLD ribbons
McKerracher & Thwaites (1999)	6	BBC CH6	stereo	FAD	unshielded diode
Rice et al (1987)	6	Clinac 6/100	stereo (40x40)	FAD	MC
Serago et al (1992)	6	Clinac 2500	stereo (50x50)	FAD	2mm diameter diode
Wierzbicki & Bissonnette (1999)	? 5	Philips SL75	stereo (50x50)	FAD	2.5mm diameter diode
Yin et al (2002)	6	Varian Clinac	stereo (40x40)	FAD	0.6mm diameter diode
Zhu et al (2000)	6	Clinac 2300CD	stereo (60x60)	FAD	1mm diameter diode

Table 5.1 Summary of recommended S_{cp} measurement or calculation method in a variety of publications, presented in Figure 5.1.

Note that in Table 5.1, the field type is either stereo (stereotactic collimators) or open (movable collimators only) and the "coll" setting is the setting on the movable collimators used in conjunction with the stereotactic fields. The range of linacs and energies is quite extensive. The data summarised in Table 5.1 above is plotted in Figure 5.1.

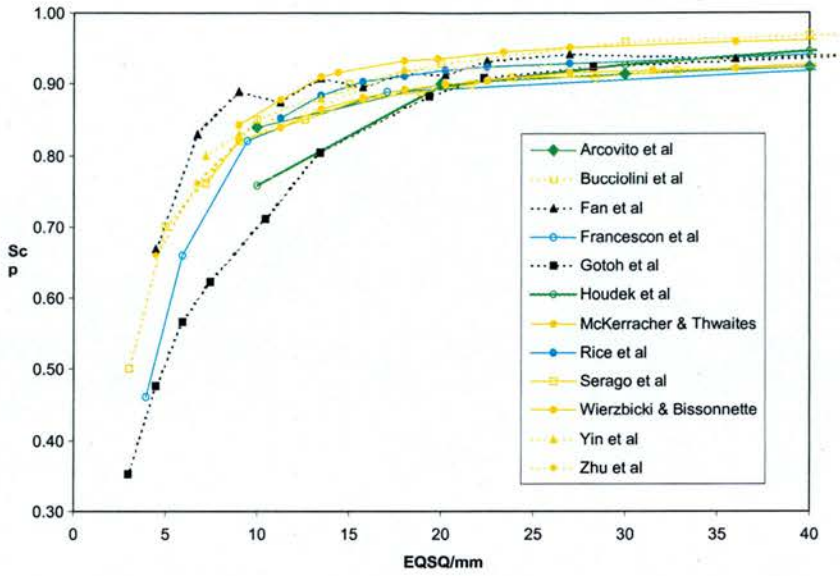

Figure 5.1 Comparison of S_{cp} measured with a variety of detectors, in several publications.

Although the range of detectors and linac types and energies is quite large, it is interesting to note that the overall spread in S_{cp} is only 5% in a 20x20mm^2 field, where S_{cp} is approximately 0.9. Below this field size, S_{cp} falls much more rapidly and the spread between data sets increases to approximately 20% in the 5x5mm^2 field. This suggests that if differences between linacs are responsible for differences in the magnitude of the drop, these differences only become significant at fields <20x20mm^2. Interestingly, one of the steepest fall offs is presented by Francescon et al (1998) whose results are based on MC calculations and therefore independent of detector size and type.

Selection of appropriate detectors

Although the extent of the literature review suggests that the measurement of S_{cp} in small fields has been investigated thoroughly, it would appear that there is still no consensus of opinion as to which detector is the most appropriate. MC is often considered to be the "gold standard" against which all measurements should be compared and it may be that in the future, MC calculations will be shown to be the most appropriate method of determining S_{cp} in small fields. However, relatively few departments have access to MC calculations and until the results have been verified comprehensively against measured data, MC remains only an option, to be considered alongside other options.

ICs, of various forms and sizes, have been shown to under-respond in most small fields due to volume averaging and probably due to their lower density which will reduce LEE in the

smaller fields. Although Rice et al (1987) accounted for this through extrapolation to zero detector size, this process is time-consuming and complicated and seems unnecessary if other types of detector can be used.

Only one publication reports on the use of MOSFETs (Francescon et al, 1998). These were shown to over-respond in the same way as a diode, due to the silicon in the sensitive volume. Although TLD, radiographic and radiochromic film were found to agree (Fan et al, 1997) and to match MC calculations (Francescon et al, 1998), their sensitivities are dependent on their annealing, processing and calibration. It is particularly important therefore that measurements with these detectors are presented with descriptions of these processes and the corresponding experimental uncertainty. This has not been done in most of the above reported work. In addition, although these detectors may be appropriate measurement devices, they are more time-consuming to use than other more straightforward detectors.

Westermark et al (2000) were the only authors to investigate a diamond and a scintillator. Although the scintillator was found to agree with the LIC, the LIC is still under development. The diamond appears to under-respond in a 4mm diameter collimator, due to volume averaging, but in larger fields it was found to match the LIC.

A conventional unshielded diode has been shown to be very useful. It has been shown to match an energy independent LIC down to a $5x5mm^2$ field (Dasu et al, 1998) and TLD chips and radiochromic film down to an 8mm collimator (Serago et al, 1992). These results imply that scatter is minimal in very small fields and energy compensation is unnecessary. Indeed, energy compensation has been shown to cause the relative outputs in small fields to be over-estimated (Dasu et al, 1998).

Finally, both Westermark et al (2000) and Lee et al (2002) recommended that S_{cp} in small fields should be measured relative to the largest small field, to minimise differences in response between detectors. Normalisation to the reference field should be investigated separately as the best detectors for the two steps may be different.

5.1.5 Aim

The primary aim of this work was to compare detectors in the measurement of S_{cp} at dmax, 1000mm FAD and determine an optimum detector to use in stereotactic collimators between 40 and 12.5mm diameter. This includes the investigation of two detectors, not previously

reported at the time of the publication of this work (1999). These were a small (0.6mm sensitive width) stereotactic diode and a 0.015cc IC. The secondary aim was to compare a more limited set of detectors in the measurement of S_{cp} at both dmax and 50mm deep in all collimators between 40 and 5mm diameter and in small square open and MLC fields between 50x50 and 10x10mm^2. These collimating systems were investigated to determine whether differences in scatter conditions had any effect on the detector responses and to compare phantom scatter factors in Chapter 7. All measurements in the stereotactic collimators were initially normalised to the 40mm collimator and the square fields to an open 50x50mm^2 field. Normalisation to the reference field was investigated separately.

The overall aim was to find a detector which was simple to use and which could preferably be used without the need for a correction factor.

5.2 Materials and Methods

5.2.1 Materials

Detectors

The initial detector comparison was carried out on the CH6 linac with the PFD, EFD, 0.125cc IC and the PP-IC, which are all standard detectors available within the department. Additional small detectors were subsequently tested as they became available, either through purchase or loan. These were the SFD, a diamond and a 0.015cc IC.

Phantoms

To measure S_{cp}, slabs of RMI were drilled to allow the long axes of the diamond, PFD, EFD and SFD to be orientated parallel to the beam CAX. All ICs were orientated conventionally, with their long axes perpendicular to the beam CAX. The 0.125cc IC was, in addition, orientated with long axis parallel to the beam CAX.

5.2.2 Methods

Detector comparison: CH6

The original detector comparison was carried out on the CH6 for collimators between 40 and 12.5mm diameter only, with a variety of detectors. S_{cp} was measured at dmax, 1000mm FAD and normalised to the 40mm collimator. Detectors were also compared to find the most appropriate method of normalising the results to the reference 100x100mm^2 field. Measurements were repeated on between two and three occasions and the average taken. All measurements in stereotactic collimators were initially normalised to the 40mm collimator.

Detector comparison: 600CD

A more precise detector comparison, with an increased number of repeats (minimum of five) and a more limited number of detectors, was carried out on the 600CD. Three beam defining systems were investigated; open fields defined by the linac jaws, MLC fields and fields defined by the stereotactic collimators. All measurements were carried out at 1000mm FAD, at both dmax and 50mm deep. The open and MLC square fields were both normalised to a $50x50mm^2$ open field defined by the movable collimators. Normalisation to the reference field was carried out by detector comparison, as before. Measurements in RMI were compared against measurements using the BDAS system, on a single occasion, for the smallest collimators. The profiles in the 5mm collimator were scanned and the zero co-ordinates set at the centre of the 50% regions. S_{cp} measurements in the 12.5, 10, 7.5 and 5mm collimators at dmax only, were then normalised to the 40mm collimator.

Linac comparison

The final data sets measured on the CH6, CH20 and 600CD were compared.

Beam profiles

Profile information from chapter 4 was used to determine an approximate value for the under-response of each detector in fields with high dose regions smaller than the sensitive widths of each detector. The amount of volume averaging was estimated by integrating the beam profiles over the area of each sensitive volume.

Statistics

On the 600CD, each measurement in each experiment was repeated on at least five separate occasions. The results were meaned and the standard deviation (s.d.) and coefficient of variation (s.d./mean x 100%) calculated. Differences between sets of measurements were considered insignificant if they were <0.3%. To determine whether differences >=0.3% were significant, a two tailed t-test was carried out.

Radiation isocentre

The position of the radiation isocentre with respect to the crosswires was determined on several occasions, using the Winston Lutz (1988) test at gantry 0^o (beam directed downwards). In all S_{cp} measurements, the geometric centre of each detector was aligned with the radiation isocentre.

5.3 Results and discussion

5.3.1 Radiation isocentre

On all machines, the radiation isocentre was found to match the crosswires to within +/- 0.2mm. As a result, the geometric centre of each detector was aligned with the crosswires.

5.3.2 CH6 measurements

Detector comparison

Figure 5.2 shows a plot of S_{cp}, normalised to the 40mm collimator and measured at dmax, 1000mm FAD, on the CH6, against collimator diameter.

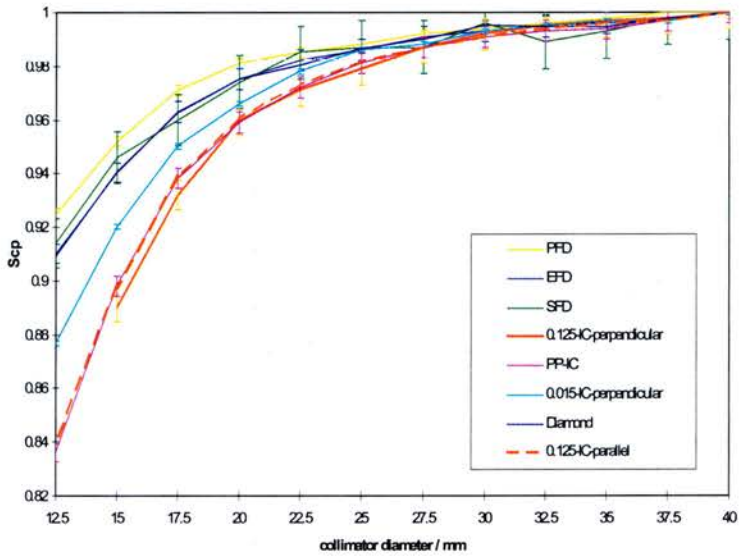

Figure 5.2 S_{cp} at dmax against collimator diameter, normalised to a 40mm collimator, for measurements made on the CH6, ECC.

The value of S_{cp} becomes detector dependent below a 27.5mm collimator. By the 20mm collimator, the spread over all detectors is 2% and in the 12.5mm collimator it has increased to over 8%. For the larger detectors, it is obvious that as the field size decreases, the entire sensitive volume does not lie within the high dose region of the corresponding profile. This will result in a signal which is too low.

It is possible to determine whether a detector is too large for measurements in a particular collimator, by considering the width of the (99%) high dose region, as discussed in Chapter 4. The approximate reduction in signal can be calculated by integrating the profile over the area of the detector. This is simplest when the detector lies symmetrically around the CAX, but is more complicated for ion chambers used in conventional orientation. For a

cylindrical ion chamber, the effective point of measurement does not lie at the geometric centre of the detector and the detector itself is not symmetrical about all axes. Figure 5.3 shows an example of the situation for an ion chamber (a) perpendicular to the beam CAX and (b) parallel to the beam CAX.

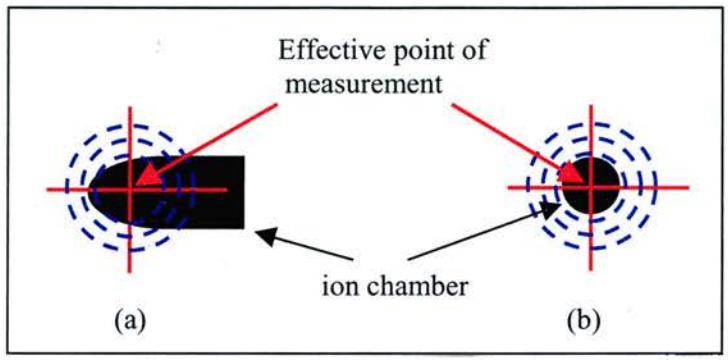

Figure 5.3 Example of the situation for an ion chamber (a) perpendicular to the beam CAX and (b) parallel to the beam CAX

Although it is possible to integrate over the volume in (a), it is more complicated. For simplicity, volume integration was only limited to detectors which lay symmetrically around the beam CAX. In addition, the conventional orientation for ICs (a) was not pursued for outputs in small fields.

The reduction in signal caused by volume averaging, is greatest in the smallest (12.5mm) collimator. Figure 5.4 shows the high dose region in the 12.5mm collimator, fitted with a fourth order polynomial.

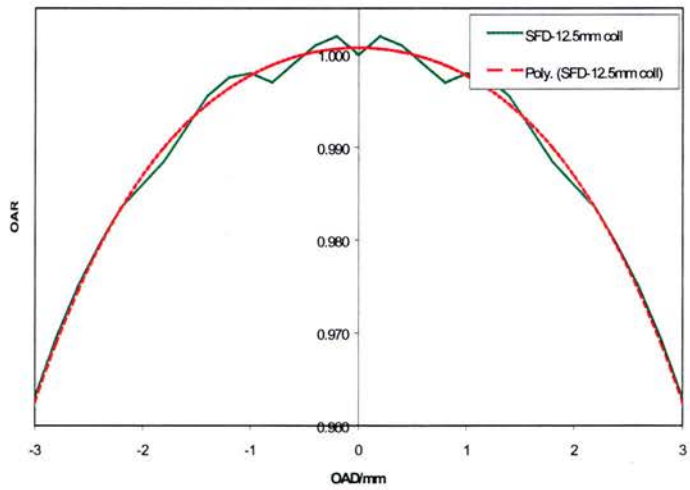

Figure 5.4 Polynomial fit to profile measured at dmax, with SFD, in 12.5mm collimator.

The approximate percentage response of each detector was calculated by integrating the above curve over the sensitive area of each detector. The calculated response for each of the detectors in the 12.5mm collimator, is shown in Table 5.2.

Detector	width / mm	% Response
Diamond	2.2	99.9
PFD/EFD	2.5	99.7
SFD	0.6	100.0
PPIC	5.0	98.9
0.125cc IC	5.5	98.5

Table 5.2 The calculated % responses for each of the detectors in the 12.5mm collimator.

The results in Table 5.2 suggest that the maximum under-response should be less than 2% in the IC. Volume averaging does not therefore explain why the 0.125cc IC orientated parallel to the beam CAX and the PPIC are both 7-8% lower than the solid state detectors in Figure 5.2. This suggests that it cannot simply be the sizes of the ICs which cause the under-responses. An additional problem is that both ICs are measuring ionisation in air, under electronic disequilibrium where the low density sensitive volume worsens the situation.

In the paper by McKerracher and Thwaites (1999), a larger correction was applied to each detector based on the widths of the high dose regions. These widths were extracted from the original profiles for each collimator and a line of best fit calculated. This simple method is not as accurate as integration of the appropriate profile and it seems that too large a correction was applied to the ion chamber results in that publication. For example, the response of the PPIC was increased by approximately 6% in the 12.5mm collimator in the original publication (Figure 7), whereas the results in Table 5.2 indicate that a correction of only 1.1% is more appropriate.

Any kind of volume integration assumes that the centre of the sensitive volume has been positioned on the beam CAX. For measurements in RMI, the geometric centre of each solid state detector was aligned with the radiation isocentre, which assumes that the centre of the sensitive volume lies at the geometric centre of each detector. This has been shown not to be the case (McKerracher and Thwaites, 2001). If the sensitive volume is not aligned with the radiation isocentre, the measured dose will be reduced. This problem can be eliminated by measuring S_{cp} in the water tank (Zhu et al, 2000), scanning the beam profile and positioning the detector at the centre of the 50% dose regions. This method is time-consuming and physically demanding (changing the collimators over the water tank) and

therefore was carried out only once, on the 600CD, to determine the magnitude of the difference.

All solid state detectors agree to within less than 2% in the 12.5mm collimator. The PFD appears to produce values of S_{cp} which are too large, as also reported by Dasu et al (1998). This is probably due to the absorption of too much scatter in the normalisation field (40mm collimator) producing too high a value of S_{cp}. S_{cp} for both unshielded diodes and the diamond are within 0.5%. Again, this is in agreement with other authors and suggests that any of these three detectors (diamond, EFD, SFD) could be used to measure accurate beam data within the field size range tested. The over-response of the EFD to scatter is not apparent in these small field sizes, due to the lack of scatter.

5.3.3 Linac comparison

The diamond, EFD and SFD, as available, were used to measure S_{cp} on the CH20 and the 600CD. The differences between detectors used on each linac were found to be comparable. S_{cp} measured with the EFD and normalised to the 40mm collimator, on all three accelerators is shown in Figure 5.5.

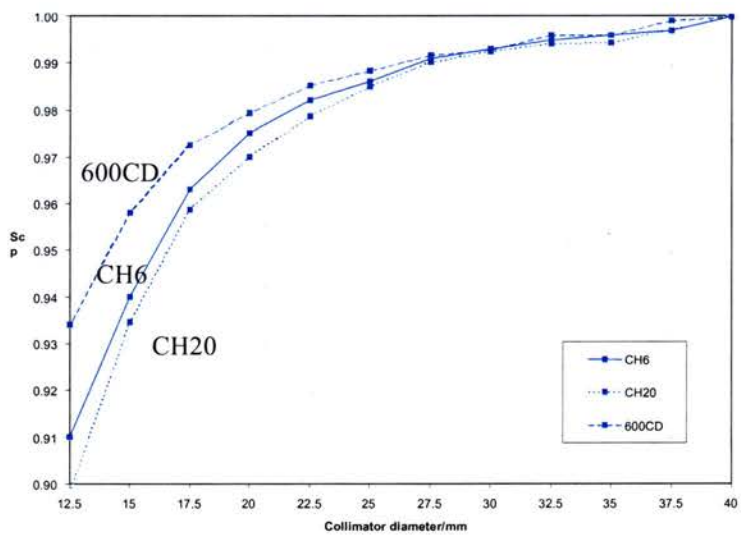

Figure 5.5 S_{cp} measured with the EFD and normalised to the 40mm collimator, on the three accelerators

Differences between the linacs begin to appear in the 25mm collimator, when normalised to the 40mm diameter collimator only and are likely to be due to differences in head scatter.

5.3.4 600CD measurements

Small stereotactic collimators

S_{cp} data in fields smaller than 12.5mm is useful for the calculation of phantom scatter factors in a large range of small field sizes. This will be discussed further in Chapter 7. However, these collimators are not used for clinical treatments at the ECC. The small collimator profiles (chapter 4) were initially integrated over the area of each of the solid state detectors. Figure 5.6 shows an example for the 5mm collimator.

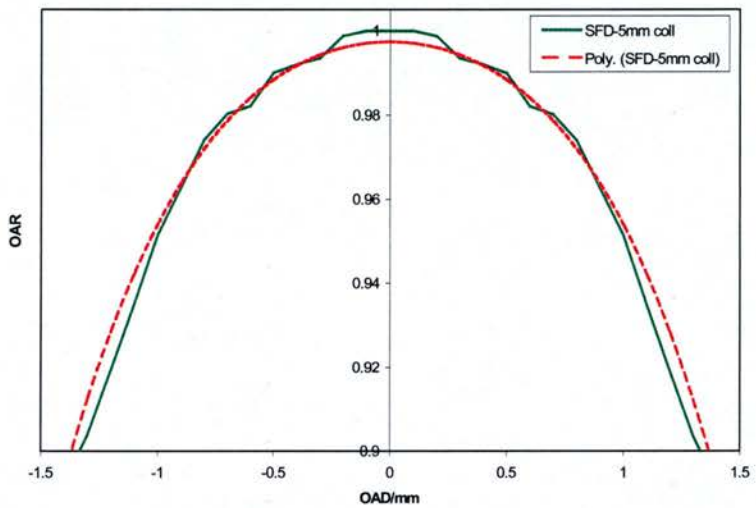

Figure 5.6 Example of polynomial fit to the profile data in a 5mm collimator.

The approximate percentage responses for the 12.5, 10 and 5mm diameter collimators were calculated and are noted in Table 5.3.

Detector	Width/mm	% Response		
		12.5mm	10mm	5mm
Diamond	2.2	99.6	99.5	96.9
PFD/EFD	2.5	99.4	99.2	94.6
SFD	0.6	100.0	99.9	99.5

Table 5.3 The calculated percentage responses in the 12.5, 10 and 5mm diameter collimators.

The results in Table 5.3 show that all detectors should be accurate to within 0.8% down to a 10mm collimator. In the smallest collimator, only the SFD lies within the high dose region, the diamond could under-respond by approximately 3% and the PFD and EFD by >5%. This shows that these detectors can only be used in this collimator size, in conjunction with a correction factor to account for the volume averaging.

As most measurements in each collimator were repeated on at least five separate occasions, the coefficient of variation, expressed as a percentage, is an indication of the reproducibility, or precision of the results, at 1 s.d.. Table 5.4 summarises the coefficient of variation. Where no value is reported, only one or two measurements were made.

	Coefficient of variation (%)		
Detector	12.5mm	10mm	5mm
Diamond	0.1	0.2	1.7
PFD	0.1	0.4	1.6
EFD	0.2	0.2	0.5
SFD	0.2	0.5	1.2
Film	-	4.3	6.5

Table 5.4 Coefficients of variation, expressed as a percentage of the mean, for each set of experiments for each detector in each collimator diameter.

Insufficient measurements were carried out in the 7.5mm collimator, simply due to time constraints. The coefficient of variation increases as the collimator diameter decreases. This is a reflection of the positional uncertainties. The reproducibility of the diamond is lower than the diodes. Notice that the reproducibility of film is very poor and is a reflection of the inconsistencies of the processing conditions. Although film processing requires a more thorough investigation in order to improve the reproducibility, this is outwith the scope of this work. As a result, film will not be investigated further.

When re-measured with the BDAS system, only the PFD and SFD measured larger values of S_{cp}. This occurred only in the 7.5 and 5mm collimators and only by between 1.5 and 2.0%. The new values of S_{cp} were at the upper limit of the range of values measured in RMI and showed that positioning errors caused the larger spread of results in the 5mm collimator. The diamond and EFD measurements did not increase when used with the BDAS system, suggesting that they were correctly positioned originally. The higher values measured with the PFD and SFD were used in Figure 5.7 which shows a plot of S_{cp} against collimator diameter, for all detectors.

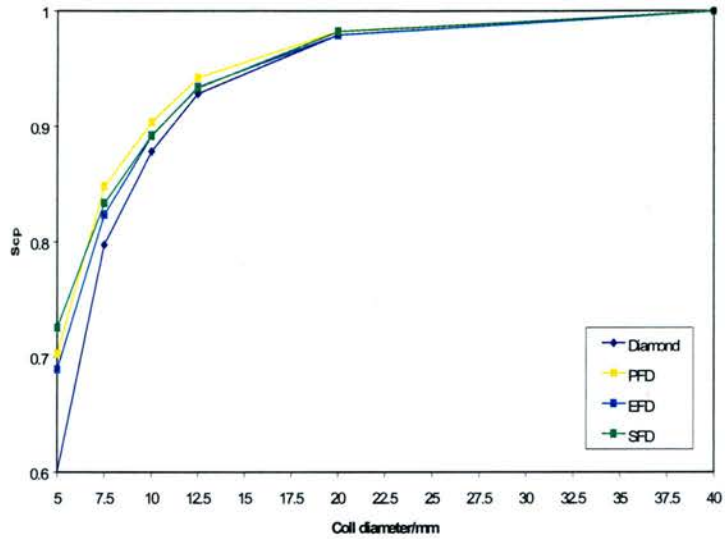

Figure 5.7 Plot of S_{cp} at dmax against collimator diameter, for all detectors. Volume averaging has not been accounted for.

In the 12.5mm diameter collimator, the spread over all detectors is approximately 1.5%. The PFD shows the highest results, again in accordance with the results of other authors (Dasu et al, 1998) and likely to be due to the absorption of too many contaminant electrons in the normalisation field. If the PFD is ignored, the spread over the three other detectors is only 0.6%. This suggests that either the diamond, EFD or SFD could be used to measure S_{cp} in the 40-12.5mm diameter collimator range. Although the diode results may be too high, due to the preservation of LEE in silicon, the effect is obviously small in the 12.5mm collimator. Below the 12.5mm diameter collimator, the effects of volume averaging must be accounted for. Figure 5.8 shows the values of Scp recalculated to account for this.

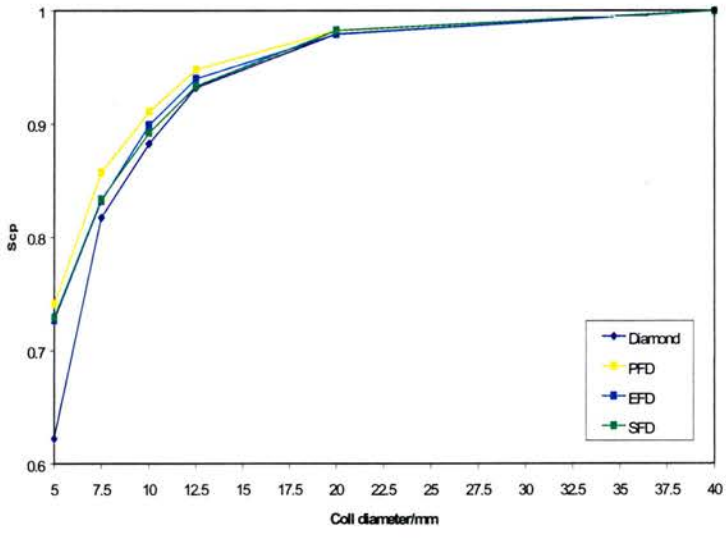

Figure 5.8. Plot of S_{cp} at dmax against collimator diameter, for all detectors, with volume averaging accounted for.

Although it is apparent that volume averaging has accounted for the differences between the diodes, the difference between the diode and diamond results is still too large in the smallest collimator. This could be a result of the preservation of LEE in silicon in the smallest fields, which would cause the diodes results to be too high. Alternatively, the problem could be an under-response in the diamond in the smallest collimator. The response of the diamond was calculated by assuming that the diamond width was 2.2mm. However, as shown in Chapter 2, the width may be larger than this. In addition, positioning the detector using the BDAS system may not have been entirely satisfactory. Scanning the profiles possibly did not result in the centre of the crystal being placed at the centre of the high dose region. Unless the size of the sensitive volume of the diamond can be determined more exactly, the diamond should not be used for measurements in field widths <10mm. At 50mm deep the coefficients of variation and the relative results between detectors were comparable with those at dmax.

Open fields

S_{cp} in small open fields were measured to determine whether differences in scatter conditions had any effect on the response of different detectors. In addition, the small field S_{cp} results were used to calculate phantom scatter factors in Chapter 7. The Inplane and Xplane profiles were integrated over the sensitive area of each detector. Figure 5.9 shows an example of the polynomial fit to the Inplane profile in the 10x10mm^2 open field.

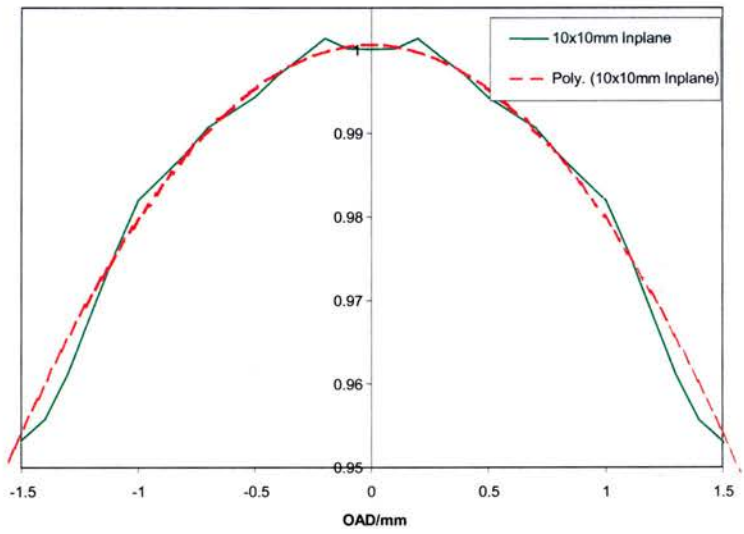

Figure 5.9 The inplane profile in the 10x10mm^2 open field.

Table 5.5 shows the calculated percentage responses in each detector in the 10x10mm^2 field, integrated over both profile directions.

Detector	Width /mm	% Response $10x10mm^2$
Diamond	2.2	99.3
PFD	2.5	98.9
EFD	2.5	98.9
SFD	0.6	100.0

Table 5.5 The calculated percentage responses in the $10x10mm^2$ field

The results in Table 5.5 show that although the diamond and larger diodes could under-estimate the dose in the smallest field, it should only be by approximately 1%.

The reproducibility of the measurement of S_{cp}, as determined by the coefficient of variation, with each detector, in the smallest fields, is summarised in Table 5.6.

	Coefficient of variation (%)	
Detector	$20x20mm^2$	$10x10mm^2$
Diamond	0.1	1.5
PFD	0.1	1.4
EFD	0.1	0.8
SFD	0.3	0.9

Table 5.6 The reproducibility of the measurements as determined by the coefficient of variation, described as a percentage of the mean.

The reproducibility of each detector in the $10x10mm^2$ field is poorer than in the 10mm diameter collimator. This is because the coefficient of variation also reflects the reproducibility of the setting of the movable collimators. This will have more effect as the field size decreases. In addition, the reproducibility will not only reflect the differences in the actual field sizes determined by the width of the 50% region, but will also reflect the corresponding change in the position of the radiation isocentre with collimator setting. Figure 5.10 shows a plot of S_{cp} against EQSQ for all four detectors, with the volume averaging accounted for.

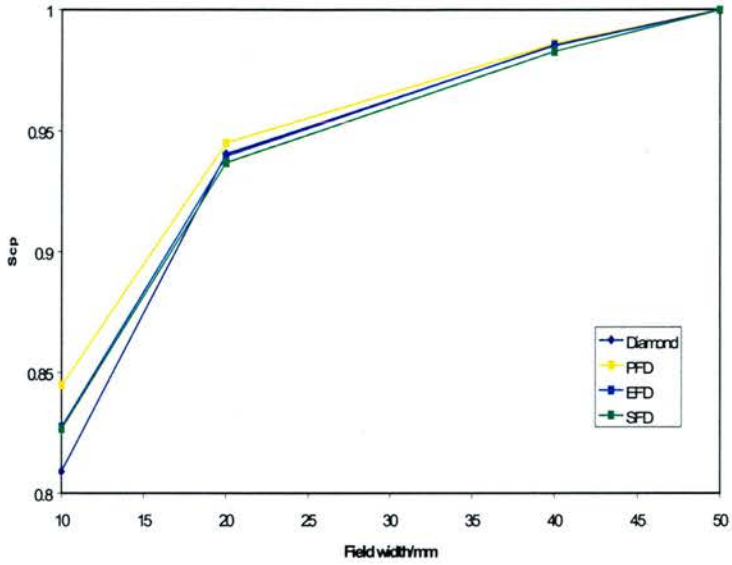

Figure 5.10 Plot of S_{cp} against EQSQ for all four detectors, with volume averaging accounted for.

The spread over all detectors in the 10x10mm^2 field is approximately 4%. The PFD results are too high, for the same reasons as before. The EFD and SFD agree, with the volume averaging accounted for, but the diamond results are lower than the diodes, by approximately 2%. As discussed previously for stereotactic fields, the diode results could be too high due to the preservation of LEE in silicon, or the diamond could be too low due to doubts over its size. Open field S_{cp} were not remeasured using the BDAS system and mispositioning could therefore account for the under-response of the diamond. However, the effect is likely to be small. At 50mm deep the uncertainties remain the same for all other detectors and the spread over all detectors is the same as that at dmax.

MLC fields

S_{cp} in small MLC fields were measured to determine whether differences in scatter conditions had any effect on the response of different detectors. In addition, the small MLC S_{cp} results will be used to calculate phantom scatter factors in Chapter 7. The 99% high dose regions were integrated over the sensitive area of each detector. Figure 5.11 shows an example of the polynomial fit to the inplane profile in the 10x10mm^2 MLC field.

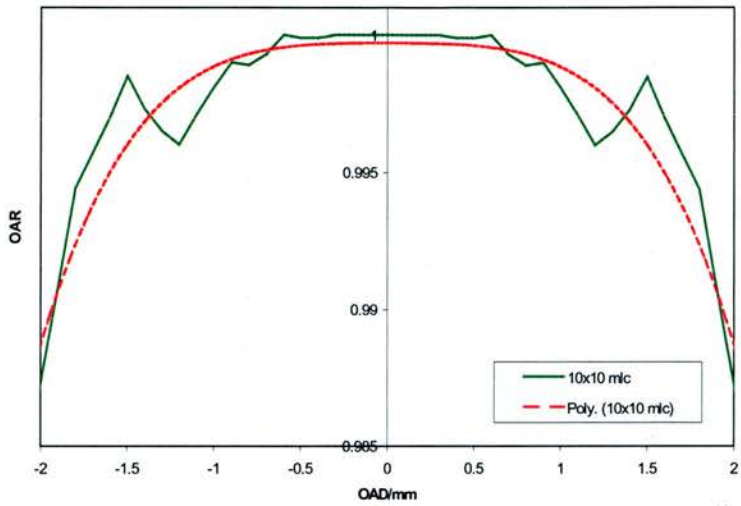

Figure 5.11. The high dose region of the inplane profile in the 10x10mm^2 field.

It should be noted that although the profile in Figure 5.11 appears somewhat strange in shape, this is the result of noise within a very small profile region (dose scale covers only 1.5%) and was not as obvious in the whole profile shown in Figure 4.14. The approximate percentage responses in each detector in the 10x10mm^2 MLC field, integrated over both profile directions, are shown in Table 5.7.

Detector	Width /mm	% response 10x10mm^2
Diamond	2.2	99.9
PFD	2.5	100.0
EFD	2.5	100.0
SFD	0.6	100.0

Table 5.7 Calculated responses for each detector in the 10x10mm^2 field

The responses are much higher in the MLC fields than in the open fields. This is due to the wider high dose region in the MLC fields shown in Figures 4.16 and 4.17 in Chapter 4. It is apparent therefore that the size of each detector is not a problem in any of the MLC field sizes investigated. As a result, all detectors should be accurate, in terms of their size only.

The reproducibility of the measurement of S_{cp}, as determined by the coefficient of variation, with each detector, in the smallest fields, is summarised in Table 5.8.

Detector	Coefficient of variation (%) 20x20 mm^2	10x10 mm^2
Diamond	0.1	0.2
PFD	0.1	0.2
EFD	0.2	0.2
SFD	0.0	0.1

Table 5.8. The reproducibility of the measurements as determined by the coefficient of variation, expressed as a percentage of the mean.

The reproducibility of the measurements is excellent and perhaps reflects the slightly larger high dose region. This is more likely to ensure that the sensitive width of each detector lies within the high dose region, rather than within the penumbra. Figure 5.12 shows a plot of S_{cp} against MLC field size for all four solid state detectors.

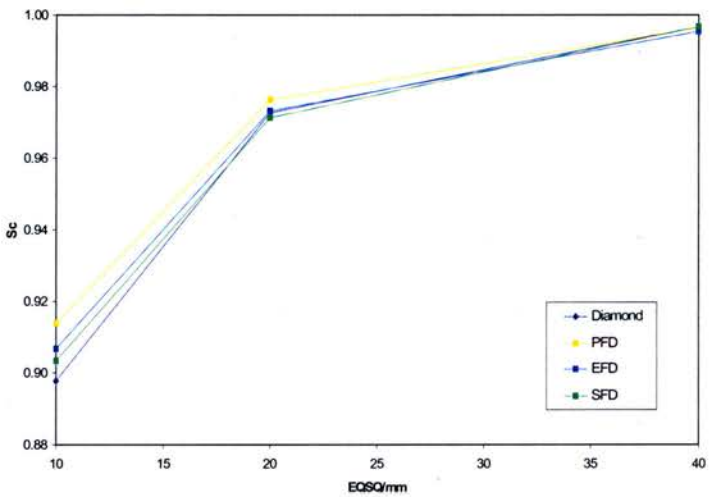

Figure 5.12 Plot of S_{cp} against MLC field size for all four solid state detectors. Volume averaging was unnecessary for all MLC field sizes.

As before, the PFD results are too high, but the other detectors agree within a range of less than 1%. The results are comparable at 50mm deep.

5.3.5 Normalisation

Overview

Initially the results for S_{cp} in stereotactic fields were renormalised from the 40mm diameter collimator, to an open 50x50mm^2 field. Measurements in all beam defining systems could then be renormalised to an open 100x100mm^2 field, at 1000mm FAD.

40mm/50x50mm^2

S_{cp} in the 40mm collimator relative to an open 50x50mm^2 was measured with a variety of detectors. The results are shown in Table 5.9, for each detector, along with the corresponding coefficient of variation (coeff. of var.).

	40mm/50x50mm^2			
Detector	dmax norm	coeff. of var.	50mm norm	coeff. of var.
Diamond	0.995	0.3	0.984	0.2
PFD	0.997	0.1	0.986	0.1
EFD	0.995	0.1	0.981	0.1
SFD	0.994	0.2	0.981	0.5
0.125cc	0.996	0.2	0.982	0.2
mean	0.995	0.1	0.983	0.2

Table 5.9 S_{cp} in the 40mm collimator relative to an open 50x50mm^2 field, with corresponding values for the coefficient of variation (coeff. of var.).

The coefficient of variation for the mean of all detectors is comparable with the coefficient of variation for each individual detector. This suggests that there are no significant differences between detectors and the average value could be used at each depth.

50x50mm^2/100x100mm^2

All detectors were compared in the normalisation of a 50x50mm^2 field to an open 100x100mm^2 field. The results are shown in Table 5.10, for each detector, along with the corresponding coefficients of variation.

	50x50mm^2/100x100mm^2			
Detector	dmax norm	coeff. of var.	50mm norm	coeff. of var.
Diamond	.954	0.1	.932	0.1
PFD	.958	0.1	.937	0.1
EFD	.952	0.2	.930	0.1
SFD	.950	0.1	.924	0.0
0.125cc	.955	0.1	.935	0.1
mean	.954	0.3	.932	0.5

Table 5.10 S_{cp} in the 50x50mm^2 field relative to the 100x100mm^2 field, with corresponding values for the coefficient of variation (coeff. of var.).

The coefficient of variation of the mean over all detectors is larger than the individual coefficients, which suggests real differences between the detectors, confirmed by t-testing. The diamond, PFD and IC are all designed for use in photon fields and are all within a range of 0.4% at dmax and 0.5% at 50mm deep. However, the PFD may be slightly too high, as the energy compensation may cause the absorption of relatively more scatter in the

100x100mm^2 field compared with the 50x50mm^2 field. The unshielded diodes are not designed for use in photon fields and are known to over-respond to scatter. As scatter will be larger in the 100x100mm^2 field, the normalisation value will be too low. The effect is greater at depth, where scatter is also larger. It is unclear why the SFD is lower than the EFD as this suggests that the SFD is more sensitive to scatter than the EFD. As discussed before, this may be due to the relatively larger effects of the connectors within the SFD, compared to the small size of the detector.

The results for the diamond, PFD and IC were meaned to obtain final 50x50mm^2/100x100mm^2 normalisation values of 0.956 and 0.935 at dmax and 50mm deep respectively, on the 600CD, with an uncertainty of +/-0.2 and 0.3% respectively (1 s.d.). Similar methods were used on the CH6 and CH20 linacs. The overall % uncertainty (1 s.d.) in Scp calculated from the reproducibility at dmax only, of each detector on the 600CD is shown in Table 5.11.

	% uncertainty in Scp		
Detector	12.5mm	10mm	5mm
Diamond	0.2	0.3	1.7
PFD	0.2	0.5	1.6
EFD	0.3	0.3	.5
SFD	0.3	0.5	1.2

Table 5.11. Overall uncertainty (dmax) in S_{cp} normalised to a 100x100mm^2 field.

5.3.6 Comparison of beam defining systems

The S_{cp} results for each of the three beam defining systems were normalised to the 100x100mm^2 field at 1000mm FAD, using the normalisations calculated above. Collimator diameters were converted to EQSQs. However, to be able to compare results between systems, the measured field widths were used, rather than the nominal field size settings. EQSQs were therefore calculated from the 50% widths measured in chapter 4 and plotted against normalised S_{cp} values (volume averaging accounted for) at dmax in Figure 5.13.

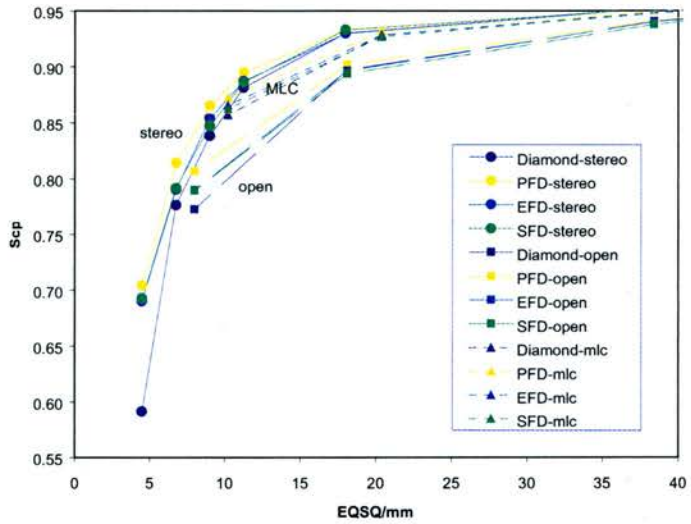

Figure 5.13 S_{cp} at dmax for each of the three beam defining systems, normalised to the reference field. Volume averaging has been accounted for.

S_{cp} values for the stereotactic and MLC fields are the most similar, due to the constant field size setting on the movable collimators of 50x50mm^2, in both types of field. The relative output factors in the open fields results are up to 4% lower as, by definition, the collimator scatter decreases with the field size setting. S_{cp} falls by up to 5% between the 40x40 and 20x20mm^2 fields. Between the 20x20 and 10x10mm^2 fields S_{cp} falls by a further 5% in the stereotactic and MLC fields and by 10% in the open fields. Below this the drop in the stereotactic collimators is between 15 and 25% dependent on the detector. All of these results are comparable with those of other authors in Figure 5.1. The same effects are displayed at 50mm deep, as shown in Figure 5.14.

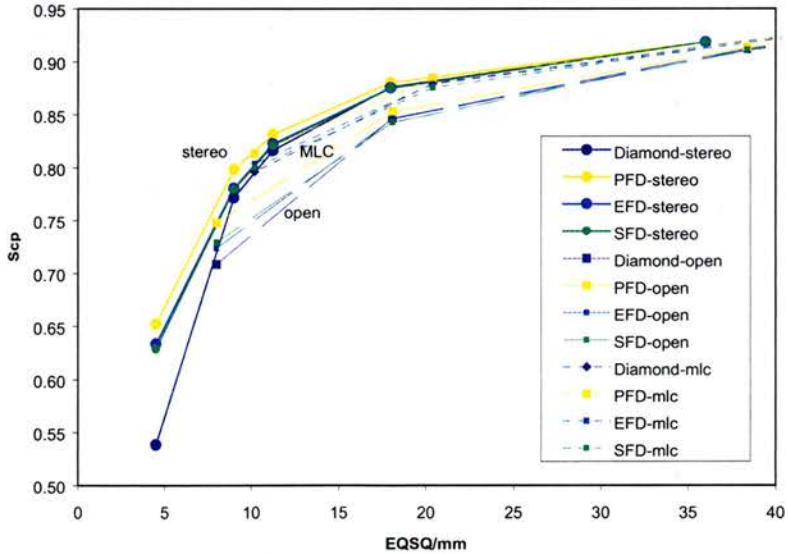

Figure 5.14. S_{cp} at 50mm for each of the three beam defining systems, normalised to the reference field. Volume averaging has been accounted for.

The differences between detectors are the same at 50mm deep, which shows that the differences are independent of depth.

5.3.7 Comparison of linacs

S_{cp} in stereotactic fields between 40 and 12.5mm diameter measured on all three linacs, with the EFD and normalised to the 100x100mm^2 field at 1000mm FAD, using an appropriate detector, are shown in Figure 5.15, along with corresponding measurements in an open 50x50mm^2 field, also at 1000mm FAD. Note that S_{cp} is plotted against collimator diameter and the 50x50mm^2 field has been plotted as its equivalent circle.

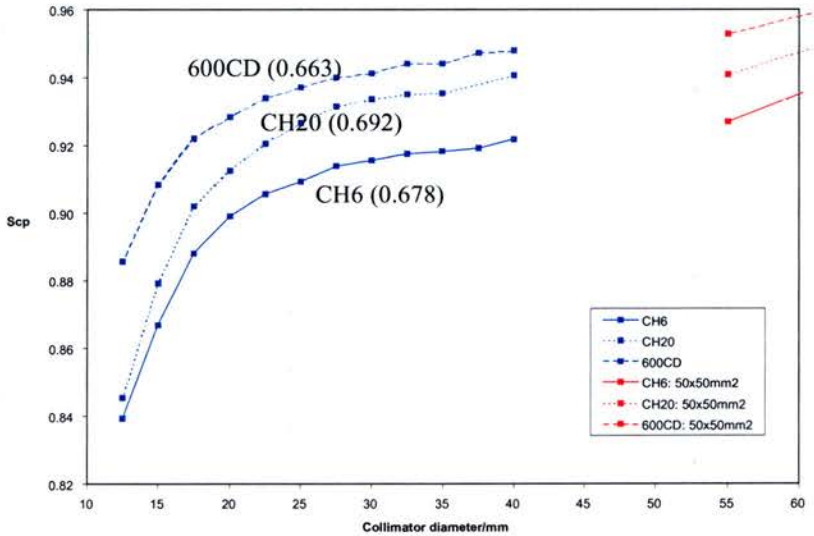

Figure 5.15. Normalised S_{cp} data in stereotactic collimators between 40 and 12.5mm diameter for all three linacs, with the EFD.

The QI for each linac is in brackets. Relative output factors are generally independent of beam energy and highly dependent on machine design. For example, the 6 and 16MV beams of the CH20 linac have identical relative outputs in regular field sizes between 40x40 and 400x400mm^2, but the relative outputs on the 6MV beams of the CH6, CH20 and 600CD are all different and do not reflect the beam qualities.

It is interesting to note that the shape of the curves on the CH6 and 600CD are similar, but the CH20 curves fall more rapidly below a 20mm collimator. This could be a real effect, or could be a result of less precise measurements, particularly in the 12.5mm collimator. Unfortunately these measurements cannot be repeated to verify the difference as the machines are no longer in use.

5.3.8 XKnife requirements

XKnife requires the input of S_{cp}, measured at dmax, 1000mm FAD and normalised to a 100x100mm^2 field, also at 1000mm FAD. These values are multiplied separately by the value of M, to relate the relative outputs to the linac calibration at 1000mm FSD, as discussed in Chapter 2. M is calculated to be 1.03 from the ratio of the relative distances of the normalisation point from the source, in both the FAD and FSD set-ups. This was confirmed by measurement, to be within +/-0.2%. Although either the diamond or the EFD could be used in collimators between 40 and 12.5mm diameter, S_{cp} was measured with the EFD on all linacs simply because the diamond was not available at the time of the commissioning of each linac. The final XKnife data (without the M factor) is shown in Table 5.12, along with the additional SFD measured data in the smaller collimators. All data has been re-calculated to account for volume averaging.

Coll /mm	S_{cp} (FAD)
40	0.950
37.5	0.949
35	0.946
32.5	0.946
30	0.943
27.5	0.942
25	0.939
22.5	0.936
20	0.933
17.5	0.924
15	0.910
12.5	0.886
10	0.847
7.5	0.791
5	0.692

Table 5.12. Final S_{cp} data (40-12.5mm diameter) measured on the 600CD, for input to XKnife, with the additional small field values.

5.4 Conclusion

Values of S_{cp} in collimators between 40 and 12.5mm diameter measured with the diamond, EFD and SFD agreed to within =<0.6%. Volume averaging was not found to be a problem within this range. The diamond and EFD were the simplest detectors to use, as the small signal on the SFD required more MU to be delivered to obtain a comparable resolution. Although the diamond does not appear to offer any advantages over the EFD within this range, it may be that the nearer water equivalence of the diamond, results in a better

estimation of Scp than for the diodes. However, the effect is small within this range and the requirement for pre-irradiation of the diamond at each measurement session could be considered to be a disadvantage, although it was not found to be a problem in this work.

Significant differences between the EFD, SFD and diamond only began to emerge in the smallest stereotactic collimators. These were due to volume averaging, uncertainty over the sizes of the detector areas and mispositioning of the centres with respect to the radiation isocentre. Volume averaging can be accounted for by integrating the profile over the size and shape of the sensitive volume. Mispositioning can be minimised by measuring S_{cp} in the water tank and placing the centre of the sensitive area midway between the 50% dose regions. This measurement technique is only necessary for the 5mm diameter collimator, although there may be a small (<1%) advantage in using it for measurements in the 7.5mm collimator.

The same conclusions regarding detectors were reached in square open and MLC fields, where the detector size was only found to be a problem for the diamond in a $10x10mm^2$ open field. This suggests that differences in scatter effects from the three beam defining systems have no effect on the relative detector responses.

Small field S_{cp} values can be normalised to the $100x100mm^2$ field using either a diamond, PFD or small IC. An unshielded diode should not be used as this may lead to an underestimation of the relative output in a $50x50mm^2$ field, albeit by less than 0.5%.

S_{cp} measured in stereotactic collimators between 40 and 12.5mm diameter were found to be independent of beam quality, but dependent on machine design.

Chapter 6

Head scatter factors

6.1 Introduction

6.1.1 Definition of S_c

The head scatter factor, S_c is defined as the ratio of the dose (D) "in-air" in the field size of interest (s) to the dose (D_{ref}) in the reference field size (s_{ref}), when both measurements are made at depth (d) and distance (f), for the same number of MU.

$$S_c = \frac{D(f, s, d)}{D_{ref}(f, s_{ref}, d)} \qquad (6.1)$$

6.1.2 Measurement of S_c

Build-up cap

Sc is generally measured in a build-up cap to achieve electronic equilibrium in all directions around the measurement point. For simplicity, build-up caps for cylindrical ion chambers conventionally have a cross-sectional radius equal to the build-up depth in the forward direction. As a result, the size of the build-up cap is dependent on the energy of the beam. Figure 6.1 shows three perspex build-up caps designed for a 0.6cc cylindrical IC, used in beams of between 15 and 6MV.

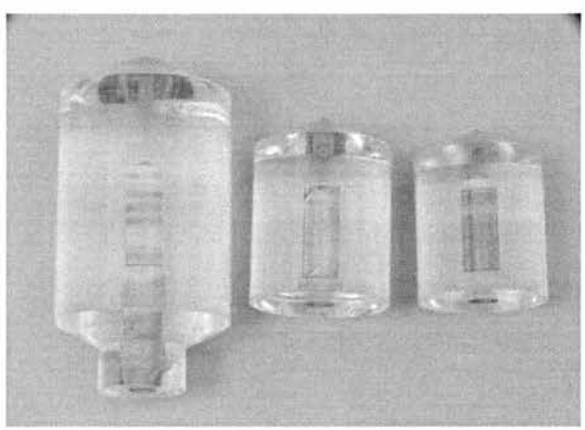

Figure 6.1. Perspex build-up caps for use with a 0.6cc IC in (from left to right) 15, 9 and 6MV beams.

A build-up cap will introduce some phantom scatter into the measurements, but if the minimum field size measured is always larger than the diameter of the build-up cap, the phantom scatter will approximately cancel out in relative measurements. Consequently, the width of the build-up cap will limit the minimum field size which can be measured. If, as is common, the minimum field size setting on a linac is 40x40mm^2, the maximum cap width must be less than 40mm in order to measure the full field size range. This size of cap will ensure lateral electronic equilibrium (LEE) in energies up to approximately 8MV. To measure the full field size range in higher energy beams, or to measure S_c in fields smaller than the build-up cap, S_c must either be measured at extended FSD, in a high density build-up cap, or under conditions of electronic disequilibrium.

Extended FSD

The advantage of measurements at extended FSD is that the field size at the isocentre is projected to a larger field size at the measurement distance and hence covers the build-up cap. However, measurements at extended FSD are only equivalent to measurements at the standard distance, if S_c is independent of FSD. Khan et al (1996) measured S_c in a build-up cap in fields >=80x80mm^2 at FSDs between 1000 and 2000mm. The results showed that S_c was independent of FSD to within 0.5%, if the field size setting at extended FSD was chosen such that the same amount of the flattening filter was "seen" from the measurement point as would have been seen from the isocentre. S_c has also been shown to be independent of FSD within the conventional field size range by other authors (Allahverdi, 1998; Allahverdi and Thwaites, 1999).

High density build-up caps

High density build-up caps can be used to measure S_c under conditions of electronic equilibrium, in field sizes at the lower end of the linac field size range. The high density material may however, cause the quality to change as a result of beam hardening. Jursinic and Thomadsen (1999) compared build-up caps of Mylar, acrylic, Al, Cu and Pb to measure S_c with a cylindrical IC (dimensions unspecified), in beams of 6, 10 and 18MV, at 1000mm FAD. Diodes with intrinsic tungsten and brass were also investigated and although their dimensions were unspecified, these appeared to be patient in-vivo dosimetry diodes (Sun Nuclear), not generally used for dosimetry measurements. In fields between 100x100 and 30x30mm^2, Sc was greater in the high density materials, by between 2 and 3%. According to the authors, in high density build-up caps, at large field sizes, secondary electrons are scattered away from the measurement point, which results in a lower signal. Measurements in fields <100x100mm^2, would therefore produce values of S_c which were too high. This

phenomenon has also been reported elsewhere, for conventional field sizes (Allahverdi, 1998; Allahverdi and Thwaites, 1999).

The mini-phantom

Recent developments in treatment planning have encouraged the use of formalisms which are based on the normalisation of dosimetric data at a depth beyond the maximum range of contaminant electrons. These formalisms require relative outputs which are measured commonly at a depth of 50, 80 or 100mm. It is obvious therefore, that S_c values measured at dmax in a build-up cap cannot be used in these formalisms. In response to this problem, van Gasteren et al (1991) designed a "mini-phantom" in which to measure S_c at depths beyond dmax. The cross-section of the mini-phantom was chosen to be 40mm in order to minimise phantom scatter, but achieve LEE in most energies of interest. Although measurements were carried out in beams of up to 25MV, the authors acknowledged that LEE would not be achieved at 25MV (dmax approximately 40mm), within a radius of 20mm. This was not thought to be important as the side scatter would be virtually independent of field size in fields > the phantom diameter. A reference depth of 50mm was chosen for energies up to 10MV and a depth of 100mm chosen for higher energies. More recently, a reference depth of 100mm for all energies, has been recommended (NCRD,1998; ESTRO, 1997).

Comparison of mini-phantom and build-up cap

It is important to note that the only difference between measurements in a mini-phantom and measurements in a build-up cap, is the depth. The argument that the width of the phantom must be wide enough to achieve lateral electronic equilibrium applies equally to measurements in either type of phantom. If Sc can be measured in a high energy beam in a mini-phantom with only 20mm (radius) of side scatter , then equally it can be measured in a build-up cap with side walls which are < the depth of dmax.

Measurements under electronic disequilibrium

Li (1995) used MC (EGS4) to calculate the radius at which lateral electronic equilibrium (LEE) occurs. At 6MV this was found to be $<1.3 g/cm^2$. S_c was measured in the field size range 360x360 to $40x40mm^2$ with a 0.12cc IC at 50mm deep in polystyrene mini-phantoms of different radii (=<LEE) and the results compared with measurements in brass build-up caps (=LEE). In fields $>100x100mm^2$, S_c was found to be higher in the mini-phantom compared to the brass caps. In fields $<100x100mm^2$, Sc was lower in the mini-phantom

compared to brass. As all differences were less than 1%, the authors concluded that electronic equilibrium need not be preserved in the measurement of S_c. However, the authors found that electron contamination was a problem in phantoms with radii <LEE and recommended that a mini-phantom or build-up cap should be wide enough to avoid electron contamination in the lateral direction. This appeared to have been a problem only in a mini-phantom of radius 5mm, in an 18MV beam. Allahverdi (1998) reported a decrease in S_c of approximately 3% measured with a 0.125cc IC in a 40mm diameter mini-phantom at dmax compared with measurements in a build-up cap with side-wall thickness of 9mm.

Direct measurement

An alternative to measuring S_c in a build-up cap or mini-phantom, is to measure S_c directly in a full scatter phantom. Lam and Ten Haken (1996) reported on a blocking technique, whereby a 50x50mm^2 field was defined by a large cerrobend cut-out. Measurements were made in a full scatter phantom, under the cut-out, for collimator settings between 50x50 and 300x300mm^2. Although the phantom scatter remained the same (constant cut-out size), the collimator scatter changed (variable collimator setting) and thus values of S_c could be obtained. This method does however assume that there are no additional scatter effects caused by the cerrobend cut-out.

Detectors

Although a cylindrical IC (0.1-0.6cc) is generally used to measure S_c in a build-up cap or mini-phantom in conventional field sizes between 400x400 and 50x50mm^2, Karlsson et al (1997) investigated the use of both a shielded and an unshielded diode. Measurements were made at the isocentre, 100mm deep in a mini-phantom, in field sizes >=50x50mm^2 and compared with the results from a 0.5cc IC. No differences >0.2% were detected between the diodes and the IC, in energies between 4 and 50MV. Although differences had been found between the detectors in the measurement of S_{cp}, these were caused mainly be the response of the diodes to phantom scatter. As phantom scatter is minimal and relatively constant in the measurement of S_c in these fields, the differences between the detectors effectively disappear.

6.1.3 Small field problems

If a mini-phantom or build-up cap with a cross-section smaller than the smallest field size is used to measure S_c in very small fields (<40x40mm^2), S_c will necessarily be measured under

conditions of electronic disequilibrium. Although Li (1995) and others (Allahverdi, 1998; Allahverdi and Thwaites, 1999) showed that this was not a significant problem for fields >40x40mm^2, the system has not been tested for smaller fields. Instead, S_c in smaller fields has generally been measured at extended FSD, or in a high density build-up cap.

The problems of detector size are the same in the measurement of both S_{cp} and S_c. A suitable detector for the measurement of S_c should therefore have a sensitive width which can lie within the high dose region of the in-air profile. Problems such as spectral change and a rapid fall off in dose at small fields are also common between the measurement of S_{cp} and S_c. Once again, the correction factors necessary to convert the detector readings to dose may now not necessarily cancel out in the field size of interest and the reference field. Again, this problem can be minimised by normalising the results to the largest small field.

6.1.4 Small field S_c in the literature

Overview

Most small field S_c measurements reported in the literature have been carried out using an IC in a build-up cap. The chamber is generally orientated with long axis parallel to the beam, to minimise the effects of volume averaging. However, it has been shown in Chapter 5 that most ICs are unsuitable for measurements in very small field sizes and it is not clear why they should be suitable for the measurement of S_c.

Literature overview

Houdek et al (1983) compared the measurement of S_c with a 0.1cc IC in an aluminium (22mm diameter) and a polystyrene (46mm diameter) build-up cap, for fields between 50x50 and 20x20mm^2 at 3000mm FSD. Both sets of measurements agreed to within 1%, although the authors did not state whether differences were random or whether measurements in one material were systematically higher than the other. Sc dropped by almost 20% between a 100x100 and 10x10mm^2 field, the latter field size being measured only with an aluminium build-up cap. The magnitude of this drop was not discussed.

Arcovito et al (1985) measured S_c with a 0.22cc IC in an aluminium build-up cap in fields down to 10x10mm^2 at 1000, 2000, 3000 and 4000mm FSD. Fields less than 40x40mm^2 were generated by adding custom-made lead collimators to the inside of the movable linac collimators. S_c was independent of FSD, although the uncertainty was not stated. S_c decreased rapidly below a 40x40mm^2 field such that the overall drop was approximately

15% between the 100x100 and 10x10mm^2 fields. However, the value of S_c tabulated in the results was 0.920, which appears to be a contradiction.

Rice et al (1987) measured S_c in stereotactic collimators between 40 and 12.5mm diameter using a 0.1cc IC in polystyrene, brass and aluminium build-up caps. The thickness of each cap was 1.5g/cm^2. In all measurements, the linac collimators were set to a constant 40x40mm^2 field. The fields defined by collimators <17.5mm diameter, covered the width of the brass cap only and as a result, brass was used in all field sizes. S_c was found to be constant and equal to the open field setting of 40x40mm^2.

Sixel and Podgorsak (1993) used an unspecified type of diode (2.5mm sensitive width) with brass build-up caps of between 2 and 3.5mm "thickness", which, from the text, must refer to the cap widths. Sc was measured in stereotactic collimators between 30 and 10mm diameter, for beam energies of 6, 10 and 18MV. In all measurements, the linac collimators were set to a constant 40x40mm^2. For all beam energies, S_c was found to be constant and equal to S_c in the open 40x40mm^2 field. This was despite the fact that the build-up cap would appear to be too large for measurements in the smallest field. S_c was found to decrease with beam energy, although the overall spread was only 2%.

Zhu and Bjarngard (1994) measured S_c in open fields between 400x400 and 8x8mm^2, with a 0.1cc IC in a Pb build-up cap (3.5g/cm wall thickness) and in an acrylic mini-phantom (40mm width) at 50mm deep. S_c appears to have been measured at either 3000 or 4000mm FAD, although this is not clear. There were no differences between measurements in the two materials. However, the 8x8mm^2 field would not have covered the mini-phantom, even at 4000mm FAD and therefore it must be assumed that not all field sizes were measured in both types of phantom. S_c was shown to drop by between 10 and 60% on four types of accelerator with energies between 6 and 10MV. The authors examined the reasons for this effect, noting that when the linac collimators were set to =<30x30mm^2, part of the opening at the top of the primary collimator was obscured when viewed from the measurement point. This was thought to have contributed to the large drop in S_c. However, the magnitude of the drop in S_c was also thought to be related to the size of the source which is related to the design of the beam bending mechanism. A linac without a beam bending device was thought to produce a relatively large spot on the target, whereas a 90° bending device was thought to focus the beam and reduce the size of the spot. However, although a 270° bending system does produce the smallest spot, a 90° bending system (unless with slalom system) actually spreads out the spot. The authors found that the linac with the, assumed, largest spot (Clinac 6/100), resulted in the largest drop in S_c and the linac with the assumed

smallest spot (Clinac 1800), resulted in the smallest drop, with the Philips SL75 lying in between. The authors also noted that the source on the SL75 must extend to 5mm from the CAX, but this would appear to be excessively large.

Heydarian et al (1996) measured S_c in stereotactic collimators between 41.0 and 8.9mm diameter, normalised to the largest collimator. The field size setting on the linac collimators was unspecified. Measurements were carried out at an extended FSD of 1580mm, with an IC, shielded diode and a diamond, each with a brass build-up cap of $1.7g/cm^2$. Although the manufacturers of each detector were stated, no detector dimensions were explicitly given. The IC and diamond agreed in fields down to 8.9mm diameter, with the diode approximately 0.5% higher. The fall in S_c with collimator diameter was fairly constant and the total drop between the 41.0 and 8.9mm diameter collimators was only 7%.

Allahverdi (1998) measured S_c in fields down to $15x15mm^2$ with a 0.125cc IC in a selection of build-up caps, at an extended FSD of 1500mm. The spread in S_c over all build-up materials was >5%, at 6MV. Measurements in brass were the highest. Measurements in perspex caps with sidewalls ranging from 12 to 21mm water equivalence were spread over approximately 3% in the smallest field. The highest value for S_{cp} measured in a perspex cap, was for sidewall thickness of 18mm. However, this is larger than the field dimensions. The total drop in S_c from the $100x100mm^2$ field was almost 30%.

Comparison of results

The methods used in each of the above publications are summarised in Table 6.1.

Author	Energy /MV	Linac	Field Type	Detector	build-up cap	FAD/ mm
Allahverdi (1998)	6	BBC CH6	□	0.125cc IC	perspex	1500
Arcovito et al (1985)	10	Toshiba LMR-13	□	0.1cc IC	polystyrene aluminium	1000-4000
Heydarian et al (1996)	6	Siemens Mevatron	○	IC, diode diamond	brass	1580
Houdek et al (1983)	9	Neptune-10	□	0.22cc IC	aluminium	3000
Rice et al (1987)	6	Clinac 6/100	○	0.1cc IC	brass	1000
Sixel and Podgorsak (1993)	10	Clinac 1800	○	diode	brass	1000 (FSD)
	6	Clinac 2300	○	diode	brass	1000 (FSD)
	18	Clinac 2300	○	diode	brass	1000 (FSD)
Zhu and Bjarngard (1994)	6	Philips SL75-5	□	0.1cc IC	Lead	3000
	6	Clinac 6/100	□	0.1cc IC	Lead	3000
	10	Clinac 1800	□	0.1cc IC	Lead	3000

Table 6.1. Summary of the methods used to measure S_c, in each of the publications presented in Figure 6.1. ○ indicates measurements in circular stereotactic collimators and □ indicates measurements in square fields.

The linac collimators were set to 40x40mm^2 for all measurements in stereotactic collimators in Rice et al (1987) and Sixel and Podgorsak (1993). Although Heydarian et al (1996) also carried out measurements in stereotactic fields, they did not specify the setting on the movable collimators and the results were only normalised to the largest collimator. All S_c measurements which were normalised to an open 100x100mm^2 field are plotted in Figure 6.2, where the squares represent open square fields defined by the movable linac collimators and the circles represent stereotactic collimators (linac collimators =40x40mm^2).

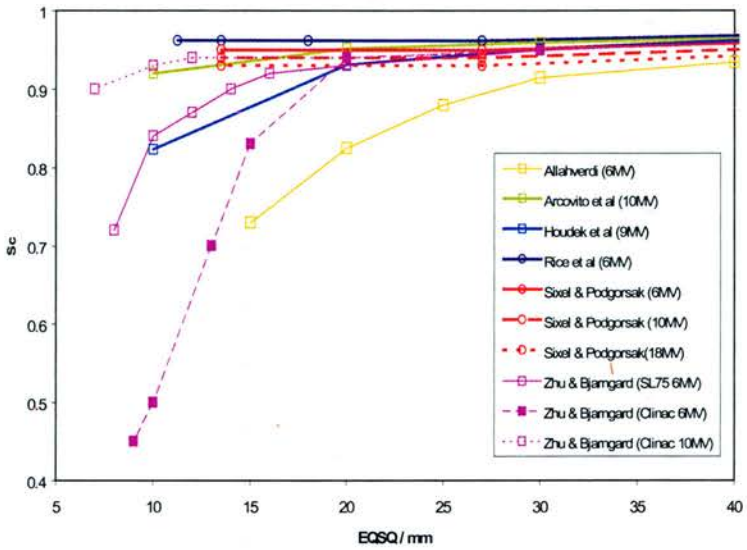

Figure 6.2. Published values of S_c, measured at dmax in stereotactic collimators and in small square fields. Data summarised in Table 6.1.

The drop in S_c is different in each publication and is dependent on either the methodology or the linac used. All measurements in stereotactic collimators show S_c to be constant with collimator diameter (Rice et al, 1987; Sixel and Podgorsak, 1993), down to 10mm. This suggests that the head scatter in stereotactic collimators within this range, is only dependent on the field size setting on the movable collimators, and not on the diameter of the stereotactic collimators. This also shows that the stereotactic collimators neither add scatter, nor shield out scatter from components above, within this range.

S_c drops with field size setting on the movable linac collimators, due to the reduction in the amount of flattening filter "seen" at the measurement point. However, it is apparent from Figure 6.2 that the magnitude of the drop is highly dependent on the design of the linac.

6.1.5 Shielding of the source

Introduction

Zhu and Bjarngard (1994) described the problem of source shielding with respect to both the size of the x-ray source on the linac and width of the aperture at the top of the primary collimator. Each of these is examined in detail, with respect to the 600CD.

Spot size

The size of the photon source, S, is determined by the size of the electron spot on the target. This is dependent on the beam bending system and on Varian linacs is only a few mm.

Shielding of the source

Figure 6.3 shows a diagrammatic view of the head of the Clinac 600CD.

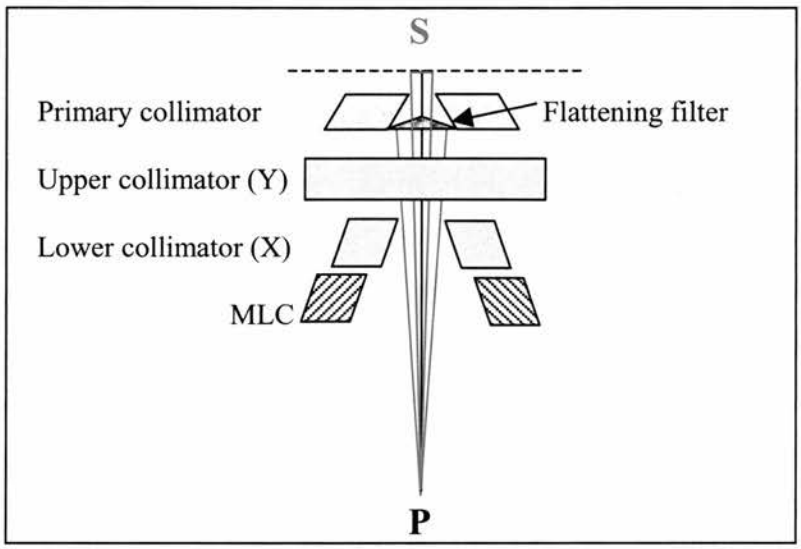

Figure 6.3. A diagrammatic view of the head of the Clinac 600CD.

The amount of scatter visible at point P will be determined primarily by the amount of the flattening filter (BFF) "seen" from the point of measurement. This will in turn be determined by the field size setting on the movable collimators, as indicated by the pink lines in Figure 6.2 above. However, the size of the incident photon beam on the BFF is determined by both the spot size and the width of the aperture at the top of the primary collimator. If either of these are obscured when viewed from the point of measurement, the scatter from the flattening filter will effectively be reduced. This may occur at very small field sizes, as indicated by the red lines in Figure 6.3 above.

It is also important to remember that the detector at P is not a point detector and has a finite size. This will mean that a different area of the flattening filter, source or top of primary collimator will be seen by each point on the sensitive area of the detector, effectively broadening the relevant areas.

6.1.6 Summary

All small field measurements require an accurate and reproducible experimental set-up. To measure Sc, the detector and phantom must both be aligned with the centre of the radiation field. This becomes increasingly difficult at extended FSD where the shadow of the crosswires may not be easily visible and the gantry sag is more significant, particularly as

both the field size and the width of the high dose region decrease. To measure S_c at the isocentre, both the detector and the phantom must be smaller than the high dose region in the collimator of interest and S_c will be measured under electronic disequilibrium. If the results are satisfactory, there is no need for a high density build-up cap.

Only Heydarian et al (1996) compared detectors (IC, shielded diode, diamond) in the measurement of small field Sc. Most other authors have used only ICs and Sixel and Podgorsak (1993) used only a diode (type unspecified). A full comparison of detectors has not therefore been carried out in the measurement of S_c.

6.1.7 Aim

There were several aims to this work. The first was to determine an optimum phantom for the measurement of S_c. Phantom sizes and materials were compared both in stereotactic collimators between 40 and 12.5mm diameter and in open fields between 40x40 and 10x10mm^2, at both dmax and 50mm. The second aim was then to use the optimum phantom width and material to compare S_c measured with a range of detectors. In addition to the above fields, small stereotactic collimators between 10 and 5mm diameter and MLC fields between 40x40 and 10x10mm^2 were also investigated. The optimum detector was then used to measure S_c in the full range of stereotactic collimators. These results were used to calculate S_p values in Chapter 7. The third aim was to investigate reasons for changes in head scatter in small fields, with respect to real changes in the head and also with respect to differences caused by the detectors and the methodology. The fourth aim was to investigate a method of normalisation. Initially, all measurements were normalised to the largest small field (40mm collimator or 50x50mm^2 open field) and therefore an optimum method of normalisation to the 100x100mm^2 reference field had to be determined. This was carried out for all solid state detectors and the 0.125cc IC, in several phantom diameters. Finally, differences between beam defining systems and linacs were investigated.

6.2 Materials and Methods

6.2.1 Materials

Detectors

The diamond, PFD, EFD and SFD were compared in all small field measurements. The 0.125cc IC was used only to compare the normalisation of the small field results to the reference 100x100mm^2 field.

Phantoms

Build-up caps (diameter 10mm, length 40mm) of solid water (WT1) and of brass, with minimum wall thickness had been designed for head scatter work in larger field sizes (Allahverdi, 1998; Allahverdi and Thwaites, 1999). In this work, these are denoted as build-up caps. Rods of brass and WT1 had also been milled for the same work to increase the effective depth of measurement in both materials, to 50mm. These, used with the build-up caps are denoted as 50mm-caps. Build-up caps and 50mm-caps were also designed without side scatter (no walls), with diameters equal to the physical diameter of each detector. These are known as build-up tops and 50mm-tops. Brass build-up caps and tops were not initially designed for the IC nor the SFD. The caps and tops for the solid state detectors are shown in Figure 6.4.

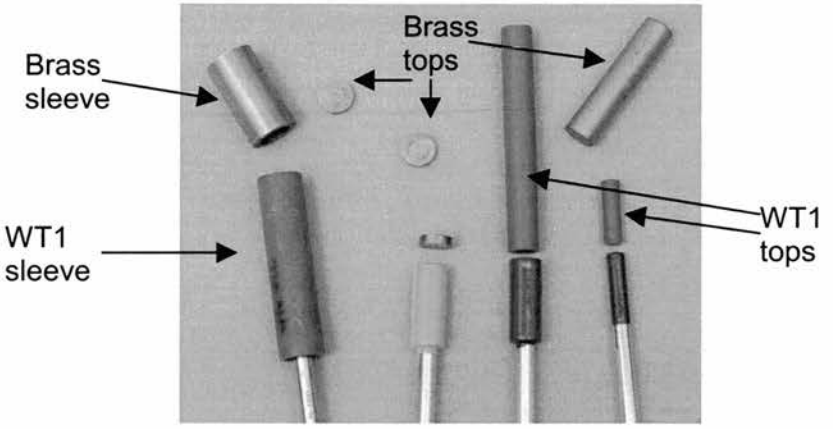

Figure 6.4. Build-up and 50mm caps and tops of brass and WT1.

Two WT1 mini-phantoms with cross-sectional diameters of 40mm had previously been made (Allahverdi, 1998; Allahverdi and Thwaites, 1999). These are shown in Figure 6.5.

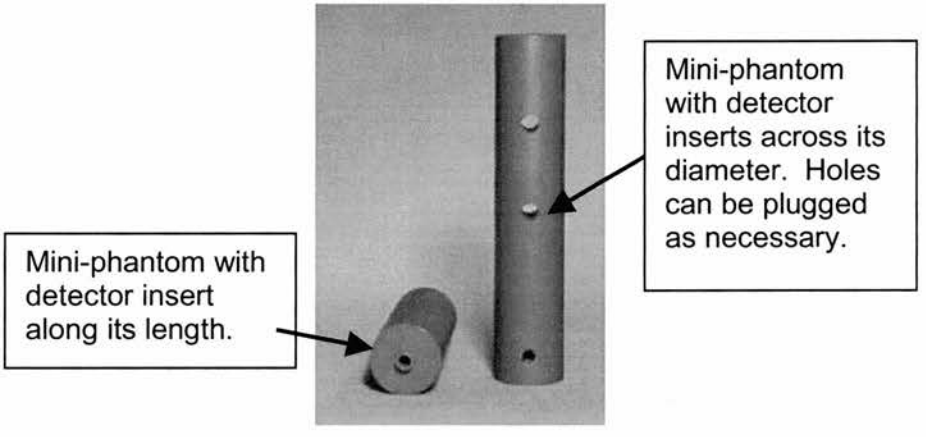

Figure 6.5. The two types of mini-phantom used; one (on the left) with detector insert along the long axis and one with the insert across the diameter.

The diamond, PFD, EFD and SFD were all used in the first type of phantom, with their long axes parallel to the beam CAX, at both dmax and 50mm. The 0.125cc IC was used both parallel and perpendicular to the beam CAX, again at both dmax and 50mm.

6.2.2 Methods

Linacs

Although S_c was measured on all three linacs, a thorough comparison of detectors and phantoms was only carried out on the 600CD. The results from the 600CD are therefore presented in full and a final comparison made with the other two linacs.

Geometry of the head

The geometry of the head of the 600CD was examined for each beam defining system, with reference to the amount of the flattening filter, primary collimator aperture and spot size, visible from the point of measurement. Figure 6.6 shows all the relevant parameters.

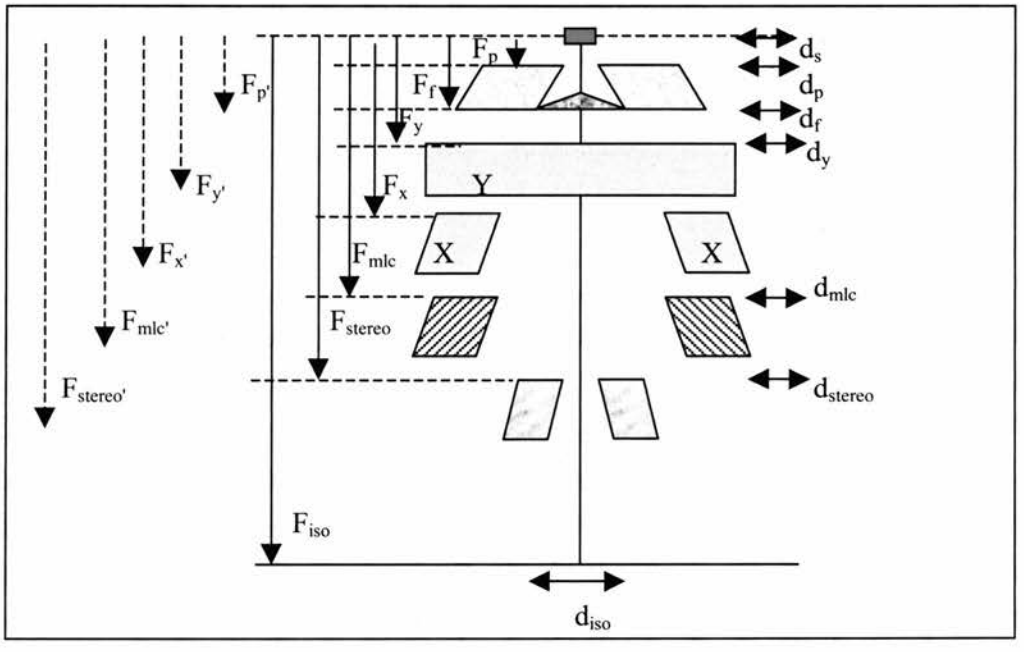

Figure 6.6. Schematic view of the geometry of the head of the 600CD, showing all the relevant parameters.

F indicates the FSD to the appropriate feature such as the Y collimators. d indicates the width of the opening at the appropriate level, for example, at the top of the primary collimator. Table 6.2 shows the values of the fixed parameters used in calculations.

Parameter	Description	mm
F_p	Distance from target to top of primary collimator	21
$F_{p'}$	Distance from target to bottom of primary collimator	113
F_f	Distance from target to base of flattening filter	113
F_y	Distance from target to top of Y moveable collimators	280
$F_{y'}$	Distance from target to bottom of Y moveable collimators	358
F_x	Distance from target to top of X moveable collimators	367
$F_{x'}$	Distance from target to bottom of X moveable collimators	445
F_{mlc}	Distance from target to top of MLC	482.5
$F_{mlc'}$	Distance from target to bottom of MLC	536
F_{stereo}	Distance from target to top of stereotactic collimator	642
$F_{stereo'}$	Distance from target to bottom of stereotactic collimator	770
F_{iso}	Distance from target to isocentre	1000
d_p	width of top of primary collimator	10.5
d_f	width of base of flattening filter	56.3
d_s	width of the source	2*

Table 6.2. Values of the fixed parameters used in calculations. * indicates the estimated value for the source width.

Table 6.3 shows the variables used in the calculations

Parameter	Description
d_y	width of top of Y moveable collimators
d_x	width of top of X moveable collimators
d_{mlc}	width of top of MLC
d_{stereo}	width of top of stereotactic collimators
d_{iso}	width of field at the isocentre

Table 6.3. Variables used in the calculation of linac head geometry.

Phantom comparison

Figure 6.7 shows the experimental set-up for the measurement of S_c in small fields, using the build-up caps and tops and the 50mm-caps and tops.

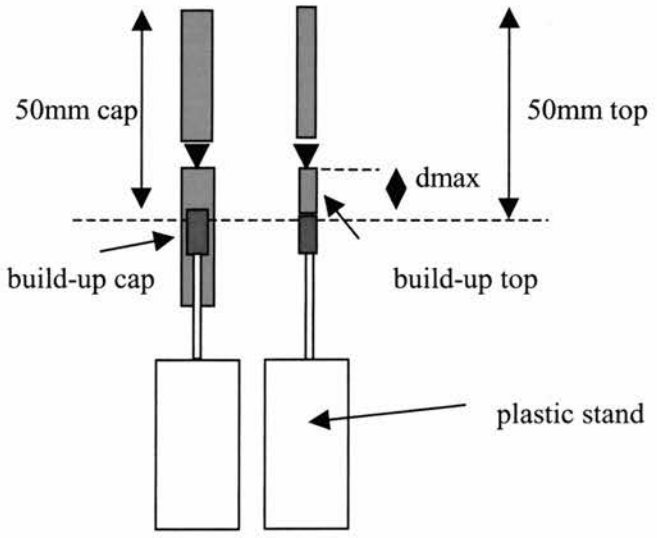

Figure 6.7. The experimental set-up for the measurement of S_c in small fields, using the build-up caps and tops and 50mm-caps and tops.

The stand was composed of the minimum amount of plastic, to both minimise scatter and ensure that the set-up was rigid and reproducible. In fields >40x40mm^2, the measurement of S_c requires that the width of the phantom is less than the minimum field size at the surface of the phantom. Table 6.4 shows the field size at the surface ($s_{surface}$) of a phantom for a field size at the isocentre (s_{iso}), when the measurement point is placed at dmax and 50mm.

	$s_{surface}$ /mm	
s_{iso} /mm	dmax	50mm
12.5	12.3	11.9
10	9.9	9.5
7.5	7.4	7.1
5	4.9	4.8

Table 6.4 Calculation of the field size at the surface ($s_{surface}$) of a phantom for measurements at dmax, for each field width at the isocentre (s_{iso}).

It is apparent that a 10mm diameter build-up cap is only suitable for measurements in fields >= 12.5mm. Measurements in smaller fields require phantoms with smaller diameters. The minimum phantom width is determined by the diameter of the outer casing of each detector. For the diamond this is 7.3mm, which implies that it can only be used at 50mm deep for fields > 7.5mm diameter. The shielded and unshielded diodes (diameter 7mm) can be used at both depths down to 7.5mm diameter and although the SFD has a diameter of only 5mm, it will also be unsuitable for measurements in the 5mm diameter collimator, unless the FSD

is extended by approximately 15mm. The comparison of phantom widths was therefore carried out in field widths >10mm.

Detector comparison

The results from the in-air profile measurements in Chapter 4 were used to estimate the response of each detector in each field, by integrating over the detector area. The detector comparison was carried out in all field sizes, with the most appropriate phantoms.

Measurements using the set-up shown in Figure 6.7 were compared against measurements using the BDAS for positioning, on a single occasion, for the smallest collimators. The profiles in the 5mm collimator were scanned using the SFD, with the WT1 build-up top or 50mm-top and the zero co-ordinates set at the centre of the 50% regions. S_c measurements in the 12.5, 10, 7.5 and 5mm collimators were then normalised to the 40mm collimator.

Normalisation

Measurements in stereotactic collimators were initially normalised to the 40mm diameter collimator (movable linac collimators set to 50x50mm^2) and those in the square fields (open and MLC) to an open 50x50mm^2 field. Normalisation of the 40mm diameter collimator to the 50x50mm^2 open field was investigated by comparing detectors and build-up caps and tops. Normalisation of the 50x50mm^2 to the 100x100mm^2 reference field was investigated by comparing detectors (including the 0.125cc IC) in the build-up caps and tops and in the mini-phantoms. All measurements were carried out at both dmax and 50mm deep.

Statistics

Each measurement in each experiment was repeated on the 600CD on at least five separate occasions. The results were meaned and the standard deviation (s.d.) and coefficient of variation (s.d./mean x 100%) calculated. Differences between sets of measurements were considered insignificant if they were <0.3%. To determine whether differences >=0.3% were significant, a two tailed t-test was carried out.

6.3 Results and discussion

6.3.1 Small field phantom comparison

Stereotactic fields

Initially, brass and WT1 caps and tops were compared in the measurement of S_c in all collimators down to 12.5mm diameter, normalised to the 40mm. The reproducibility of the measurements, as determined by the coefficient of variation (coeff. of var.) in the 12.5mm collimator, relative to the 40mm collimator, is shown in Table 6.5.

	coeff. of var. (% of mean)			
Detector	WT1 cap	WT1 top	Brass cap	Brass top
Diamond	0.1	0.1	0.1	0.3
PFD	0.2	0.2	0.2	0.4
EFD	0.2	0.1	0.3	0.5
SFD	0.4	0.3	-	-

Table 6.5. The coefficients of variation, expressed as a percentage, for each set of measurements (12.5/40mm collimators).

The results in Table 6.5 show that the reproducibility of each measurement set was within 0.5%. Although this is good, the measurements are less reproducible than in the measurement of S_{cp} in the corresponding collimator. This is because, for S_c, the detector stem must be fixed in air, parallel to the beam CAX. This is quite difficult without a more rigid set-up than that shown in Figure 6.7. However, it is not apparent why the brass measurements appear to be less reproducible than those in WT1. The mean values for each measurement set are compared for build-up caps and tops of RMI and brass, in Table 6.6.

	S_c (12.5/40mm collimators)					
Detector	WT1 cap	WT1 top	Brass cap	Brass top	mean	coeff. of var.
Diamond	.989	.988	.988	.988	0.988	0.1
PFD	.989	.988	.990	.989	0.989	0.1
EFD	.989	.988	.990	.991	0.990	0.1
SFD	.988	.991	-	-	0.990	0.2
mean	0.989	0.989	0.989	0.989		
coeff. of var.	0.1	0.2	0.1	0.2		

Table 6.6. S_c (12.5/40mm collimators) at dmax for each detector and phantom.

The mean values for each detector were averaged over all caps and tops (row mean) and the coefficients of variation calculated. These were comparable with the individual coefficients in Table 6.5 and show that there are no significant differences between phantoms. The

mean values of S_c for each phantom were averaged over all detectors (column mean) and again the coefficient of variation showed no significant differences between detectors. The coefficient of variation increased at 50mm (up to 0.8% for the PFD), due to increased difficulties in aligning the detector and phantom with the beam CAX at 50mm deep. A comparison of brass and RMI at 50mm deep showed a 0.3-0.5% increase in S_c in the brass for all detectors ($p=<0.1$). Weber et al (1997) also reported a 0.3% increase in S_c in fields $<50x50mm^2$, at 4MV, in brass, due to a slight increase in the quality of the beam. As the effect is likely to be less at dmax, it was probably masked by experimental uncertainties. The S_c values for each detector, with each type of build-up, at both dmax and 50mm, in the 12.5mm collimator are summarised in Figure 6.8.

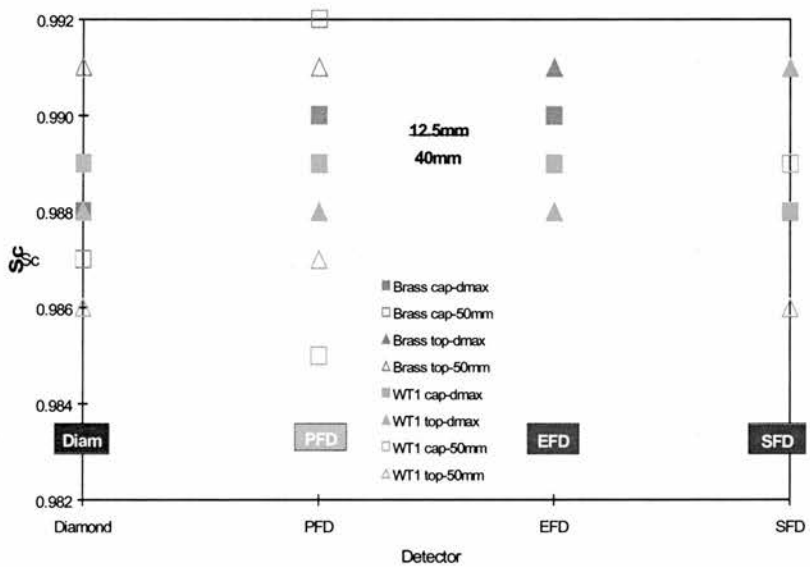

Figure 6.8. Summary of the S_c values for each detector, with each type of build-up, at dmax and 50mm in the 12.5mm collimator

Although it was shown in Table 6.6 that there were no significant differences between phantoms, it is apparent that there is a very small, consistent, difference between the brass and WT1. Although the spread in results over all detectors and phantoms is only of the order of 0.7%, there is a small increase in S_c in brass. This is probably due to the increase in beam quality which predominantly affects the silicon diodes, due to their energy dependence, but may also be due to secondary electron effects. Monte Carlo modelling is really required to explain the effect in full.

Open fields

Although a 10mm diameter phantom is unsuitable for measurements in a 10x10mm^2 field, some measurements had previously been carried out and are worth considering. The reproducibility, as determined by the coefficient of variation, is shown in Table 6.7.

	coeff. of var. (% of mean)			
Detector	WT1 cap	WT1 top	Brass cap	Brass top
Diamond	1.6	0.9	0.6	0.7
PFD	0.7	0.5	1.1	0.9
EFD	1.4	1.2	0.7	0.5
SFD	0.9	0.6		

Table 6.7. The coefficients of variation, expressed as a percentage, for each set of measurements (10x10/50x50mm^2 open fields).

The coefficients of variation are higher in the open fields than in the stereotactic fields, which is a reflection of the reproducibility of the field size setting. The results for S_c measured at dmax with each detector, in the 10x10mm^2 field are shown in Table 6.8.

	Sc (10x10/50x50mm^2 open fields)					
Detector	WT1 cap	WT1 top	Brass cap	Brass top	mean	coeff. of var.
Diamond	.876	.899	.87	.903	0.887	1.9
PFD	.899	.912	.915	.924	0.913	1.1
EFD	.89	.904	.903	.924	0.905	1.6
SFD	.896	.927			0.912	2.4
mean	0.890	0.911	0.896	0.917		
coeff. of var.	1.1	1.3	2.6	1.3		

Table 6.8. Sc (10x10/50x50mm^2) at dmax for each detector and each phantom.

The mean values for each detector were averaged over all caps and tops (the row mean) and the corresponding coefficient of variations calculated. These were greater than the individual coefficients for each measurement set. This shows that there are real differences between phantom materials. The mean values for each cap and top were averaged over all detectors (the column mean) and again the coefficient of variation is larger. This shows that there are also real differences between detectors. The measurements in the build-up caps could be smaller than those in the build-up tops, due to a lack of phantom scatter in the small field measurements, as calculated in Table 6.4.

The relative results at 50mm were the same as those at dmax, although again the coefficients of variation were larger, due to the increased set-up difficulties at 50mm. Figure 6.9 shows

a summary of the Sc values for each detector, for the build-up tops only, at both dmax and 50mm, the 10x10mm^2 open field, relative to the 50x50mm^2.

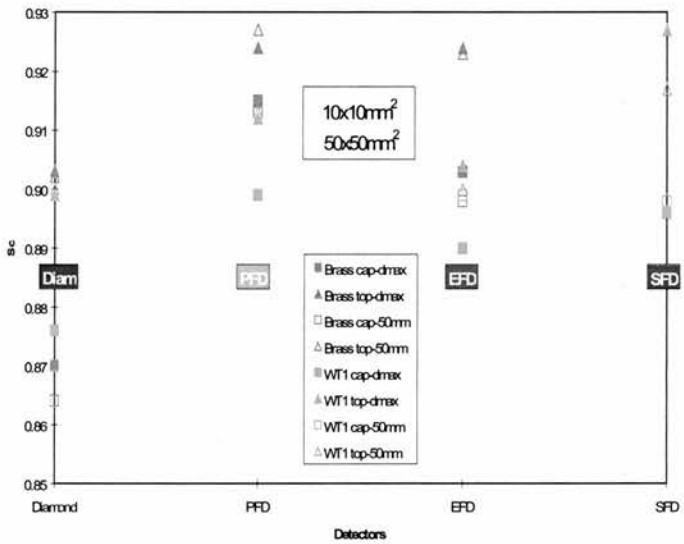

Figure 6.9. Sc values for each detector, with each type of build-up, at both dmax and 50mm, in the 10x10mm^2 open field relative to the 50x50mm^2 field.

The results for all detectors are spread over 3%, which is more than for the stereotactic collimators. Although there is also increased uncertainty in the measurements in the open fields, there does appear to be a much larger increase in S_c in the brass than was shown in the 12.5mm diameter collimator. Again, this must be due to spectral changes and secondary electron effects in the brass. As there are likely to be more secondary electrons in the open fields compared with the stereotactic collimators, the effects are probably enhanced. However, Monte Carlo modelling is required to explain the effect in full.

Summary

Although both the build-up tops and caps are suitable for measurements in stereotactic collimators between 40 and 12.5mm diameter, only the tops are suitable for smaller collimators and for measurements in the open 10x10mm^2 field. As brass has been shown to produce higher values of Sc than in WT1, possibly due to spectral changes and secondary electron effects, build-up tops of WT1 with diameters equal to the diameters of each detector were chosen as the most suitable phantoms for S_c measurements in small fields.

6.3.2 Detector comparison: stereotactic fields

Overview

All detectors were compared in each field situation using the WT1 build-up and 50mm tops. The in-air profiles reported in Chapter 4 were used to determine the response in each detector. In addition, the geometric aspects of the linac head in the stereotactic field situation were investigated with respect to changes in scatter in small collimators.

Detector response

The high dose region of each in-air profile, measured with the SFD, was fitted with a fourth order polynomial. Figure 6.10 shows an example for the 5mm collimator.

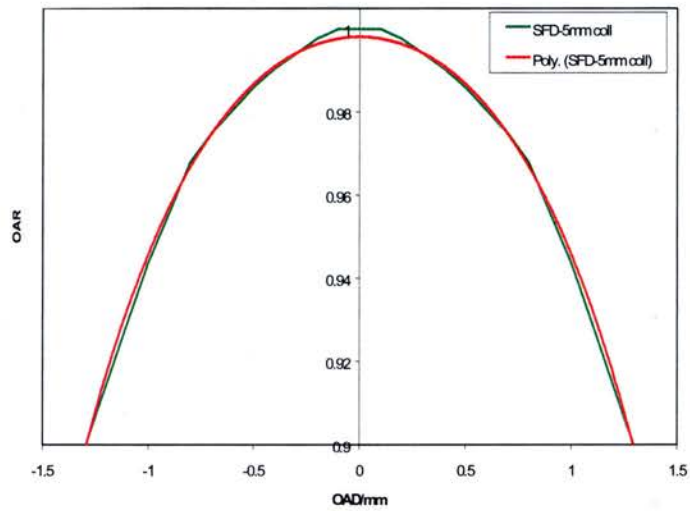

Figure 6.10. In-air profile in the 5mm collimator, measured with the SFD and fitted with a fourth order polynomial.

The profile was integrated over the sensitive area of each detector to determine the amount of under-response caused by its finite size. The results of the integration give an approximate value for the percentage response in the detector, as shown for the 10 and 5mm diameter collimators in Table 6.9.

Detector	sensitive width / mm	% Response 12.5mm coll.	10mm coll.	5mm coll.
Diamond	2.2	99.9	99.8	96.3
PFD/EFD	2.5	99.9	99.7	93.8
SFD	0.6	99.9	99.9	99.5

Table 6.9 Calculated responses for each detector in the 10 and 5mm collimators.

Only the SFD has a sensitive width (0.6mm) which is small enough to be positioned within the 99% isodose of all collimators. The maximum sensitive widths of the other detectors (2.2-2.5mm) lie within the 99% isodose of all collimators other than the 5mm diameter where they may under-respond by approximately 4%.

Reproducibility

The reproducibility, in terms of the coefficient of variation, of the measurements of S_c in the build-up tops, for collimators between 12.5 and 5mm diameter is shown in Table 6.10.

	coeff. of var. (%)		
Detector	12.5mm	10mm	5mm
Diamond	0.1	0.2	0.3
PFD	0.2	0.2	1.1
EFD	0.1	0.1	1.1
SFD	0.3	0.5	1.2

Table 6.10. Coefficients of variation, expressed as a percentage, for each set of experiments for each detector in each collimator diameter.

Only one or two measurements were carried out in the 7.5mm collimator, due to time constraints and therefore a corresponding coefficient of variation could not be calculated. The coefficient of variation in the 20-10mm diameter range is <0.3% for all detectors other than the SFD, which is <0.5%. In the 5mm collimator this increases to 1.2% for all detectors.

When re-measured using the BDAS system, only the PFD and SFD measured values of S_c which were higher than those originally measured with the set-up in Figure 6.6. Increases of 1.5-3% were only apparent for measurements in the 7.5 and 5mm collimators and these values were at the upper limit of the original range of values. This suggests that positioning errors caused the larger spread of results in the smallest collimator. The highest increase occurred with the SFD in the 5mm collimator, which produced a value of S_c which was almost 3% higher than that measured conventionally. The EFD and diamond were thought to have been positioned correctly in the original measurements.

S_c results

The higher values were used to complete the curves in Figure 6.11 which shows S_c measured at dmax, with each detector, in the WT1 build-up top.

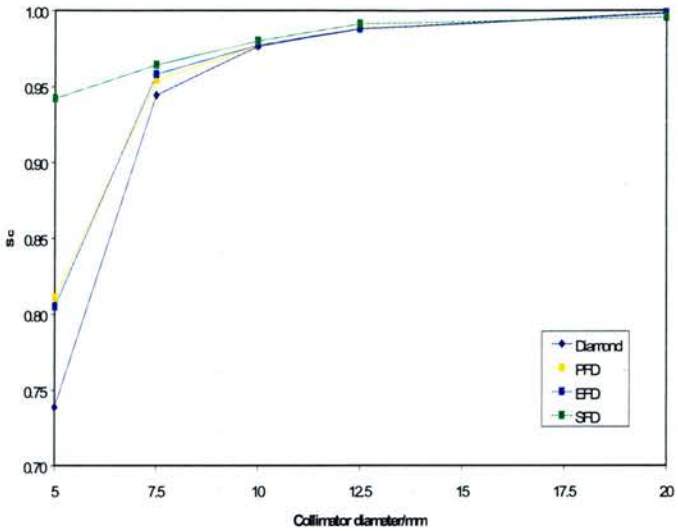

Figure 6.11. S_c measured at dmax, with each detector, in the WT1 build-up top.

There are no significant differences between the detectors for collimators in the 20-10mm diameter range. Below a 10mm collimator, there is a large drop in S_c, which is very detector dependent and due in part to the effects of volume averaging. Figure 6.12 shows the S_c results above, but with the effects of volume averaging accounted for.

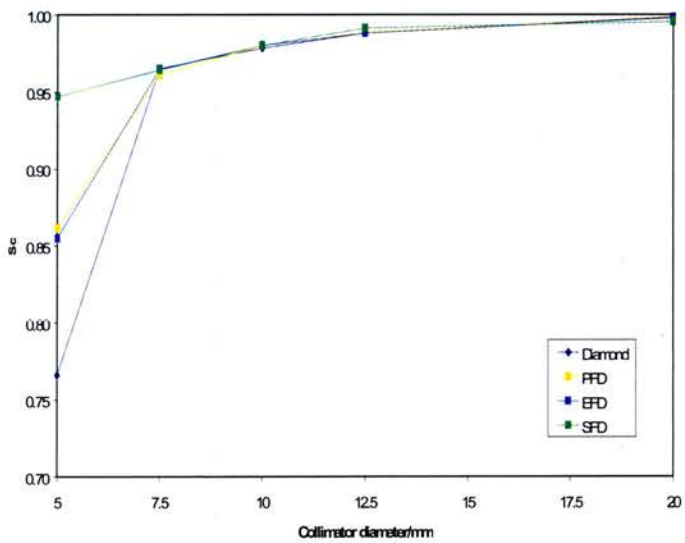

Figure 6.12. Sc measured at dmax, with each detector, in the WT1 build-up top, with the effect of volume averaging accounted for.

It is apparent that volume averaging does not account for the differences between detectors in the 5mm diameter collimator, where there is a spread in S_c of approximately 18% over all detectors. There were no significant differences between the results at dmax and those at 50mm. The possible reasons for the differences between detectors are examined individually.

Detector size

Volume averaging may be less accurate for the diamond, due to uncertainties over the size of the plate, as discussed in Chapter 2.

Positioning

Although the effects of positioning have been dealt with by carrying out measurements using the BDAS system, this is only accurate to approximately =/-0.2mm. A positioning error of only 0.2% may still have a large effect on the measured dose, particularly in a collimator where the width of the high dose region is only of the order of 1mm. In addition, there was a problem with the positioning of the diamond, as discussed in Chapter 5.

Phantom size

The calculated beam widths at the phantom surface in Table 6.4 showed that the size of the build-up top was actually too big for measurements in the 5mm diameter collimator, with all detectors. This was because the field size at the surface of each build-up top, was less than the diameter of the top. The effect was smallest for the SFD and greatest for the diamond as it has the largest diameter (7.3mm) and requires the widest top. The effect of the use of a phantom which is too wide will be too include some phantom scatter in the normalisation field (40mm) that will be missing in the small field (5mm). This will lead to a value of S_c which is too low. However, it may be more important to consider the width of the high dose region rather than the field size defined at the 50% level. This is for two reasons; the fall off in dose is very fast and the penumbra accounts for a much larger proportion of the beam. If the high dose region dose not entirely cover the phantom in both fields, S_c will be underestimated. Although this may affect measurements in all collimators <12.5mm diameter, from Figure 6.11 it only appears to be significant in the 5mm collimator where the width of the high dose region is of the order of 1mm.

Spectral changes

As reported in Chapter 5, the calculation of S_c from the ratio of two detector readings assumes that the correction factors necessary to convert the reading to dose are the same in both field sizes. This may not be the case in very small fields without electronic equilibrium. This is more likely to affect the diode results, but the magnitude of the error can only be calculated through Monte Carlo modelling.

Source shielding

Zhu and Bjarngard (1994) reported that the large drop in S_c found on some linacs was due to the design of the linac head, particularly with respect to the size of the source and the width of the aperture at the top of the primary collimator. The inability to "see" the entire aperture or source, from the point of measurement in any field size, would lead to a large drop in Sc. Figure 6.13 shows the head of the 600CD in the stereotactic field situation.

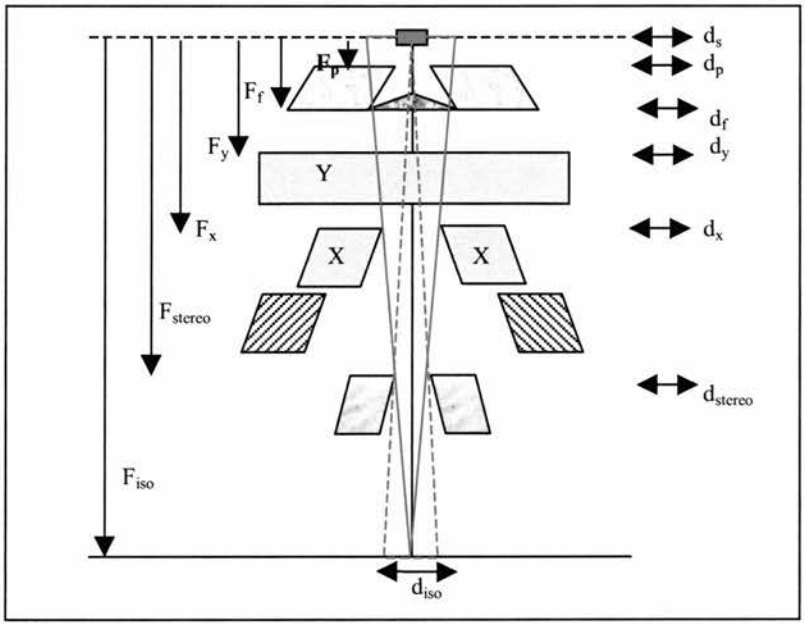

Figure 6.13. Schematic diagram of the head of the 600CD in the stereotactic field situation.

In all measurements in stereotactic fields, the movable linac collimators are set to a constant 50x50mm^2 field. As discussed previously, the amount of head scatter detected at the point of measurement is primarily dependent on the amount of the flattening filter "seen" from the point of measurement. It is important therefore to determine whether it is the position of the movable linac collimators, or the diameter of the stereotactic collimator, which limits the amount of the flattening filter seen. The setting on the linac collimators is considered first. The stereotactic collimator diameter at the isocentre (d_{iso}) which corresponds to the 50mm width on the X and Y collimators separately can be calculated from the distances in Table 6.2, as shown in Table 6.11.

width	Y collimators	X collimators
d_{stereo}	$\frac{1000 - F_{stereo}}{1000 - F_y} . d_y$ = 7.0mm	$\frac{1000 - F_{stereo}}{1000 - F_x} . d_x$ = 10.4mm
d_{iso}	$\frac{1000}{F_{stereo}} . d_{stereo}$ = 10.9mm	$\frac{1000}{F_{stereo}} . d_{stereo}$ = 16.2mm

Table 6.11. Calculation of diameter of stereotactic collimator equivalent to an open $50x50mm^2$ field.

These results show that a point detector used to measure S_c in all collimators with X >16.2mm will "see" the same amount of the flattening filter as the open ($50x50mm^2$) field. The minimum collimator diameter to which this is applicable, is the 17.5mm diameter. Although this suggests that the head scatter will not change in collimators down to 17.5mm diameter, measurements in larger diameters will include scatter from the sides of the movable linac collimators and transmission through the edges. As a result, there is likely to be a very small drop in S_c down to a 17.5mm diameter collimator. Figure 6.14 shows a complete set of S_c values, measured with the EFD and build-up top down to 12.5mm diameter and the SFD and build-up top between 12.5 and 5mm diameter.

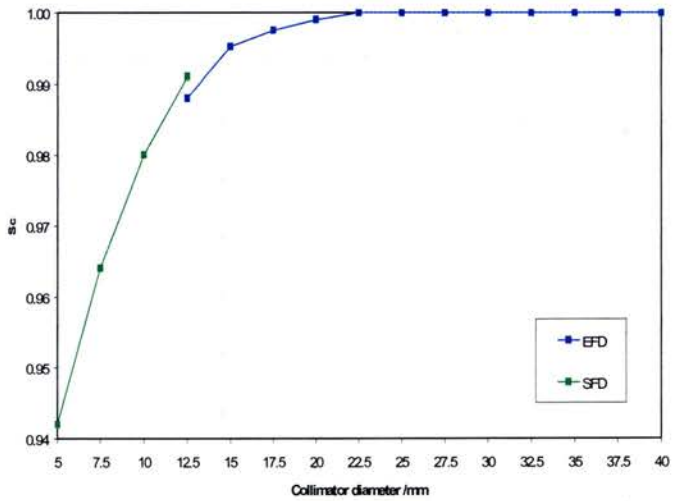

Figure 6.14. S_c measured with the EFD and SFD and corresponding build-up tops, in all stereotactic collimators.

There is a drop in S_c of <1% down to a 12.5mm diameter collimator. The slightly higher value of S_c measured with the SFD (+0.3%) in the 12.5mm collimators is within the experimental uncertainty. Although no drop in S_c down to a 12.5mm collimator was reported by Rice et al (1987) and Sixel and Podgorsak (1993) this is likely to have been due

to the smaller ($40x40mm^2$) field size setting on the linac collimators. However, for collimators <17.5mm diameter, the head scatter is primarily determined by the projection of the stereotactic collimator on to the flattening filter. However, the head scatter may also be affected by shielding of the source, or the aperture at the top of the primary collimator. The collimators at which the entire source, or primary collimator aperture are not "seen" at the point of measurement, are calculated in Table 6.12.

width	Source	Primary collimator
d_{stereo}	$\frac{1000 - F_{stereo}}{1000} . d_s = 0.7mm$	$\frac{1000 - F_{stereo}}{1000 - F_p} . d_p = 3.8mm$
d_{iso}	$\frac{1000}{F_{stereo}} . d_{stereo} = 1.1mm$	$\frac{1000}{F_{stereo}} . d_{stereo} = 6.0mm$

Table 6.12. Calculation of the collimator diameter at the isocentre (d_{iso}) at which the entire source or aperture at the top of the primary collimator, will be seen from the point of measurement.

The entire (estimated at 2mm) source will not be visible from the measurement point only in collimators with diameters =<1mm, which means that the entire source will be visible in the 40-5mm range of collimator diameters. The entire aperture at the top of the primary collimator will not be visible from the point of measurement in collimators with diameters <6mm, which will only affect measurements in the 5mm diameter, collimator.

Discussion

The true head scatter in stereotactic fields >=17.5mm diameter is predominantly determined by the setting on the movable linac collimators. Below this collimator diameter, S_c decreases as the amount of flattening filter visible at the point of measurement is determined predominantly by the collimator diameter. In the 5mm diameter collimator, some of the scatter from the aperture at the top of the primary collimator may be shielded, due to the small size of the collimator.

However, the head scatter measured by different detectors is affected by several other parameters. The finite size of the detector will cause volume averaging to occur, although the magnitude of this effect is no more than 6% for the EFD and PFD in the 5mm diameter collimator. Positioning of the detectors can also result in a reduction of S_c, although this is likely to be less than 3%. The size of the phantom will also lead to some under-estimation of S_c, which is only significant in the 5mm diameter collimator. This is due to the inclusion

of phantom scatter in the 40mm diameter collimator, which is missing in the smallest collimator. Although this effect could be minimised by carrying out measurements in the smallest collimator at extended FSD, the effect of changes in electron contamination would also have to be investigated as the FSD would have to be increased to approximately 2000mm. This leads to additional set-up difficulties which again require further investigation. Finally, spectral changes may affect the conversion of a detector reading to dose, in the field size of interest and in the normalisation field. It is apparent therefore, that all of these effects contribute to an underestimation of S_c and only Monte Carlo modelling can provide detailed answers as to the magnitude of each of these effects.

6.3.3 Detector comparison: Open fields

Overview

All detectors were compared in each field situation using only the WT1 build-up tops and 50mm tops. The in-air profiles reported in Chapter 4 were used to determine each detector response. In addition, the geometrical aspects of the linac head in the open field situation were investigated with respect to changes in scatter in small open fields.

Detector response

The high dose region of each in-air profile, measured with the SFD, was fitted with a fourth order polynomial. Figure 6.15 shows an example for the 10x10mm^2 open field.

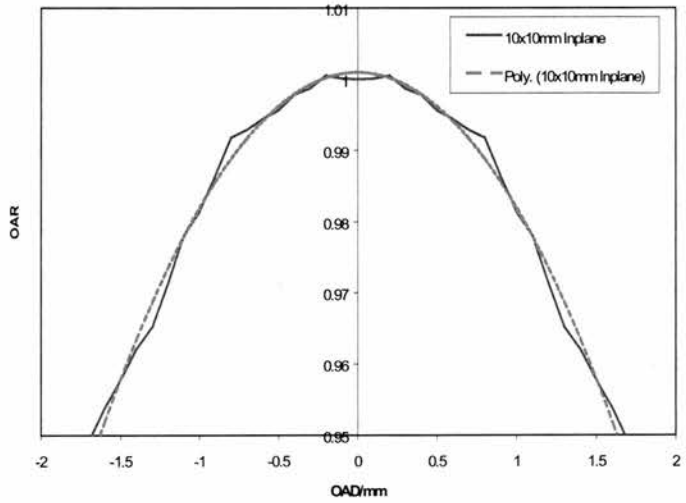

Figure 6.15. In-air profile in a 10x10mm^2 open field, measured with the SFD and fitted with a fourth order polynomial.

The Inplane and Xplane profiles were integrated over the sensitive area of each detector to determine the amount of under-response caused by its finite size. The results of the integration give an approximate value for the percentage response in the detector, as shown for the 10x10mm^2 field in Table 6.13.

Detector	Diameter / mm	% Response
Diamond	2.2	99.4
PFD/EFD	2.5	99.0
SFD	0.6	100.0

Table 6.13. Calculated responses for each detector in the 10x10mm^2 field.

In terms of detector size only, the maximum under-response of any detector should be <1%.

Reproducibility

The reproducibility, in terms of the coefficient of variation, of the measurements of S_c in the build-up tops, for open fields is shown in Table 6.14.

	coeff. of var. (%)	
Detector	20x20mm^2	10x10mm^2
Diamond	0.1	0.9
PFD	0.1	0.5
EFD	0.1	1.2
SFD	0.5	0.6

Table 6.14. Coefficients of variation, expressed as a percentage, for each set of experiments for each detector in each open field size.

The coefficient of variation is 0.5% for the SFD and 0.1% for the other detectors in the 20x20mm^2 field, increasing to 0.5-1.2% in the smallest field. This is a reflection not only of the positional difficulties, but also the reproducibility of the field size setting determined by the movable collimators (+/-2mm, as determined in Chapter 4). Measurements were not repeated in the BDAS system. Although this was partly due to time constraints, it was also noted that S_c only increased in the 5mm diameter stereotactic collimator and by <3%. The increase, if any, in the 10x10mm^2 open field is likely to be much less.

Sc results

Figure 6.16 shows S_c measured at dmax, with each detector, in the build-up top. Volume averaging has been accounted for.

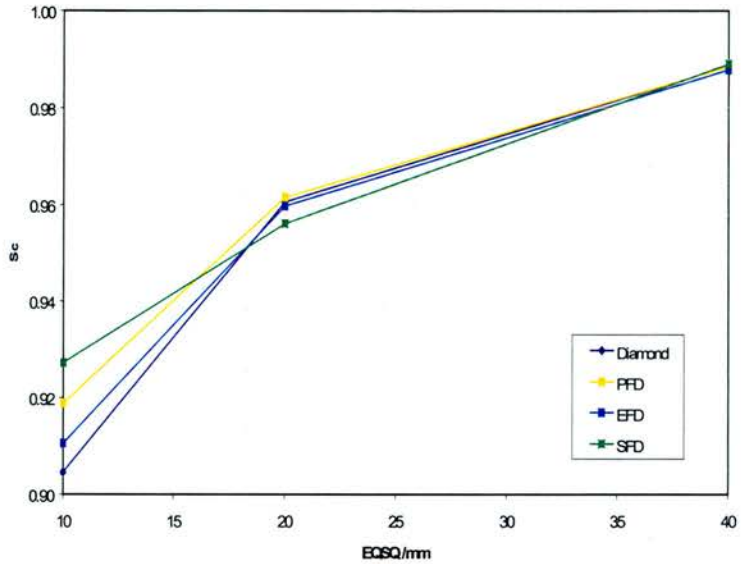

Figure 6.16. S_c in open fields measured at dmax, with each detector, in the build-up top, with the effects of volume averaging accounted for.

It is apparent once again, that volume averaging does not account for all the differences between detectors as the total spread in Sc in the 10x10mm^2 field is approximately 3%. The fact that the PFD is lower than the SFD in the smallest field, suggests that mispositioning could account for 1-2% of the difference. However, it is also worth investigating the effects of source shielding in the open field situation.

Source shielding

The head design is considered in the open field situation, as shown in Figure 6.17.

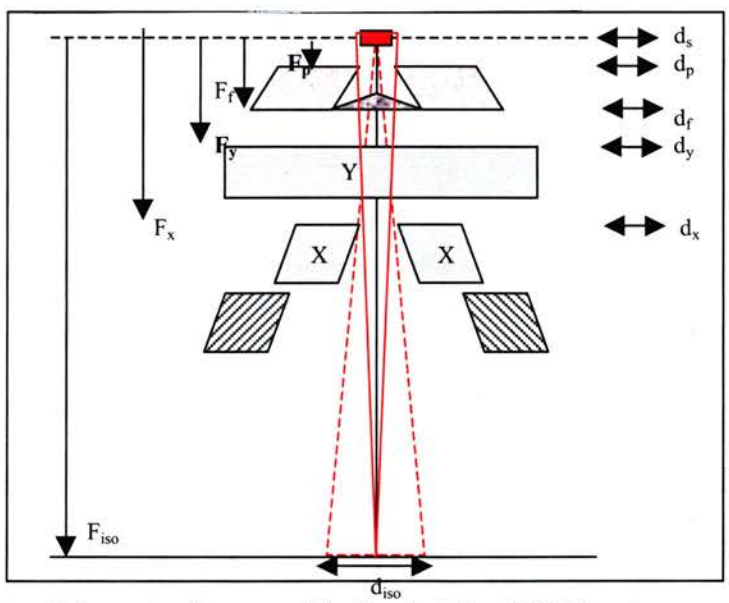

Figure 6.17. Schematic diagram of the head of the 600CD in the open field situation.

The open field widths at which the entire source, or primary collimator aperture are not "seen" at the point of measurement, are calculated in Table 6.15.

Parameter	Source	Primary collimator
d_y	$\frac{1000 - F_y}{1000} \cdot d_s = 1.4mm$	$\frac{1000 - F_y}{1000 - F_p} \cdot d_p = 7.7mm$
d_{iso}	$\frac{1000}{F_y} \cdot d_y = 5.1mm$	$\frac{1000}{F_y} \cdot d_y = 27.5mm$
d_x	$\frac{1000 - F_x}{1000} \cdot d_s = 1.3mm$	$\frac{1000 - F_x}{1000 - F_p} \cdot d_p = 6.8mm$
d_{iso}	$= \frac{1000}{F_y} \cdot d_x = 3.4mm$	$\frac{1000}{F_y} \cdot d_x = 18.5mm$

Table 6.15. Calculation of the field width at the isocentre (d_{iso}) at which the entire source or aperture at the top of the primary collimator, will be seen from the point of measurement.

The entire source will therefore be visible in all open field measurements. The entire aperture at the top of the primary flattening filter will however not be visible from the point of measurement for fields with X<18.5mm and Y<27.5mm. This will reduce Sc in both the 20x20 and 10x10mm^2 fields.

Summary

The same problems noted for measurements of S_c in stereotactic fields, exist for measurements in open fields. The effects are less, simply because the field size range measured is smaller. The magnitude of the effects of source shielding and spectral changes can only be accurately determined with Monte Carlo modelling.

6.3.4 Detector comparison: MLC fields

Overview

All detectors were compared in each MLC field situation using only the WT1 build-up tops and 50mm tops. The in-air profiles reported in Chapter 4 were used to determine the reduction in detector response over the sensitive area of each detector. In addition, the geometrical aspects of the linac head in the MLC field situation were investigated with respect to changes in scatter in small MLC fields.

Detector response

The high dose region of each in-air profile, measured with the SFD, was fitted with a fourth order polynomial. Figure 6.18 shows an example for the 10x10mm^2 MLC field.

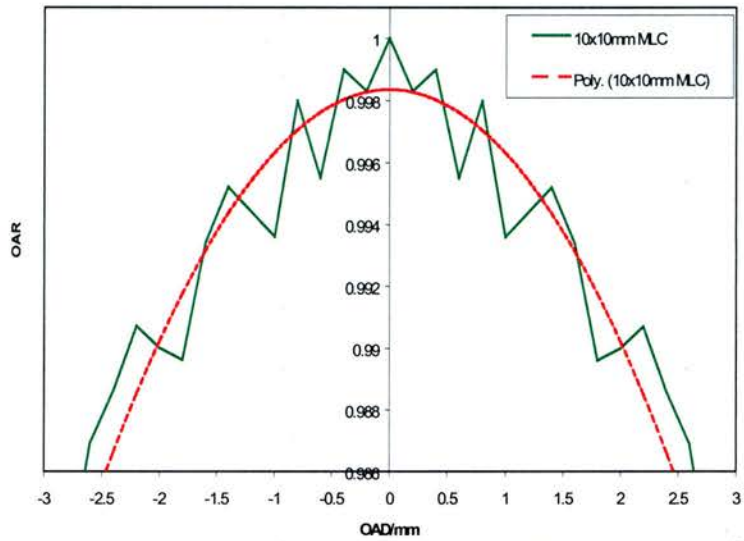

Figure 6.18. In-air profile measured with the SFD in a 10x10mm^2 MLC field

The Inplane and Xplane profiles were integrated over the sensitive area of each detector to determine the amount of under-response caused by its finite size. The results of the integration give an approximate value for the percentage response in the detector, as shown for the 10x10mm^2 MLC field in Table 6.16.

Detector	Diameter /mm	% Response
Diamond	2.2	99.8
PFD/EFD	2.5	99.8
SFD	0.6	99.8

Table 6.16. Calculated responses for each detector in the 10x10mm^2 field.

In terms of detector size only, there should be minimum under-response in any detector.

Reproducibility

The reproducibility, in terms of the coefficient of variation, of the measurements of S_c in the build-up tops, for open fields is shown in Table 6.17.

Detector	coeff. of var. (%) 20x20mm^2	10x10mm^2
Diamond	0.1	0.1
PFD	0.1	0.1
EFD	0.1	0.2
SFD	0.2	0.2

Table 6.17. Coefficients of variation, expressed as a percentage, for each set of experiments for each detector in each MLC field size.

The coefficients of variation are all very small, which shows that the positioning is good. As the high dose regions are wider in the MLC fields than in the open fields (Chapter 4), repositioning of each detector using the BDAS system was considered to be unnecessary.

Figure 6.19 shows S_c measured at dmax, with each detector, in the build-up top.

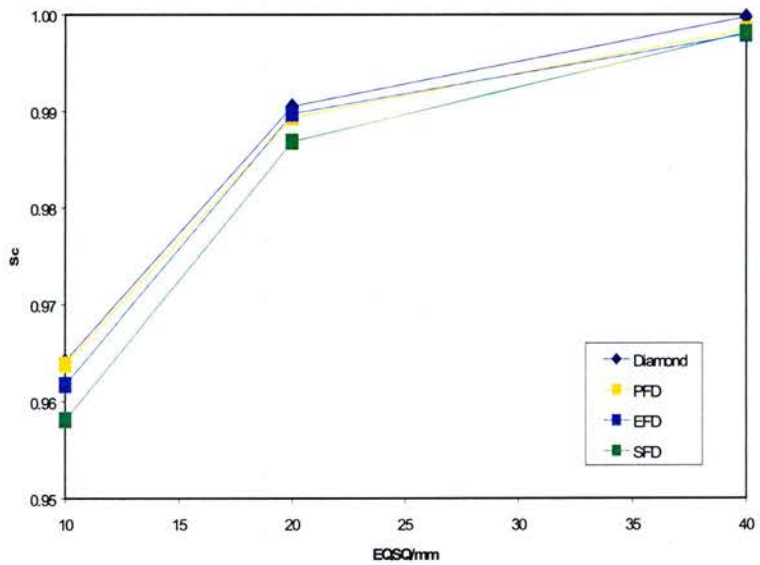

Figure 6.19. S_c measured at dmax, with each detector, in the RMI build-up top.

The spread over all detectors is 0.4% in the 20x20mm^2 field and 0.6% in the 10x10mm^2. There were no significant differences between the results at dmax and those at 50mm. Although there are some differences between detectors, the effect is very small. The effect of source shielding in MLC fields is investigated for interest only.

Source shielding

The head design in the MLC field situation is shown in Figure 6.20.

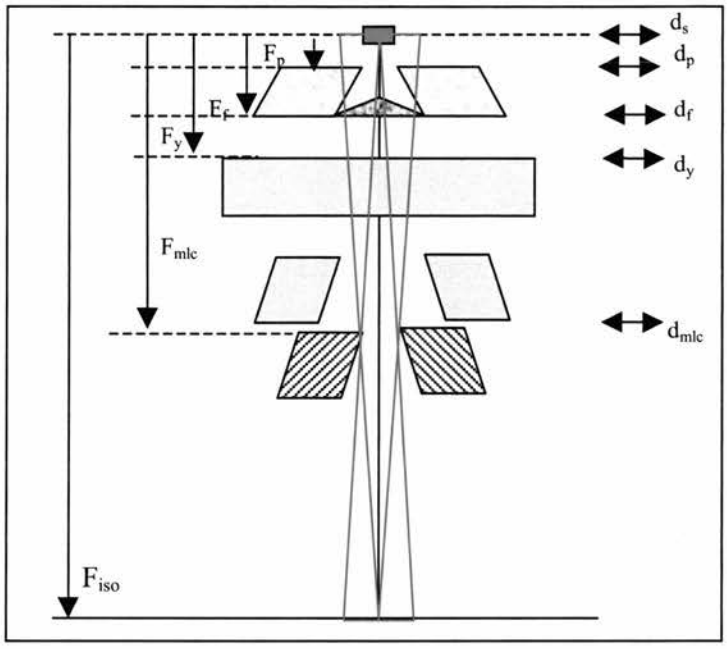

Figure 6.20. Schematic diagram of the head of the 600CD in the MLC field situation.

In all measurements in MLC fields, the movable linac collimators are set to a constant field size of 50x50mm^2. As discussed previously, the amount of head scatter detected at the point of measurement is primarily dependent on the amount of the flattening filter "seen" from the point of measurement. It is important therefore to determine whether it is the position of the movable linac collimators, or the width of the MLC opening, which limits this amount. The setting on the linac collimators is considered first. The MLC width at the isocentre (d_{iso}) which corresponds to the 50mm width on the X and Y collimators separately can be calculated from the distances in Table 6.2, as shown in Table 6.18.

width	Y collimators		X collimators	
d_{mlc}	$\frac{1000 - F_{mlc}}{1000 - F_y} . d_y$	= 10.1mm	$\frac{1000 - F_{mlc}}{1000 - F_x} . d_x$	= 15.0mm
d_{iso}	$\frac{1000}{F_{mlc}} . d_{mlc}$	= 20.9mm	$\frac{1000}{F_{mlc}} . d_{mlc}$	= 31.1mm

Table 6.18. Calculation of width of MLC equivalent to open 50x50mm^2 field.

Head scatter is therefore dependent mainly on the MLC setting for fields of 20x20 and 10x10mm^2. The MLC field widths at which the entire source, or primary collimator aperture are not "seen" at the point of measurement, are calculated in Table 6.19.

Parameter	Source	Primary collimator
d_{mlc}	$\frac{1000 - F_{mlc}}{1000} \cdot d_s = 1.0mm$	$\frac{100 - F_{mlc}}{100 - F_p} \cdot d_p = 5.6mm$
d_{iso}	$\frac{1000}{F_{mlc}} \cdot d_s = 2.1mm$	$\frac{100}{F_{mlc}} \cdot d_{mlc} = 11.5mm$

Table 6.19. Calculation of the MLC field width at the isocentre (d_{iso}) at which the entire source or aperture at the top of the primary collimator, will be seen from the point of measurement.

The entire (estimated at 2mm) source will not be visible in fields <2.0mm width, which is again not relevant for any of the MLC field measurements in this work. The entire aperture at the top of the primary flattening filter will not be visible from the point of measurement for MLC settings <11.5mm^2, which may affect measurements in the 10x10mm^2 MLC field.

Summary

Although the effects are small, the same S_c problems in stereotactic and open fields, exist for measurements in MLC fields. The magnitude of the effects of source shielding and spectral changes can only be accurately determined with Monte Carlo modelling.

6.3.5 Normalisation

40mm/50x50mm^2

There were no differences in the readings for each detector between a 40mm collimator and the 50x50mm^2 field. This shows that the head scatter remains the same on addition of the largest stereotactic collimator. Normalisation to the 100x100mm^2 reference field can therefore be carried out in the same way for all field types.

50x50mm^2/100x100mm^2

At the ECC, S_c is generally measured at dmax in a mini-phantom. To relate the results in small fields to those in more conventional field sizes, it is necessary to investigate the differences between phantom diameters in the normalisation of the 50x50mm^2 field to the 100x100mm^2. This was carried out using each detector, in three different types of phantom; the 40mm diameter mini-phantom, the build-up and 50mm caps and tops. In the mini-phantoms and caps, the 0.125cc IC was only used with long axis parallel to the beam CAX.

The purpose of these measurements was to ensure that S_c was independent of phantom diameter. The coefficient of variation for each detector is shown in Table 6.19.

	coeff. of var. (%)		
Detector	mini-phantom	build-up cap	build-up top
Diamond	0.0	0.1	0.1
PFD	0.1	0.1	0.3
EFD	0.1	0.1	0.1
SFD	0.2	0.3	0.1
0.125cc IC	0.1	0.1	

Table 6.19 Table of coefficients of variation, as percentages, for repeat measurements, in the three phantom diameters, with each detector, at dmax.

The precision of the measurements is very high, showing that the experimental set-up was reproducible for each detector and phantom. Figure 6.21 shows the results at dmax.

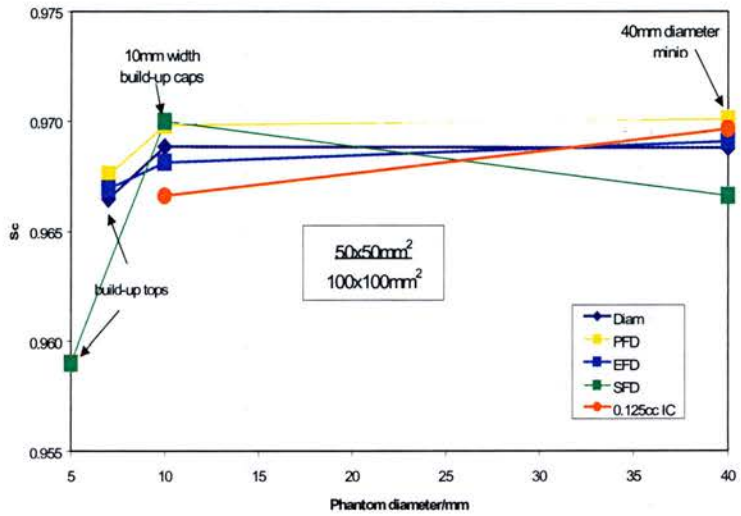

Figure 6.21. Graph of S_c at dmax, against phantom diameter for a 50x50mm^2 field relative to the 100x100mm^2 reference field.

The spread over all phantoms and detectors is only 1% and if the SFD results are excluded, the spread is only 0.5%. This suggests that S_c measured in a 50x50mm^2 field relative to a 100x100mm^2 field is virtually independent of the phantom diameter. At this field size S_c can be measured under electronic disequilibrium, as also reported by Li et al (1995). This also means that the small field results can be normalised to the reference field using measurements in any of the above phantom diameters, with any of the above detectors (other than the SFD) to within 0.5%.

Although the differences between phantoms are very small, they are reproducible and S_c does appear to decrease slightly with decreasing phantom diameter. The reason for this is

unclear and could be thought to be due either to a decrease in phantom scatter, or an increase in the effects of electron contamination. In terms of phantom scatter, although the 100% isodose will entirely cover the mini-phantom in a 100x100mm^2 field, only the 93% isodose will cover the mini-phantom in a 50x50mm^2 field. As a result, there will be some missing phantom scatter in the 50x50mm^2 measurement, which could result in a value of S_c which is too low. Phantom scatter differences cannot therefore explain the decrease in S_c with phantom diameter. Electron contamination will have the largest effect in the smallest diameter phantom where electrons to the sides of the detectors will most easily reach the sensitive volume. As electron contamination will be greater in the normalisation field, the resulting S_c will be too low. This is therefore the most likely explanation for the small drop in S_c with phantom diameter. The drop will be largest for the SFD because it is the smallest diameter detector and will have the smallest diameter build-up top. S_c measured with the 0.125cc IC in the build-up cap may be slightly too low due to the air within the measurement volume which may make the detector and phantom behave more like a water equivalent detector with a smaller phantom diameter.

The results were averaged over all detectors in each phantom. The IC was excluded from the build-up cap results and the SFD excluded from the build-up top results. The final normalisation values in the mini-phantom, build-up cap and top were 0.969, 0.969 and 0.967 respectively. The mini-phantom and build-up cap values were chosen for normalisation to exclude the additional effects of electron contamination. The same relative effects (and precision) were found at 50mm deep, as shown in Figure 6.22.

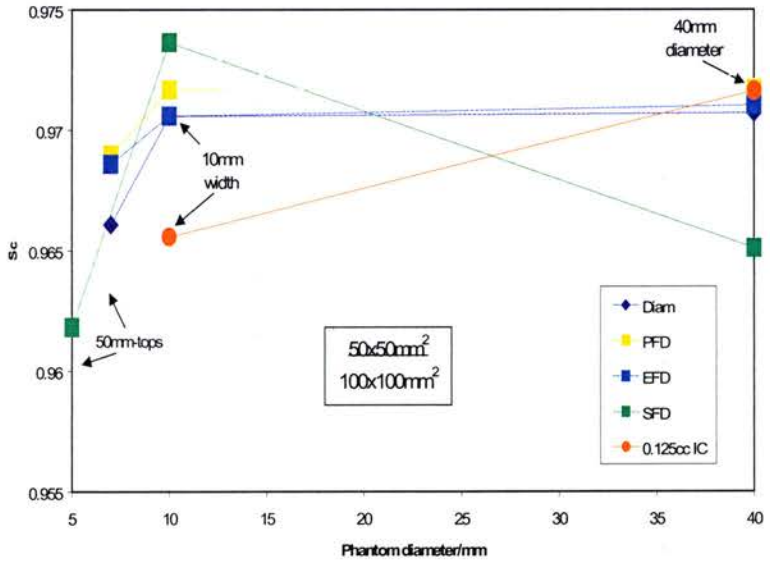

Figure 6.22. Graph of S_c at 50mm deep, against phantom diameter for a 50x50mm^{2}field relative to the 100x100mm^2 reference field.

Averaging was carried out as before, yielding values of 0.971, 0.971 and 0.968 in all three phantoms respectively, with a coefficient of variation maximum of 0.2%. Comparing these results with those at dmax, yields p values of <0.01, 0.06 and 0.2 respectively, which suggests that there is a depth dependence, but only of the order of 0.2%. The response of the SFD in the mini-phantom is curious and may be related to the same effect apparent in the normalisation of S_{cp} in Chapter 5 (Table 5.10).

Comparison of beam defining systems

All S_c (dmax) measurements were therefore normalised to the reference field using 0.969. As no significant differences (>0.2%) were found between measurements at dmax and 50mm, one set was used for both depths. Figure 6.23 shows a plot of the results. Note that the EQSQ widths are measured widths (Chapter 4), rather than nominal field size settings.

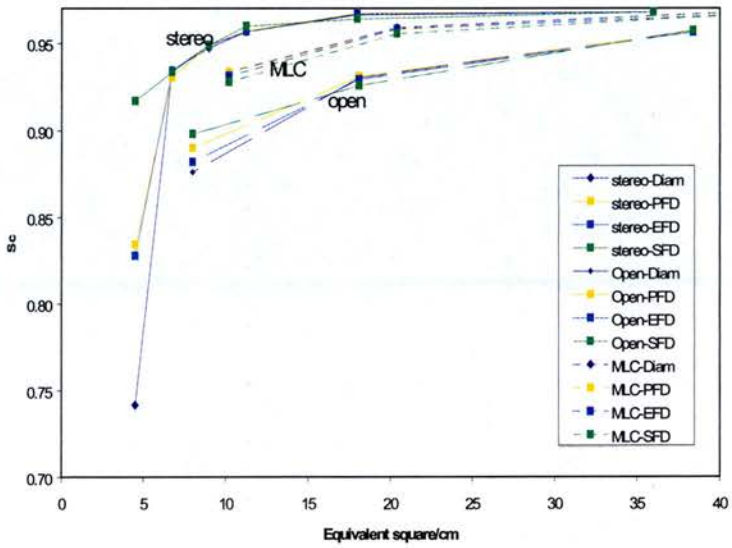

Figure 6.23. Comparison of S_c measured in all three beam defining systems, normalised to a 100x100mm^2 field.

Fields shaped with the stereotactic collimators show the smallest drop in S_c, of approximately 1.2%, between 40x40 and 10x10mm^2 equivalent square. The MLC shaped fields show a 3.5% fall off in this region, and the open fields over 6%. The larger fall off in the open fields is to be expected as, by definition, S_c decreases as the setting on the movable collimators decreases. In both the stereotactic and MLC fields the setting on the movable linac collimators is the same for all beam areas.

6.3.6 Linac comparison

It is important to note that the measurements carried out on the other two linacs were not as extensive, nor as precise, as those carried out on the 600CD. S_c on the CH6 and CH20 linacs are therefore subject to a larger uncertainty. In addition, only S_c at dmax, in stereotactic collimators were measured. Figure 6.24 shows a comparison of SFD results.

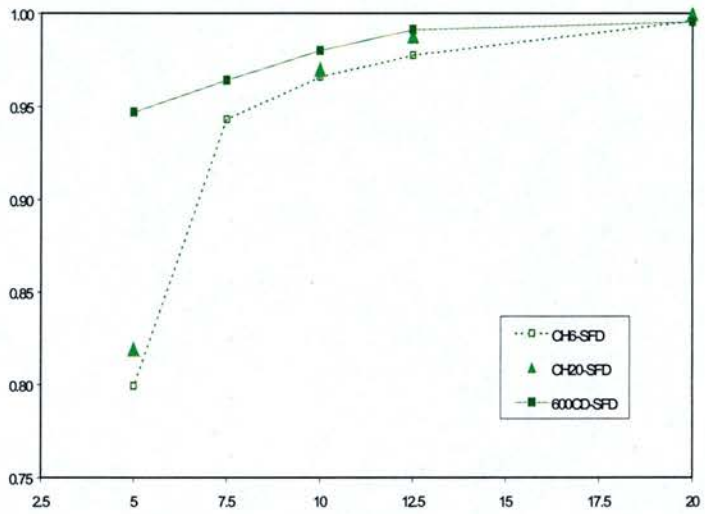

Figure 6.24. Comparison of S_c measured with the SFD on all three linacs, in all stereotactic collimators.

The differences between linacs appear to be <2%, other than in the 5mm collimator, where the results on the CH linacs are almost 15% lower than those on the 600CD. This may be due to real differences between linacs, with particular reference to shielding of the aperture at the top of the primary collimator, but will also be due to less precision in the measurement of S_c on the CH linacs.

6.3.7 XKnife Requirements

Although XKnife does not require the input of S_c values, these were required for collimators between 40 and 10mm diameter, for the calculation of S_p. The final set of values used is shown in Table 6.20.

Coll /mm	S_c
40	0.968
37.5	0.968
35	0.968
32.5	0.968
30	0.968
27.5	0.968
25	0.968
22.5	0.968
20	0.967
17.5	0.965
15	0.962
12.5	0.960
10	0.949
7.5	0.934
5	0.917

Table 6.20. Final table of S_c values on the 600CD.

6.4 Conclusion

No significant differences between phantom diameters or materials, detectors or depths were found for stereotactic collimators in the 40-12.5mm range. Measurements with brass were approximately 0.5% higher, probably due to spectral changes. In open fields between 50x50 and 10x10mm^2, measurements in tops were higher than those in caps, by approximately 2%. This was thought to be due to too much phantom scatter in the cap measurements in the larger field. Although there were no significant differences between depths, there were differences between detectors in the smallest field.

The under-response of each detector due to volume averaging in small collimators (<12.5mm diameter) and small square fields (10x10mm^2) did not entirely account for the differences between detectors. Additional under-response was firstly due to the widths of the build-up tops in the 5mm diameter collimator, which caused some phantom scatter to be measured in the normalisation field and be excluded from measurements in the smallest field. Spectral changes could mean that the conversion of detector reading to dose is not the same in the normalisation field and the field size of interest, which could also lead to errors.

Although there were large differences between detectors at small field sizes, all detectors measured a significant drop in S_c at small field sizes. This was thought to be due to

shielding of the aperture at the top of the primary collimator which was independent of detector, but dependent on beam defining system.

Small field S_c could be normalised to the reference field using measurements in any of the phantoms investigated, to within 0.2%. Any detector, other than the SFD could be used for normalisation measurements although an IC should really only be used in a mini-phantom due to positional difficulties. The comparison of results between beam defining systems was as expected. Setting $50x50mm^2$ on the movable linac collimators for all stereotactic fields ensured that the head scatter remained approximately constant (excluding the effects of transmission and scatter from the movable collimators) at collimators >=17.5mm diameter. Below this the scatter is determined primarily by the diameter of the collimator. Although a similar effect is noticed with the MLC, this is not relevant for routine clinical work as the linac collimators will generally be positioned close to the edge of the MLC. This will however be relevant in the IMRT situation and head scatter will have to be determined for both the setting on the linac collimators and the MLC setting.

The differences between linacs were minimal, other than in the smallest collimator. This was either due to linac head design or experimental uncertainties.

In all of the above, it is important to be able to distinguish between real changes in head scatter and apparent changes caused by the measurement system. Real changes are caused primarily by the amount of the flattening filter visible from the point of measurement, but, at very small field sizes, also by the amount of the aperture at the top of the primary collimator visible from the measurement point. Although this latter effect changes the effective primary, it is still a real, measurable effect and reflects a real change in S_c. Apparent changes are caused by the size of the detector volume and to a lesser extent, the phantom material. The width of the phantom may have a significant effect in the smallest field and although measurements could be carried out at extended FSD, there needs to be a fuller examination of the smallest field. In addition, spectral changes may cause differences in the correction factors necessary to convert the detector reading to dose. Although the detector volume can be accounted for with volume averaging, the other effects require further investigation. Ideally, this should be with Monte Carlo modelling.

Chapter 7

Phantom scatter factors

7.1 Introduction

7.1.1 Definitions

Back scatter factor

A back scatter factor (BSF) is the ratio of the total absorbed dose (D) on the CAX in a field size (s) at the surface of a phantom (d_0) to the absorbed dose (D_0) at the same point due to effective primary only, with the same collimator opening.

$$BSF = \frac{D(s, d_0)}{D_0(s, d_0)} \qquad (7.1)$$

Peak scatter factor

A peak scatter factor (PSF) is the ratio of the total absorbed dose (D) on the CAX in a field size (s) at dmax (d_m) to the absorbed dose (D_0) at the same point due to effective primary only, with the same collimator opening.

$$PSF = \frac{D(s, d_m)}{D_0(s_0, d_m)} \qquad (7.2)$$

Normalised peak scatter factor

A normalised peak scatter factor is the ratio of the PSF in the field size of interest (s) to that in a reference field (s_{ref}), usually 100x100mm^2.

$$NPSF = \frac{PSF\ (s)}{PSF\ (s_{ref})} \qquad (7.3)$$

Phantom scatter factor

A phantom scatter factor (S_p) is the ratio of the dose (D) in a field (s) to the dose (D_{ref}) in the reference field size (s_{ref}), at depth (d) and FSD=f, for the same collimator opening.

$$S_p = \frac{D(s, d)}{D_{ref}(s_{ref}, d)} \quad (7.4)$$

When S_p is measured at dmax, it is analogous to an NPSF. However, S_p can be measured at any depth to conform with the reference depth used in any particular formalism. Because scatter increases with depth, S_p values are also depth dependent.

7.1.2 Measurement of scatter factors

BSF

BSFs are generally only defined, measured and used at orthovoltage energies and below (=<400kV), where the maximum dose is at, or very close to the surface. As a BSF is the ratio of the dose at the surface of a phantom, to that in air at the same point in the same irradiation conditions, BSFs can be measured only in field sizes > the size of the detector.

PSF

PSFs are defined, measured and used at higher energies, where the maximum dose lies at a significant depth below the surface. They are measured as the ratio of the dose at dmax in a phantom, to that in-air at the same point, in a build-up cap. As the build-up cap is designed to provide electronic equilibrium, its size increases with increasing energy. PSFs can only be measured in field sizes > the dimensions of the build-up cap and therefore the minimum field size measurable is limited by the size of the build-up cap and hence the energy.

NPSF and S_p

As a result of the limitations described above, it is difficult to obtain absolute PSFs for small field sizes, particularly for high energies. This is because an increasing amount of attenuation and scatter will occur as the size of the build-up cap and the energy increases, thus affecting the in-air measurements. For this reason, NPSFs are more commonly measured and used, as the amount of attenuation and scatter in the field size of interest and in the reference field, will approximately cancel. In addition, as the ratio of PSFs is most often used in calculations, the substitution of the ratio of NPSFs will be satisfactory.

An NPSF can be measured from the ratio of a relative output in phantom, to a relative output in air, when both sets of data have been measured at the same depth and distance from the source and are normalised to the same reference field. Equation 5.2 in Chapter 5

can therefore be used to calculate NPSFs (S_p values at dmax) from values of S_{cp} and S_c which have also been measured at dmax.

$$S_p = S_{cp} / S_c \qquad (7.5)$$

This equation can also be used to calculate S_p at any other depth, if S_{cp} and S_c are also measured at the same depth. S_p values at a depth beyond dmax are used in formalisms which are also based on a depth beyond dmax, as discussed previously.

Although both NPSF and S_p are commonly extracted from measurements of S_{cp} and S_c, they can also be measured directly in a full scatter phantom. Khan (1980) achieved this by setting the movable collimators to a constant field size and using blocks placed at the phantom surface to produce a range of beam areas. However, this method assumes that the blocks do not change, or contribute to, the head scatter. Similarly, S_p can be determined by carrying out measurements in phantoms of different cross-sectional sizes, again for the same collimator setting (Khan, 1994). NPSF and S_p values can also be calculated analytically from differential scatter factors (dSAR) or from Monte Carlo.

7.1.3 Tables of scatter factors

BJR (Supplement 25)

Following the approach laid down by its predecessors (Supplements 17,11,10), BJR Supplement 25 contains tables of BSF, PSF and NPSFs (Burns; Jordan; McKenzie; Smith, 1996). BSFs are tabulated for ortho and kilovoltage x-ray units and PSFs for Cs-137 and Co-60 units. PSFs and BSFs decrease with field size as the phantom scatter decreases. More exactly, the total absorbed dose tends towards the primary as the field size tends towards zero. BSFs and PSFs are therefore normalised to 1.0 at zero field size.

The tables of data in the supplements have been compiled from the analysis of a large range of data supplied to the BJR Working Party by numerous radiotherapy centres. The data encompassed a wide range of linac designs and beam energies. On analysis of the NPSF data for MV x-ray beams, it was noted by the Working Party that no systematic differences were apparent with beam energy. The Co-60 PSFs were renormalised to 1.0 in a 100x100mm^2 field to produce NPSFs and compared with the values for MV x-rays. Again, no significant differences were apparent. As a result, BJR contains a single set of NPSFs for all MV beams (Co-60 and x-rays between 2 and 50MV). This indicates energy

independence within the experimental uncertainties of the data supplied. At first this seems surprising, as scatter is clearly energy dependent. However, although the scatter decreases with increasing energy (all other parameters considered to be equal), it also increases with depth. As the depth of dmax increases with energy, this effect counterbalances the decrease and these two effects appear to cancel within the experimental uncertainties in the BJR compilation (Jordan 1996).

Storchi and van Gasteren (1996)

Storchi and van Gasteren (1996) used S_{cp} data measured in a full scatter phantom and S_c data measured in a 40mm diameter mini-phantom to produce a table of S_p values at 100mm depth, for use in formalisms based on a depth beyond dmax. Measurements were made in fields between 400x400 and 40x40mm^2 and normalised to 100x100mm^2, for energies between 4 and 25MV. Figure 7.1 shows a plot of the final tabulated S_p data, for the full range of beam qualities and the NPSF data from BJR Supplement 25, for comparison.

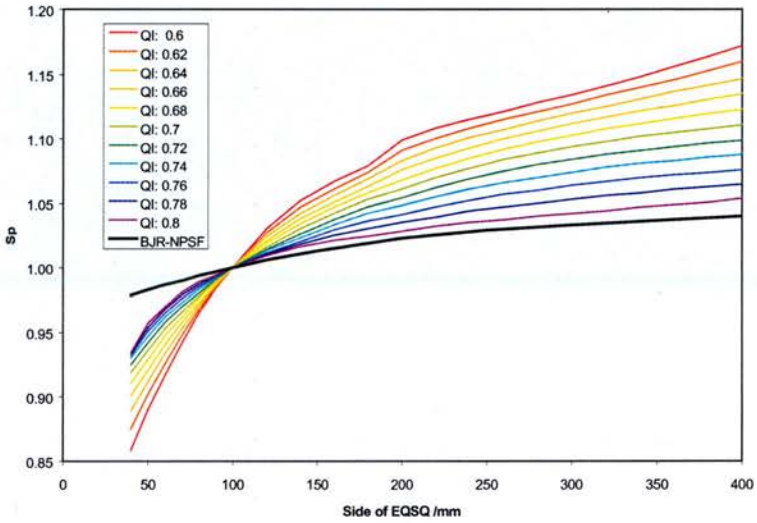

Figure 7.1 S_p data at 100mm deep, for beam energies between 4 and 25MV from Storchi and van Gasteren (1996). NPSF data from BJR Supplement 25.

The expected increase in S_p and NPSF (BJR) with increasing field size and hence, phantom scatter, is clearly seen. NPSF was found to be independent of beam quality, S_p increases with quality in fields < the normalisation field (100x100mm^2) and decreases with quality in larger fields, reflecting the decrease in phantom scatter at the point of measurement as the beam energy increases. The 'kinks' in the S_p data for QI = 0.6 and 0.62 at a field size of approximately 200x200mm^2, are real and imply that there are possibly some smoothing or typing errors in the original paper.

7.1.4 Small field problems

As S_p is most commonly extracted from S_{cp} and S_c measurements, accurate Sp data for small fields relies on the accurate measurement of both S_{cp} and S_c. The uncertainties in S_p will therefore be a combination of the uncertainties in each of these. However, the problems associated with S_{cp} (Chapter 5) and S_c (Chapter 6) measurements may or may not have an effect on the calculated values of S_p, depending on whether or not the effects cancel out.

7.1.5 Small field S_p in the literature

Overview

S_p data at dmax (NPSF) and normalised to a 100x100mm^2 reference field, have been published for small square fields and circular stereotactic fields. No small field S_p data at any other depth has been published to date.

Literature review

Houdek et al (1983) obtained small square field S_p data from measured (10MV) S_{cp} (TLD ribbons) and S_c (0.1cc IC, Al build-up cap, extended FSD) data. The decrease in S_p from the reference field to a 10x10mm^2 field was approximately 8%.

Arcovito et al (1985) also obtained small square field S_p data from measured (9MV) S_{cp} (TLD) and Sc (0.22cc, Al build-up cap, extended FSD) data. The decrease in S_p from the reference field to a 10x10mm^2 field was approximately 9%.

Rice et al (1987) calculated S_p data from EGS4 Monte Carlo (MC) S_{cp} data and measured S_c (0.1cc IC, brass build-up cap) data, for both small square and circular stereotactic fields. The linac collimators were set to 40x40mm^2 for all S_{cp} calculations and Sc measurements and S_c found to be constant for all stereotactic collimators. S_p fell by approximately 12% between the reference field and the 12.5mm diameter collimator.

Chierego et al (1993) obtained S_p from measured TMRs (Markus, 0.6cc IC) and PDDs (Markus), which had been corrected for detector size. The curve of NPSF values between 100x100 and 10x10mm^2 showed a total drop in NPSF of approximately 15%. An extrapolated curve showed a drop of only 4%, but this was not discussed.

Haider and El-Khatib (1994) measured S_p directly from S_{cp}/S_c in fields >=40x40mm^2. S_p in fields down to 10x10mm^2 were obtained using the density scaling theorem of O'Conner

(1957). This theorem assumes that the ratio of primary to scatter is the same in two materials of different density, if the phantom dimensions are scaled in proportion to the ratio of the densities. In practice, the authors assumed that a small field S_p measured in water, was equal to S_p in a larger field of lower density. The size of the larger field was calculated using the ratio of the electron densities. The mean value of S_p measured in both balsa and cedar wood dropped by approximately 30% between a 100x100 and 10x10mm^2 field.

Li (1999) used EGS4 MC to calculate PSFs for Co-60. Less than 4% drop in NPSF was reported between the 100x100 and 10x10mm^2 fields.

Comparison of results

A summary of the methods used in each of the above publications is presented in Table 7.1.

Author	Year	Energy /MV	Linac	Field Type	Method
Arcovito et al	1985	10	Toshiba LMR-13	□	$S_p=S_{cp}/S_c$
Chierego et al	1993	6	Siemens Mevatron 6700	○	TMRs and PDDs
Haider & El-Khatib	1994	10	Clinac 2100C	□	Density scaling theorem.
Houdek et al	1983	9	Neptune-10	□	$S_p=S_{cp}/S_c$
Li et al	1999	6	Siemens KD2	□	EGS4
Rice et al	1987	6	Clinac 6/100	○	$S_p=(MC)S_{cp}/S_c$

Table 7.1 Methods used in each of the above publications to obtain S_p.

Values of S_p from the publications in Table 7.1 are plotted against EQSQ in Figure 7.2.

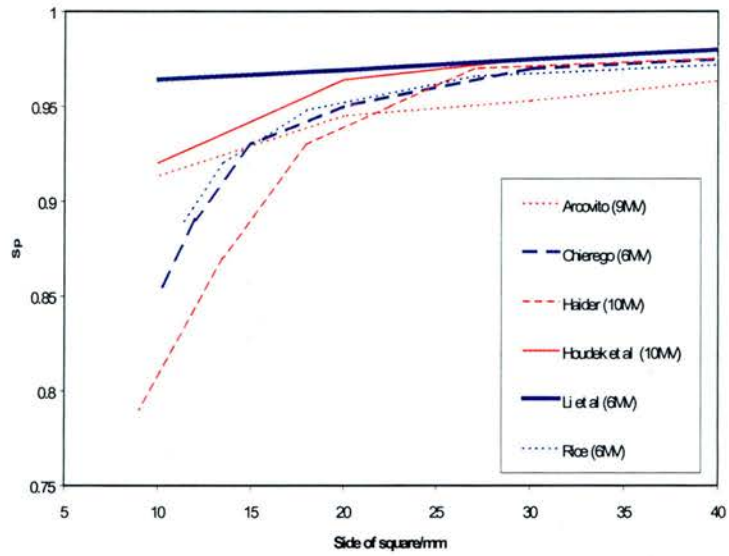

Figure 7.2. S_p from the publications in Table 7.1 plotted against EQSQ.

S_p at dmax (NPSF) is expected to be independent of beam quality if the energy independence reported in BJR can be extended to smaller fields. S_p should then only be dependent on the beam area at the surface of the phantom. The spread over the 6MV beams (navy) is comparable with the spread over the higher energy beams (red) and no quality dependence is discernible. This suggests that it is the range of experimental and calculation methods which have led to the differences between data sets. Although Li et al (1999) are the only authors to have used MC, their results show a surprisingly small drop in S_p, which does not seem to be reasonable. The overall spread in S_p values in a $10x10mm^2$ field is >15%, which shows the magnitude of the possible error in small field S_p data.

7.1.6 Aim

The primary aim of this work was to compare measured values of S_p, extracted from S_{cp} and S_c data measured with each detector, at both dmax and 50mm in all three beam defining systems and identify the possible magnitude and likely causes of differences. The secondary aim was to obtain S_p data at dmax (NPSF) in stereotactic collimators between 40 and 10mm diameter and compare the results on all three linacs.

7.2 Methods

S_p was obtained using equation 7.5 for each detector, beam defining system and field size, at both dmax and 50mm, using the S_{cp} (Table 5.12) and S_c (Table 6.20) results in Chapters 5 and 6 respectively, which had been corrected for detector size. The uncertainty in each ratio

of S_{cp}/S_c was calculated as the quadrature sum of the square of the coefficients of variation of each parameter for each detector, in each field size. Uncertainties are therefore expressed as +/- percentage uncertainty at 1s.d.

7.3 Results and discussion

7.3.1 Calculation of S_p

Stereotactic collimators

The (+/-) percentage uncertainties (1s.d.) in the calculation of S_p, are shown in Table 7.2.

	% uncertainty (1s.d.)		
Detector	12.5mm	10mm	5mm
Diamond	0.3	0.4	2.0
PFD	0.3	0.5	2.0
EFD	0.3	0.3	1.2
SFD	0.4	0.8	1.7

Table 7.2 Uncertainties in S_p (stereotactic collimators), expressed as a percentage of the mean.

The uncertainties increase with decreasing collimator diameter due to the problems in the measurement of both S_{cp} and S_c in the smallest collimator. Figure 7.3 shows a plot of S_p at dmax against EQSQ (not collimator diameter). Note that the points are based on measured beam widths rather than nominal field size setting. These results are analogous to NPSFs.

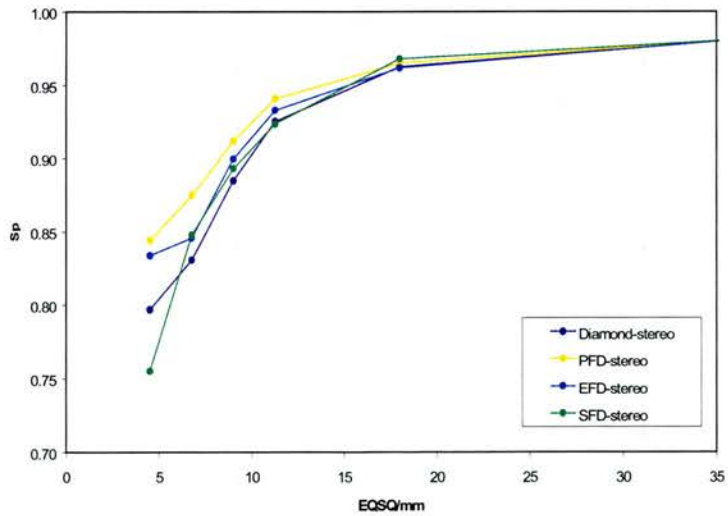

Figure 7.3. S_p calculated at dmax for the stereotactic beam defining system, using S_{cp} and S_c data corrected for detector size.

S_p should be independent of the detector used, if all uncertainties in the measurement of S_{cp} and S_c cancel out. However, differences in S_p are apparent between detectors, in Figure 7.3. This is because although some of the measurement features in both situations (S_{cp} and S_c), which could have had an effect on the detector response, may cancel out in the calculation of S_p, some may not. For example, the effect of shielding of the primary collimator aperture will cancel out in the calculation of S_p as this is inherent to both sets of measurements. However, the effect of spectral changes may not cancel as the spectrum will be different in the measurement of each parameter. The effects of detector size will cancel, if S_{cp} and S_c values have been adjusted to account for the effects of detector size. The effects of detector size will not cancel in uncorrected values of S_{cp} and S_c because the amount of volume averaging is dependent on the shape of the profile, which will be different for the in-phantom and in-air situations. The effect of LEE may not cancel because this too may be different in the in-phantom and in-air situations. The effect of the absorption of too much phantom scatter in the PFD will not cancel out. Values of S_{cp} were over-estimated with the PFD, but no over-estimation occurred in the measurement of S_c. S_p is therefore still over-estimated for the PFD.

Finally, the effect of the phantom width in the measurement of S_c in the smallest collimator will not cancel. The build-up top was too wide for measurements with the SFD in the 5mm diameter collimator and therefore S_c was underestimated. This will result in a value of S_p which is too high. The effect will increase with detector (and hence phantom) diameter. Although this should suggest that the highest value of S_p should be measured with the diamond, it was shown in Chapters 5 and 6 that both volume averaging and positioning of the diamond using the BDAS system may not have entirely accounted for the shape of the crystal. S_{cp} measured with the diamond was 10% lower than that measured with the PFD or EFD and 5% lower for S_c in the 5mm diameter collimator and therefore S_p for the diamond is approximately 5% lower than for the PFD or EFD. Figure 7.4 shows a plot of S_{cp}, S_c and S_p against EQSQ (measured) for the EFD and SFD only.

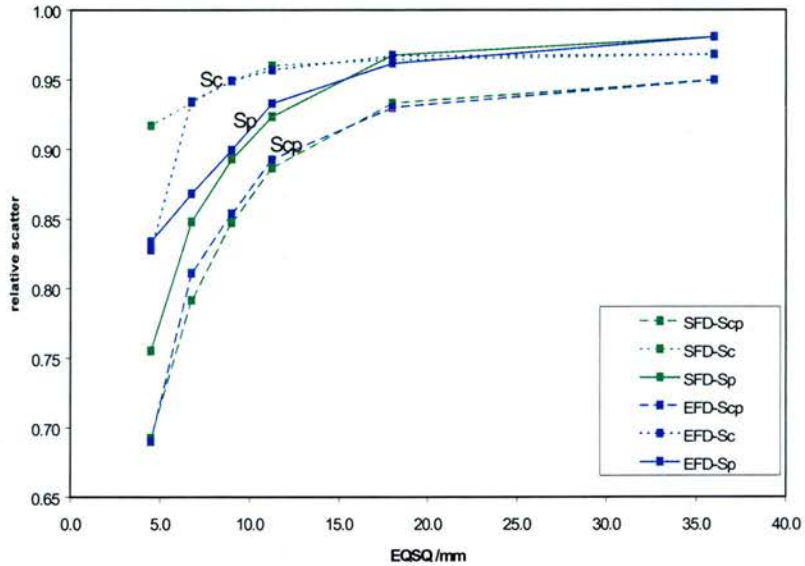

Figure 7.4. Plot of S_{cp}, S_c and S_p against EQSQ for the EFD and SFD, for the stereotactic collimators.

The large drop in S_c measured with the EFD has caused the over-estimation of S_p in the smallest collimators. Although it would seem that the SFD is therefore a more appropriate detector in the smallest collimators, it should be remembered that the S_p value calculated from SFD measured data for the 5mm collimator is also too high, due to the underestimation of S_c caused by the phantom width.

Open fields

The uncertainties in the calculation of S_p, expressed as percentages of the means at 1 s.d., are shown in Table 7.3.

	% Uncertainty (1s.d.)	
Detector	$20x20mm^2$	$10x10mm^2$
Diamond	0.1	1.7
PFD	0.1	1.5
EFD	0.1	1.4
SFD	0.6	1.1

Table 7.3 Uncertainties in S_p (open fields), expressed as percentage of the mean.

The increase in uncertainties in the $10x10mm^2$ field is a reflection of the positional uncertainties and the reproducibility of the field size setting on the movable collimators. In addition, the high dose region is smaller than for the 10mm width stereotactic field (Figure 4.16). Figure 7.5 shows a plot of S_p against measured EQSQ for measurements at dmax, in

which the effects of volume averaging have been corrected for. These results are analogous to NPSFs.

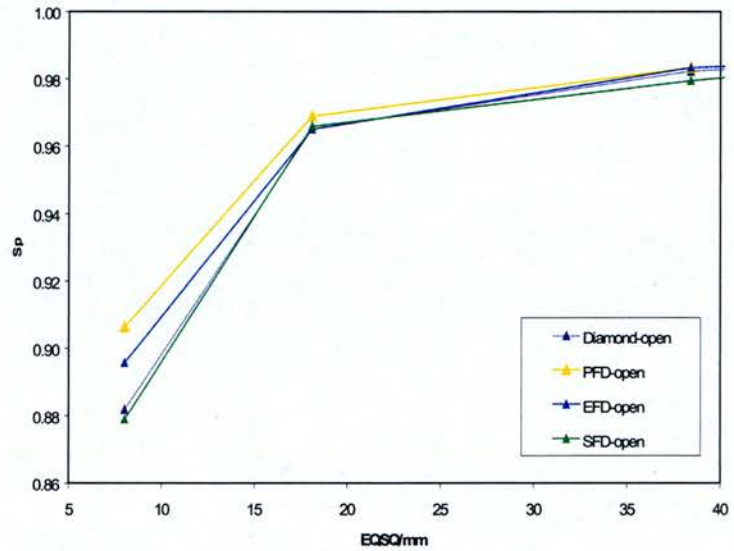

Figure 7.5. Plot of S_p against EQSQ for measurements at dmax in open fields.

The spread over all detectors is just over 2% in the smallest field size. Differences between detectors echo the corresponding differences in the measurement of S_{cp} and S_c. The PFD values are also over-estimated, for the same reasons as before. S_{cp}, S_c and S_p for the EFD and SFD are compared in Figure 7.6 against measured EQSQ.

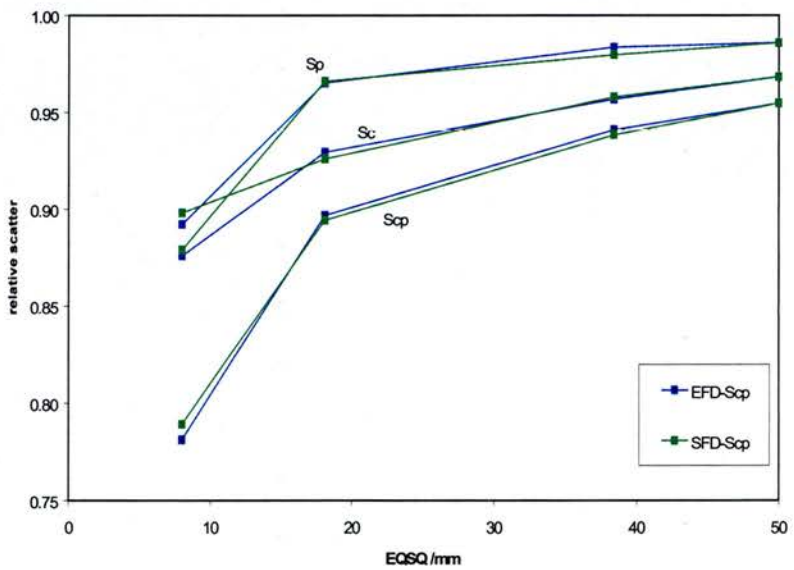

Figure 7.6. S_{cp}, S_c and S_p for the EFD and SFD in open fields.

Once again, at the smallest field size, the under-estimation of S_c measured with the EFD has caused S_p to be over-estimated.

MLC fields

The uncertainties in the calculation of S_p, expressed as percentages of the means at 1 s.d., are shown in Table 7.4.

Detector	% uncertainty (1s.d.) $20x20mm^2$	$10x10mm^2$
Diamond	0.1	0.2
PFD	0.1	0.2
EFD	0.2	0.2
SFD	0.5	1.3

Table 7.4 Uncertainties in S_p (MLC fields), expressed as percentage of the mean.

The experimental uncertainty is improved in the MLC fields, due to the wider high dose region. This decreases the effects of the positional inaccuracies. Figure 7.7 shows a plot of S_p against measured EQSQ for measurements at dmax. This time there were no volume averaging effects in either S_{cp} or S_c. These results are again analogous to NPSFs.

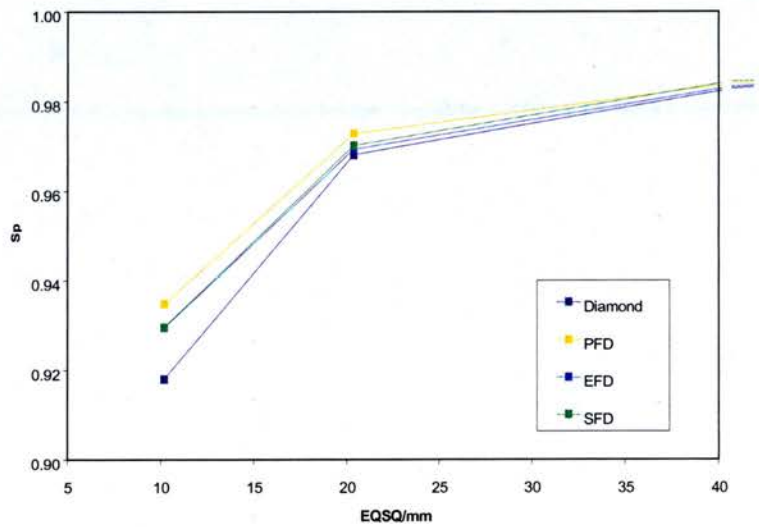

Figure 7.7. Plot of S_p against EQSQ for measurements at dmax, in MLC fields.

The spread over all detectors in the smallest field is approximately 2%. Again, this is due to the same differences between detectors in the measurement of S_{cp} and S_c. S_{cp}, S_c and S_p measured with the EFD and SFD are compared in Figure 7.8.

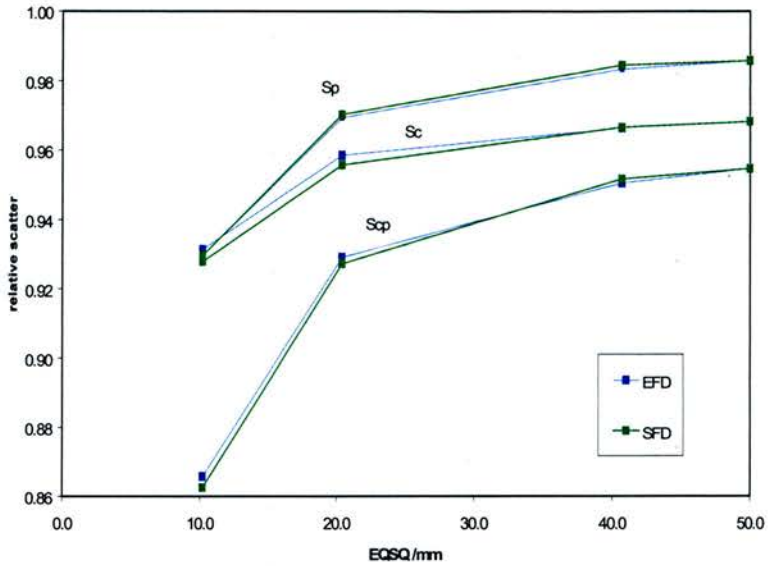

Figure 7.8. S_{cp}, S_c and S_p for the EFD and SFD in MLC fields.

The differences between the detectors are reduced in the MLC fields, due to the wider high dose regions.

7.3.2 Comparison of beam defining systems

S_p should be dependent only on the beam area at the surface of the phantom and therefore independent of the beam defining system. S_p against measured EQSQ, calculated for all three beam defining systems are compared at dmax in Figure 7.9.

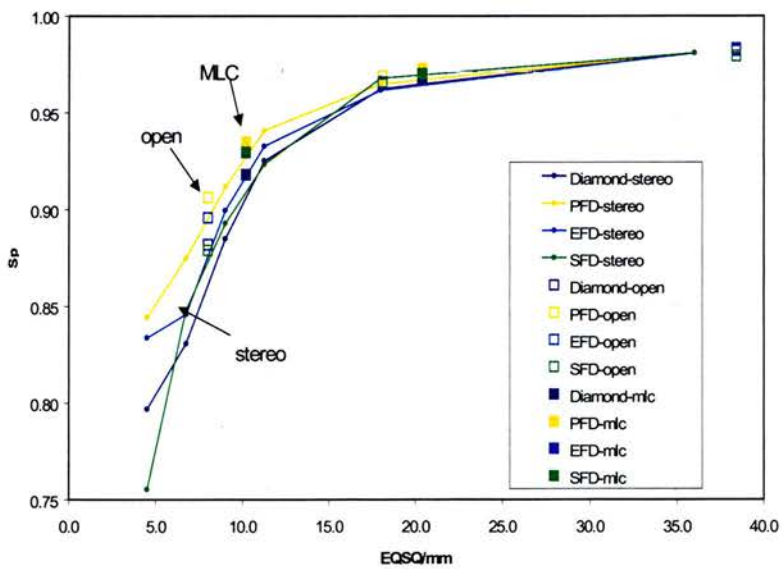

Figure 7.9. S_p calculated at dmax for all three beam defining systems.

The maximum difference between S_p in each beam defining system, is approximately 1.5%, within the field size ranges measured. The differences are due to the experimental uncertainties and the specific measurement features in each situation. The most appropriate S_p results for fields <20x20mm^2 are those calculated from SFD measured data, as this minimises the effect of the phantom width. However, the magnitude of the effect of the increase in LEE caused by the silicon is unknown, although it is likely to be small in the smallest collimator. S_p against measured EQSQ calculated at both dmax and 50mm for measurements with the SFD are compared with those of the EFD in Figure 7.10.

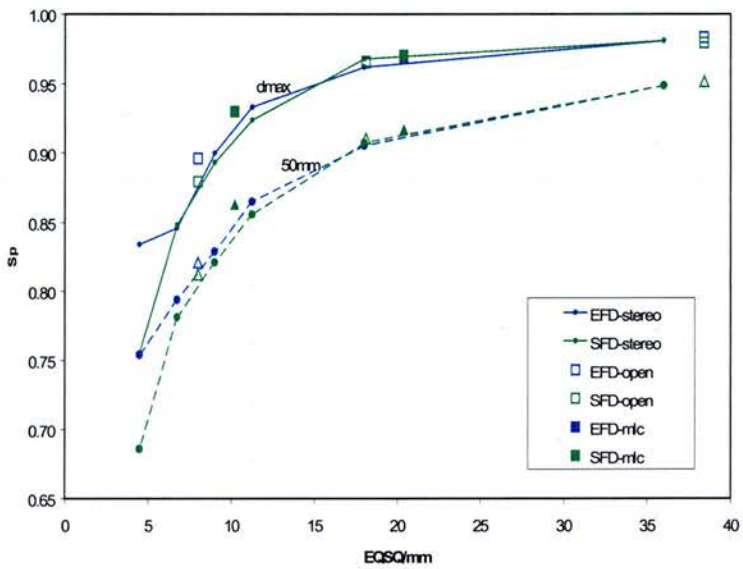

Figure 7.10. S_p calculated at both dmax and 50mm deep for all three beam defining systems, for the EFD and SFD only.

The effects are similar at both depths and it is likely that the EFD measurements have resulted in values of S_p which are too high.

7.3.3 Comparison of linacs

S_p data sets extracted from EFD (down to 15mm collimator) and SFD (smallest collimators) measured data on all three linacs are compared in Figure 7.11.

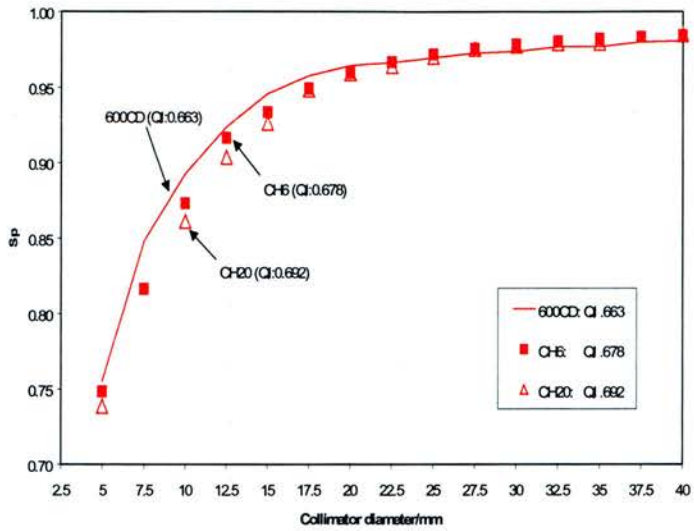

Figure 7.11. Comparison of S_p calculated data on all three linacs.

The maximum difference between curves is 3% in a 10mm diameter collimator. This may be the result of a quality dependence which is apparent only in fields <40x40mm^2. However, it could also be due to inaccuracies in the measurements on the two CH linacs.

7.3.4 XKnife data

XKnife does not require the input of S_p values. However, values of S_p calculated at dmax (NPSF) are required to calculate TMRs from PDDs in Chapter 8. Table 7.5 shows the final values of S_p at dmax for the stereotactic collimators.

Coll/mm	S_p at dmax
40	0.981
37.5	0.980
35	0.977
32.5	0.977
30	0.974
27.5	0.973
25	0.970
22.5	0.966
20	0.964
17.5	0.957
15	0.946
12.5	0.924
10	0.893
7.5	0.848
5	0.755

Table 7.5. Table of S_p at dmax for stereotactic collimators.

However, it should be remembered that values for the 5mm diameter collimator may be underestimated.

7.3.5 Comparison with other authors

The results in Table 7.5 are compared with those of other authors in Figure 7.12.

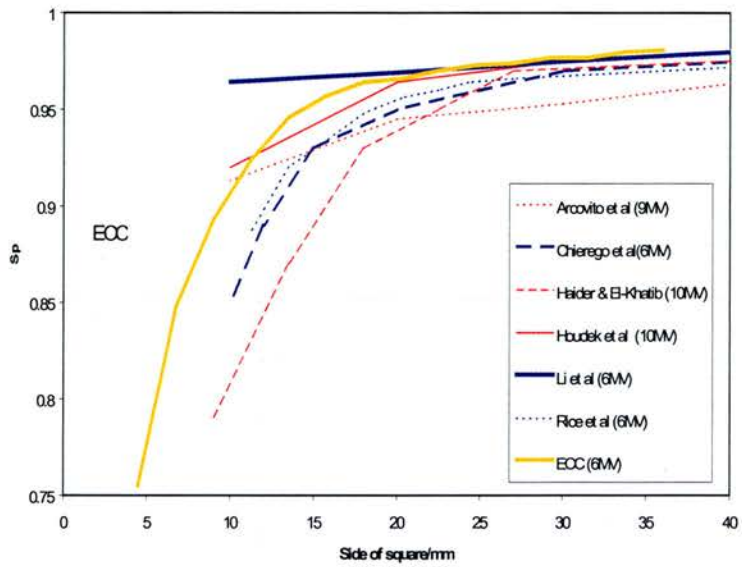

Figure 7.12. Comparison of ECC results for S_p calculated at dmax, with those of other authors.

The ECC results are for the largest range of field sizes and therefore show the largest drop in S_p.

7.4 Conclusion

S_p has been extracted at dmax and 50mm, from S_{cp} and S_c data measured with a range of detectors. S_p has been shown to be dependent on the detectors used, but independent of the beam defining system. The accuracy of S_p data calculated from equation 7.5 relies on the accuracy of the measured data for S_{cp} and S_c.

S_p should be independent of the detector used, if all uncertainties in the measurement of S_{cp} and S_c cancel out. However, differences in S_p are apparent between detectors, in Figure 7.3. This is because some of the measurement features in both situations (S_{cp} and S_c), which could have had an effect on the detector response, may cancel out in the calculation of S_p, but some may not. For example, the effect of shielding of the primary collimator aperture will cancel out in the calculation of S_p as this is inherent to both sets of measurements.

However, the effect of spectral changes may not cancel as the spectrum will be different in the measurement of each parameter. The effects of detector size will cancel, if S_{cp} and S_c values have been adjusted to account for the effects of detector size. The effects of detector size will not cancel in uncorrected values of S_{cp} and S_c because the amount of volume averaging is dependent on the shape of the profile, which will be different for the in-phantom and in-air situations. The effect of LEE may not cancel because this too may be different in the in-phantom and in-air situations. The effect of the absorption of too much phantom scatter in the PFD will not cancel out. Values of S_{cp} were over-estimated with the PFD, but no over-estimation occurred in the measurement of S_c. S_p is therefore still over-estimated for the PFD.

Finally, the effect of the phantom width in the measurement of S_c in the smallest collimator will not cancel. The build-up top was too wide for measurements with the SFD in the 5mm diameter collimator and therefore S_c was underestimated. This will result in a value of S_p which is too high. The effect will increase with detector (and hence phantom) diameter. Although this should suggest that the highest value of S_p should be measured with the diamond, it was shown in Chapters 5 and 6 that both volume averaging and positioning of the diamond using the BDAS system may not have entirely accounted for the shape of the crystal.

Although differences in S_p were reported on the three linacs tested, the measurement on the CH linacs may have been less precise as a full investigation of the methodology was only carried out on the 600CD.

Differences between the ECC results and those of other authors show that for fields <12.5mm diameter, experimental differences can have large effects. This indicates that the accurate determination of S_p data in the full field size range may only be achieved through MC modelling of both the beam and the detectors, which is outwith the scope of this work.

A final table of S_p was produced, although S_p in the 5mm diameter collimator is likely to have been over-estimated. However, as the calculation of TMRs relies on the ratio of two NPSF values for field sizes which are close together, the error in TMR is likely to be small.

Chapter 8

Tissue maximum ratios

8.1 Introduction

8.1.1 Definitions

Tissue phantom ratio

In a similar way to PDDs, tissue phantom ratios (TPRs) also characterise the fall off in dose with depth along the beam CAX. They are equal to the dose (D) at depth (d) divided by the dose at the reference depth (d_0), but for the measurement point held at a constant FAD.

$$TPR(d, s, FAD) = D(d)/D(d_0) \qquad (8.1)$$

TPRs can be normalised to any depth d_0, dependent on the formalism used. Formalisms based on a depth beyond dmax will use TPRs normalised to the same depth. TMRs are generally expressed as a ratio, but are stated in this work as a percentage, for convenience.

Tissue maximum ratio

A tissue maximum ratio (TMR) is a special case of the TPR, in that d_0 is equal to dmax. TMRs are used for formalisms which are based on dmax.

8.1.2 Measurement of TMRs

Water tank

TMRs can be measured in a water scanning tank (BDAS system) equipped with computer control of both the detector position and the water level. The detector is held at a constant FAD for each measurement and the water level increased in small increments. Although several tank manufacturers offer this facility as an "add-on" to the basic BDAS facility, the measurements are time consuming and often fraught with practical difficulties. This is primarily because the water has to be filled from the reservoir under computer control and

the water depth has to be fed back accurately to the software as each signal is sampled. The same detectors are used in the measurement of TMR as are used in PDD measurements.

Solid water measurements

TMRs can be measured much more easily in a solid water phantom. The detector is inserted in the phantom and the effective point of measurement located at the isocentre. The depth is increased by placing slabs of material on top of the detector. Although this is a simple technique, the measurements are again time-consuming, particularly if repeat measurements are carried out to determine the experimental uncertainty. In addition, care must be taken to ensure that the detector remains at the isocentre as the depth is increased, as couch sag with increasing weight of phantom could move the detector out of position. An adjustment to the couch height may therefore be necessary at greater depths.

8.1.3 Calculation of TMRs

PDDs can be converted to TMRs using equation 2(a) in Appendix B of BJR supplement 25 (Burns 1996):

$$TMR(d, s) = \frac{1}{100} \times PDD[d, f, sf/(f+d)] \times \frac{PSF[sf/(f+d)]}{PSF[sf/(f+d_m)]} \times \frac{(f+d)^2}{(f+d_m)^2} \qquad (8.2)$$

where d is the depth of interest, d_m is the depth of dmax and s is the field size at the FSD, f. This formula is applicable to PDDs which have been measured at f. The field sizes used in PDDs and PSFs must also have been defined at f. Although the above equation requires a ratio of PSFs, these are substituted with NPSFs (S_p values at dmax) for high energy beams.

PDD

In equation 8.2, the TMR is calculated for a field size s at the isocentre, from a PDD which has the same field size s at depth d and therefore a smaller field size at the phantom surface, equal to sf/(f +d). For example, the calculation of TMRs for a 12.5mm collimator, at depths of 100 and 200mm will require PDDs for collimators of diameters 11.4 and 10.4mm respectively. In order to calculate TMRs for all collimators in the range of 40-12.5mm diameter, PDDs for fields down to 10mm diameter are required.

Scatter correction

The ratio of PSF (or NPSF, or S_p at dmax) for two different field sizes in equation 8.2, is known in this work as the scatter correction. The scatter correction is required to account for the different amounts of phantom scatter in the TMR field size (s) at an FAD of f, compared to that in the PDD situation, where the field size s has been projected to the phantom surface at FSD f. The different field sizes and hence amounts of scatter are caused by the differences in divergence between the PDD and TMR situations. This will generally be a small correction at depths close to dmax, but will increase with increasing depth.

ISL correction

The effect of the ISL in the measurement of relative depth dose, is to further decrease the dose at depth in addition to the effect of attenuation. For TMR measurements, the measurement point is always located at the isocentre and therefore the relative dose at a given depth is greater than in the PDD (field size defined at the surface) situation. Removing the ISL from the relative PDD in equation 8.2 accounts for this. The effect of ISL is negligible at depths close to dmax, but increases as the depth increases and is 1% at 20mm deep and 40% at 200mm deep. As TMRs do not exhibit the effects of the ISL, they are FSD independent and are often used in isocentric based calculation systems. They are particularly useful for rotational treatments, as the change in FSD at each increment of gantry angle does not need to be accounted for.

8.1.4 Small field problems

Measured TMRs in small fields are subject to the same problems as the equivalent PDDs. In particular, these are the size of the detector (volume averaging) and the position of the reference (for BDAS measurements). However, when using a BDAS, there will be less uncertainty in the alignment between the detector and the beam CAX as the depth increases, compared to PDDs. This is because the detector position always remains the same and is not dependent on the accuracy of the tank depth control. However, there are other practical problems, such as the difficulty of changing the stereotactic collimators (if used) over a tank which has been positioned such that the detector is at the isocentre, at a large depth. As the distance between the end of the stereotactic collimators and the isocentre is only 230mm, the maximum depth which could be measured is very limited, as there should be a gap between the end collimators and the water surface.

TMRs measured in RMI will be subject to the same uncertainties as PDDs measured in RMI, although there will be the additional problem of the couch sag. If TMRs are calculated rather than measured, they will be subject to the uncertainties inherent in the measured PDD and the NPSF ratios.

8.1.5 Small field TMRs in the literature

Overview

Most small field TMRs reported in the literature have been measured directly, either using a BDAS system, or in a solid water equivalent phantom. Although film was rejected by several authors for the measurement of PDDs (Chapter 3), some authors have used it to measure TMRs, placing it perpendicular to the beam under different thicknesses of phantom. Although film is subject to potentially large uncertainties caused by the calibration and processing conditions, it is notable that no authors have commented on this with respect to TMR measurements.

Measured TMRs

Rice et al (1987) measured TMRs at 6MV in a polystyrene phantom with both a parallel plate (5.4mm effective diameter) and a cylindrical IC (internal diameter 3.5mm). TMRs measured with each detector were within 0.5% in collimators between 40 and 12.5mm, to a depth of 200mm.

Serago et al (1992) compared film, a parallel plate IC (PPIC, dimensions unspecified) and a diode (2mm sensitive width, shielding unspecified) to measure TMRs in a solid water phantom at 10MV. The detectors agreed to within 3% to a depth of 300mm, in a 8.4mm diameter collimator. The reproducibility of film was not discussed, nor the calibration method. The PPIC results were the highest and the diode and film results appeared to match, although differences were difficult to extract from the graphs. The PPIC was subsequently selected to measure TMRs in a range of energies between 24 and 4MV, although the reason for its selection is unclear.

Chierego et al (1993) measured TMRs at 6MV with a (0.055cc) PPIC and a cylindrical IC (0.6cc) in a water tank and film in a solid water phantom. All measurements were corrected for detector size using depth dependent correction factors calculated from Rice et al (1987). In addition, PDDs were measured in the water tank with the PPIC and converted to TMRs. Results were only presented for measurements in a $15x15mm^2$ field. The uncertainty on the

PPIC was the smallest, at +/-0.6% and this was therefore considered to be the optimum detector to use. The 0.6cc IC results had an uncertainty of +/-1% and varied from 2.9% higher than the PPIC at 30mm deep, to 0.2% higher at 150mm deep. The uncertainty on film was +/-1.8% and was within 0.5% of the PPIC around dmax, but diverged to a maximum difference of 1.6% lower at a depth of 150mm.

Haworth and Perry (1993) used a photon diode (2.5mm sensitive width, long axis parallel to CAX) to measure TMRs in a water tank (BDAS). These were compared with TMRs measured in a solid water phantom (detector perpendicular to the CAX), at 6MV. The maximum difference between the two set-ups was 1% down to a depth of 250mm, in collimators between 30 and 5mm.

Rustgi et al (1995) measured TMRs in a solid water phantom with a diamond (2.7mm sensitive width) and a photon diode (2.2mm sensitive width) both with long axes parallel to the CAX and a PPIC (5.4mm active diameter), in a 12.5mm collimator, at 6MV. The maximum difference between detectors was 2% at a depth of 250mm. The authors noted that there was no over-response to low energy photons because an energy compensated diode was used. However, it has been shown that scatter effects in small fields are minimal.

Gotoh et al (1996) found agreement to within 2.7% between TMRs measured with film and a micro-IC (external diameter 3.2mm) at 10MV, for depths up to 175mm, in collimators between 31 and 11mm diameters. No uncertainties were presented for film.

Heydarian et al (1996) used a diamond (size unspecified) and shielded diode (2.5mm sensitive width), both with long axes parallel to the beam CAX, in the water tank, at 6MV. Film was used in a solid water phantom. All results were compared with MC (EGS4). The diode was found to under-respond by 2 and 3% in the 23 and 7mm collimators respectively at 200mm deep. The diamond over-responded by 1.1 and 1.6% and film over-responded by 3.8 and 5.5% in the same field sizes, at the same depths. The responses of the diode and diamond were thought to be due to their dose-rate dependency and the film due to its over-response to low energy photons.

Das et al (1996) compared a diamond (2.7mm sensitive width) and a 0.125cc IC to measure TMRs in a water tank at 6MV, in "larger" collimators (diameters unspecified) and found that the results from each detector agreed to within +/-0.5% for depths down to 200mm. Although film was also used, no results were presented. A full set of TMRs for collimators between 50 and 12.5mm was measured with the diamond.

Fan et al (1997) measured TMRs with a 0.1cc IC (axis perpendicular to beam CAX) in 40-20mm diameter cones and used TLD in smaller cones down to 5mm diameter, at 6MV. All measurements were carried out in a polystyrene phantom. However, as measurements were only made with one detector type in each collimator, results could not be compared.

Francescon et al (1998) used both a 0.002cc PP micro-chamber (PPMC) and radiochromic film to measure TMRs using a BDAS system and compared the results with MC. However, the authors do not explain how they positioned film accurately within the water. In a 10.5mm diameter field, the PPMC was 0.3% lower than MC at a depth of 30mm and 1.1% higher at 150mm deep. The radiochromic film was 0.3% higher and 1.7% lower at the same depths. These results were considered to be in good agreement.

Zhu et al (2000) used a diode (1mm sensitive width) and film to measured TMRs in 7.5 and 5mm diameter collimators, in a polystyrene phantom. Their results on a 6MV beam of a Varian Clinac 2300CD compared favourably with the TLD results of Fan et al (1997) on a 6MV Clinac 1800. However, film was found to significantly over-estimate the dose at a depth of 150mm in both collimators, by approximately 3%.

van Battum et al (2002) measured TMRs with a shielded diode (2.5mm sensitive width) ,in collimators between 50-5mm diameter, in a 6MV beam, at depths beyond the build-up region only. The results were compared with calculated TMRs (see next section).

Calculated TMRs

The conversion of small field PDDs to TMRs using the BJR-25 equation, has been reported in only two publications to date. Chierego et al (1993) converted PDDs to TMRs using NPSF values which had been calculated through a comparison of measured TMR and PDD values. However, this appears to be a circular argument. As differences of up to 2.4% were found between the measured and calculated TMRs in a $15x15mm^2$ field, it is possible that the work was reported incorrectly.

McKerracher and Thwaites (1999) calculated TMRs from average PDDs measured with a selection of detectors and NPSF values taken from Rice et al (1987). The inclusion of the NPSF correction was found to improve the match between calculated and measured TMRs in the 12.5mm diameter collimator only. This work will be discussed in the results section.

van Battum et al (2002) used a unique method to calculate TMRs from PDDs. Although it was based on equation 2(a) in BJR-25, the ratio of NPSFs was approximated by the ratio of S_{cp} values for two other field sizes. A comparison of the calculated and measured (2.5mm sensitive width shielded diode) TMRs in a 5mm diameter collimator produced random differences only, of up to 2% at a depth of 200mm and 3% at 300mm. The method was found to be satisfactory within the desired experimental uncertainty, although no problems were discussed regarding the size of the diode with respect to the 5mm collimator.

Comparison of results

One field size (closest to 10mm width) has been selected from each publication for comparison, as summarised in Table 8.1.

Author	Energy /MV	Linac	Field Type	Field width/mm	Data presented
Chierego et al (1993)	6	Siemens Mevatron 6700	□	15	PPIC
Das et al (1996)	6	Clinac 600SR	○	12.5	Film
Fan et al (1997)	6	Varian Clinac 1800	○	12.5	TLD + 0.1cc IC
Francescon et al (1998)	6	Siemens Mevatron	○	10.5	MC BEAM
Gotoh et al (1996)	10	Varian Clinac 2100C	○	11.6	Film
Haworth and Perry (1993)	6	Philips	○	10	Diode
Heydarian et al (1996)	6	Siemens Mevatron KD-2	○	7	EGS4
McKerracher & Thwaites (1999)	6	BBC CH6	○	12.5	Calculated from PDD
Rice et al (1987)	6	Varian Clinac 6/100	○	12.5	PPIC
Rustgi et al (1995)	6	Siemens KD2	○	12.5	diamond
Serago et al (1992)	6	Varian Clinac 6/100	○	12.5	PPIC
van Battum et al (2002)	6	Varian 2300 C/D	○	20	Calculated from PDD
Zhu et al (2000)	6	Varian Clinac 2300CD	○	7.5	Diode

Table 8.1 Summary of data extracted from the above literature review, for circular (○) and square (□) fields.

The range of measurements taken from the above table, is shown in Figure 8.1.

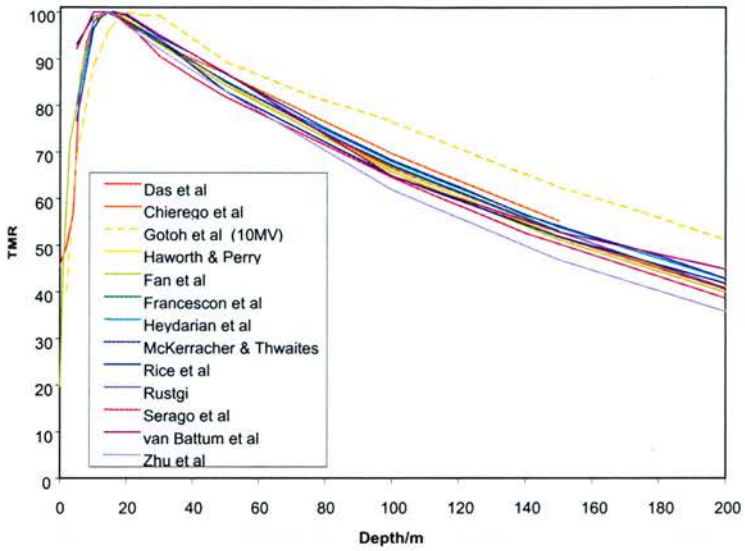

Figure 8.1 Comparison of TMR results in a variety of publications, as summarised in Table 8.1.

The spread over all 6MV data sets is approximately 10% and although a variety of beam widths is presented, the spread is higher than expected from quality alone and may be due to the different experimental techniques. Gotoh et al (1996) are the only authors to present results for 10MV and the resulting TMR curve is much higher than the highest 6MV data, by approximately 10% (TMR) at a depth of 100mm. The BJR-25 TMR data for a $40x40mm^2$ field shows an increase of only 2% (TMR) over the same range of energies, at 100mm deep. It is clear therefore, that although all authors have reported results which they consider to be accurate and representative of the data measured, the magnitude of the spread between results suggests that the measurement method plays a larger role than was suggested in any of the publications.

8.1.6 Aim

The aim of this work was firstly to compare TMRs calculated from PDDs and NPSFs, with TMR point measurements in solid water, made with a selection of detectors, in collimators between 40 and 12.5mm diameter and to determine the magnitude of the NPSF correction (equation 8.2).

8.2 Materials and Methods

8.2.1 Materials

A limited number of spot checks of TMR were made at different times, in solid water (RMI), with the diamond, EFD and PFD.

8.2.2 Methods

At the time of the commissioning of the stereotactic facility at the ECC (1994), the BDAS system in use did not have a functioning TMR facility. In addition, the measurement of TMRs in all collimators, in a full range of depths was considered to be too time consuming. PDDs were therefore converted to TMRs using NPSFs, according to equation 8.2. On the CH6, NPSFs were taken from Rice et al (1987), as discussed in McKerracher and Thwaites (1999). However, the extracted S_p (dmax) data from Chapter 7 were used in the calculations on the 600CD. To facilitate the calculation of the scatter correction, the S_p values at dmax from Chapter 7 (Table 7.5) were fitted to a curve using Origin version 6 software package (Microcal Software Inc, USA).

Spot checks of TMRs were also measured in solid water with the EFD, in the 40 and 12.5mm diameter collimators. A few measurements were also made with the PFD and the diamond. In each case, the effective point of measurement was set to the isocentre at 1000mm FAD. Measurements were only carried out on between one and three occasions. TMRs were smoothed and averaged as appropriate.

8.3 Results and discussion

8.3.1 Calculated TMRs

S_p curve fitting

The S_p values calculated at dmax in Chapter 7 (Table 7.5) were fitted to a Growth/Sigmoidal curve using the Hill function in the Origin software. The fit to the entire data set (40-5mm diameter) yielded an R^2 of 0.998 and a maximum difference between calculated and fitted S_p data of 0.5%. However, S_p was underestimated by 0.5% in collimators between 20 and 15mm diameter and matched the S_p values in the smallest collimators. As the data in the smallest collimators were subject to greater uncertainties and as S_p was required only for collimators between 40 and 10mm diameter, the curve fit was repeated for S_p data in this range only. R^2 was 0.998 for the new curve and the maximum difference between

calculated and fitted S_p values was 0.2%. The final equation to calculate S_p in a collimator of diameter s, is:

$$S_p = 0.984\ s^{2.19} / (3.55^{2.19} + s^{2.19}) \qquad (8.3)$$

It should be noted that equation 2(a) of Appendix B in BJR-25 (equation 8.2 here) requires NPSF data for field sizes defined at the phantom surface, at fixed FSD. S_p values in Table 7.5 in Chapter 7 have been measured at 1000mm FAD and the field sizes have been defined at the isocentre. However, the effect of the ISL will cancel due to the use of the ratio of NPSF used in equation 8.2 and the effect of the field size difference will be very small. In a 40mm collimator, the difference in field size is 0.6mm, which corresponds to an insignificant difference in S_p. In the 12.5mm collimator S_p is changing rapidly, but the field size change is only 0.2mm, which corresponds to a change in TMR of <0.1%.

Spreadsheet calculation

TMRs were calculated from PDDs and ratios of S_p at dmax (NPSF) in Excel. An example of a spreadsheet calculation is shown in Appendix 3, for the 12.5mm diameter collimator.

Scatter correction

The maximum scatter correction (ratio of S_p) is 2.7% in a 12.5mm collimator at 220mm and 1.2% at 100mm deep, which lowers the TMR value at that point. The correction is smallest in the 40mm diameter collimator, at only 0.2% of the TMR value at the same depth.

Uncertainties

The uncertainties in the calculated TMRs can be estimated from the uncertainties in the PDDs and the ratio of NPSFs. For collimators between 40 and 12.5mm diameter, the uncertainty in the PDDs (reproducibility only) was approximately +/-0.5%. In the 12.5mm collimator, the coefficient of variation for the calculation of S_p was <0.5%. However, as the ratio of Sp values is used, the uncertainty will be much less than this and is estimated here as +/-0.2%. The total uncertainty, at 1s.d. can therefore be estimated as +/-0.5% at 1s.d.. However, it should be noted that uncertainties due to extrapolation etc are unaccounted for.

8.3.2 Measured TMRs

Uncertainties

TMRs were measured on between only one and three occasions with the diamond, PFD and EFD. The overall reproducibility was +/-0.7%, which can be taken to be an uncertainty of +/-0.4% at the 1s.d. level. Measurements with the EFD were repeated again at a much later date and found to match the previous results.

8.3.3 Calculated compared with measured TMRs

Figure 8.2 shows calculated and measured TMRs for the 40mm collimator.

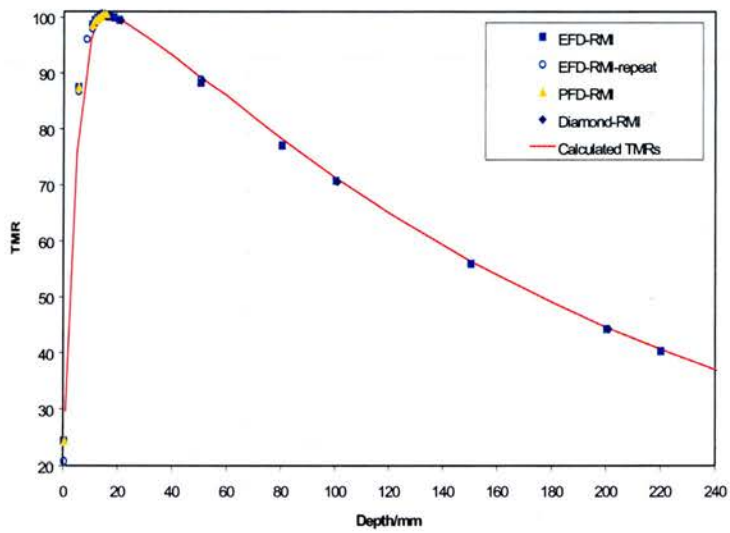

Figure 8.2 Calculated and measured TMRs for the 40mm collimator.

The differences between the average of the measured results in the 40mm diameter collimator and the calculated TMRs are shown in Table 8.2 for depths beyond dmax.

Depth /mm	Calculated TMR	Diamond measured TMR	% difference	EFD measured TMR	% difference
20	99.5	99.3	0.2	99.4	0.1
50	89.3	88.6	0.8	88.2	1.2
100	71.4	70.6	1.1	70.7	1.0
150	56.6	-	-	56.0	1.1
200	44.7	44.3	0.9	44.4	0.7

Table 8.2. Comparison of calculated and measured (EFD and diamond) TMRs in the 40mm diameter collimator.

Although the calculated and measured TMRs agree to within the quoted experimental uncertainties, there appears to be a systematic difference between the two data sets. Measured TMRs are approximately 1% lower than those calculated, as measured with both detectors. The differences are larger in the region around dmax, as shown in Figure 8.3.

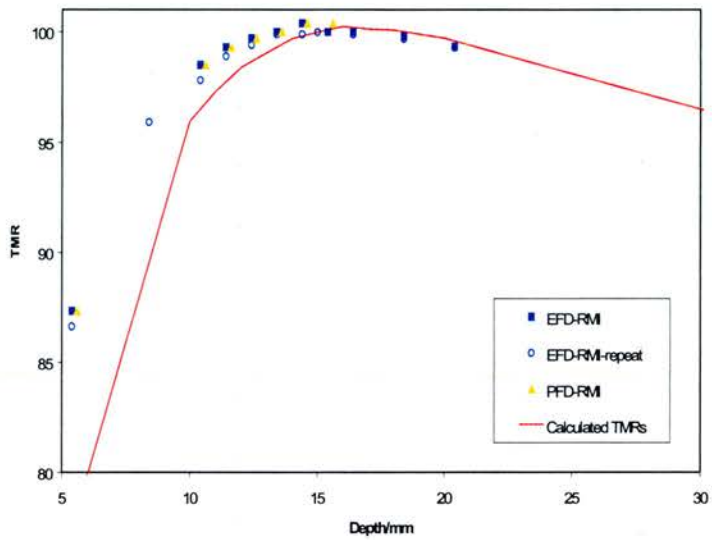

Figure 8.3 Calculated and measured TMRs for the 40mm collimator, in the region around dmax.

In the region around dmax, both the PFD and EFD measurements show a small shift in the position of dmax towards the surface. This is the same difference reported for the PDDs (Chapter 3) and is for all the same reasons, primarily the difficulties in smoothing the data in the build-up region. However, it could also be due to a systematic error in the depth; either in the set-up of the tank (for PDD), or in the RMI measurements.

Alternatively, the differences could be due to differences in detector response between the two methods of obtaining TMRs. As has been discussed previously, diodes are dose rate dependent. In the PDD measurements, the dose rate decreases due to both the depth and the distance. In the TMR measurements the dose rate is changing only with depth. These differences could affect the results. Figure 8.4 shows similar results in the 12.5mm collimator.

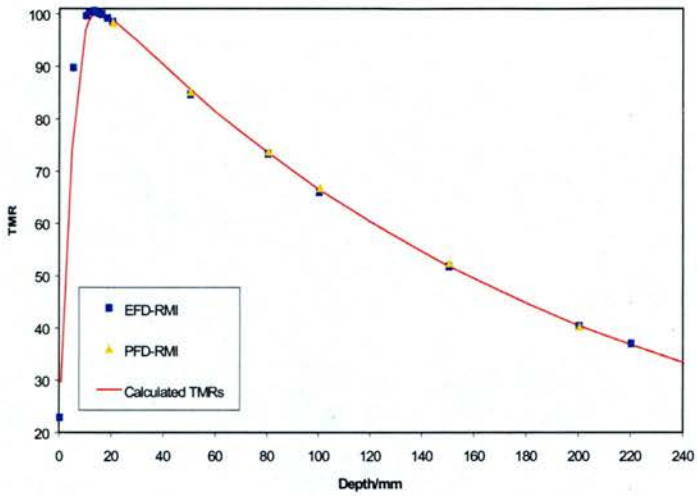

Figure 8.4 Calculated and measured TMRs for the 12.5mm collimator.

The differences between the mean measured and the calculated TMRs are shown in Table 8.3 for depths beyond dmax.

Depth /mm	Calculated TMR	PFD measured TMR	% difference	EFD measured TMR	% difference
20	99.0	98.2	0.8	98.4	0.6
50	85.6	85.1	0.6	84.6	1.2
100	66.2	66.8	-0.9	66.0	0.3
150	51.6	52.4	-1.5	51.8	-0.4
200	40.3	40.3	0.0	40.5	-0.5

Table 8.3. Comparison of calculated and measured (EFD and diamond) TMRs in the 12.5mm diameter collimator.

In the 12.5mm collimator, the differences between the measured and calculated TMRs show a possible tilt in either data set. This could be due to uncertainties in the NPSF data in small field sizes, requiring a larger NPSF correction at shallow depths and a smaller one at deeper depths. Alternatively it could the result of a problem with the measured data. This requires further investigation. Figure 8.5 shows the region around dmax.

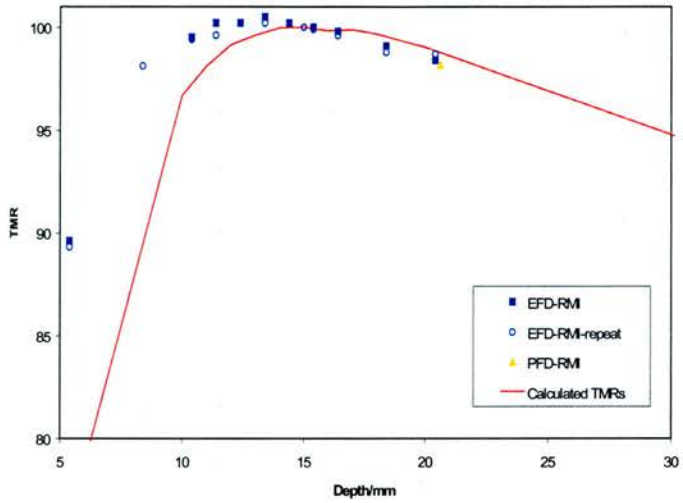

Figure 8.5. Calculated and measured TMRs for the 12.5mm collimator, in the region around dmax.

These differences are comparable with those in the 40mm diameter collimator. The same effects were also found in the 30 and 20mm diameter collimators.

Data smoothing

All calculated TMR curves were adjusted by averaging between the measured and calculated values. This results in a total uncertainty of +/-0.9% 1s.d.. The results were then smoothed in the same manner as the PDDs in Chapter 3 i.e. by plotting TMR against collimator diameter for each depth of measurement and fitting straight lines. The TMRs in all collimators are shown in Figure 8.6.

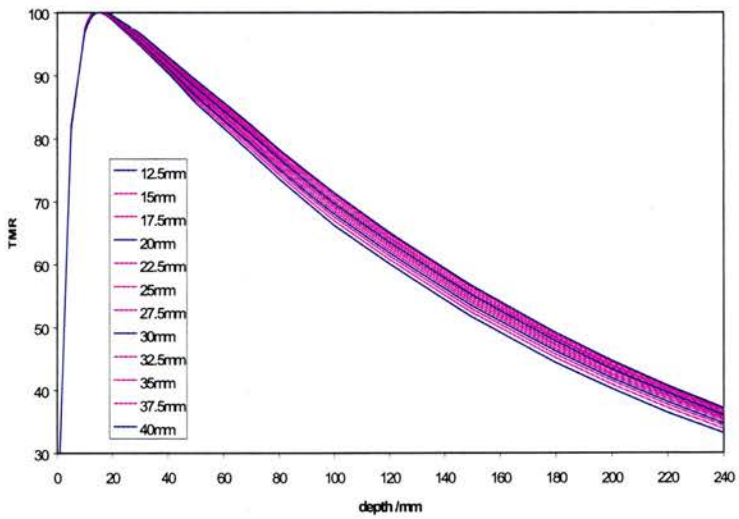

Figure 8.6 Final smoothed TMRs in all collimators on the 600CD.

The shift in dmax between the smallest and the largest collimators is apparent in Figure 8.7

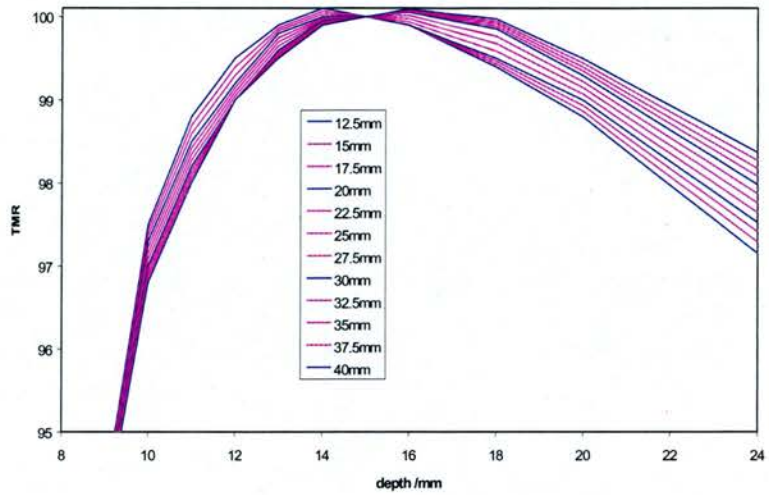

Figure 8.7. Final smoothed TMRs around dmax, in all collimators on the 600CD.

8.3.4 Comparison with CH6

PDDs were converted to TMRs on the CH6 using equation 8.2. S_p values at dmax, taken from Rice et al (1987) were used as the NPSF values in the equation, as S_p data had not been measured for this linac at that time. However, Rice et al provided Sp data only down to a 12.5mm diameter and as a result, data in beam widths down to 10mm were extrapolated. The ratio of S_p (NPSF) values resulted in a maximum correction to the PDD, of 4.5% at 200mm deep in a 12.5mm collimator. On the 600CD, the maximum correction resulting from the 600CD measured S_p values, was 3.3% at the same depth and collimator diameter. Using the correction based on Rice et al for the 600CD data, produces TMRs which are approximately 0.8% (TMR) lower than those calculated using the S_p data in Chapter 7. TMRs in the 40 and 12.5mm diameter collimators on the 600CD, calculated using the S_p data in Chapter 7 are compared with TMRs calculated using the data in Rice et al and with the calculated data for the CH6, in Figure 8.8.

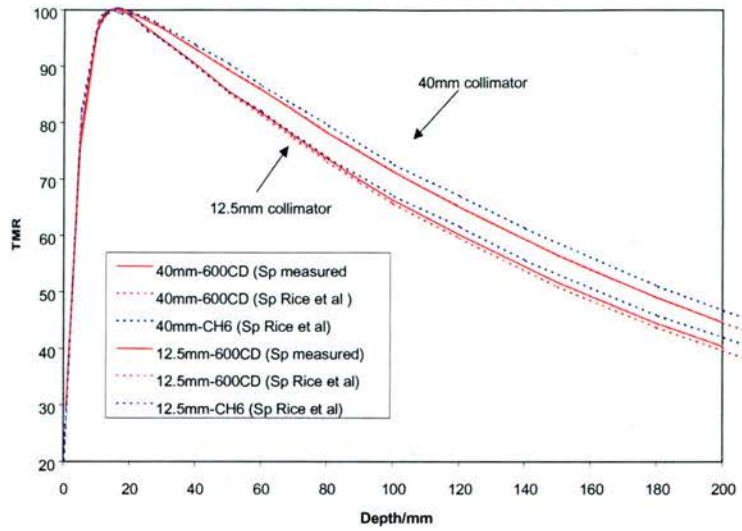

Figure 8.8 Comparison of TMRs on the 600CD and CH6, calculated from Chapter 7 S_p values (600CD only) and from data in Rice et al (600CD and CH6).

It is obvious that the TMRs on the CH6 (blue) are higher than those on the 600CD (red) by approximately 5% (local dose) at a depth of 200mm. This corresponds to approximately the same difference in PDD local dose (Figure 3.22) between the two linacs. However, the CH6 TMRs have been calculated using the S_p values in Rice et al and the TMRs on the 600CD have been calculated using the measured S_p values. To compare the difference caused by using the two different S_p data sets, the TMRs on the 600CD have been calculated using each S_p data set. The red solid lines in Figure 8.8. represent TMRs calculated from PDDs and measured S_p values and the dashed lines represent TMRs calculated from the same PDDs but S_p values taken from Rice et al (1987). These two sets of TMRs are indistinguishable in the 40mm collimator, but in the 12.5mm diameter collimator the use of the measured S_p values results in a TMR curve which is approximately 2% (local dose) higher at 200mm deep than that calculated with the data from Rice et al.

8.3.5 Comparison with BJR-25

As a final point of interest, measured PDDs and calculated TMRs for the 40mm diameter collimator, on the 600CD were compared with PDDs and TMRs taken from BJR-25 6MV beam data for a 40x40mm^2 field, which is the smallest field size tabulated. Figure 8.9 shows the results, including PDDs and TMRs for the 12.5mm diameter collimator.

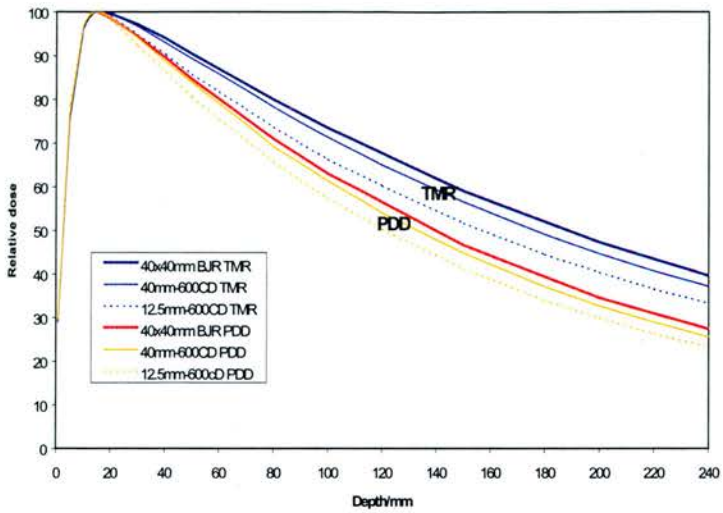

Figure 8.9. Comparison of PDD and TMR data for the 40 and 12.5mm diameter collimators on the 600CD with 40x40mm^2 data in BJR-25.

Although the QI for the BJR data is not stated explicitly, the dose at 100mm deep in a 100x100mm^2 field is 67.5%. On the 600CD it is 66.5%. The BJR data is therefore representative of a higher energy beam and this is reflected in the higher PDD and TMR data. TMRs are higher than PDDs primarily because the effect of the ISL has been removed from the measurements at depth. At shallow depths, the scatter correction is very small simply because the field size change caused by divergence is also very small.

8.3.6 XKnife data

XKnife requires the input of TMRs for the full range of collimators used. In the ECC, collimators between 40 and 12.5mm diameter are used clinically. The corresponding TMR data calculated for the 600CD from measured PDD and extracted S_p (dmax) data and shown in Figure 8.6 is tabulated in Appendix 4.

8.4 Conclusion

TMRs calculated from PDDs and the ratio of Sp (dmax) values are subject to the uncertainties in both sets of data. The overall uncertainty in calculated TMRs has been shown in this work, to be +/- 0.5% (1 s.d.). The ratio of S_p values lowers the calculated TMRs by a very small amount in the larger collimators (0.2-0.5%), but in the 12.5mm collimator the correction is greatest and is 1% at 100mm deep and 2.7% at 200mm deep. The use of Rice et al (1987) S_p values resulted in TMRs which were too low by

approximately 1.8% at 200mm in the smallest collimator. This error was caused by extrapolation at the smaller field sizes.

The uncertainty in TMRs measured in solid water was estimated as +/-0.7%, but this is the total spread over very few repeats. Although this means that the calculated and measured TMRs agreed within the experimental uncertainty, there does appear to be a systematic difference between the two methods. TMRs calculated in the 40mm collimator were approximately 1% (of the value) higher than a few points measured with the diamond and EFD, at depths beyond 50mm. In the 12.5mm collimator the differences were less systematic although the calculated TMRs ranged from 1% higher to 1% lower. The reason for a systematic error could be due to positioning errors, or a dose-rate effect, as discussed previously. Differences in the build-up region were due to the PDD extrapolation problem in this region, as also reported previously. In conclusion TMRs can be calculated from PDDs to within an accuracy of +/-0.5%.

Chapter 9

Verification of the dose to the isocentre

9.1 Introduction

9.1.1 Verification

Overview

All radiotherapy techniques require verification of some kind, whether it is through measurements of dose in a phantom (in-vitro) or by measurements of dose on or in the patient (in-vivo). Verification of a new technique in a phantom is particularly useful as the phantom can be scanned and planned in a similar way to a patient. The geometry and set-up of the phantom and isocentre can be checked, as can the dose to specific points. Finally, the overall dose distribution can be checked. Verification can be used to confirm the overall accuracy of the system, from the imaging and planning processes at the beginning, to the treatment stages at the end. It is useful both within a department as part of the overall quality assurance programme and between departments, to audit the dosimetry, planning and treatment processes.

Geometrical set-up

An accurate geometrical set-up is dependent on precise patient positioning and the mechanical constraints of the linac, couch and lasers. To achieve this, customised immobilisation devices must be individually fitted to reproduce the patient position between all imaging (CT, MR, simulator etc) and treatment modalities. Exact transfer of patient images and beam co-ordinates must also be carried out between the imaging, planning and treatment equipment, to ensure consistency of data. The coincidence of the crosswires, lasers, beam CAX and centre of rotation of the gantry, and collimator, must lie within a sphere of, at worst, diameter 4mm (IEC, 1989). However, as agreement to within +/-1mm can be achieved on the majority of modern linacs, most departments work to within this smaller limit.

The geometrical set-up is frequently verified using radio-opaque markers embedded in a phantom. The difference between the known (measured) and calculated (on the planning system) positions is an indication of the overall geometric accuracy. However, in the patient situation, accuracy is likely to be reduced as a result of patient movement (voluntary or involuntary), breathing and internal organ motion.

Relative dose distribution

The accuracy of the calculated relative dose distribution is dependent on the data input to the planning system in terms of OARs, PDDs, TMRs etc. It is also dependent on the planning algorithm, with particular reference to the modelling of inhomogeneities and lack of scatter. Finally, it is dependent on the accuracy of the imaging information, which in turn is dependent on CT slice thickness, and separation etc. ICRU 42 (1987) states that the difference between measured and computed dose distributions should be <2% relative dose within regions of constant dose and <2mm between isodose lines, in regions of high dose gradient.

The relative dose distribution can be measured in a phantom using TLD, film or gel. Although each TLD chip can supply only 1D information, arrays of TLDs can be used to obtain 3D data. However, the overall resolution is likely to be poor and the process is time-consuming. A single sheet of film can provide 2D information and if banks of films are used, 3D data can be extracted. However, the calibration and reproducibility of film is dependent on the accuracy of the processing conditions and the specific irradiation conditions (e.g. film perpendicular or parallel to beam CAX) and optimising these can be a lengthy process. Although gel is the only type of dosimeter which can provide full 3D information, it is also the most expensive and time-consuming and as a result, its use is not as yet routine.

Absolute dose

The accuracy of the calculated dose to the isocentre is also a function of the planning system input data, algorithms, imaging data and relative outputs. The accuracy of the measured dose is dependent primarily on the traceable calibration for the detector used. ICRU 24 (1976) states that the dose delivered to a specific point in a patient should be at worst, within +/- 5% of the prescribed dose, although other assessments of recommended accuracy, based on dose-effect curve information, suggests about 3% at the 1s.d. level (IPEM 81,

1999). The dose at the isocentre (or any point of interest) is usually measured with an ion-chamber in a phantom at a predefined point.

Phantoms

Various types of phantom have been in use for a number of years. The Rando anthropomorphic phantom (Alderson et al, 1962) remains popular and is the most anatomically correct phantom. It is most often used in conjunction with TLD or film. Semi-anatomic phantoms (Thwaites, 1996; Thwaites and Allahverdi, 1997; Thwaites et al, 2003) are useful for intra and inter-departmental audit and can be used in conjunction with film, TLD and ion chambers. These phantoms are most suitable for the verification of coplanar beams. The verification of target co-ordinates generally requires the design of an in-house phantom (Hartmann et al, 1993; Yeung et al, 1993), although some commercial phantoms are available.

9.1.2 Small field problems

Geometry

The geometrical accuracy of the linac, couch and lasers for stereotactic treatments, must be better than that for conventional treatments. Tsai et al (1991) and Hartmann et al (1993) both recommended coincidence within a 1mm diameter sphere for stereotactic treatments. The overall geometrical accuracy of a stereotactic treatment will again depend on the immobilisation device, the quality of the imaging data and the accurate transfer of co-ordinates between the imaging modality, planning system and treatment machine. A more precise patient immobilisation system is required for stereotactic treatment, such as the fixed or relocatable frames discussed in Chapter 1. Smaller CT slice thickness and separation are also required to minimise errors in patient outline and tumour localisation. However, as a scan of the whole head is required, there may have to be a compromise between slice thickness and total number of slices.

Dose and distribution

The accuracy of the delivered dose and dose distribution, in all types of treatments, is dependent on the input beam data. As the measurement of small field beam data is much more complex than for more routine types of treatment, the verification of that data is also more complex. The measurement of absolute dose in small fields introduces additional problems. The calibration of several small types of detectors must be investigated carefully

as the correction factors applied to convert a detector reading to dose may not apply in the small field situation. In addition, verification of the dose delivered from several non-coplanar arcs requires a thorough investigation of the directional response of each detector.

Phantom

A dedicated phantom is required for the verification of stereotactic treatments. It must be attachable to the appropriate stereotactic frame, should mimic the shape of the head and allow the use of non-coplanar beams.

9.1.3 Small field verification in the literature

Introduction

The verification of various aspects of stereotactic treatments has been described in several publications. Although dedicated phantoms have been designed commercially, or in-house, many of the procedures outlined below are complex and unsuitable for use on a more routine basis, particularly as part of a regular quality assurance programme.

Target position verification

Yeung et al (1993) investigated individual spatial uncertainties and overall spatial accuracy using targets in an acrylic cylinder. Localisation was found to be most accurate for conventional angiography (0.38 +/-0.1mm) and least accurate for CT slices with 4mm spacing (1.6 +/-0.5mm).

Coffey et al (1993) verified target position with ferrous-sulphate gel and although there was "excellent" agreement between the target co-ordinates and the machine isocentre, it was not quantified. More usefully, Hartmann et al (1993) looked at errors in the determination of known target co-ordinates and found agreement to within 1mm using CT and x-ray.

O'Brien and Fung (1994) located 1mm diameter markers of known co-ordinates relative to the centre) of an acrylic phantom, to within 1.2mm, as determined by CT and digital subtraction angiography (DSA).

Ramani et al (1995) localised markers embedded in an acrylic phantom at known co-ordinates to within the voxel size for CT ($1x1x1mm^2$) and MR ($1.2x1.2x3.0mm^3$). However, for DSA, the error was >2.5mm at the periphery of the image.

Verellen et al (1999) used 0.2cm lead beads in an anthropomorphic phantom and found agreement between the known co-ordinates and those localised with CT, to within 0.8mm, at 95% confidence.

Linac, couch and lasers

Winston and Lutz (1988) developed a method for checking the coincidence of the radiation isocentre with the lasers, which was later adapted by Warrington et al (1994). Tsai et al (1991, 1996) also developed methods for testing the stability of the isocentre and found agreement to within 0.3mm.

Gibbs et al (1992) tested the coincidence of the crosswires and lasers on five Varian accelerators. A root mean square error between +/-0.06 to 0.08mm was found in the plane of rotation and between +/-0.17 to 0.35mm perpendicular to that plane. This demonstrates the achievable accuracy on similar Varian linacs.

Treuer et al (2000) developed a method for looking at the stability of the isocentre with respect to the lasers and found agreement to within 0.3mm.

Verification of dose and dose distribution

Coffey et al (1993) planned a typical 18mm collimator Gamma Knife treatment on a commercial water filled phantom and verified the absolute dose with TLD powder embedded in ferrous gel. The dose to the isocentre was measured on several different occasions and found to differ from calculation by between +4.2% and -3.7%. The authors did not make any comment regarding the acceptability of these results, nor the reproducibility.

Guan et al (1993) used gel, TLD and radiochromic film in an anthropomorphic head phantom. Nine non-coplanar arcs were planned with a 10mm collimator. The gel showed "qualitative" agreement with the calculated dose distribution. Agreement between the prescribed dose and the dose measured with TLD was within 5% in the high dose region, but at the 10% dose level, there was a disagreement of almost 30%. Radiochromic film also showed agreement in the high dose region, but a 20% difference at the 50% level. According to the authors, the largest problem was in determining the isocentre co-ordinates in the phantom, for each dosimeter used.

Ramani et al (1994) used radiochromic film in an acrylic phantom. The isocentre dose was measured to within +/-3% of the calculated dose in a plan which incorporated a 20mm diameter collimator. The 90 and 50% isodoses were measured to within +/-1mm and the 10% to within 5mm.

Ravindran et al (2001) verified the dose in mMLC plans in a commercial acrylic phantom. Plastic inserts were used to simulate different lesions and film and TLD used for verification. TLDs were found to match the expected dose in the target to within 3%, but in regions of high dose gradient the deviations were 5-9%. Film measured the dose to the isocentre to within 2%, but differed by up to 8% at off axis distances. Transverse and sagittal plane isodose distributions agreed with calculated values to within 1-2mm.

O'Brien and Fung (1994) used a TLD array to measure profile widths and found these to differ from calculated widths by up to 5mm.

Duggan and Coffey (1996) used a micro-ionisation chamber (0.009cc) in a commercial water filled phantom. The mean dose to the IC was calculated by averaging the dose over the orthogonal projections of the isodose curves in the final plan. The measured doses for plans incorporating collimators of between 32 and 16mm diameter were within 2% of the calculated doses. For the 7.5 and 5mm collimators, the differences were 5.8 and 7.5% respectively.

Ertl et al (1997) used TLD in a RANDO phantom to verify the treatment of an eye on the Gamma Knife. The measured dose to isocentre was found to be within +/-1.6% of the calculated dose. To verify the dose to different parts of the eye, a TLD array was inserted into a human cadaver. The measured dose was found to be within 3% of the calculated dose at the back of eye, but up to 30% less than the calculation at the front of the eye. However, measurements at the surface of a phantom are subject to the largest uncertainty.

Cosgrove et al (1999) used film in a cubic, solid water phantom to verify the dose distribution from several six-field, non-coplanar mMLC plans. Measured isodoses >=50% matched calculated isodoses to within 1mm, but deviations of up to 5mm were found in the low dose region. Absolute dose measurement with film differed from the calculated dose by up to 6%. Although TLD in a Rando phantom matched the calculated dose to within +/-2%, the reproducibility was +/-4%.

Cosgrove et al (2000) used polyacrylamide gel (PAG) in a perspex and glass phantom to confirm non-coplanar conformal plans. The areas enclosed by particular isodoses differed from the calculated areas by between 2 and 8%, with a reproducibility of +/-5%. However, the absolute dose was found to be on average 23.5% higher than the calculation. This was thought to show the unsuitability of gel for the measurement of absolute dose.

Perks et al (1999) verified the dose in a 32.5mm collimator non-coplanar arc plan and a four field conformal plan. A 0.2cc IC was used in a hemispherical water filled perspex phantom. Although the maximum percentage difference for a single arc was 3.2% in the stereotactic plan, the overall difference was only 0.3% in the dose to the isocentre. In the fixed field plan, the maximum single field difference was 2.4%, with an overall difference in the total dose to the isocentre of 0.6%.

Verellen et al (1999) measured the dose to the isocentre in a perspex phantom for a stereotactic plan to within 2% with TLD.

Robar and Clark (2000) used a multiple-film cassette box in a water-filled anthropomorphic phantom to verify a five-arc, 30mm collimator, plan. Monte Carlo simulation showed that as the number of films increased, so too did the photon attenuation. As a result, there was a compromise between spatial resolution and dose perturbation. Although the planned and measured 80% isodoses matched to within 1.5mm, there were differences of up to 3.2mm in regions of low dose.

Grebe et al (2001) used both a polymer gel phantom and a 0.3cc IC in a water filled glass phantom. Conformal plans for target volumes between 7 and 9cc were produced with 5 arcs. The measured 50 and 90% isodoses were within 1-2mm of the planned isodoses and the dose to the isocentre was within +/-2%. The authors noted that the BANG polymer gel method required approximately 12hrs for planning, irradiation and measurement, excluding analysis.

McKerracher and Thwaites (2002) compared a 0.125cc IC against a diamond and a shielded, unshielded and stereotactic diode in the measurement of the dose to the isocentre. These measurements will be presented and discussed in the results section.

Comparison of results

Table 9.1 summarises the verification processes described in each of the above papers.

Authors	Target co-ords	Linac geometry	Absolute dose	Relative dose
Coffey et al (1993)	✔		✔	
Cosgrove et al (1999)			✔	✔
Cosgrove et al (2000)			✔	✔
Duggan and Coffey (1996)			✔	
Ertl et al (1997)			✔	
Guan et al (1993)				✔
Gibbs et al (1992)		✔		
Grebe et al (2001)			✔	✔
Hartmann et al (1993)	✔			
McKerracher and Thwaites (2002)			✔	
O'Brien and Fung (1994)	✔			✔
Perks et al (1999)			✔	
Ramani et al (1994)			✔	✔
Ramani et al (1995)	✔			
Ravindran et al (2001)			✔	✔
Robar and Clark (2000)				✔
Treuer et al (2000)		✔		
Tsai et al (1991)		✔		
Tsai et al (1996)		✔		
Verellen et al (1999)		✔	✔	
Warrington et al (1994)		✔	✔	
Winston and Lutz (1988)		✔		
Yeung et al (1993)	✔			

Table 9.1. Summary of verification processes in the above literature review.

Summary

Although polymer gels have been shown to be useful in measuring the dose distribution, they are messy, expensive and time-consuming and unsuitable for use on a regular basis. TLD arrays are easier to use, but the process is still time consuming and the reproducibility and resolution is less than ideal. Film, if calibrated and processed appropriately, is therefore the most useful detector for verification of the dose distribution.

In terms of the measurement of absolute dose, gel has been shown to exhibit large inconsistencies. TLD is much more accurate, but with a lack of precision. Ion chambers have been shown to be both accurate and precise, but are generally unsuitable for measurements in small fields. Other types of detectors have not been tested in the measurement of the delivered dose to the isocentre.

9.1.4 Verification of stereotaxy at the ECC

Although target co-ordinates, relative dose distribution and absolute dose should all be tested as part of the verification process, this work is concerned only with the verification of the absolute dose to the isocentre. Verification of the basic geometrical aspects of the stereotactic process at the ECC was carried out originally by Radionics as part of the XKnife installation process. ECC staff then borrowed the geometric phantom on several occasions to test new scanners and recently this phantom has been purchased. Verification of the dose distribution is currently being studied, but as this requires a thorough investigation of film types (X-Omat V, EDR and Gafchromic) in addition to a review of the calibration and processing conditions, analysis of appropriate scanners (x-ray densitometer, laser scanner, document scanner) and the design of a new phantom. This will be undertaken as future work.

9.1.5 Aim

The aim of this work was to develop a simple, reproducible technique to verify the dose to the isocentre in a selection of typical treatment plans, for the full range of clinical collimators, 40-12.5mm diameter. This involved the design of a phantom which could be attached to the GTC frame. The most appropriate detector to use in the phantom was determined by testing the symmetry, directional response and calibration of a range of small detectors. A technique was developed to measure the dose to the isocentre on a routine basis, in a simple and reproducible manner. The verification method was also incorporated into the departmental quality assurance programme.

9.2. Methods and Materials

9.2.1 Materials

Detectors

The diamond, PFD, EFD, SFD and 0.125cc IC were all compared to determine the most appropriate detector. All measurements were carried out on the 600CD only.

Phantom

A solid water phantom was designed and constructed in-house as shown in Figure 9.1.

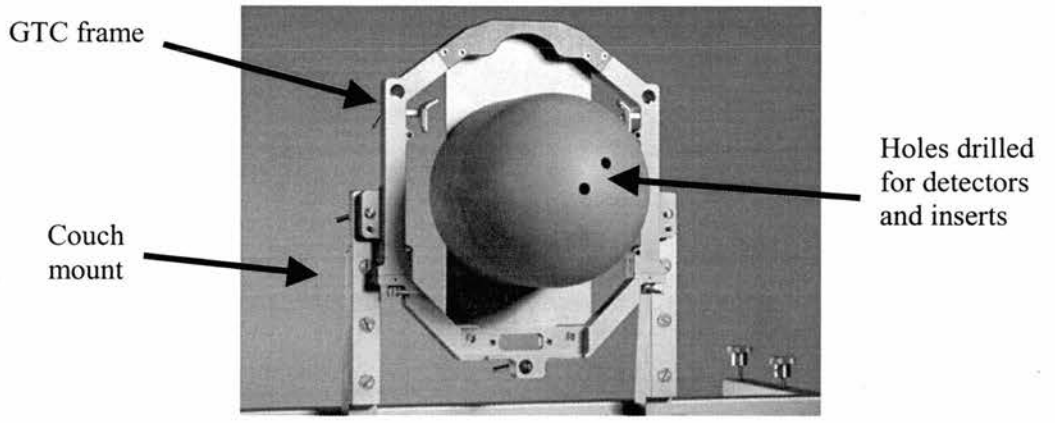

Figure 9.1. Photograph of the stereotactic phantom attached to the GTC frame.

The phantom is made of WT1, an epoxy-resin based water equivalent phantom material produced at St Bartholomew's Hospital in London. The design was loosely based on the water-filled phantom used at the Royal Marsden in London (Perks et al, 1999). It was attached to the GTC relocatable stereotactic frame via a steel baseplate. The shape of the phantom is basically cylindrical, terminating in an 8cm radius hemispherical section furthest from the frame. 1cm diameter holes were drilled the full length of the phantom both at the centre and at 3cm off axis. Inserts of the same material were made to fit the holes and to hold each of the detectors under investigation. Figure 9.2 is a diagrammatic view.

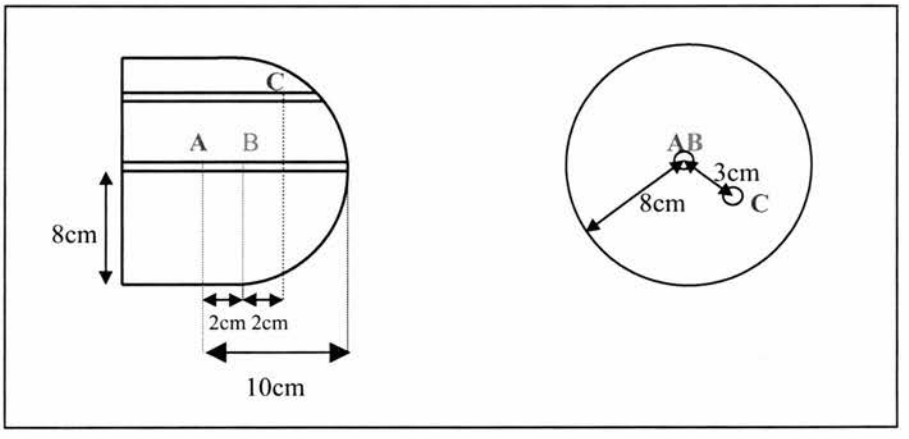

Figure 9.2. Diagram of the stereotactic phantom, viewed in cross-section from the side and the end. A and B are points lying along the central hole and C lies in the off-axis hole.

Position A is located within the cylindrical section of the phantom, 10cm from the hemispherical end and in the middle of the central hole. Position B is also located in the

middle hole, but at 2cm from A, towards the hemispherical end, at the origin of the hemisphere. Position C is located in the off-axis hole, at 4cm from A along the axis of the central hole. The accuracy of the position of the holes and the effective point of measurement within each detector sleeve were both +/-0.2mm.

Image data

XKnife version 3.0, in use at the time, limited the maximum number of slices to 64. In order to scan the whole of the phantom, CT slices of 3mm thickness and separation had to be used. The slices were transferred via the local network to the planning system.

9.2.2 Methods

Radiation isocentre

The position of the radiation isocentre with respect to the position of the lasers was determined using the Winston Lutz test (1988) at the four principal gantry angles (0, 90, 180, 270). The centre of the measurement volume for each detector was placed at the mean position of the radiation isocentre, averaged over all arcs, for each individual plan. The coincidence of the couch rotation with the radiation isocentre was tested at the time of acceptance. An overhead laser was also purchased to allow adjustments for isocentre drift (+/-1mm) to be made at each floor angle.

Symmetry

Symmetry is defined in this work as the relative radial response around the axis of the detector, as shown in Figure 9.3.

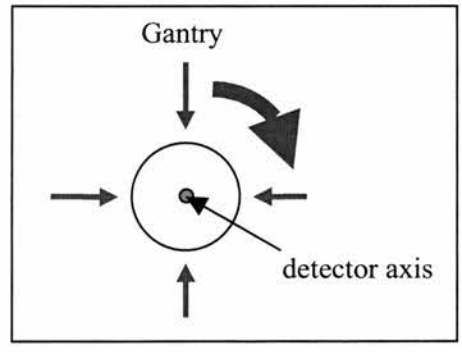

Figure 9.3. Direction of detector symmetry, as defined in this work.

Symmetry was measured by placing the effective point of measurement for each detector at position A in the phantom. Position A was then placed at the radiation isocentre, averaged over the four principal gantry angles. Measurements were initially made at 0° couch, for static beams positioned at the four principal gantry angles, then at gantry 0°, with each detector rotated around its axis, to achieve the same beam-detector alignments. This verified whether or not the phantom and set-up were symmetrical and whether or not the dose variation with gantry angle, on the linac was acceptable (+/- 0.5%).

Measurements were carried out for gantry positions between 0° and 350° in 10° intervals and the response at each angle was normalised to that at 0°. Moving the detector 1mm in the superior-inferior direction assessed misalignment between the radiation isocentre and the effective point of measurement. This was achieved using spacers of 0.5 and 1mm.

Directional dependence

Directional dependence is defined here as the change in response of the detector at any angle, around the end of the detector axis, as shown in Figure 9.4.

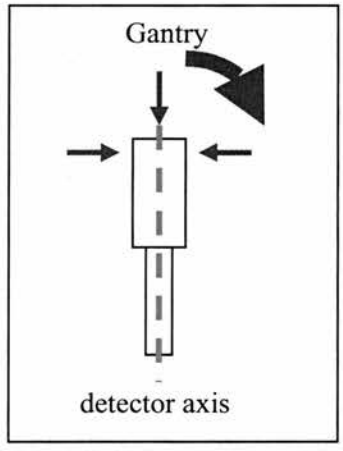

Figure 9.4. Direction of detector directional dependence, as defined in this work

The centre of the measurement volume was placed at position B, the couch rotated to 90° and measurements made in static beams at 10° intervals from gantry 0 to 180°. The response at each angle was normalised to that at the calibration geometry for each detector. The diode was then turned through 90° and the measurements repeated, to compare the results over two axes. Measurements of directional dependence beyond 0 and 180° gantry limits would require the use of a spherical phantom and would only be necessary if inferior arcs were used in treatment planning. To avoid the potential for gantry-couch collision, inferior arcs are not used in the ECC. As a result, these gantry angles were not measured.

Exposures

For both symmetry and directional dependence, exposures of 100MU were used for all detectors other than the SFD. The small signal on the SFD resulted in poor resolution on the electrometer reading and this necessitated the use of exposures of 500MU.

Correction factors

Correction Factors (CFs) were calculated as the inverse of the directional dependence. An effective angle (γ) was calculated from each combination of gantry (θ) and floor (α) angle:

$$\gamma = \theta \sin \alpha \qquad (9.1)$$

A curve was fitted to a plot of CF against effective angle, using Origin version 6 (Microcal Software Inc, MA, USA). CFs were then integrated over the appropriate gantry arc at each floor angle, to obtain one average CF for each beam. It is important to note that measurement of the directional dependence includes the effects of asymmetry and averaging the results over all axes increases the uncertainty.

Calibration

Each detector was calibrated against the 0.125cc IC following the procedures outlined in the IPSM Code of Practice (IPSM, 1990) and using factors traceable to the UK Primary Standards (NPL). Although the standard calibration conditions used in this department are fixed FSD, all detectors were calibrated under isocentric conditions to match the set-up used in the measurement of the relative output factors. The reference conditions were:

* $100 \times 100 mm^2$ field size
* 50mm deep
* 1000mm FAD
* water equivalent phantom (WT1)

A CAL factor was then obtained for each detector:

$$CAL = \frac{R(IC) \times Recombination \times TP \times Fx}{R(detector)} \qquad (9.2)$$

where R(IC) is the reading on the electrometer for the 0.125cc IC and R(detector) is the reading on the appropriate electrometer for each detector. Fx is the traceable calibration factor for the 0.125cc IC and electrometer combination (x), to convert the reading to dose in water, at the appropriate beam quality. TP is the temperature and pressure correction applied to the IC reading. CAL factors were also measured in a 50x50mm^2 field to investigate conditions nearer the stereotactic situation. This was to determine whether the Fx factor was still appropriate for use in fields <50x50mm^2, where the scatter conditions and beam spectrums are different.

XKnife data

The final beam data described in Chapters 4 (OARs), 5 (S_{cp}) and 8 (TMRs) were entered into the XKnife TPS and used to calculate the dose and distribution for each plan on the 600CD.

Calculation of dose

Equation 9.3 described the calculated, or planned dose to the isocentre (D_c) on XKnife:

$$D_c = MU \times TMR(d_{av}, s) \times S_{cp} \times M \qquad (9.3)$$

where MU is the number of MU delivered per beam and TMR(d_{av}, s) is the TMR at a mean depth of d_{av} averaged over the entire arc. S_{cp} is the relative output factor for the field size s at the isocentre and M is the factor to convert the FAD situation to the beam calibration FSD conditions. It is calculated geometrically from the ISL as 1.03.

Measured dose

The measured dose (D_m) for each detector was obtained from:

$$D_m = R \times CAL \times CF(\gamma) \times OP \ (\times TP) \qquad (9.4)$$

where R is again the reading on the electrometer, CAL is the calibration factor to convert each detector reading to dose and CF(γ) is the correction factor to account for directional dependence at the effective gantry angle γ. OP is the routine output correction for the machine on the day of measurement and the TP correction is applied only to the IC measurements.

Single arcs

Single field rotations at position A were planned with the couch at 0° for gantry rotations of 20° to 120° and 240° to 340°. The dose to the isocentre for each arc was calculated for 200MU. These single arcs were used to verify the methodology before proceeding to full treatment plans.

Plans

The general approach in the ECC is to use 4-5 arcs for a patient's treatment, selected to avoid sensitive structures and shape the dose distribution. A plan for each collimator size was designed to include a variety of typical arcs and couch positions. The isocentre was positioned at B, the centre of the hemispherical region, to obtain arcs of equal depth. MUs were calculated to give 17.5Gy to the 90% dose region, which is the prescription used in the ECC for the single fraction treatment of arterio-venous malformations (AVMs). The plan parameters are shown in Table 9.2.

Plans at position B							
Beam	Couch	Gantry start	Gantry end	mean depth/mm	Dose per arc /cGy	40mm MU	12.5mm MU
1	15	20	120	80	648.1	848	972
2	345	240	340	80	648.1	848	972
3	60	50	90	80	259.3	339	388
4	300	240	300	80	388.9	509	584

Table 9.2. Plan parameters for a typical stereotactic plans at position B.

To test the validity of the method for isocentres of different depths, plans were also calculated at position C, the off axis position. The plan parameters for this position are shown in Table 9.3.

Plans at position C							
Beam	Couch	Gantry start	Gantry end	mean depth/mm	Dose per arc /cGy	40mm MU	12.5mm MU
1	15	20	120	65.5	648.1	793	901
2	345	240	340	41	648.1	717	797
3	60	50	90	42.6	259.3	288	321
4	300	240	300	35.4	388.9	421	465

Table 9.3. Plan parameters for a typical stereotactic plan at position C.

An example of the plan at position B, for the 12.5mm diameter collimator is shown in Appendix 5.

Uncertainties

In all experiments, measurements were carried out on at least three separate occasions. The mean, standard deviation (s.d.) and coefficient of variation were calculated. The uncertainties in the calculated dose were calculated from the beam and image data input to the planning system. The uncertainties in the measured dose were calculated from the uncertainties in the electrometer reading, detector calibration, calculation of correction factors and phantom and detector positional uncertainties. In each case, the overall uncertainty (1s.d.) was calculated as the square root of the summed squares of all constituent parts.

9.3 Results & Discussion

9.3.1 Radiation isocentre

The lasers were found to match the mean position of the radiation isocentre to within a sphere of diameter 1.5mm +/-0.2mm. The maximum difference was caused by gantry sag between 0 and 180^0. As no treatments are ever delivered through gantry 180^o due to the higher density impression and mounting materials at the posterior side of the frame, the actual drift per arc is much smaller. The mean position of the radiation isocentre was calculated for each arc individually and the maximum drift from the start angle to the end angle calculated to be <1.0mm i.e. the positional uncertainty on each arc was +/-0.5mm. In terms of TMR, this constitutes an uncertainty of only +/-0.2 TMR (+/-0.3% of local TMR).

9.3.2 Detector properties

Symmetry

The measured symmetry of each detector is shown in Figure 9.5.

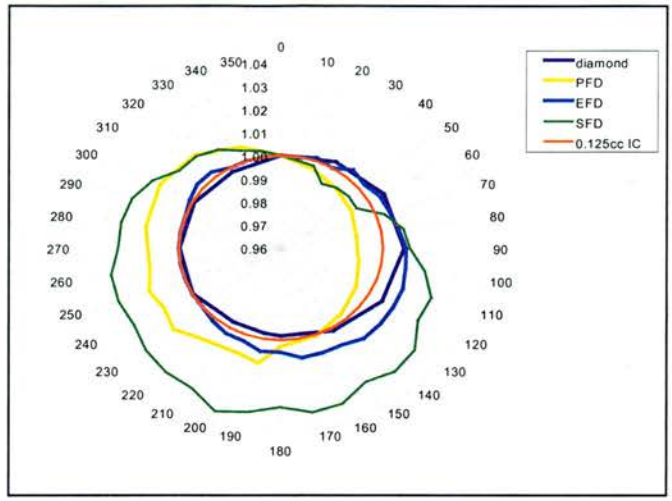

Figure 9.5. Graph of symmetry against gantry angle (couch 0°), for each detector. Values normalised to the response at gantry 0°.

All detectors, other than the ion chamber, exhibit some degree of asymmetry. The maximum variation in ion chamber readings was 0.2%, with a reproducibility of +/-0.2%. This suggests that the construction and geometry of the phantom and set-up is symmetrical and that there are no significant fluctuations in dose with gantry angle. The diamond and the EFD show asymmetry of up to approximately 1% and the PFD and the SFD up to 1.5% and 3.5% respectively. The reproducibility of each detector was 0.2%, other than the SFD, which was 2%. Agreement between measurements with the detector in a fixed position (gantry rotated) and with the detector rotated (fixed gantry angle) showed that detector asymmetry alone was responsible for the results. This confirmed the observations above on phantom and linac uncertainties.

It is interesting to note that there is a line of approximate symmetry for each detector. To minimise the above problem in all further experiments, each detector was rotated around its axis to align the line of symmetry with the beam CAX at gantry 0°. Unfortunately, accurate rotation is physically quite difficult as each detector cable tends to pull in a particular direction.

For solid state detectors, the effective centre of the measurement volume is usually assumed to lie on the CAX of the detector. The results in Figure 9.5 clearly show that this is not the case. Small amounts of asymmetry displayed by the EFD, PFD and diamond are not significant for measurements in routine x-ray beams, but may present problems when trying to align the centre of the detector with the centre of a small beam. This may affect the

measurement of OARs and PDDs in very small fields. However, according to the manufacturers, the results are not surprising. In the case of the EFD, the materials surrounding the chip may not be uniform and the chip itself may not lie at the exact centre of the encapsulation. In addition, there are electrical connections and other design features which are not cylindrically symmetric. The same is true of the PFD but with the additional problem that the high density material used for energy compensation may not be spatially uniform. The larger asymmetry displayed by the SFD is due to the difficulties of placing the very small chip, perfectly horizontally, in the centre of the diode casing and the relatively larger effects of connectors and wires etc. The fact that the SFD measurements are the least reproducible may in part be due to the small signal and also because small differences in position between measurement sessions will lead to greater differences in symmetry. Diamonds are naturally grown and therefore unlikely to be symmetrical. In addition, Westermark et al (2000) found that the two electrodes attached to the diamond crystal, were of different thicknesses, which may also account for some asymmetry.

The percentage asymmetry for each detector was converted to a percentage change in TMR and then to a depth in water. The possible shifts in the effective point of measurements away from the geometric centres were calculated to be 1.2mm (EFD), 2.7mm (PFD), 1.1mm (diamond) and 4.2mm (SFD). However, the true shifts will typically be less than these values because the asymmetry in response is also due to the inhomogeneities of construction described above, as must obviously be the case for the SFD as the shift is comparable with the detector size.

When the detector was moved by 0.5 and 1mm in the superior-inferior direction (using the spacer), in the 40mm collimator, there was no change in signal. However, in the 12.5mm collimator, the signal increased when the detector was move inferiorly by 1mm, by less than 1% at gantry 0° and almost 2% at gantry 180°. This indicates that the effective point of measurement was not in fact placed at the radiation isocentre. This was due to the use of an average radiation isocentre position and will cause more of a problem in the small collimator because of the sharp fall off in dose.

Directional dependence

Figure 9.6 shows the directional dependence of each detector, averaged across the two main axes and averaged across both sides of the CAX in order to minimise the effect of asymmetry. All values were normalised to the response at the calibration orientation for

each detector. For an ion chamber, this was gantry 0° and for all other detectors this was gantry 90°.

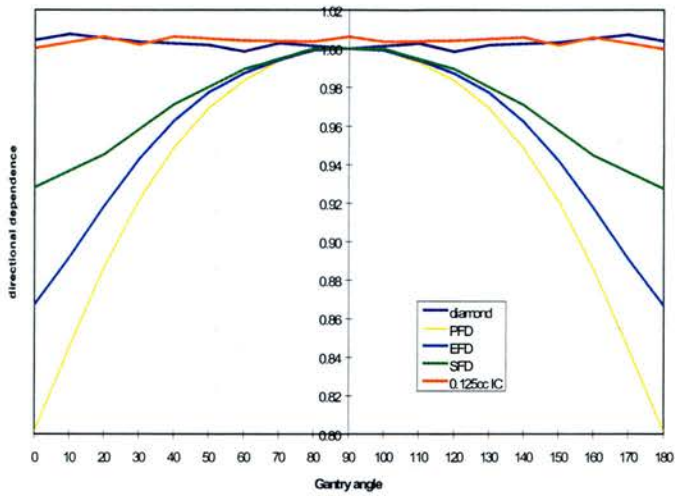

Figure 9.6. Graph of directional dependence against gantry angle for couch at 90° and gantry between 0 and 180°. Values normalised to the response at the calibration orientation for each detector.

The results for the PFD, EFD and SFD follow a parabolic shape with minimum responses of 80, 87 and 93% respectively at gantry 0° and 180°. The reproducibility is better than 0.5% for the EFD, and the measurements across the two axes are the same. The reproducibility of the PFD is also within 0.5%, but with a maximum difference between axes of +/-2%. The reproducibility of the SFD measurements is 0.2%, with a maximum difference between axes of +3% to -1%. In addition, there is a maximum of 2% difference between each half of the curve (0 to 90° and 90 to 180°).

Directional dependence is an inherent property of diodes. Rikner and Grusell (1985) measured the maximum directional dependence at 85 and 95% for the PFD and EFD respectively, at 50mm deep in an 8MV narrow beam. However, the directional dependence measured above in this work, is larger than that measured by Rickner and Grusell. This could be due to the difference in depth of measurement.

The difference in directional dependence across the two axes for each of the diodes, is caused mainly by the asymmetry, which will contribute to the measured response at each gantry angle. The magnitude of the differences above approximately agree with the values of asymmetry at the corresponding positions. Small inconsistencies are due to the different set-ups for the measurement of the two parameters as symmetry is measured at position A and directional dependence at position B. The asymmetry in directional dependence will

lead to uncertainties in the CFs, which are based on average values of directional dependence.

The diamond exhibits a small amount of directional dependence whereby the response increases by 1% when it is irradiated with its long axis perpendicular to the beam. This is probably due to the non-symmetrical and non-uniform shape of the diamond crystal. The 0.125cc IC also has an increase in response of around 1% when irradiated with its long axis parallel to the beam, possibly due to the shift in the effective point of measurement from one orientation to the other. The reproducibility is better than 0.5% for both detectors and the measurements across the two axes are the same.

As the directional dependence for the diodes follows a parabolic shape, and the ion chamber and diamond are approximately linear, the expected values for any combination of couch and gantry angle can be predicted. However averaging the results for the SFD will lead to much larger uncertainties than for the other detectors, due to the large degree of asymmetry. Although it would be more appropriate to calculate CFs in 3D for the SF, this is an unnecessary complication unless the other detectors prove to be unsuitable. For this reason, the SFD was not used in any dose measurements in the phantom.

Correction factors

Correction factors to account for the directional response of each detector were calculated as the inverse of the Origin fits to the above data., for each effective angle. The difference between the Origin fitted values and the mean measured values was less than 0.3% for each detector. An average CF was calculated by integrating over all effective angles, for each arc. An example of the CFs calculated for the EFD for couch and gantry angles between 0 and 90^{o} is shown in Appendix 6.

Calibration factors

Table 9.4 shows CAL values averaged over five sets of measurements for each detector calibrated against the IC in both a $100x100mm^2$ field and a $50x50mm^2$ field.

detector	CAL factors 100x100mm^2	coeff. of var.	50x50mm^2	coeff. of var.	50x50mm^2 c.f. 100x100mm^2
Diamond	0.0926	0.4	0.0928	0.4	0.3
PFD	0.0243	0.5	0.0242	0.5	-0.2
EFD	0.0368	0.6	0.0369	0.5	0.4
SFD	0.3968	0.2	0.4017	0.2	1.2
0.125cc IC	1.0000	-	1.0000	-	0.0

Table 9.4 Comparison of calibration factors (CAL values) for each detector in a small (50x50mm^2) and a large (100x100mm^2) field.

The precision, as indicated by the coefficient of variation, is approximately 0.5%. Column six shows the differences between the calibration in the 50x50mm^2 field and the 100x100mm^2 field, which are all within the experimental uncertainties for each detector, other than for the SFD. The SFD has a significantly higher calibration factor in the 50x50mm^2 field, which suggests that the over-response of an unshielded diode due to the larger scatter in the 100x100mm^2 field is greater for the SFD than for the EFD. This over-response was also shown in chapter 5 and indicates that the SFD is unsuitable for measurements in large fields. The reason for the over-response may be due to the relatively larger effect of connectors (probably high density) and other materials, relative to the small size of the detector. The agreement between the calibration factors for each detector relative to the 0.125cc IC in both field sizes suggests that if the changes in beam spectrum in the small field affect the correction factors to convert reading to dose, they are independent of the detector used. However, this does not prove that the same is true in very small fields.

The CAL factors for the diodes in Table 9.4 were between 10 and 20% lower than those measured two months previously. During that period, the PFD and EFD had been subject to a cumulative dose of approximately 200Gy and the SFD to approximately 1000Gy, which must have decreased their responses. However, the cumulative doses to the PFD and EFD are less than the recommended re-calibration limits (1000Gy) for patient diodes and the percentage decrease in calibration is much higher than the 0.5% expected (Essers and Mijnheer, 1999). As a result, CAL values were measured for each detector against the IC, in a 50x50mm^2 field, on a regular basis.

9.3.3 Uncertainties

Position

Positioning uncertainties in the verification process are comparable with the treatment process. For example, errors introduced by the CT slice thickness can lead to uncertainties of position of +/- 1mm (Yeung et al 1993). Although the treatment process includes errors introduced by the patient, phantom measurements introduce other uncertainties. The absolute depth of the effective point has uncertainty associated with it, quoted as +/-0.15mm for the diode. In addition, each sleeve is drilled with an uncertainty of approximately +/- 0.1 mm. These uncertainties were minimised during the symmetry and directional dependence measurements by finding the position of the maximum signal, which implies coincidence between the effective point and the radiation isocentre.

Calculated dose

The overall uncertainty in the calculated dose is a result of the uncertainties in the TMR, S_{cp} and absolute calibration of the MU chamber, in addition to uncertainties in the imaging data. The calculation is described in Appendix 7 and the total uncertainty in D_c calculated to be +/-0.9% (1 s.d.), for all collimators between 40 and 12.5mm diameter.

Measured dose

The uncertainty in the measured dose is detector dependent and is due to the uncertainty in each of the parameters in equation 9.4 and the positional uncertainties. The calculations are shown in Appendix 7 and the results for each detector listed in Table 9.5.

Detector	% uncertainty in D_m (1 s.d.)
Diamond	0.7
PFD	1.2
EFD	0.6
0.125cc IC	0.6

Table 9.5. Overall uncertainty in the measured dose (D_m) for each detector. Complete calculations are shown in Appendix 7.

The largest uncertainty is associated with the PFD, due primarily to the larger asymmetry.

9.3.4 Dose measurements in single arcs

Radiation isocentre

The coincidence of the mean radiation isocentre with the effective point of measurement was tested by comparing measurements in the 12.5mm collimator with and without a selection of small spacers. As the signal was maximised when the 1mm spacer was inserted, this was included in each of the following measurements.

40mm collimator

Table 9.6 shows the results for rotations at position A (40mm collimator) for all detectors other than the SFD.

	Rotations at position A: 40mm collimator							
		20° to 120°			240° to 340°			
Detector	D_c cGy	D_{m1} cGy	coeff. of var.	diff c.f. D_c (%)	D_{m2} cGy	coeff. of var.	diff c.f. D_c (%)	diff c.f. D_{m1} (%)
Diamond	152.8	154.5	0.4	1.1	152.8	0.1	0.0	-1.1
PFD	152.8	151.6	0.3	-0.8	154.5	0.2	1.1	1.9
EFD	152.8	153.3	0.3	0.3	152.5	0.5	-0.2	-0.5
0.125cc IC	152.8	153.1	0.2	0.2	152.6	0.3	-0.2	-0.3

Table 9.6. Comparison of the measured dose (D_{m1}, D_{m2}) against the calculated dose (D_c) for single arcs at position A, with a 40mm collimator.

The reproducibility of all measurements is within 0.5%. The difference between the calculated dose (D_c) and the measured dose (D_m) is between -0.8 and 1.1%, the largest differences being for the PFD and diamond. There are differences between measurements at one side of the phantom (D_{m1}) compared with the other (D_{m2}). These are =< 0.5% for the EFD and 0.125cc IC, 1.1% for the diamond and 1.9% for the PFD. These values are consistent with the measured asymmetry of each detector, which was averaged over the CAX in the calculation of the correction factors for the directional response.

12.5mm collimator

The results in the 12.5mm collimator for all detectors other than the SFD and 0.125cc IC are shown in Table 9.7.

	Rotations at position A: 12.5mm collimator							
		20° to 120°			240° to 340°			
Detector	D_c cGy	D_{m1} cGy	coeff. of var.	diff c.f. D_c (%)	D_{m2} cGy	coeff. of var.	diff c.f. D_c (%)	diff c.f. D_{m1} (%)
Diamond	133.2	134.7	0.3	1.1	133.9	0.2	0.6	-0.6
PFD	133.2	134.7	0.5	1.1	137.3	0.3	3.1	1.9
EFD	133.2	134.4	0.3	0.9	133.6	0.4	0.3	-0.5

Table 9.7. Comparison of the measured dose (D_{m1}, D_{m2}) against the calculated dose (D_c) for single arcs at position A, with a 12.5mm collimator.

The reproducibility of all measurements is again within 0.5%. The difference between the calculated dose (D_c) and the measured dose (D_m) is between 0.3 and 3.1%, the largest differences being for the PFD. Again there are differences between measurements at one side of the phantom (D_{m1}) compared with the other (D_{m2}), of the order of 0.5% for the diamond and EFD and 1.9% for the PFD. These values are again consistent with the measured asymmetry of each detector.

Summary

The differences between the expected and measured doses for these single fields give some indication of the errors introduced both by calculating the CF(γ) only at each increment of 10° gantry rotational fields and by averaging the directional dependence over the two axes. The 0.125cc IC is the only symmetrical detector and the consistent difference of -0.3% from one side is an indication of asymmetry in the set-up of the phantom, or in the phantom itself, which was not apparent in the measurements of asymmetry.

9.3.5 Dose measurements in plans at position B

40mm collimator

The values of D_c for the plan at position B are shown in Table 9.2 as the dose per arc in cGy. Table 9.8 shows D_c again and the difference between D_m and D_c for each arc and for the total dose to the isocentre, for the 40mm diameter collimator.

		Plans at position B: 40mm collimator (D_m cf D_c)							
		Diamond		PFD		EFD		0.125cc IC	
Beam	D_c /cGy	Diff. (%)	coeff. of var.	Diff. (%)	coeff. of var.	Diff. (%)	coeff. of var.	Diff. (%)	coeff. of var.
1	648.1	0.3	0.6	-3.3	0.4	-0.6	0.9	-0.1	0.4
2	648.1	-0.7	0.9	-2.2	0.5	-1.4	1.0	-0.4	0.4
3	259.3	0.2	0.3	-1.8	0.7	0.0	0.7	0.4	0.4
4	388.9	-0.2	0.3	-1.8	0.7	-0.4	0.9	-0.2	0.2
Total	1944.4	-0.2	0.0	-2.4	0.5	-0.8	0.9	-0.1	0.3

Table 9.8. Comparison of the difference between the measured dose and the calculated dose for plans at position B, with the 40mm collimator.

The reproducibility (coefficient of variation) is better than 1% for each set of measurements. The most reproducible results are for the 0.125cc IC, probably because its symmetry ensures that small rotational uncertainties have no effect. The differences between D_c and D_m for the total dose to the isocentre are within 0.9% for all detectors, other than the PFD, which is too low by 2.4%. The differences between D_c and D_m for each individual arc are within 0.4% for the 0.125cc IC and 0.7% for the diamond. Agreement is good for the EFD in all but one of the beams, which is 1.4% lower that the calculated value. The differences are largest for the PFD, particularly at couch and gantry angles with the largest correction factors. At these positions, the curve describing the directional dependence is the steepest and therefore averaging the CF over the entire arc becomes less precise.

12.5mm collimator

Table 9.9 shows the difference between D_m and D_c for each arc and for the total dose to the isocentre, for plans at position B, with the 12.5mm diameter collimator.

		Plans at position B: 12.5mm collimator(D_m cf D_c)					
		Diamond		PFD		EFD	
Beam	D_c /cGy	Diff. (%)	coeff. of var.	Diff. (%)	coeff. of var.	Diff. (%)	coeff. of var.
1	648.1	0.2	0.3	-2.3	0.9	-0.7	0.7
2	648.1	0.1	0.2	-0.6	0.3	-1.2	0.9
3	259.3	0.1	0.3	-0.2	0.5	0.7	0.8
4	388.9	0.1	0.3	0.7	0.6	0.7	0.6
Total	1944.4	0.1	0.3	-0.9	0.5	-0.4	0.8

Table 9.9. Comparison of the difference between the measured dose and the calculated dose for plans at position B, with the 12.5mm collimator.

The reproducibility is again better than 1% for each set of measurements. The results for the EFD and the diamond are comparable with those for the 40mm collimator, which suggests that each detector has been positioned accurately within the 12.5mm collimator. The diamond shows the smallest differences between D_c and D_m. The PFD again shows the largest differences although the results for individual beams appear to be slightly better than for the 40mm collimator. However, for both collimators, the PFD is consistently low, which suggests a systematic error. Although this could be investigated further, it is unnecessary when the EFD can be used to obtain accurate and reproducible results to within 0.9% and the diamond can be used to obtain accurate and reproducible results to within 0.3%, in both cases for each individual beam and the total dose to the isocentre.

9.3.6 Dose measurements in plans at position C

40mm collimator

Table 9.10 shows the difference between D_m and D_c for each arc and for the total dose to the isocentre, for a plan with the 40mm collimator at position C. Only one single measurement has been made at this position to date, simply to verify that variations in depth and isocentre position do not affect the results and therefore no coefficients of variation are presented.

	Plans at position C: 40mm collimator(D_m cf D_c)			
Beam	Diamond	PFD	EFD	0.125cc IC
1	-0.4	-2.2	-0.8	-0.4
2	-0.6	-2.2	-0.7	-0.2
3	0.2	0.5	1.6	1.0
4	-0.3	0.2	0.4	-0.2
Total	-0.4	-1.4	-0.2	-0.1

Table 9.10. Comparison of the difference between the measured dose and the calculated dose for plans at position C, with a 40mm collimator.

These results are comparable with those at position B in the 40mm collimator. The diamond and the 0.125cc IC show the best results. The maximum differences are 0.6% for the diamond and 1.0% for the 0.125cc IC. All differences are =<1.6% for the EFD and =<2.2% for the PFD.

12.5mm collimator

Table 9.11. shows the difference between D_m and D_c for each arc and for the total dose to the isocentre, for the 12.5mm diameter collimator at position C.

	Plans at position C: 12.5mm collimator(D_m cf D_c)		
Beam	Diamond	PFD	EFD
1	-1.1	-2.1	-1.3
2	-1.1	-2.1	-1.0
3	-0.3	1.5	1.8
4	-1.3	1.3	0.4
Total	-1.0	-0.9	-0.5

Table 9.11 Comparison of the difference between the measured dose and the calculated dose for plans at position C, with a 12.5mm diameter collimator.

The 12.5mm collimator results for the PFD and the EFD are comparable, but for the diamond they are slightly higher. This may be because of positioning uncertainties. However, the results confirm that the method can be applied to plans at other positions within the available channels in the phantom.

9.3.7 Quality Assurance

The above verification technique has been incorporated into the quality assurance programme at the ECC and is carried out on an annual basis. For each check, the phantom is CT scanned and the images are transferred to XKnife where a typical plan is created for one collimator (a different collimator is selected on each occasion). For collimators >=32.5mm, the IC is used and for all other collimators, the diamond. Its calibration is verified against the IC at each measurement session. If the measured dose per beam differs from the calculated dose by >2%, all stereotactic treatments are stopped until the differences are resolved. If the differences are between 1 and 2% then further investigations should be carried out, but stereotactic treatments can continue. However, neither of these situations has ever arisen.

9.4 Conclusion

A simple, reproducible method of verifying the dose to the isocentre in two typical stereotactic plans, for a large (40mm) and a small (12.5mm) collimator has been developed. The symmetry and directional dependence of response for a range of detectors was investigated and correction factors calculated to account for them. The stability of response for each detector was investigated over time and the recommendation made that diodes should be calibrated on a regular basis, in a 50x50mm^2 field to be closer to the stereotactic situation.

The 0.125cc IC was found to be appropriate for use in collimators down to 32.5mm diameter. In all collimators, the diamond was within 1.3% and the EFD within 1.8%. Either of these detectors can therefore be used to verify the dose to the isocentre to within 2%. However, the simplest detector to use, is the diamond as it requires a minimum correction for directional dependence and is much more stable over time compared with a diode. However, in the absence of a diamond, an EFD, or even a PFD could be used to verify the dose to the isocentre in all collimators between 40 and 12.5mm diameter, if the detectors are calibrated appropriately and account is taken of the directional dependence. The asymmetry of the stereotactic diode and the fact that it underestimates the dose in a $50x50mm^2$ field make it unsuitable for this type of work.

It is important to note that the verification of the accuracy of the calculated dose does not necessarily confirm the delivered dose. The calculated dose is itself dependent on the input measured data and if both the input data and the verification technique are flawed in exactly the same way, a false positive could be obtained. This would mean that the verification process could confirm that the measured dose matched the calculated dose when in fact the delivered dose was still incorrect.

Most of the beam data sets in Chapters 4-8 were measured with the EFD. The measured dose to the isocentre has been confirmed with the EFD, which shows internal consistency, but does not confirm that the delivered dose is correct. However, the fact that the dose to the isocentre has also been confirmed with the diamond and the PFD, in all collimators, and the ion chamber in the larger collimator does suggest that both the measured data and the verification process are correct. It is good practice therefore to verify the dose to the isocentre with a different detector from the one used to measure the data.

The verification technique is simple, inexpensive and time-effective and has been incorporated into the departmental quality assurance programme. The verification of the dose to the isocentre with several different detectors validates the final data sets obtained in each of the previous chapters. The author has proposed this technique as the basis for an audit of all stereotactic facilities in the UK.

Chapter 10

Conclusion

10.1 Small field problems

The analysis of the absolute and relative dosimetry of small x-ray beams is not straightforward. The interpretation of the data within different sets of measurements requires a thorough knowledge of the specific beam and detector properties. Beam properties which are unique to the small field situation are the lack of electronic equilibrium (at 6MV, fields <30mm width), the lack of scatter outside the field, the steep fall off in dose within the penumbra region (fields defined by stereotactic collimators), the changes in beam spectrum, both in-air and in-phantom and the changes in head scatter.

Although it is obvious that the measurement of dose within a small field requires the use of a small detector, the unique beam properties outlined above may have an effect on the response of that small detector. For relative dose measurements in more conventional field sizes (400 to 40mm width), it is generally assumed that the correction factors required to convert a detector reading to dose are the same in the field size of interest and in the reference field. A ratio of detector readings can therefore be substituted for the ratio of doses, assuming that the effective point of measurement of the detector is accounted for. However, in small fields this may not be the case. For example, LEE may be preserved in the normalisation field of 40mm width, but not in a width of 20mm or less. In addition, photon scatter is a smaller proportion of the total dose in the smaller field. As a result, the detector response may not be the same in both situations. The composition of a small detector may also have an effect on its response in the small field, which is not apparent in a more conventional field size. This may be the case for the sensitive detector material, but also for the larger relative effect of connecting wires etc and of the detector housing. Again this may be particularly significant in regions of electronic disequilibrium.

In short, it is difficult to determine whether a set of relative detector measurements in small fields is a reflection of the true change in relative dose for a particular situation, or is a reflection of the properties of the detector used. Throughout this work it has become apparent that the only way to accurately determine the true change in relative dose may be

through modelling of both the beam and the detector. However, it is important to distinguish between problems which affect the sizes of fields used clinically within a department and those which affect field sizes which, to be used clinically, would require a greater degree of sophistication in terms of the overall accuracy of the system.

Within the ECC, clinical treatments with small fields are limited to stereotactic collimators within the range of 40-12.5mm diameter. These field sizes are fairly typical of the ranges commonly used in centres employing the stereotactic technique in the UK and smaller fields are only used on the Gamma Knife units. The question then remains as to how the dose can be measured with acceptable accuracy within these field sizes. In particular, it is necessary to know whether a single detector could be used for all measurements, or whether several should be compared. If the latter is the case, then it is important to know which types of detectors are the most useful and whether it is necessary to purchase one that has been designed specifically for stereotactic use. In addition, it is also important to determine the best experimental method for each measurement set, in terms of accuracy and precision primarily, but also of simplicity. This work has been an attempt to address these questions and point to the way ahead for measurements in small beams.

10.2 Appropriate detectors and methods

10.2.1 Clinical range 40-12.5mm diameter

Overview

Several types of detectors were compared in the measurement of PDDs, TMRs, OARs, S_{cp}, S_c and S_p, in addition to an investigation of the measurement of the dose to the isocentre. The types of more commonly available detectors which were compared were a shielded (PFD) and unshielded (EFD) diode, a 0.125cc cylindrical IC (0.125cc IC), a Markus parallel-plate IC (PP-IC) and film. Three new detectors were also investigated. No results had previously been published (prior to McKerracher and Thwaites, 1999) for measurements with a small (0.6mm sensitive width) unshielded diode (SFD) and a PinPoint 0.015cc cylindrical IC. Although there were published results for the use of a diamond, the literature was somewhat limited on its use in small fields.

PDDs

PDDs measured with all relevant detectors were within a range of <2% local dose at 100mm deep (normalisation to dmax) in the largest (40mm) collimator. However PDDs measured

with the PFD were slightly higher than those measured with the other detectors. This effect increased as the field size decreased and was thought to be due to too much absorption in the tungsten shielding at dmax. PDDs measured with the ICs agreed with the other detectors in the largest collimator, but became higher than the other detectors as the field size decreased, due to the partial volume effect. As a result, the unshielded diodes were selected as the most appropriate detectors with which to measure PDDs in the field size range of 40-12.5mm diameter. The EFD was found to be more suitable than the SFD due to its high signal to noise ratio compared with the SFD. Although the diamond may also be suitable, the design of the M connector makes it more difficult to set up in a BDAS system, unless a suitable cable holder is made.

An accurate experimental set-up for the measurement of PDDs requires that they are measured using a BDAS scanning system. Beam profiles should be scanned at at least two depths and the effective centre of the detector sensitive volume aligned with the beam CAX determined as midway between the 50% dose levels, before commencing PDD measurements. The reference signal should be taken directly from the linac MU chamber, or the reference detector placed above the stereotactic collimators (if used).

OARs

The effects of volume averaging can be exhibited most clearly in the measurement of profiles. For measurements in circular fields the effect is enhanced due to averaging in two dimensions; across the sharp dose gradient at the edge of the beam and across the shape of the circular field. Although the detector size can be extrapolated to zero and the profile shape corrected, this method is time consuming and requires several small detectors of the same type, but with different internal diameters. If possible, the use of a smaller detector is preferred to eliminate the need for these corrections.

OARs measured with the 0.125 and 0.015cc ICs exhibited the effects of volume averaging and produced peunumbras which were too wide. However, all diodes and film were found to be in agreement over the collimator range of 40-12.5mm diameter. As the sensitive width of the detectors ranged from 2.5mm to 0.6mm, it was concluded that volume averaging for the sizes of diodes used was not a significant problem within this field size range. The SFD did however measure a slightly sharper profile in the 12.5mm diameter collimator and the width of the 90% region was found to be 0.3mm greater than that measured with the other detectors. However, it was not apparent whether the SFD was measuring a truer profile due to its smaller size, or whether it was over-sharpening the profile due to the effect that silicon

has on the LEE. Although it might be thought that the larger diodes (more silicon) should increase the amount of over-sharpening, it has been suggested (Beddar et al 1994) that the effect is counter-balanced by the effect of volume averaging. The validity of the sharper profile could be determined simply by film measurements if the film resolution could be improved without increasing the noise. Although this should be possible, the 1mm maximum resolution was a feature of the limitations of the scanning densitometer. Methods of improving this are currently being examined within the ECC.

In summary, a PFD, EFD, SFD and film could be used in all collimators, but with a small uncertainty (<0.3mm) in the 12.5mm diameter collimator. The experimental set-up was simplest for film used in slabs of solid water. Profiles were measured with the diodes using a BDAS scanning system. Profiles should be scanned along both axes several times until the effective centre of the detector is coincident with the centre of the 50% dose regions, to within +/-0.2mm. This was the accuracy of the BDAS system in use at the time. The reference signal should be obtained in the same manner as for PDDs.

S_{cp}

S_{cp} was measured most easily in a solid water phantom. However, the geometric centre of the detector should be placed at the beam CAX. Steps should therefore be taken to determine the position of the radiation isocentre with respect to the crosswires or the lasers. Although this assumes that the centre of the sensitive volume is aligned with the centre of the detector, the positional misalignment does not appear to have had any significant effect within the field size range of 40-12.5mm diameter. Measurements of S_{cp} in small fields should be normalised to an appropriate intermediate field, such as a 50x50mm^2 or a 40mm diameter collimator. Normalisation to the reference field (100x100mm^2) should be carried out separately with a detector such as an IC, PFD or diamond.

The effect of volume averaging within the clinical field size range was also minimal at approximately 0.5% for the diamond and larger diodes. However, volume averaging should still be accounted for by integrating over the detector shape. The agreement in S_{cp} values to within 0.6% in a 12.5mm collimator, for the diamond, EFD and SFD showed that the alignment was satisfactory and that volume averaging almost entirely accounted for differences between detectors. Values of S_{cp} measured with the PFD were approximately 1% higher than those measured with the other detectors and this was thought to be due to the over-absorption of scatter in the tungsten shielding, which would predominantly affect measurements in the normalisation field. The two unshielded diodes were approximately

0.6% higher than the diamond and it is not apparent whether the diode S_{cp} were higher as a result of the (small) effect of the silicon or the diamond S_{cp} were lower due to mispositioning of the diamond or innaccurate volume averaging over its shape. This difference could only be resolved through modelling. However, within the 40-12.5mm field size range, it is reasonable to assume that any of the above detectors could be used to measure S_{cp}.

S_c

It was shown that S_c could be measured simply, reproducibly and accurately under conditions of electronic disequilibrium using a small build-up top of water-equivalent material, equal in diameter to that of the detector housing. The agreement in S_c values measured with the diamond, PFD, EFD and SFD was 0.3% in the 12.5mm diameter collimator, when volume averaging was taken into account. This showed that differences between detectors were minimised in the measurement of S_c. This was probably due to the lack of phantom scatter which would otherwise have led to differences in response between the detectors. Again, all measurements should be normalised initially to the appropriate intermediate field size and further normalisation to the reference field should only be carried out with any of the above detectors other than the SFD.

S_p

The accuracy of S_p data relies on the accuracy of the measured data for S_{cp} and S_c. S_p should, in theory, be independent of the beam defining system and the detector used, if all uncertainties in the measurement of S_{cp} and S_c cancel out. Although differences between S_p in each of the three beam defining systems were within the overall experimental uncertainty, there was a 2% spread in values of S_p over all detectors, in the 12.5mm diameter collimator. However, the spread was only 1% over the unshielded diodes and the diamond. S_p measured with the PFD was too high simply because S_{cp} measured with this detector was also too high. The spread over the other detectors was a reflection of the spread over the corresponding measurements of S_{cp} and S_c, for the reasons discussed above.

TMR

The measurement of TMR data is particularly problematic for small fields. Although software exists to measure TMRs directly in the tank, the small distance between the end of the stereotactic collimators and the isocentre (ECC = 230mm) makes this difficult and changing the collimators between measurements may actually require the whole tank to be

moved out the way. TMRs can be measured more simply in RMI but the method is time consuming if data in a full range of collimators, at all depths, is required.

TMRs can be calculated from PDDs and the ratio of S_p (dmax) values. However, these calculated TMRs are subject to the uncertainties in both data sets. However, it is good practice to both calculate TMRs and compare them with measurements in solid water. Although calculated and measured TMRs agreed within the experimental uncertainty, there did appear to be a systematic difference between the two methods, which was a maximum of +/-1% in the 12.5mm diameter collimator. The reason for this difference was not clear and further investigation is required.

Dose to the isocentre

The symmetry, directional response and calibration of the 0.125cc IC, diamond, PFD, EFD and SFD were all investigated with a view to using them to measure the dose delivered to the isocentre. The small signal on the SFD and its relatively large asymmetry excluded it from measurements of the dose to the isocentre. The directional dependence of the other detectors was accounted for with the use of correction factors. Each detector was calibrated against the 0.125cc IC in a $50x50mm^2$ field and the 0.125cc IC calibrated against a calibrated Farmer according to the IPSM code of practice.

A suitable phantom was designed to be attached to the GTC. The 0.125cc IC was found to be appropriate for use in the phantom to verify the dose to the isocentre in collimators down to 32.5mm diameter. In all collimators, the diamond was within 1.3% and the EFD within 1.8% of the calculated dose and therefore either of these detectors could be used to verify the dose to the isocentre to within 2%. The simplest detector to use was the diamond as it required a minimum correction for directional dependence and was much more stable over time compared with a diode. The use of the diamond to confirm the dose to the isocentre for data measured primarily with an EFD, suggests that both the measured data and the verification process were correct. It is good practice therefore to verify the dose to the isocentre with a different type of detector from the one used to measure the data. The verification technique is simple, inexpensive and time-efficient and has been incorporated into the departmental quality assurance programme.

10.2.2 Smaller fields

PDDs

In fields <12.5mm width, all the above measurement problems were enhanced. The comparison of extrapolated and measured PDDs produced some significant differences, the reasons for which were not completely resolved. Although it was apparent that a very small detector, such as the SFD was required to ensure that volume averaging did not cause the PDDs to be over-estimated at greater depths, positional difficulties could still have led to problems. Although alignment was very difficult in the smallest field size, a misalignment of the detector at dmax would have caused the PDDs to be too high. In fact, the PDDs measured with the SFD were lower than those extrapolated from the EFD. Either the EFD was misaligned in the 12.5mm diameter collimator, or the extrapolation technique is flawed in small field sizes. The latter is likely, particularly as it has been shown that there is a relatively larger shift in the dmax position towards the surface in very small fields, which would lead to inaccuracies in the extrapolation technique.

OARs

In the measurement of profiles, significant differences between detectors began to emerge in fields < 12.5mm. Although the SFD measured the sharpest profile, it was not clear whether this was a result of its smaller size in relation to the EFD and film, or was a result of the increase in LEE in silicon. This problem could be resolved by improving the resolution of film, or more precisely, through modelling. As the in-air and in-phantom profiles were different, both situations would have to be modelled separately.

S_{cp}

The EFD, SFD and diamond were found to be the most suitable detectors for the measurement of S_{cp} in fields between 40 and 12.5mm diameter. However, differences between the three detectors began to emerge in fields less than this. Volume averaging in the smallest fields was much more significant, particularly in the 5mm diameter collimators where the response of the EFD was calculated to be approximately 94.6%. Positioning was also much more important although repositioning of the SFD using the BDAS system increased S_{cp} by a maximum of 2% in the 5mm collimator. However, neither of these effects (volume averaging, detector mispositioning) could account for the >10% spread over all three detectors in the 5mm diameter collimator. The only way to accurately resolve these differences would be to model both the beam and the detector.

S_c

Differences between detectors also began to emerge in the measurement of S_c in fields <12.5mm diameter. Although differences in S_{cp} were only 0.3% in the 7.5mm diameter collimator, in the 5mm diameter collimator, the spread over all detectors was almost 20%. The SFD measured a drop in S_c of only 5% between the 40 and 5mm diameter collimators, whereas the diamond measured a drop of almost 25%. It was shown that a large drop in S_c was to be expected in the smallest stereotactic field due to the shielding of the aperture at the top of the primary collimator. However, the magnitude of this effect could only truly be investigated though modelling. Although the SFD might measure a value of S_c which is too high due to the preservation of LEE in silicon, the diamond value may be too low due to detector mispositioning or the use of a phantom (build-up top) which is too wide. Again, the reasons for these differences could only be resolved through modelling.

S_p

Differences in S_p measured with each detector increased below a 12.5mm diameter collimator. These were due to differences in the experimental situations for both S_{cp} and S_c, which did not cancel out, such as changes in beam spectrum, shielding of the aperture at the top of the primary collimator, the effect of LEE and the effect of the phantom width. For the PFD there was the additional problem of the absorption of too much phantom scatter in the normalisation field in the Scp measurements only. Once again, these effects can only be accounted for through modelling.

10.3 Conclusion

It would appear from the above, that other than a very small amount (0.5%) of volume averaging, no corrections are necessary for measurements in stereotactic collimators within the 40-12.5mm diameter range. The magnitude of the effects of volume averaging is dependent on the beam defining system and profile measurements are therefore required in each measurement situation. Measurements in all fields within this range can be accurately carried out using a selection of the above detectors, as appropriate. Measurements with the diamond using the BDAS system were not investigated due to the awkward design of the "M" connector, which makes it more difficult to position accurately within the water tank. However, BDAS measurements with the diodes proved to be satisfactory. The diamond did however offer an advantage in the verification of the dose to the isocentre and it is useful to have a small, near-tissue equivalent detector available to verify measurements carried out

predominantly with diodes. However, the manufacturers should review the design of the cable.

The SFD did not offer any advantages within the clinical field range and indeed was less useful than the conventional unshielded diode due to the very low signal. The 0.015cc PinPoint IC did not offer any advantages over the diodes as it was still too large for measurements within the full clinical field size range. Although corrections could have been applied to the data, this appears to be unnecessary when the diodes appeared to be satisfactory.

The differences between detectors and uncertainties in the measurements, increase in fields <12.5mm width. However the problems are really only significant in the 5mm diameter collimator. It is apparent that in terms of its size, only the SFD is suitable for measurements in the very smallest fields, although the effect of the silicon and of the relatively larger volume of connectors and other materials within the detector housing need to be examined. To accurately resolve the differences between detectors it is necessary to model both the beam and the detector. Paskalev et al (2001) did precisely this for the measurement of PDDs and OARs only, in two fields of 5 and 1.5mm diameter. Their work highlights the complexity of the calculations necessary in order to model both the beam and the detector

10.4 Future work

This author has proposed an audit of all stereotactic facilities within the UK. This is likely to involve measurements with the diamond detector, in the verification phantom developed in this work. The development of a method for the verification of the dose distribution is currently underway and will be carried out in conjunction with similar work for IMRT.

The commissioning of IMRT has recently commenced within the ECC and the conclusions reached in this work will be applied to measurements in small IMRT portals. The differences in detector response in the small field and large field situations outlined in this work highlight the problems that may occur in measurements in IMRT fields which are a combination of small and large fields.

Finally, to further investigate the measurement of dose in very small fields it is necessary to carry out Monte Carlo modelling of both the beams and the detectors. In order to do this, more detailed detector information is required from the manufacturers. Detector and small field modelling is likely to form part of a proposal for a research project.

Appendix 1

PDD data on 600CD

The following table shows the final table of PDDs, calculated in Chapter 3. d indicates the depth in mm.

	Collimator diameter /mm												
d	**10**	**12.5**	**15**	**17.5**	**20**	**22.5**	**25**	**27.5**	**30**	**32.5**	**35**	**37.5**	**40**
0.9	30.5	30.5	30.4	30.3	30.3	30.2	30.2	30.1	30.0	30.0	29.9	29.9	29.8
5	79.0	78.8	78.7	78.5	78.3	78.1	77.9	77.7	77.5	77.3	77.2	77.0	76.8
10	97.4	97.3	97.3	97.2	97.2	97.2	97.2	97.1	97.1	97.1	97.1	97.0	97.0
11	98.5	98.5	98.5	98.4	98.4	98.4	98.4	98.3	98.3	98.3	98.3	98.2	98.2
12	99.6	99.5	99.5	99.4	99.4	99.4	99.3	99.3	99.2	99.2	99.2	99.1	99.1
13	99.9	99.9	99.8	99.8	99.8	99.8	99.7	99.7	99.7	99.7	99.6	99.6	99.6
14	100.1	100.1	100.1	100.1	100.1	100.1	100.1	100.1	100.1	100.1	100.1	100.1	100.1
15	100.0	100.0	100.0	100.0	100.0	100.0	100.0	100.0	100.0	100.0	100.0	100.0	100.0
16	99.8	99.8	99.8	99.8	99.8	99.8	99.8	99.9	99.9	99.9	99.9	99.9	99.9
17	99.4	99.5	99.5	99.5	99.5	99.5	99.6	99.6	99.6	99.6	99.7	99.7	99.7
18	99.1	99.1	99.1	99.1	99.2	99.2	99.2	99.3	99.3	99.3	99.3	99.4	99.4
20	98.1	98.1	98.1	98.2	98.2	98.3	98.3	98.4	98.4	98.5	98.5	98.6	98.6
30	92.0	92.2	92.4	92.5	92.7	92.8	93.0	93.2	93.3	93.5	93.7	93.8	94.0
40	86.2	86.4	86.6	86.8	87.1	87.3	87.5	87.7	87.9	88.1	88.3	88.5	88.7
50	80.2	80.5	80.8	81.1	81.4	81.7	82.0	82.3	82.6	82.9	83.2	83.5	83.7
60	75.2	75.5	75.8	76.1	76.5	76.8	77.1	77.4	77.7	78.0	78.4	78.7	79.0
70	70.3	70.6	70.9	71.3	71.6	71.9	72.3	72.6	73.0	73.3	73.6	74.0	74.3
80	65.5	65.8	66.1	66.4	66.7	67.0	67.3	67.7	68.0	68.3	68.6	68.9	69.2
90	61.1	61.4	61.8	62.1	62.5	62.9	63.2	63.6	63.9	64.3	64.7	65.0	65.4
100	56.9	57.3	57.7	58.1	58.4	58.8	59.2	59.6	59.9	60.3	60.7	61.0	61.4
120	50.1	50.4	50.7	51.1	51.4	51.7	52.1	52.4	52.8	53.1	53.4	53.8	54.1
150	41.0	41.3	41.6	41.9	42.3	42.6	42.9	43.2	43.5	43.9	44.2	44.5	44.8
180	33.7	34.0	34.3	34.6	34.9	35.2	35.5	35.7	36.0	36.3	36.6	36.9	37.2
200	29.7	30.0	30.2	30.5	30.7	31.0	31.2	31.5	31.8	32.0	32.3	32.5	32.8
220	26.1	26.4	26.7	26.9	27.1	27.4	27.6	27.8	28.1	28.3	28.6	28.8	29.0
240	23.2	23.3	23.6	23.8	24.0	24.2	24.4	24.6	24.8	25.1	25.3	25.5	25.7

Appendix 2

OAR data on 600CD

The following table shows the final table of OARs, calculated in Chapter 4. OAD indicates the off axis distance in mm.

	Collimator diameter/mm											
OAD	**12.5**	**15**	**17.5**	**20**	**22.5**	**25**	**27.5**	**30**	**32.5**	**35**	**37.5**	**40**
0	1.000	1.000	1.000	1.000	1.000	1.000	1.000	1.000	1.000	1.000	1.000	1.000
1.2	0.995	0.997	0.998	0.998	0.999	0.999	1.000					1.001
1.8	0.990	0.994	0.995	0.996	0.998	0.999	0.999				1.001	1.001
2.4	0.981	0.987	0.992	0.994	0.997	0.998	0.998	0.999	1.000	1.000		1.001
3	0.963	0.982	0.988	0.991	0.995	0.997	0.000	0.000	0.999	1.000	1.000	
3.6	0.941	0.967	0.982	0.988	0.993	0.996	0.997	0.998	0.999	0.999	1.000	1.001
4.2	0.903	0.951	0.972	0.983	0.990	0.994		0.997		0.000	1.000	
4.8	0.840	0.925	0.962	0.978	0.987	0.993	0.995	0.996	0.997	0.998	0.999	1.000
5.4	0.724	0.891	0.945	0.969	0.982	0.990						
6		0.833	0.925	0.958	0.978	0.987	0.991	0.994	0.996	0.997	0.999	0.999
6.6	0.382	0.725	0.893	0.945	0.972	0.981						
7.2	0.236	0.569	0.842	0.927	0.958	0.977	0.986	0.989	0.993	0.995	0.997	0.998
7.8	0.139	0.395	0.741	0.897	0.946	0.972						
8.4	0.092	0.244	0.591	0.851	0.925	0.964	0.975	0.985	0.988	0.992	0.994	0.996
9	0.065	0.146	0.411	0.764	0.893	0.949						
9.6		0.097	0.256	0.624	0.847	0.931	0.960	0.978	0.982	0.988	0.991	0.993
10.2	0.037	0.069	0.153	0.449	0.757	0.903						
10.8			0.103	0.287	0.612	0.863	0.933	0.960	0.974	0.983	0.988	0.990
11.4		0.040	0.075	0.172	0.437	0.781	0.906					
12	0.021	0.033	0.000	0.114	0.279	0.648	0.867	0.933	0.957	0.974	0.981	0.986
12.3			0.052				0.835	0.923				
12.6				0.083	0.171	0.473	0.793					
13.2	0.018	0.022	0.036	0.063	0.114	0.313	0.668	0.874	0.933	0.958	0.972	0.980
13.8				0.050	0.084	0.195	0.509	0.809	0.920			
14.4	0.000	0.019	0.025	0.040	0.065	0.129	0.345	0.690	0.874	0.930	0.959	0.972
15	0.015	0.017	0.023	0.034	0.052	0.094	0.217	0.528	0.813	0.907	0.951	0.967
15.6				0.029	0.043	0.071	0.143	0.359	0.699	0.869	0.937	0.959
16.2				0.025	0.036	0.057	0.102	0.223	0.538	0.802	0.917	0.948
16.8			0.019	0.022	0.031	0.046	0.078	0.144	0.368	0.680	0.886	0.935
17.4		0.015			0.027	0.039	0.062	0.105	0.228	0.520	0.833	0.916
18				0.020	0.025	0.033	0.051	0.081	0.149	0.353	0.735	0.887
18.6					0.023	0.029	0.043	0.065	0.109	0.224	0.587	0.834
19.2			0.015		0.022	0.026	0.037	0.054	0.084	0.150	0.420	0.741
19.8						0.024	0.033	0.046	0.068	0.110	0.274	0.598
20.4	0.012	0.013	0.000	0.017	0.019		0.029	0.039	0.057	0.086	0.179	0.435
21						0.021	0.027	0.034	0.048	0.070	0.127	0.286
21.6							0.025	0.031	0.041	0.058	0.098	0.185
22.2							0.023		0.037	0.049	0.078	0.131
22.8									0.032	0.042	0.064	0.100
23.4				0.014	0.015	0.017	0.000	0.024	0.029	0.037	0.054	0.080
24							0.018		0.026	0.033	0.046	0.065
24.6									0.024	0.029	0.040	0.055

25.2					0.013	0.014	0.016	0.018		0.026	0.035	0.047
25.8										0.024	0.032	0.041
26.4										0.022	0.028	0.036
27							0.014		0.018	0.021	0.026	0.033
27.6										0.019	0.024	0.030
28.2										0.018	0.022	0.027
28.8										0.017	0.021	0.025
29.4								0.013	0.014	0.016	0.020	0.023
34										0.013	0.014	0.016
40	0.012	0.013	0.013	0.013	0.013	0.013	0.013	0.013	0.013	0.013	0.013	0.013
200	0.015	0.015	0.015	0.015	0.015	0.015	0.015	0.015	0.015	0.015	0.015	0.022

Appendix 3

TMR spreadsheet calculation

Example of spreadsheet calculation of TMR from PDD and NPSF, in the 12.5mm diameter collimator.

Field size (1) for PDD (1) & NPSF (1)

Field size (2) for NPSF(2)

Depth/ mm	Sf (f+d)	Sf (f+dm)	PDD (10)	PDD (12.5)	PDD (1)	NPSF (1)	NPSF (2)	NPSF(1) NPSF(2)	$\frac{(f+d)^2}{(f+dm)^2}$	TMR
0.9	12.5	12.3	30.5	30.5	30.5	0.926	0.924	1.002	0.972	29.7
5.0	12.4	12.3	79.0	78.8	78.8	0.925	0.924	1.001	0.980	77.4
10.0	12.4	12.3	97.4	97.3	97.3	0.925	0.924	1.001	0.990	96.4
11.0	12.4	12.3	98.5	98.5	98.5	0.925	0.924	1.001	0.992	97.8
12.0	12.4	12.3	99.6	99.5	99.5	0.924	0.924	1.000	0.994	99.0
13.0	12.3	12.3	99.8	99.9	99.9	0.924	0.924	1.000	0.996	99.5
14.0	12.3	12.3	100.1	100.1	100.1	0.924	0.924	1.000	0.998	99.9
15.0	12.3	12.3	100.0	100.0	100.0	0.924	0.924	1.000	1.000	100.0
16.0	12.3	12.3	99.8	99.8	99.8	0.924	0.924	1.000	1.002	100.0
17.0	12.3	12.3	99.43	99.5	99.4	0.924	0.924	1.000	1.004	99.8
18.0	12.3	12.3	99.05	99.1	99.1	0.924	0.924	1.000	1.006	99.6
20.0	12.3	12.3	98.08	98.1	98.1	0.923	0.924	0.999	1.010	99.0
30.0	12.1	12.3	92.00	92.2	92.2	0.922	0.924	0.998	1.030	94.7
50.0	11.9	12.3	80.20	80.5	80.4	0.920	0.924	0.995	1.070	85.7
60.0	11.8	12.3	75.20	75.5	75.4	0.918	0.924	0.994	1.091	81.7
70.0	11.7	12.3	70.30	70.6	70.5	0.917	0.924	0.993	1.111	77.8
80.0	11.6	12.3	65.50	65.8	65.7	0.916	0.924	0.991	1.132	73.7
90.0	11.5	12.3	61.10	61.4	61.3	0.915	0.924	0.990	1.153	69.9
100.0	11.4	12.3	56.90	57.3	57.1	0.913	0.924	0.988	1.175	66.3
120.0	11.2	12.3	50.10	50.4	50.2	0.911	0.924	0.985	1.218	60.3
150.0	10.9	12.3	41.00	41.3	41.1	0.906	0.924	0.981	1.284	51.8
180.0	10.6	12.3	33.70	34.0	33.8	0.902	0.924	0.977	1.352	44.6
200.0	10.4	12.3	29.70	30.0	29.7	0.899	0.924	0.973	1.398	40.5
220.0	10.2	12.3	26.10	26.4	26.1	0.897	0.924	0.970	1.445	36.6

Appendix 4

TMR data for 600CD

The following table shows the final table of TMRs, calculated in Chapter 8. d indicates the depth in mm. Note that the values on this page have been smoothed from those in Appendix 3 (see section 8.3.3).

	Collimator diameter / mm											
d	12.5	15	17.5	20	22.5	25	27.5	30	32.5	35	37.5	40
0.9	29.7	29.6	29.5	29.5	29.4	29.3	29.3	29.2	29.2	29.1	29.0	29.0
5	81.0	81.0	81.0	81.0	81.3	81.5	81.8	82.0	82.0	82.0	82.0	82.0
10	97.5	97.4	97.4	97.3	97.2	97.2	97.1	97.0	97.0	96.9	96.9	96.8
11	98.8	98.7	98.6	98.5	98.4	98.4	98.3	98.2	98.2	98.1	98.1	98.0
12	99.5	99.4	99.3	99.2	99.2	99.1	99.1	99.0	99.0	99.0	99.0	99.0
13	99.9	99.9	99.8	99.8	99.8	99.7	99.7	99.6	99.6	99.6	99.5	99.5
14	100.1	100.1	100.0	100.0	100.0	100.0	100.0	100.0	99.9	99.9	99.9	99.9
15	100.0	100.0	100.0	100.0	100.0	100.0	100.0	100.0	100.0	100.0	100.0	100.0
16	99.9	99.9	99.9	99.9	99.9	100.0	100.0	100.1	100.1	100.1	100.1	100.1
18	99.4	99.4	99.5	99.5	99.6	99.7	99.8	99.9	99.9	99.9	99.9	100.0
20	98.8	98.9	98.9	99.0	99.1	99.2	99.2	99.3	99.4	99.4	99.5	99.5
30	94.7	94.9	95.1	95.3	95.5	95.7	95.9	96.0	96.2	96.4	96.5	96.7
40	90.2	90.5	90.8	91.0	91.3	91.5	91.7	92.0	92.2	92.4	92.6	92.8
50	85.6	86.1	86.4	86.8	87.1	87.5	87.8	88.1	88.4	88.7	89.0	89.3
60	81.7	82.2	82.6	83.0	83.4	83.7	84.1	84.4	84.8	85.1	85.5	85.8
70	77.7	78.2	78.7	79.1	79.5	79.9	80.3	80.7	81.0	81.4	81.8	82.1
80	73.6	74.2	74.7	75.2	75.6	76.0	76.4	76.8	77.1	77.5	77.9	78.3
90	69.8	70.5	71.0	71.5	71.9	72.4	72.8	73.2	73.6	74.0	74.4	74.8
100	66.2	66.9	67.5	68.0	68.5	68.9	69.3	69.8	70.2	70.6	71.0	71.4
120	60.1	60.8	61.3	61.8	62.3	62.7	63.1	63.5	63.9	64.3	64.7	65.1
150	51.6	52.3	52.9	53.4	53.8	54.3	54.7	55.1	55.5	55.8	56.2	56.6
180	44.4	45.2	45.7	46.2	46.6	47.0	47.4	47.8	48.1	48.5	48.8	49.2
200	40.3	41.0	41.5	42.0	42.4	42.8	43.1	43.5	43.8	44.1	44.4	44.7
220	36.5	37.3	37.8	38.2	38.6	39.0	39.3	39.6	39.9	40.2	40.5	40.8

Appendix 5

XKnife plan at position B

XKnife 3.0 (29/ 8/101) **Beam Set-Up Sheet**

Patient: BARTS (A1) Hospital: WGH-LA1 Time: 17:18:58

BEAM # 1

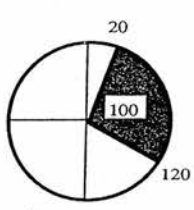

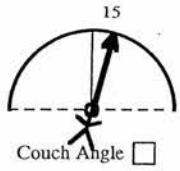

Isocenter: 1
Beam: 1
Collimator: 1.25

D= Dose to Isocenter	
W= Wt.	0.333
Dt= D x W	
Depth	8.01
Ψ	
MU= Dt / Ψ	
R	100
MU/R	

BEAM # 2

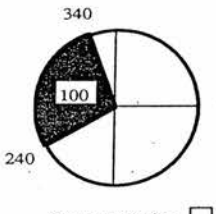

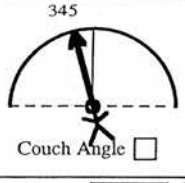

Isocenter: 1
Beam: 2
Collimator: 1.25

D= Dose to Isocenter	
W= Wt.	0.333
Dt= D x W	
Depth	8.01
Ψ	
MU= Dt / Ψ	
R	100
MU/R	

BEAM # 3

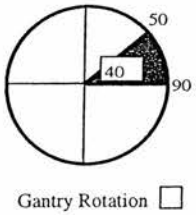

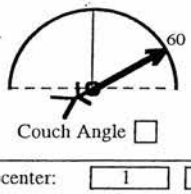

Isocenter: 1
Beam: 3
Collimator: 1.25

D= Dose to Isocenter	
W= Wt.	0.133
Dt= D x W	
Depth	8.01
Ψ	
MU= Dt / Ψ	
R	40
MU/R	

BEAM # 4

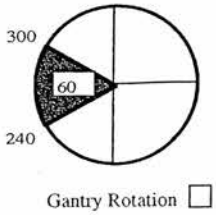

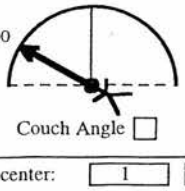

Isocenter: 1
Beam: 4
Collimator: 1.25

D= Dose to Isocenter	
W= Wt.	0.200
Dt= D x W	
Depth	8.01
Ψ	
MU= Dt / Ψ	
R	60
MU/R	

Appendix 6

CFs for EFD

The following table shows an example of the CF(γ)s to account for the directional dependence of the EFD, used in Chapter 8.

		gantry (θ)									
		0	10	20	30	40	50	60	70	80	90
floor (α)	0	1.155	1.155	1.155	1.155	1.155	1.155	1.155	1.155	1.155	1.155
	10	1.155	1.148	1.142	1.136	1.129	1.123	1.118	1.112	1.106	1.101
	20	1.155	1.142	1.130	1.118	1.107	1.097	1.087	1.077	1.068	1.060
	30	1.155	1.136	1.119	1.103	1.088	1.075	1.062	1.051	1.041	1.032
	40	1.155	1.131	1.110	1.090	1.073	1.057	1.044	1.032	1.022	1.015
	50	1.155	1.127	1.102	1.080	1.061	1.044	1.031	1.020	1.011	1.005
	60	1.155	1.124	1.096	1.072	1.052	1.035	1.022	1.012	1.005	1.001
	70	1.155	1.121	1.092	1.067	1.046	1.029	1.016	1.007	1.002	1.000
	80	1.155	1.120	1.089	1.081	1.042	1.026	1.013	1.005	1.001	1.001
	90	1.155	1.119	1.088	1.062	1.041	1.025	1.012	1.005	1.001	1.001

Appendix 7

Calculation of Uncertainties

A.7.1 Overview

All uncertainties in this work are calculated as the square root of the sum of the squares of each individual percentage uncertainty, at 1 s.d.. Although the uncertainty in TMR and S_{cp} is dependent on the collimator diameter, the uncertainty is only calculated for the 12.5mm diameter collimator, where it is a maximum within the clinical range (collimators 40 to 12.5mm diameter). The uncertainty is calculated only for those detectors which were used in the measurement of the dose to the isocentre. The SFD was rejected because of its large asymmetry and therefore its overall uncertainty is not calculated. The relative uncertainty in the Farmer calibration of the linac is stated within the department to be +/-0.25% at 1 s.d., based on the distributions of repeated relative calibrations (dose/MU). All uncertainties are calculated relative to the internal departmental beam calibration only.

A.7.2 Calculation of uncertainties in the calculated dose (D_c)

Equation 9.3 in Chapter 9 described the calculation of the dose to the isocentre (D_c) for each stereotactic plan under investigation:

$$D_c = MU \times TMR(d_{av}, s) \times S_{cp}(s) \times M \qquad (9.3)$$

The uncertainties in D_c are therefore dependent on the uncertainties in the TMR, S_{cp} and the adherence to the ISL (M), relative to the standard beam calibration. As the calculation is relative to the absolute beam calibration, the uncertainty in MU is considered to be nil. The uncertainty in the daily output variation is considered only in the calculation of the uncertainties in the measured dose. The uncertainties in TMR, S_{cp} and M are described in the appropriate chapters, in terms of their overall reproducibility only. The calculated uncertainty is also dependent on the uncertainty in position, which is determined primarily by the CT slice thickness. In the case of 3mm slices, the uncertainty is +/-1.5mm, which equates to +/-0.7% dose at 80mm deep. The total percentage uncertainty in D_c, arising from random errors only, is calculated in Table A.7.1 for the 12.5mm collimator.

Parameter	TMR	S_{cp}	M	CT	Total (D_c)
%uncertainty (1 s.d.)	0.5	0.2	0.2	0.7	0.9

Table A.7.1. Random % uncertainties (1s.d.) in the calculated dose (D_c), for the 12.5mm diameter collimator. Based on reproducibility only.

A.7.3. Calculation of uncertainties in the measured dose (D_m)

Overview

Equation 9.4 in Chapter 9 described the calculation of the measured dose (D_m) for each stereotactic plan under investigation:

$$D_m = R \times CAL \times CF(\gamma) \times OP \ (\times TP) \qquad (9.4)$$

The uncertainties in the measured dose (D_m) are therefore dependent of the uncertainties in each of the above. These are, the uncertainties in the reading (R) on each electrometer, for each detector, the calibration factor (CAL) for each detector, the correction factor for the directional dependence (CF), the daily output on the linac and the temperature and pressure correction (where appropriate). Each of these will be considered in turn.

Calibration factor

The CAL factor was described in equation 9.2:

$$CAL = \frac{R(IC) \times Recombination \times TP \times Fx}{R(detector)} \qquad (9.2)$$

The total percentage uncertainty in CAL can therefore be calculated for each detector individually.

	% uncertainty (1s.d.) CAL					
Detector	R(IC)	Recomb.	TP	Fx	R(detector)	Total (CAL)
Diamond	0.01	0.05	0.08	0.25	0.01	0.27
PFD	0.01	0.05	0.08	0.25	0.03	0.27
EFD	0.01	0.05	0.08	0.25	0.05	0.27
0.125cc IC	0.01	0.05	0.08	0.25	0.01	0.27

Table A.7.2 Random % uncertainties (1s.d.) in the calibration factor (CAL) for each detector.

Directional dependence CF(γ)

The uncertainty in the CF(γ) is a result of the uncertainty in the calculation of directional dependence at each gantry angle, averaged over two axes and meaned across the central axis. The uncertainty is therefore calculated individually for each detector. The total uncertainty in the best fit and that caused by averaging over the asymmetry is assumed to be 2 s.d., such that the uncertainty at 1s.d. is half of those values. The uncertainty determined from the reproducibility of measurements, is 1s.d.. The overall random uncertainty is calculated in Table A.7.3.

		% uncertainty (1s.d.) CF(γ)		
Detector	Reproducibility	Best fit	Asymmetry	Total (CF(γ))
Diamond	0.3	0.2	0.3	0.5
PFD	0.4	0.1	1.0	1.1
EFD	0.3	0.1	0.3	0.4
0.125cc IC	0.3	0.3	0.1	0.4

Table A.7.3. Random % uncertainties (1s.d.) in the correction factor CF(γ) for directional dependence.

The magnitude of the uncertainty is dependent on the asymmetry of each detector. The directional dependence was averaged over two main axes and therefore the uncertainty caused by the asymmetry is inherent in the correction factor and is largest for the PFD.

Linac output

The uncertainty in the daily linac output is the result of the uncertainty in the reading on the Farmer chamber (0.02%), the TP correction (0.08%) and in the overall stability of repeat output measurements (0.25%). The total uncertainty is therefore 0.26%.

Position

The uncertainty in the measured dose is also a result of mispositioning between the effective point of measurement and the radiation isocentre. Although there is a drift in the radiation isocentre within each arc, this was averaged and the use of the spacer to maximise the dose reduced the uncertainty to +/-0.25mm. This is equivalent to an uncertainty in dose of approximately +/-0.2%.

Overall uncertainty

The overall uncertainty for each detector is calculated in Table A.7.4.

	% uncertainty (1s.d.) D_m						
Detector	R	CAL	CF	OP	TP	Position	Total (D_m)
Diamond	0.01	0.27	0.5	0.26	-	0.3	0.7
PFD	0.03	0.27	1.1	0.26	-	0.3	1.2
EFD	0.05	0.27	0.4	0.26	-	0.3	0.6
0.125cc IC	0.01	0.27	0.4	0.26	0.08	0.3	0.6

Table A.7.4. Random % uncertainties (1s.d.) in the measured dose (D_m).

These uncertainties have been calculated for the 12.5mm diameter collimator at a depth of 80mm only. Although uncertainties for larger collimators and shallower depths will be less, the above figures were used as an indication of the uncertainty in each calculation in Chapter 9.

Appendix 8

List of publications relevant to thesis

Peer reviewed papers

Assessment of new small-field detectors against standard field detectors for practical stereotactic beam data acquisition.
C. McKerracher & D.I. Thwaites. *Phys Med Biol* 44: 2143-2160 (1999)

Verification of the dose to the isocentre in stereotactic plans.
C McKerracher & D I Thwaites. *Radiotherapy & Oncology* 64: 97-107 (2002)

Abstracts at conferences

World Congress on Medical physics and Biomedical Engineering. Nice 1997.
Acquisition and verification of beam data for stereotactic radiotherapy. C McKerracher & D I Thwaites. *Medical & Biological Engineering & Computing*. 35 (Suppl 2): 1045 (1997)

17th Annual ESTRO meeting. Edinburgh 1998
Comparison of shielded, unshielded and mini diode to measure and verify stereotactic beam data. C McKerracher & D I Thwaites. *Radiotherapy & Oncology* 48(Suppl 1): S52 (1998).

VI International Conference on Medical Physics. Patras 1999
Collimator and phantom scatter factors for small fields. C McKerracher & D I Thwaites. *Physica Medica* 15(3): 169-170 (1999)

6th Biennial ESTRO meeting on "Physics for Clinical Radiotherapy". Seville 2001
Verification of the dose to the isocentre in stereotactic plans. C McKerracher & D I Thwaites. *Radiotherapy & Oncology* 61 (Suppl 1): S24 (2001)

IPEM Biennial Radiotherapy Meeting. Southampton 2002
Determination of differences between experimental conditions for measurements of collimator scatter factors. C McKerracher & D I Thwaites. *Conference proceedings* (2002).

21st Annual ESTRO meeting. Prague 2002
Analysis of methodology for scatter measurements in small fields. C McKerracher & D I Thwaites. *Radiotherapy & Oncology* 64 (Suppl 1): S43 (2002)

World Congress on Medical physics and Biomedical Engineering. Sydney 2003.
Phantom scatter factors for standard, shaped and square fields. D I Thwaites, C McKerracher, A Allahverdi. *Int Fed Med Phys Biol Eng* ISBN 1 877040 14 2

Prizes

Jack Fowler-University of Wisconsin Young Investigator Award for "The dosimetry of small x-ray beams for stereotactic radiotherapy". (ESTRO, 2003)

Appendix 9

Phys Med Biol 44: 2143-2160 (1999)

Phys. Med. Biol. **44** (1999) 2143–2160. Printed in the UK PII: S0031-9155(99)00538-2

Assessment of new small-field detectors against standard-field detectors for practical stereotactic beam data acquisition

C McKerracher and D I Thwaites

Oncology Physics, Clinical Oncology, Western General Hospital, Crewe Road, Edinburgh, EH4 2XU, UK

E-mail: carolyn.mckerracher@ed.ac.uk and david.thwaites@ed.ac.uk

Received 5 January 1999, in final form 28 May 1999

Abstract. Two new detectors (0.015 cm^3 ion chamber from PTW, 0.6 mm diameter diode from Scanditronix AB) designed specifically for use in small stereotactic fields were compared against similar, more routine, detectors (0.125 cm^3 ion chamber, parallel plate chamber, shielded and unshielded diodes and film). Percentage depth doses, tissue maximum ratios, off-axis ratios and relative output factors were compared for circular fields in the 40–12.5 mm diameter range, with a view to identifying the optimum detector for stereotactic beam data acquisition. Practical suggestions for beam data collection and analysis are made, with an emphasis on what is achievable practically in radiotherapy departments where the primary demand is to provide a routine service. No single detector was found to be ideal, and neither of the two new measurement devices had any significant advantages over more routine devices, in the situations measured. Although the new 0.015 cm^3 ion chamber was an improvement on a 0.125 cm^3 ion chamber in the measurement of profiles, it was still too large when compared with a diode. The new small diode had a low signal to noise ratio which made reliable data difficult to extract and its only advantage is possibly improved resolution in fields smaller than the range tested. The use of a larger unshielded diode is recommended for all measurements, with the additional cross-checking of data against at least one small ion chamber and film. A simple method of obtaining reliable output data from the detectors used is explained.

1. Introduction

Stereotactic radiotherapy performed on a linear accelerator is, by now, an established technique. However, the measurement of the beam data required for a particular planning system continues to present problems. Rice *et al* (1987) advised that both the lack of lateral electronic equilibrium and the steep fall-off in dose in the penumbra of small fields, necessitate the use of small detectors. It has been suggested (Higgins *et al* 1995, Bjarngard *et al* 1990) that the maximum inner diameter should be smaller than the beam radius. As the most common field sizes used in stereotactic treatments are circles with diameters ranging from 40 to 10 mm, an optimum detector to measure all fields should have a sensitive width (as 'seen' by the radiation beam) of less than 5 mm. Increasing use is also being made of field sizes in the 10–4 mm range, which would require a detector with sensitive width less than 2 mm. This presents a much greater problem which will not be dealt with here. Film, diodes and small ion chambers have all been recommended (AAPM 1995), but new specifically designed detectors continue to be developed.

A diamond detector (Rustgi 1995) has been shown to be reliable for small-field measurements, primarily due to its non-directional dependence (compared with an energy compensated diode), near tissue equivalence, small volume and small active diameter

0031-9155/99/092143+18$30.00 © 1999 IOP Publishing Ltd

(2 to 4 mm). However, the detector is expensive, difficult to obtain and has been shown to exhibit dose rate dependence when used with particular electrometers (Norrgard *et al* 1998). Dasu *et al* (1998) tested a small liquid ionization chamber which compared well with both shielded and unshielded diodes and could be calibrated and used for absolute dosimetry. Francescon *et al* (1998) investigated several new types of detector, radiochromic film, a new parallel plate chamber, MOSFETs and TLD 800 microcubes, all with comparable results. However, the radiochromic film was found to be equivalent to radiographic film, the parallel plate chamber is not available commercially, the MOSFETs were not compared against conventional dosimetry diodes and TLDs have always been laborious to use. Other authors have investigated radiochromic film with promising results (Sanders *et al* 1993, McLaughlin *et al* 1994, Somigliana *et al* 1999), but whether it can be used to obtain more accurate data than those obtained with conventional detectors is still unproven.

Although the specific advantages of these new detectors are significant, the question remains as to whether it is necessary to purchase a special detector for stereotactic measurements, or whether the detectors generally available within most departments will suffice? Accuracy and precision should be weighed against ease of use, availability, cost and, importantly, the ability to use the detector in verification measurements and audits. Although the use of one detector to acquire all the necessary data would be welcome, Podgorsak (1992) points out that it is 'good practice' to compare several different types. In addition, if it is the case that standard dosimetry devices are adequate, it is important to assess the relative merit of each device in measuring a particular beam parameter and consequently apply experimental limitations to each. Although Monte Carlo data have been used to calculate small-field beam data (Heydarian *et al* 1996), there are still problems in defining the spectrum for small fields (Bjarngard *et al* 1990) and it does not eliminate the need for detectors for verification measurements in phantoms.

In this paper, several detectors, including two new commercial ones developed for small-field work, are compared in the measurement of percentage depth doses (PDDs), tissue maximum ratios (TMRs), off-axis ratios (OARs) and relative output factors in stereotactic fields. The merits of each detector are assessed in all measurement situations with a view to producing acceptably accurate beam data for all circular field sizes in the range of 40–12.5 mm diameter. The new commercial detectors are a 'mini' diode (sensitive diameter 0.6 mm) from Scanditronix AB and a small 'PinPoint' ion chamber (0.015 cm^3) from PTW. Both detectors are compared against the larger detectors of the same type to ascertain whether they present significant advantages over their predecessors.

2. Materials

2.1. Linac and accessories

All measurements were carried out on an ABB CH6 6MV linac, adapted for stereotactic treatments via an add-on system from Radionics. This incorporates a stainless steel tertiary collimator housing, which is bolted on to the face plate of the linac, and 12 tertiary collimators made of cerrobend. The collimators are slotted into the housing and are held in place at the linac source end by a shoulder region and a screw cap at the opposite end towards the isocentre. They are drilled with divergent holes which produce circular field sizes from 40 to 12.5 mm diameter at isocentre. Although Radionics produce smaller collimators, 12.5 mm was considered to be at the lower end of usefulness for the types of lesions to be treated. A 50 × 50 mm field setting is always set on the secondary collimators to ensure that head scatter from the standard machine components remains constant.

Table 1. Summary of detectors used and their most important properties.

Manufacturer	Detector type	Volume (cm^3)	P_{eff} (mm)	Active size (mm)	Physical size (mm)
Scanditronix	Shielded diode	29×10^{-5}	+0.6†	2.5	7
Scanditronix	Unshielded diode	29×10^{-5}	+0.4†	2.5	7
Scanditronix	Unshielded mini diode	1.7×10^{-5}	+0.5†	0.6	5
PTW	Ion chamber	0.125	−1.4†	$d = 5.5$	6.5+
			+4.5‡	$l = 6.5$	$0.75w$
PTW	PinPoint ion chamber	0.015	−0.5†	$d = 2$	$5 + 0.7w$
			+3.4‡	$l = 5$	
PTW	Markus parallel plate ion chamber	0.05	+0.03†	5	6(30*)
Kodak	X-Omat V film				
Tobias	Point densitometer	N/A	0	1 mm spot size	

P_{eff} is the effective point of measurement.
† Distance along beam CAX.
‡ Distance from the tip of the chamber along its own axis.
d = chamber diameter (cross section).
l = chamber length (along axis).
w = chamber wall thickness.
Active size is the maximum dimension 'seen' by the radiation beam.
* Overall dimension including additional material surrounding the sensitive area of the Markus.

2.2. Detectors

The detectors used and their most important properties are summarized in table 1. An unshielded diode is a p-type silicon detector and is generally used in electron beams ('electron diode'). In megavoltage photon beams it overestimates the dose at large depths and field sizes due to the increased sensitivity of a silicon detector to low-energy photons. A shielded diode is an energy compensated diode ('photon diode') which has been empirically modified to absorb some of this low-energy scatter through the addition of a layer of high atomic number material immediately behind the chip (Gager *et al* 1977, Rikner and Grusell 1985). Although the properties of the two types of diode differ significantly, many papers on stereotactic measurements do not indicate which type of diode has been used. The mini diode from Scanditronix is an unshielded diode with a smaller sensitive area, specifically designed for stereotactic beam measurements. The PinPoint ion chamber from PTW has also been specifically designed for stereotactic beams and has a small sensitive volume. Although the Markus parallel plate ion chamber has an active diameter of 5 mm it is surrounded by other materials, mainly PMMA, which extends the overall physical dimension to 30 mm. This may have a perturbing effect at smaller field sizes. It can be seen that the detectors with the largest sensitive dimensions are the PTW ion chambers and the Markus parallel plate chamber, although all are very close in size to the radius of the smallest beam (6.25 mm). The Tobias is a point densitometer with 1 mm spot size. Film must be positioned and moved manually on the measurement point.

3. Methods

The XKnife software from Radionics requires the input of TMRs, OARs and relative output factors, which is typical of most stereotactic planning packages. All detectors were compared for four collimator sizes, 40, 30, 20, 12.5 mm, and intermediate collimators were measured with a more limited set of detectors.

3.1. Tissue maximum ratios

The TMR software option was not available on the version of RFA300 (Scanditronix) water scanning tank software in use. As a result, PDDs were measured and converted to TMRs.

PDDs were initially measured in the water scanning tank at 1000 mm focus to surface distance (FSD) with all diodes and both cylindrical ion chambers. Spot checks were made in a water substitute plastic material (RMI) with the same detectors and the parallel plate chamber. Film was orientated parallel to the beam central axis, sandwiched between slabs of RMI and calibrated with a sensitometric curve produced by films exposed at the depth of dose maximum, perpendicular to the beam. Williamson (1981) notes that this method used for conventional beams produces errors greater than 5% for 25 MV and up to 30% for cobalt-60, and advocates a more complex method of calibration. These errors are due to the increased sensitivity of film to low-energy photons, resulting in larger errors at greater depths. However, as stereotactic beams have much less scatter, the film response may not vary as greatly with depth in these situations.

PDDs were converted to TMRs using the method described in *Br. J. Radiol.* (suppl 25) (1996). This method includes the ratio of peak scatter factors (PSFs), which are extremely difficult to measure for small fields. Limited literature is available, although phantom scatter factors for stereotactic field sizes at 6 MV have been measured by Rice *et al* (1987) and Chierego *et al* (1993) and at 10 MV by Houdek *et al* (1983). As the curve of phantom scatter factors against field size is steepest at small field sizes, the ratio of two field sizes will be more significant. To determine the magnitude of the correction and how it relates to measured data, TMRs are calculated both with the Rice *et al* (1987) PSF values and without any correction. Both results are compared with TMR spot check measurements in RMI.

Doses close to the surface and in the build up region were measured with the larger diodes and the parallel plate chamber in RMI. The depth of dose maximum was measured in RMI with the larger diodes, the PinPoint chamber and the parallel plate chamber.

3.2. Off-axis ratios

The Radionics software requires the input of profiles at only one depth of 50 mm. Divergence in small stereotactic fields over the depths relevant to head treatments (approx 0–150 mm) has been reported to be insignificant (Rice *et al* 1987, Das *et al* 1995). The use of a tertiary collimator system results in a very steep fall in dose in the penumbra region. To accurately resolve the dose in the penumbra, the detector has to be as small as possible. It has been well documented (Dawson *et al* 1984, 1986, Sibata *et al* 1991) that ion chambers broaden the apparent penumbra and are unsuitable for profile measurements. This is true even when they are used unconventionally with their long axis parallel to the beam central axis to minimize their sensitive width. Conversely, the sensitive width of a diode can be reduced by orientating it with its long axis perpendicular to the beam, but Beddar *et al* (1994) and Dasu *et al* (1998) both advise against using diodes in this orientation.

All diodes (long axes parallel to beam CAX) and both cylindrical ion chambers (long axes perpendicular to beam CAX) were used in the water scanning tank, with an isocentric set up of 1000 mm focus to detector distance (FDD) at 50 mm depth. Film was used perpendicular to the beam central axis, in RMI, with the same geometrical set-up and read out on the point densitometer.

The widths of the relevant isodoses (100–95%) were also analysed for each collimator size with respect to the size of the detector used. This information was used to judge whether a particular detector could measure the central uniform dose accurately, or whether dose inhomogeneity within the detector sensitive volume had an effect on the measurement.

3.3. Relative output factor

The output factor for each collimator was measured relative to a 100 × 100 mm field, under isocentric conditions of 1000 mm FDD, at a constant depth of dose maximum of 15 mm. Relative output factors were measured with all detectors, including film, in RMI. The ion chambers were connected to an NE 2620 electrometer; 300 V bias was set for the 0.125 cm^3 ion chamber and parallel plate and 90 V for the PinPoint. The diodes were connected to a single channel on a DPD6 monitor from Scanditronix. Three exposures of 200 monitor units (2 Gy) were made in each measurement situation.

Output factors for larger open fields in the 100–40 mm square range were also measured with the shielded and unshielded diode, the 0.125 cm^3 ion chamber, the Markus chamber and a 0.6 cm^3 Farmer ion chamber which would normally be used for more routine field sizes. This was carried out to assess the relative response of each of these detectors in larger fields to aid in adapting the information to stereotactic fields.

4. Results

4.1. Tissue maximum ratios

Figure 1(*a*) shows all the PDD measurements in a 40 mm collimator. All detector measurements are closely matched, with the exception of those for film which are approximately 3.5% higher at greater depths. The measurements with the shielded diode are approximately 1% higher than the mean of the results of the other detectors. Figure 1(*b*) shows a greater spread of approximately 1.5% between the measurements for each detector other than film in the 12.5 mm collimator. The measurements with the PinPoint chamber lie highest at greater depths. It is difficult to determine whether the differences between the other detectors are real, or are a result of measurement uncertainty. The film measurements are approximately 2.5% lower than the mean of the others.

Figure 2(*a*) shows the 40 mm collimator PDD values near the depth of dose maximum (d_{max}). Each curve is normalized at 100 mm depth to show the relative response of each detector at d_{max}. The unshielded diode shows the largest relative response but closely matches that of the ion chamber. The maximum spread of relative responses is only 0.7% between the unshielded and shielded diode with the Markus chamber and PinPoint lying in between. Figure 2(*b*) shows the measurements in the 12.5 mm collimator. The maximum spread of relative responses increases to approximately 2.5% with the difference between diodes increasing slightly to 1%, but this increase may only be due to experimental uncertainty. Each ion chamber has a lower response with respect to the diodes than in the larger field size.

The position of d_{max} when analysed carefully in RMI, decreases from approximately 15.6 mm for the 40 mm collimator, to 15 mm for both 30 and 20 mm collimators and 13.8 mm for the 12.5 mm collimator, averaged over all detectors. Although noise in each of the systems causes the measured d_{max} to vary by up to ± 1 mm, a field size dependence can still be seen. The surface dose varies between 10 and 20%, measured with the diodes and parallel plate chamber, but noise in the measurements is too large to extract any field size dependence.

The average of all the curves was taken for each collimator, the results smoothed and converted to TMRs.

Figure 3(*a*) shows a comparison of TMRs calculated from PDDs, both with and without a PSF correction and measured (point measurements) TMRs for a 40 mm collimator. There is

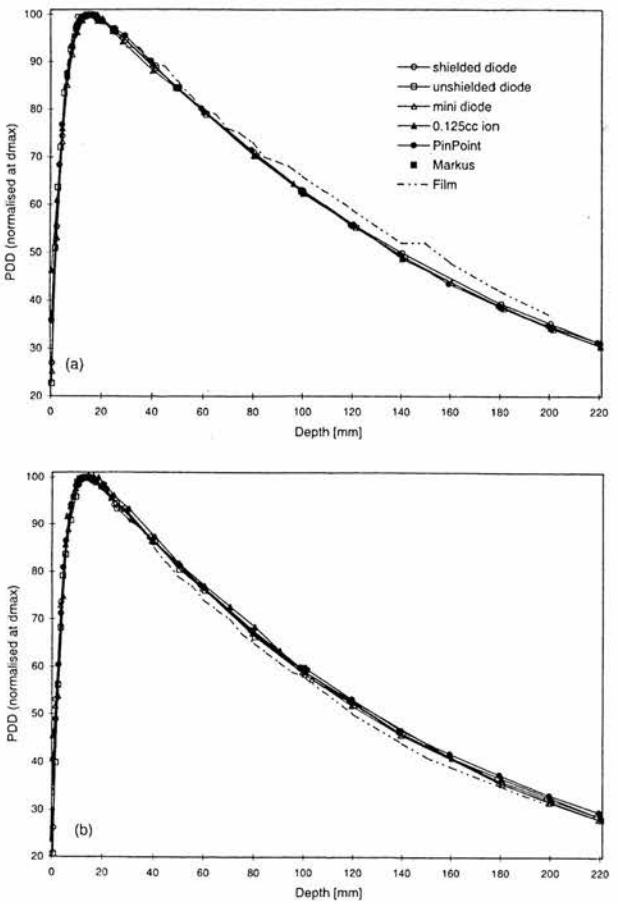

Figure 1. Measured PDDs normalized at d_{max} against depth in (*a*) a 40 mm collimator and (*b*) a 12.5 mm collimator.

no significant difference between any of the curves. Figure 3(*b*) shows the same comparison for the 12.5 mm collimator. For this field size, there is a difference between TMRs calculated with and without the PSF correction. The maximum difference is less than 2% at the largest depths (>100 mm). Less than 1% difference exists over the range of depths between 60 and 100 mm. Measured data fit the curve which includes the PSF correction.

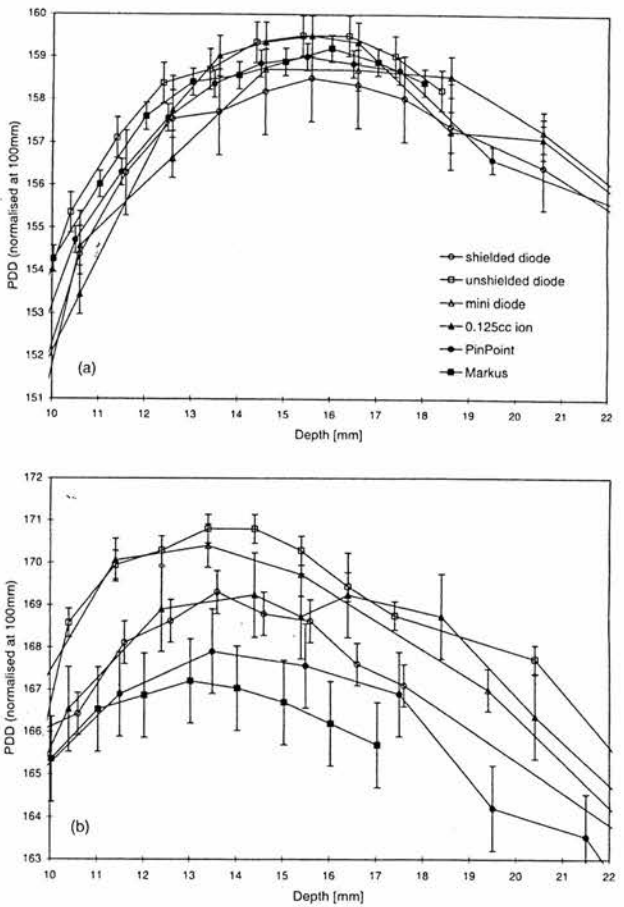

Figure 2. Measured PDDs near d_{max} normalized at 100 mm depth against depth in (*a*) a 40 mm collimator and (*b*) a 12.5 mm collimator.

4.2. *Off-axis ratios*

Figure 4(*a*) shows the measured OARs for a 40 mm collimator. As expected, the 0.125 cm^3 ion chamber broadens the apparent penumbra. The results for the shielded, unshielded and mini diodes are indistinguishable and match well with film. However, the values outside the field for

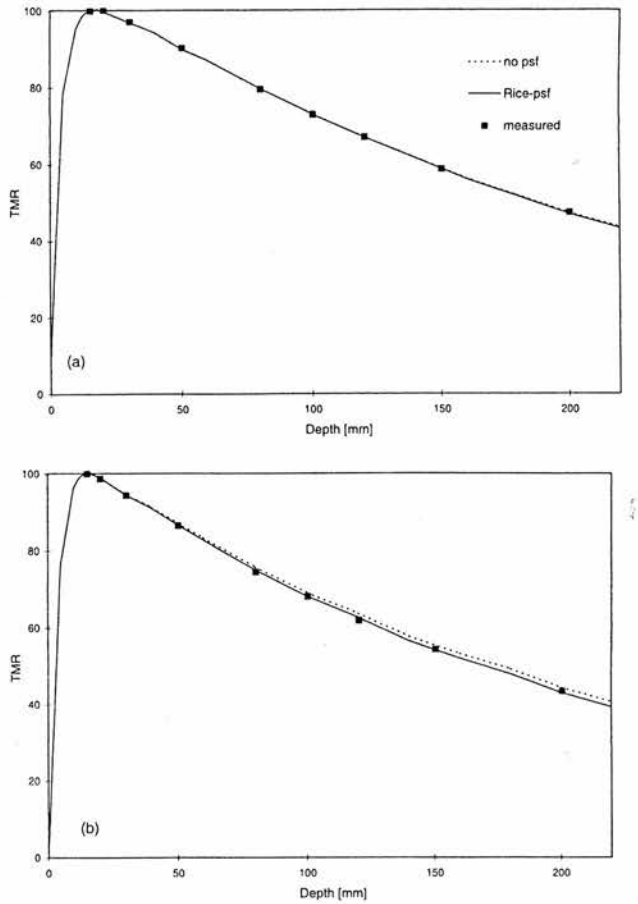

Figure 3. Calculated and measured TMRs against depth in (*a*) a 40 mm collimator and (*b*) a 12.5 mm collimator, normalized at d_{max}.

film are higher than those for the diodes. The PinPoint chamber is a significant improvement on the larger ion chamber, although the dose is still underestimated in the shoulder region. The measurements in the 12.5 mm collimator are shown in figure 4(*b*). At this field size the measurements with the 0.125 cm^3 ion chamber are much worse, as expected. The shielded and unshielded diodes match and the mini diode appears to produce a wider high-dose region.

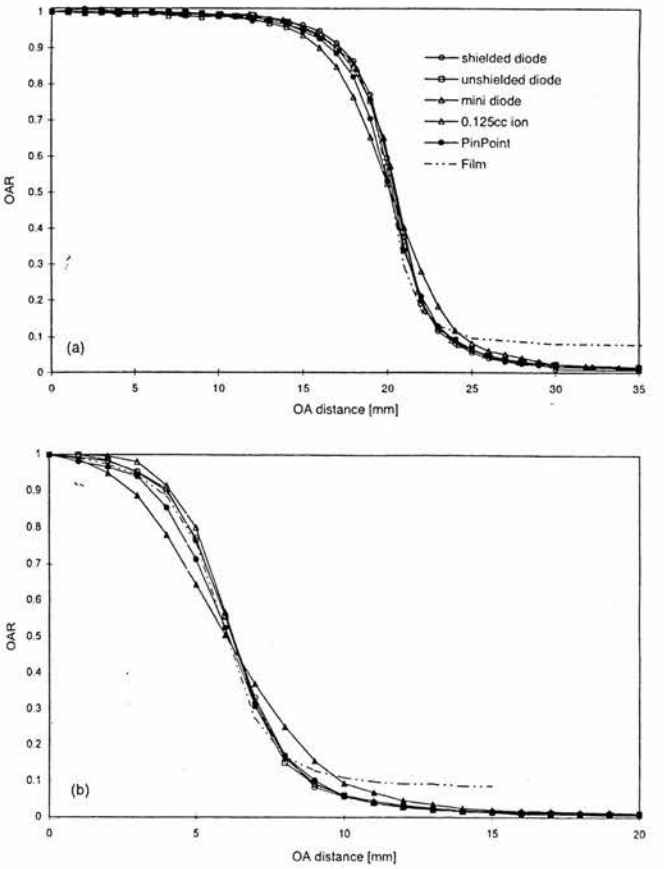

Figure 4. Measured OARs against off axis distance in (*a*) a 40 mm collimator and (*b*) a 12.5 mm collimator, normalized at beam CAX.

Although the PinPoint chamber is an improvement on the larger ion chamber, it underestimates the dose in the shoulder region significantly. Again, film overestimates the dose outside the field.

Figure 5 shows a graph of the width of six isodoses (100–95%), extracted from the OAR data and plotted against collimator size. The best fit lines have been calculated via linear regression and only a section of the data (up to 10 mm isodose width) is shown. The maximum

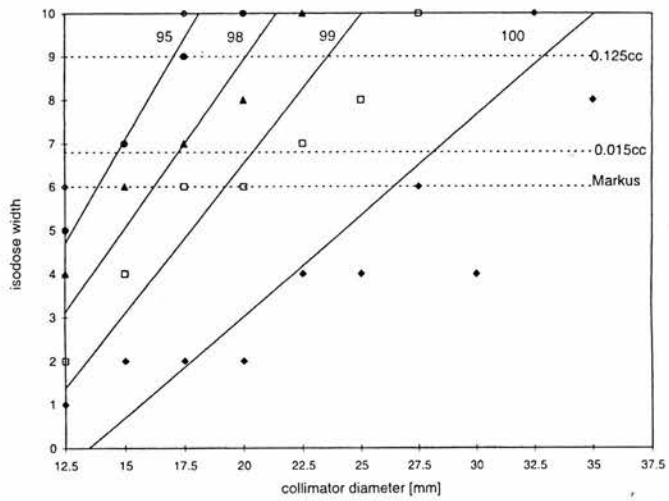

Figure 5. Best fit lines for measured isodose widths against collimator diameter, with effective maximum physical dimension superimposed for each ion chamber.

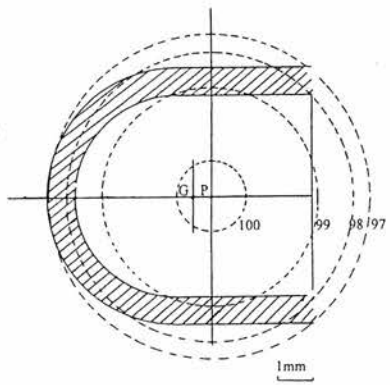

Figure 6. 0.125 cm^3 ion chamber measurement volume (full lines) with major isodose curves (100, 99, 98, 97; broken lines) superimposed. The hashed area indicates the chamber wall. *G* is the geometrical centre of the chamber measurement volume, *P* is the effective point of measurement.

effective physical dimension of each ion chamber, as 'seen' by the beam, is superimposed. These values for the cylindrical ion chambers have been calculated as twice the effective point of

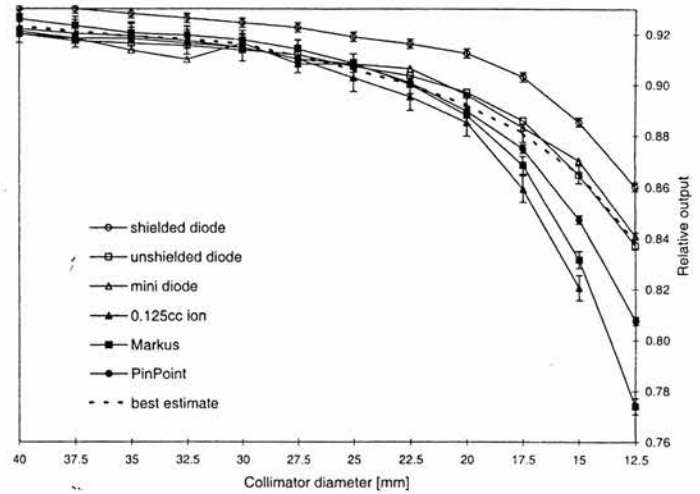

Figure 7. Measured relative output factors (normalized to 100 × 100 mm square open field) and calculated 'best estimate' against collimator diameter.

Table 2. Smallest collimator sizes (in mm) with isodose regions (100, 99, 98%) which fully encompass the physical and sensitive dimensions of each ion chamber.

	0.125 cm^3 cylindrical	PinPoint cylindrical	Markus parallel plate
Physical dimension	9*	6.8*	6
100%	< 35	< 30	< 27.5
99%	< 25	< 22.5	< 20
98%	20	< 17.5	< 17.5
Sensitive dimension	7.5*	5.4*	5
100%	< 30	< 27.5	< 27.5
99%	< 22.5	< 20	< 20
98%	< 20	< 17.5	< 17.5

* Effective dimension calculated by placing the detector with the effective point of measurement at the field centre.

measurement (along the chamber axis, from the tip). This is because the geometrical centre of the measurement volume is not placed at the central axis of the beam due to the asymmetry of the chamber volume. Figure 6 shows an example of the 0.125 cm^3 chamber placed within the 20 mm collimator distribution. *P* is the effective point of measurement of the chamber and is placed at the beam CAX. *G* is the geometrical centre of the chamber measurement volume. Table 2 summarizes some of the data which can be extracted from figure 5.

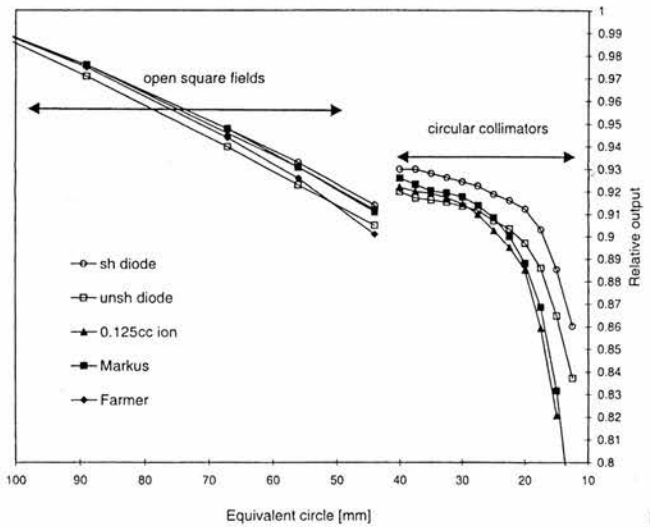

Figure 8. Measured relative output factors (normalized to 100 × 100 mm square open field) against equivalent circle diameter for open square fields and stereotactic collimators.

4.3. Relative output factors

Figure 7 shows a graph of the relative output factors for each collimator, normalized to a 100 mm × 100 mm square open field. There is a large difference between the measurements made with each detector, which increases with decreasing collimator size. The shielded diode curve is higher than the others and the two unshielded diodes match well, although the error bars on the mini diode are larger due to noise. The measurements with each of the three ion chambers begin to fall off as their size becomes more significant compared to the field size. The construction of the 'best estimate' curve is discussed in section 5.3.

Figure 8 shows output factors measured in larger open fields and some measured in the circular stereotactic fields with a few detectors, both sets measured at d_{max} at 1000 mm FDD. The field sizes have been converted to equivalent diameters (*Br. J. Radiol.* (suppl 25) 1996) and normalized to 100 mm square field (111 mm equivalent diameter). Again, in the open fields the shielded diode measurements are highest, but the curve is closely matched with both the 0.125 cm^3 cylindrical and the Markus parallel plate chamber measurements. The Farmer chamber values begin to fall off noticeably for field sizes below the 50 × 50 mm square (56 mm equivalent diameter) and the unshielded diode measures values which are consistently lower than the other detectors. Similar trends are observed when a 50 × 50 mm square field is set and the stereotactic collimators are added.

5. Discussion

5.1. Tissue maximum ratios

All detectors (other than film) are well matched in the measurement of PDDs at the largest field size, although the behaviour of the shielded diode, if real and not the result of experimental uncertainty, is the opposite of that which might first be expected. The characteristics of the unshielded diode make it more likely to over-respond at depth but instead it matches well with the ion chambers at depth and in terms of absolute response at d_{max}. This suggests that there are negligible changes in response from low-energy photons at depth, at this field size. The shielded diode has been designed to partially absorb low-energy scatter and if this scatter is insignificant, the diode might under-respond due to over absorption. This appears to be the case at d_{max} where the relative signal is reduced compared with the unshielded diode. The fact that the depth dose curve is too high at greater depths suggests that the problem of the energy over-compensation is more significant at d_{max} than at depth, i.e. the compensation tends towards being more correct at greater depths.

The larger spread between the measurements and the decrease in ion chamber response with respect to the diodes at d_{max} in the smallest collimator is partly due to increased experimental uncertainty and partly due to the ion chambers being too large to measure the dose accurately. The detector size problem is greatest at d_{max} and will tend to decrease with depth because of divergence. The effect of this will be to produce depth dose curves tending to be too high at depth. This is only observed for the PinPoint chamber in the smaller field. It is not observed for the 0.125 cm^3 chamber, suggesting that the effect may be obscured by experimental uncertainties. The difference between the shielded and unshielded diodes at d_{max} was also noted by Dasu *et al* (1998) who suggested that this reflected differences in response to contaminant electrons. These differences also reflect in part the experimental uncertainties associated with each detector.

The biggest problem in measuring PDDs in the water scanning tank is the size of the reference detector which is used to normalize out any machine output fluctuations. Although attempts are being made to reduce the size of measurement detectors, little thought has been given to the reference detector which perturbs the beam when placed in a homogeneous region. If possible, the reference signal should be taken directly from the linac, or the detector should be localized above the stereotactic collimators. In the Radionics system, this would involve drilling a hole in the tertiary collimator housing above the level of the shoulder region.

In accordance with other authors (Arcovito *et al* 1985, Rice *et al* 1987, Serago *et al* 1992, Sixel and Podgorsak 1993, Fan *et al* 1996–7), the depth of d_{max} was found to decrease as field size decreases. This antithesis to large open fields is not related to electron contamination but is in part due to the increasing effect of phantom scatter as field size increases and possibly also in part due to the effects of tertiary collimator scatter as suggested by Arcovito *et al* (1985). However, the statistical noise inherent to measurements at d_{max}, and the problems in setting up a detector at the exact depth with respect to the effective point of measurement, means that a constant value of 15 mm for all collimators is a reasonable approximation in this 6 MV beam (Serago *et al* 1992, Das *et al* 1995, Fan *et al* 1996–7). Statistical noise also obscures any field size dependence of the surface dose, as also noted by Sixel and Podgorsak (1993) and Das *et al* (1995).

PDDs converted to TMRs without the use of PSFs may result in an error of up to 2% for the smallest collimator at the larger depths. However, this error may be acceptable if larger collimator sizes are generally in use. As the PSFs used were measured for a particular collima-

tion system with an ion chamber, size effects and secondary electron effects may influence the values obtained and therefore their extension to other set-ups may not be entirely appropriate. Future measurements of PSF values for the Radionics system with diodes is required.

5.2. Off-axis ratios

Dawson *et al* (1984) suggests that using a diode in the penumbral region measures something closer to the photon fluence distribution whilst an ion chamber measures something closer to a dose distribution. Although the measurement of a dose distribution is the most desirable, the accuracy of the ion chamber is reduced in small fields where there is a steep fall-off in dose throughout the chamber volume, which leads to a broadening of the penumbra. Dawson consequently recommends the use of a shielded diode. However, Beddar *et al* (1994) recommend an unshielded diode as the detector of choice. Metcalfe *et al* (1993) looked at both diodes to measure penumbra in a 100 × 100 mm 6 MV beam and discovered little difference at d_{max}, but a difference of 1.5 mm at 200 mm deep, and therefore recommend a shielded diode. However, at relevant depths in the head and at smaller field sizes, this difference is unlikely to be a problem. Alternatively, various methods have been employed to correct ion chamber measurements: Sibata *et al* (1991) use both deconvolution of a single detector size and extrapolation of several detectors to zero diameter. However, neither of these methods agree totally with film and both seem to assume a circular cross section with a measurement volume placed symmetrically at the centre of the beam. This approximation is only true when cylindrical ion chambers are used with their long axes parallel to the beam central axis.

In figures 4(*a*) and (*b*) the ion chambers do not adequately resolve the dose in the penumbra, as expected. All the diodes match well with film, except in the low-dose region outside the field where film produces values which are too high. This is due to the difficulties in obtaining an accurate film calibration at low doses, background subtraction, processor inconsistencies and the poor resolution of the densitometer at low optical densities. There was no significant difference between the shielded and unshielded diodes at 50 mm depth. The mini diode shows increased resolution at the smallest field size, which suggests it may have an advantage in the measurement of smaller stereotactic fields. However, the small collecting volume leads to noisy data and therefore smoother data are required to assess this advantage more fully. A longer sampling time could be applied, but has practical problems of experimental time and potential machine output fluctuations.

An alternative to conventional film is radiochromic film, sold under the brand name of GafChromic™ (GAF Chemicals Corp.). It is unique in that it is insensitive to daylight, turns a blue colour on exposure to x-rays and has a higher resolution than conventional film (Chu *et al* 1990). A recent AAPM report (Niroomand-Rad *et al* 1998) recommends techniques for the calibration, exposure and analysis of radiochromic film. It has been used to measure off-axis ratios and dose distributions for stereotactic fields on the Gamma Knife unit (Sanders *et al* 1993, McLaughlin *et al* 1994, Somigliana *et al* 1999) and on a linac (Guan *et al* 1993, Somigliana *et al* 1999). However, the results have all been comparable with those for radiographic film, or, in the case of the Gamma Knife, with the manufacturer's provided data. The advantage of radiochromic film appears to be in terms of its use practically, rather than a dosimetric advantage.

5.3. Relative output factors

The detector of choice for the measurement of relative output factors is an ion chamber. However, in small fields the size of an ion chamber will result in an underestimation of the

dose if the entire chamber is not contained within the central uniform dose region, as shown in figure 6. Although a diode is not generally used to measure output factors, Karlsson *et al* (1997) compared both shielded and unshielded diodes with an ion chamber and found little difference in the 100–50 mm range for open square fields. Small differences were found between the shielded and unshielded diode due to their different responses to low-energy scatter. As stereotactic fields have much reduced scatter, the extension of the information obtained in open square fields to the stereotactic field situation may not be entirely correct. As a result, the question of which curve is most accurate is not easy to answer. Two issues must be addressed; how to predict the effect of dose inhomogeneity within an ion chamber and how to assess the accuracy of diode measurements at these small field sizes.

In terms of dose inhomogeneity, deconvolution of detector size or extrapolation to zero seem appropriate correction methods but they are complicated for the reasons discussed previously and they require measurements with several ion chambers of different sizes. A less mathematical approach is to consider the physical position of each chamber within each field, as in figure 6. The information contained in figure 5 and table 2 can be used to do this. For example, it is obvious that if both the sensitive and physical dimensions of the ion chamber fit within the 100% isodose, then the chamber will measure accurately. If both are within the 99% isodose then the answer is also likely to be accurate and to be within less than 1% of the true value. By consideration of each isodose in turn, the expected accuracy of each chamber can be predicted. To partially construct the 'best estimate' curve, the measurements with each chamber are averaged in each collimator, down to approximately the 25 mm diameter. Below this, the estimated accuracy of each chamber is considered at each smaller collimator size. Note that although the maximum dimensions of the PinPoint and the Markus chamber are similar, the Markus chamber values fall off faster, possibly due to the non-tissue equivalent material surrounding the sensitive volume.

The second issue can be partly resolved by consideration of the results in figure 7. Assuming that the 0.125 cm^3 chamber and the Markus chamber are both correct in a 40 × 40 mm open field and a 40 mm diameter collimator, the shielded diode shows an enhanced response as the field size decreases. Conversely, the unshielded diode underestimates the dose in both the open fields and the stereotactic collimators, although the effect decreases with collimator size such that the unshielded diode curve crosses that of the ion chamber at around a 25 mm collimator. It seems prudent to assume that the unshielded diode becomes more reliable at smaller fields because of the reduction in scatter.

Using all of this information, the 'best estimate' curve is constructed. In the largest collimators it matches best with an average of the ion chambers and at the smallest fields matches best with both unshielded diodes. Overall, the 'best estimate' matches closest with the unshielded diode. This empirical approach, although not strictly mathematical, is useful because it encourages consideration of the physical dimensions of both the dose distribution and the detector and can be applied easily to measurements with any device.

One type of detector not reported for output measurements was film. Although radiographic film was originally tested, inconsistencies in the processor and general non-reproducibility led to it being abandoned. However, some authors have investigated both radiographic and radiochromic film in the measurement of relative outputs, with promising results. Somigliana *et al* (1999) used both types of film and a diode to measure relative outputs on both the Gamma Knife and a linac. All three detectors produced equivalent results on the linac for collimator diameters between 24 and 14 mm. On the Gamma Knife, differences were reported for helmets with collimator diameters between 14 and 4 mm. However, in this case, the directional dependence of a detector becomes important because of the geometrical set-up of the sources. The diode (probably unshielded, although not specified explicitly in

the paper) has inherent directional dependence which may affect the measurements. As a result, the different results for the diode and film cannot be directly transferred to the linac situation. Francescon *et al* (1998) also used both types of film on a linac but reported very little difference between the two down to a 4.4 mm diameter collimator. Although Bjarngard *et al* (1990) also reported the use of radiochromic film to measure relative outputs, the results were not presented.

6. Conclusions

It is not necessary to purchase a special detector for stereotactic measurements for field diameters in the 40–12.5 mm range. Any small detector can be used to measure depth doses, the greatest problem being the placement of a reference detector in the beam in such a way that it does not affect the field detector readings. The rule of thumb that a detector must be smaller than the radius of the beam to measure profiles has been shown to break down. Although the PinPoint chamber complies with this, it does not accurately resolve the dose in the penumbra. Profiles should instead be measured with film and a diode, shielded or unshielded. The diode should be used with its long axis parallel to beam CAX and care should be taken to compare the results outside the field.

The measurement of relative output factor presents the largest problem because no detector is ideal and only a comparison between different detectors highlights the weaknesses of each. Although manufactures have put an emphasis on improving the resolution in the penumbra, the problems in measuring relative output factors are largely ignored. An unshielded diode has been shown to be the most reliable detector, but should be compared with a small ion chamber and one other device. Ion chambers should have maximum active dimensions within the 100% isodose and all detectors should be compared in a few larger open fields.

In terms of the new detectors investigated, a mini diode may be most appropriate for smaller fields below 12.5 mm if the signal to noise ratio can be improved. Although an increase in measurement time (about five times as long) is one solution, frequently it may not be practical. However, the treatment of fields smaller than 10 mm on a linear accelerator introduces many other problems of accuracy, possibly larger than those associated with inadequate resolution of the penumbra. In the 40–12.5 mm range, the PinPoint chamber may resolve the penumbra if used with its long axis parallel to the beam axis, but this more cumbersome set-up seems unnecessary when film and diodes are satisfactory.

No single detector, from the selection tested, can be used on its own to obtain reliable stereotactic beam data in the circular field size range 40–12.5 mm. Neither is the purchase of a stereotactic-specific detector necessary, nor the use of complicated data correction methods. Reliable stereotactic data can be obtained simply by careful comparison of three or more small detectors—ion chamber, unshielded diode, film. For output verification, one other detector is advised.

Fields smaller than 12.5 mm remain a problem. Although the measurement of PDDs and OARs is unlikely to present any dosimetric difficulties, the accurate determination of the output presents a greater challenge. The small ion chambers used in this study were too large in the 12.5 mm collimator and therefore cannot be used for smaller fields. Although the unshielded diodes may still be small enough, they should be used alongside another type of small detector. It may be that GafChromic film offers a method of determining the validity of the diode results and vice versa, but it should be assessed against ion chamber and diode measurements primarily in the larger collimators. This may be the subject of future work.

References

AAPM 1995 Stereotactic radiosurgery *AAPM Report* 54 (New York: American Institute of Physics)

Arcovito G, Piermattei A, D'Abramo G and Andreasi Bassi F 1985 Dose measurements and calculations of small radiation fields for 9MV x-rays *Med. Phys.* **12** 779–84

Beddar A S, Mason D J and O'Brien P F 1994 Absorbed dose perturbation caused by diodes for small field photon dosimetry *Med. Phys.* **21** 1075–9

Bjarngard B E, Tsai J-S and Rice R K 1990 Doses on the central axes of narrow 6MV x-ray beams *Med. Phys.* **17** 794–9

Br. J. Radiol. 1996 Central axis depth dose data for use in radiotherapy, equation 2(a) *Br. J. Radiol* (suppl 25) 156

Chierego G, Francescon P, Cora S, Colombo F and Pozza F 1993 Analysis of dosimetric measurements in linac radiosurgery calibration *Radiother. Oncol.* **28** 82–5

Chu R D H, Van Dyk G, Lewis D F, O'Hara K P J, Buckland B W and Dinelle F 1990 GafChromic™ dosimetry media: a new high dose, thin film routine dosimeter and dose mapping tool *Radiat. Phys. Chem.* **35** 767–73

Das I J, Downes M B, Corn B W, Curran J, Werner-Wasik M and Andrews D W 1995 Characteristics of a dedicated linear accelerator-based stereotactic radiosurgery-radiotherapy unit *Radiother. Oncol.* **38** 61–8

Dasu A, Lofroth P-O and Wickman G 1998 Liquid ionization chamber measurements of dose distributions in small 6 MV photon beams *Phys. Med. Biol.* **43** 21–36

Dawson D J, Harper J M and Akinradewo A C 1984 Analysis of physical parameters associated with the measurement of high-energy x-ray penumbra *Med. Phys.* **11** 491–7

Dawson D J, Schroeder N J and Hoya J D 1986 Penumbral measurements in water for high-energy x-rays *Med. Phys.* **13** 101–4

Fan C J, Devanna W G, Leybovich L B, Kurup R G, Hopkins B J, Melian E, Anderson D and Glasgow G P 1996–7 Dosimetry of very small (5–10 mm) and small (12.5–40 mm) diameter cones and dose verification for radiosurgery with 6-MV x-ray beams *Stereotact. Funct. Neurosurg.* **67** 183–97

Francescon P, Cora S, Cavedon C, Scalchi P, Reccanello S and Colombo F 1998 Use of a new type of radiochromatic film, a new parallel-plate micro-chamber, MOSFETs, and TLD 800 microcubes in the dosimetry of small beams *Med. Phys.* **25** 503–11

Gager L D, Wright A E and Almond P R 1977 Silicon diode detectors used in radiological physics measurements. Part 1: Development of an energy compensating shield *Med. Phys.* **4** 494–8

Guan T Y, Almond P R, Park H C, Lindberg R D and Shields C B 1993 Imaging of radiation dose for stereotactic radiosurgery *Med. Dosim.* **18** 135–42

Heydarian M, Hoban P W and Beddoe A H 1996 A comparison of dosimetry techniques in stereotactic radiosurgery *Phys. Med. Biol.* **41** 93–110

Higgins P D, Sibata C H, Siskind L and Sohn J W 1995 Deconvolution of detector size effect for small field measurement *Med. Phys.* **22** 1663–6

Houdek P V, Van Büren J M and Payos J V 1983 Dosimetry of small radiation fields for 10MV x-rays *Med. Phys.* **10** 333–6

Karlsson M G, Karlsson M, Sjogren R and Svensson H 1997 Semiconductors in output fctor measurement *Radiother. Oncol.* **42** 293–6

McLaughlin W L, Soares C G, Sayeg J A, McCullough E C, Kline R W, Wu A and Maitz A H 1994 The use of a radiochromic detector for the determination of stereotactic radiosurgery dose characteristics *Med. Phys.* **21** 379–88

Metcalfe P, Kron T, Elliott A and Wong T 1993 Dosimetry of 6 MV x-ray beam penumbra *Med. Phys.* **20** 1439–45

Niroomand-Rad A *et al* 1998 Radiochromic film dosimetry: recommendations of AAPM Radiation Therapy Committee Task Group 55 *Med. Phys* **25** 2093–115

Norrgard F S E, Sipila P M, Kulmala J A J and Minn H R I 1998 Dose characteristics of in-house-built collimators for stereotactic radiotherapy with a linear accelerator *Phys. Med. Biol.* **43** 1545–56

Podgorsak E B 1992 Physics for radiosurgery with linear accelerators *Neurosurg. Clin. North Am.* **3** 9–34

Rice R K, Hansen J L, Svensson G K and Siddon R L 1987 Measurements of dose distributions in small beams of 6 MV x-rays *Phys. Med. Biol.* **32** 1087–99

Rikner G and Grusell E 1985 Selective shielding of a p-Si detector for quality independence *Acta Radiol. Oncol.* **24** 65–9

Rustgi S N 1995 Evaluation of the dosimetric characteristics of a diamond detector for photon beam measurements *Med. Phys.* **22** 567–70

Sanders M, Sayeg J, Coffey C, Patel P and Walsh J 1993 Beam profile analysis using GafChromic films *Stereotact. Funct. Neurosurg.* **61** (suppl 1) 124–9

Serago C F, Houdek P V, Hartmann G H, Saini D S, Serago M E and Kaydee A 1992 Tissue maximum ratios (and other parameters) of small circular 4, 6, 10, 15 and 24 MV x-ray beams for radiosurgery *Phys. Med. Biol.* **37** 1943–56

Sibata C H, Mota H C, Beddar A S, Higgins P D and Shin K H 1991 Influence of detector size in photon beam profile measurements *Phys. Med. Biol.* **36** 621–31

Sixel K E and Podgorsak E B 1993 Build up region of high-energy x-ray beams in radiosurgery *Med. Phys.* **20** 761–4

Somigliana A *et al* 1999 Dosimetry of Gamma Knife and linac-based radiosurgery using radiochromic and diode detectors *Phys. Med. Biol.* **44** 887–97

Williamson J F, Khan F M and Sharma S C 1981 Film dosimetry of megavoltage photon beams: A practical method of isodensity-to-isodose curve conversion *Med. Phys.* **8** 94–8

Appendix 10

Radiotherapy & Oncology 64: 97-107 (2002)

ELSEVIER

Radiotherapy and Oncology 64 (2002) 97–107

RADIOTHERAPY & ONCOLOGY

www.elsevier.com/locate/radonline

Verification of the dose to the isocentre in stereotactic plans

Carolyn McKerracher*, David I. Thwaites

Oncology Physics, Edinburgh Cancer Centre, Western General Hospital, Edinburgh EH4 2XU, Scotland, UK

Received 31 January 2002; received in revised form 12 April 2002; accepted 10 June 2002

Abstract

Background and purpose: The aim of the study was: (a) to develop a simple, reproducible, technique to verify the dose to the isocentre, in a typical stereotactic treatment plan, for collimators from 12.5 to 40 mm in diameter; (b) to investigate a variety of detectors to compare different approaches; and (c) to introduce the technique into a quality assurance programme.

Material and methods: The symmetry, directional response and stability of calibration of a small 0.125 cm^3 ion chamber, a diamond and three types of diode (photon, electron and stereotactic) were tested. Correction factors were calculated to account for directional dependence, where appropriate and calibration factors were obtained to convert each reading to absorbed dose in water. Single arcs and typical four arc treatments were planned on XKnife and the dose to the isocentre verified in phantom with each usable detector.

Results: The ion chamber showed no asymmetry, the stereotactic diodes exhibited 4% and the others 1–2%. Maximum directional dependence was 1% for the ion chamber and diamond and 7–20% for the diodes. Correction factors were calculated to account for this. Only the response of the diodes decreased with cumulative dose; the response of the other detectors remained constant. The ion chamber, electron diode and diamond measured the dose in single arcs to within 1.5% of calculation, in the 40 and 12.5 mm collimators. The photon diode was within 3.5 and 2.5% in the largest and smallest collimators, respectively.

Conclusion: A simple method of verification was developed. The ion chamber, the diamond and the electron diode were found to be the best detectors to verify the dose to the isocentre in a typical multiple arc treatment for collimators between 40 and 12.5 mm in diameter. The technique has been incorporated into a quality assurance programme, using the ion chamber and diamond, on a twice yearly basis.

© 2002 Elsevier Science Ireland Ltd. All rights reserved.

Keywords: Stereotactic; Verification; Diodes; Diamond

1. Introduction

The introduction of any new radiotherapy technique to a department requires both the accurate measurement of the necessary beam data and a robust method of verification. The acquisition of stereotactic beam data is well documented in the literature [17,11], although the absence of a single, useful detector continues to prompt further research. The geometrical aspects of verification are also well documented [10,2], along with analyses of the set-up errors involved [7,19] but there is very little literature available on the dosimetric verification of stereotactic treatments.

There are two main aspects of dosimetric verification; verification of the planned dose distribution, and verification of the delivered dose. The accuracy of the dose distribution is dependent on the accuracy of the measurement of beam data such as off-axis ratios (OARs), percentage depth doses (PDDs) or tissue maximum ratios (TMRs), the accuracy of computed tomographic (CT) information, the planning system algorithm, and on the geometric set-up. Verification of all of these aspects is important to ensure both that the target volume is covered and critical structures avoided. The accuracy of the measurement of the delivered dose is dependent on the overall uncertainty associated with the calibration of a detector and the geometric set-up. Verification of the dose delivered is important in stereotactic treatments, as in all radiotherapy treatments, as clinical outcome is linked to target dose [12,13,16]. This paper is concerned only with the verification of the delivered dose, not the dose distribution.

The limited literature available on the subject of dosimetric verification of stereotactic treatments implies that it is not simple. Techniques are often complex and time consuming and the results are very dependent on the experimental set-up. Coffey et al. [1] used thermoluminescent dosimetry (TLD) powder and ferrous gel in a commercial water filled phantom, to measure both the absolute dose and the dose distribution. The differences between the measured and calculated doses differed from 0.1 to 4.5%. Guan et al. [6] used gel, TLD and radiochromic film in a head phantom. The experiments revealed differences between the expected

* Corresponding author.

0167-8140/02/$ - see front matter

© 2002 Elsevier Science Ireland Ltd. All rights reserved.

PII: S0167-8140(02)00142-1

and the measured dose from 5.5% to just less than 50%. Duggan and Coffey [3] used a micro-ionisation chamber (0.009 cm^3) in a commercial anthropomorphic phantom. The results for collimators between 16 and 32 mm diameter were within 2% of the calculated dose and their method appears robust, reproducible and accurate. Perks et al. [14] used a similar method, but with a larger ionisation chamber (0.2 cm^3) and only a 32.5 mm diameter collimator.

Commissioning of the stereotactic technique in this Cancer Centre began in 1994. As a result, a verification technique had to be developed based on the detectors available at that time. The smallest ion chamber was a 0.125 cm^3 cylindrical chamber and the smallest detectors were a photon and an electron diode. The technique had to be used to verify the dose delivered to the isocentre for a typical stereotactic plan, for all sizes of collimators. It had to be simple and reproducible and easy to implement on a routine basis as part of a quality assurance program.

Ion chambers are important detectors to use in the verification process as their calibration and use are well established and their properties and behaviour well understood. The main problem with a 0.125 cm^3 chamber is that it is too large to use in anything other than the largest collimators. Although diodes have the advantage of size, the directional dependence [15] is a problem, particularly in the measurement of non-coplanar beams. In addition, although they can be calibrated, their response changes with cumulative dose [4]. Consequently, any verification technique would have to take account these problems.

Recently a diamond detector and a stereotactic diode have been acquired. The main advantages of a diamond are its size, tissue equivalence and directional independence [8]. The stereotactic diode has the advantages of being smaller [17] and having less directional dependence than the conventional diodes.

Overall, the aim was to develop a technique to verify the dose to the isocentre, in a typical treatment plan, for all sizes of collimator. By investigating and accounting for the properties of a number of detectors, a range of methods could be used to incorporate the technique into a department's quality assurance programme.

2. Methods and materials

2.1. Detectors and electrometers

The detectors investigated and their corresponding properties are indicated in Table 1. The electron diode (EFD) is an unshielded diode recommended for use in electron beams and small ($<10\times10$ cm^2) photon beams. The stereotactic diode (SFD) is also an unshielded diode with an increased resolution, recommended for use in photon fields $<10\times10$ cm^2. The photon diode (PFD) is a shielded diode designed for use in photon fields only. It is energy compensated to attempt to match the response of an ion chamber in megavoltage photon beams $>10\times10$ cm^2. The manufacturer states that for relative output measurements in fields $<10\times10$ cm^2, any of the three diodes can be used, although the SFD is recommended for fields $<2\times2$ cm^2. The EFD, the PFD and the SFD were attached in turn, to the same channel on a DPD6 (Scanditronix) electrometer. The sensitivity of the channel was maximised.

The diamond is a solid state detector incorporating a naturally grown crystal. It was attached to a Unidos (PTW) electrometer and a bias of 100 V set. Prior to each measurement session, the diamond was pre-irradiated with a dose of approximately 10 Gy, according to the manufacturer's instructions.

The 0.125 cm^3 ion chamber (IC) was attached to a Farmer electrometer (NE Technology, Reading, UK) with a bias of 250 V.

The conventional orientation for these diodes and the diamond is with the cylindrical housing (long axes) parallel to the beam axis. A cylindrical ion chamber is, however, conventionally orientated with its long axis perpendicular to the beam. These conventional orientations were used for calibration.

2.2. Stereotactic hardware

The stereotactic hardware was purchased as a package (Radionics Inc). It includes a collimator housing, which is fixed to the base plate of the head of the linac, twelve divergent collimators with diameters in the range 40–12.5 mm (at the isocentre), a couch mount and a Gill–Thomas–Cosman (GTC) relocatable stereotactic frame [5].

Table 1
Summary of detectors used and their most important properties

Manufacturer	Detector type	Abbreviation	Volume (cm^3)	P (eff) [a] (mm)	Active size (mm)	Physical size (mm)
Scanditronix AB, Uppsala, Sweden	Electron diode	EFD	29×10^{-3}	+0.4[b]	2.5	7
Scanditronix	Stereotactic diode	SFD	1.7×10^{-3}	+0.5[b]	0.6	5
Scanditronix	Photon diode	PFD	29×10^{-3}	+0.6[b]	2.5	7
PTW, Freiburg, Germany	Ion chamber (W233642)	IC	0.125	−1.4[b]	$d=5.5$	6.5
				+4.5[c]	$l=6.5$	+0.75w
PTW	Diamond	Diam	1.8×10^{-3}	+1	2.2	7.3

[a] P(eff) is the effective point of measurement.
[b] Indicates distance along beam CAX.
[c] Indicates distance from the tip of the chamber along its own axis. d, chamber inner diameter (cross section); l, chamber inner length (along axis); w, chamber wall thickness. Active size is the dimension of the sensitive area directed towards the radiation beam.

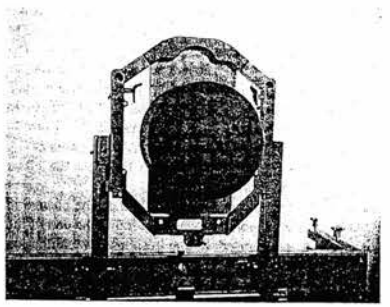

Fig. 1. Photograph of the stereotactic phantom attached to the GTC frame. Note the two 1 cm diameter holes drilled for the detectors and inserts.

2.3. Phantom

The phantom is shown in Fig. 1. It is made of WT1, an epoxy-resin based water equivalent phantom material, produced at St Bartholomew's Hospital in London. The design was loosely based on the water-filled phantom used at the Royal Marsden in London [14] and was attached to the GTC relocatable stereotactic frame. The shape is basically cylindrical, terminating in an 8 cm radius hemispherical section furthest from the frame. One centimeter diameter holes were drilled to full length of the phantom both at the centre and at 3 cm off-axis. Inserts of the same material were made to fit the holes and to hold each of the detectors under investigation.

Fig. 2 shows a diagrammatic view of the phantom. Position A is located within the cylindrical section of the phantom, 10 cm from the hemispherical end and in the middle of the central hole. Position B is also located in the middle hole, but at 2 cm from A, towards the hemispherical end, at the origin of the hemisphere. Position C is located in the off-axis hole, at 4 cm from A.

The phantom was CT scanned with 3 mm slice thickness and separation and the slices transferred via the local network to the planning system.

2.4. Planning system

XKnife version 4.1 (Radionics Inc) was used to plan the treatments. The beam data on XKnife was measured according to previously published recommended methods [11], although the final output figures in the planning system have since been updated to those measured with the diamond.

Monitor units (MU) are calculated as:

$$MU = D/\Psi$$

where D is the delivered dose and Ψ is the XKnife relative scatter factor. This is a measured output, normalised to our reference geometry (10×10 cm^2, 100 cm FSD, dmax) and multiplied by the TMR. It should be noted that although the standard calibration conditions in this department are FSD, XKnife requires that collimator outputs be measured under isocentric conditions.

2.5. Linac

All measurements were carried out on a Varian (Palo Alto, USA) 600CD 6 MV accelerator (quality index (TPR(20/10) = 0.663). The gantry and couch angles are set according to Fig. 3.

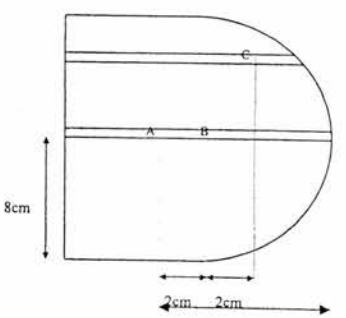

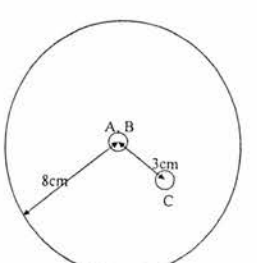

Fig. 2. Diagram of the stereotactic phantom, viewed in cross-section from the side and the end. A and B are points lying along the central hole and C lies in the off-axis hole.

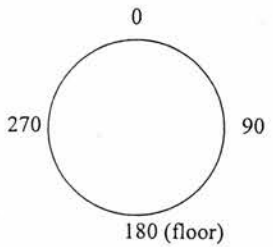

Gantry angle settings

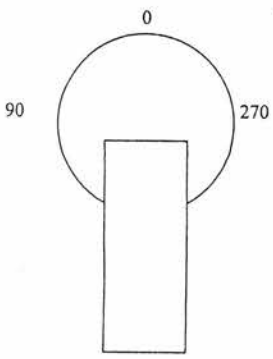

Couch angle settings

Fig. 3. The orientation of the gantry angles, viewed towards the gantry and the floor angles, viewed from above.

2.6. Symmetry and directional dependence

The symmetry and directional dependence of each detector is shown in Fig. 4. Symmetry is defined here as the relative radial response around the axis of the detector. It was measured by placing the effective point of measurement for each detector at position A in the phantom. Position A was then placed at the position of the radiation isocentre, averaged over the four principal gantry angles. The couch was positioned at 0° and measurements were initially made in static beams at the four principal gantry angles. These were compared with the results for the gantry fixed at 0° but with each detector rotated around its axis to achieve the same beam-detector alignments. This ensured that the phantom and set-up were symmetric and that there was an acceptable linac dose variation with gantry angle (±0.5%). The measurements were then carried out for gantry positions between 0 and 350° in 10° intervals. The response at each angle was normalised to the response at 0°. Changes in detector response caused by moving the detector 1 mm in the superior–inferior direction were also investigated by adding a 1 mm spacer to the channel to assess the effect of positional misalignment.

Directional dependence is defined here as the change in response of the detector at any angle, around the end of the detector axis, normalised to the response at calibration geometry. It was measured by placing the centre of the measurement volume at position B, rotating the couch to 90° and making measurements in static beams at 10° intervals from gantry 0 to 180°. The diode was then turned through 90° and the measurements repeated, to compare the results over

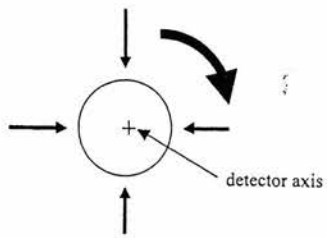

Symmetry

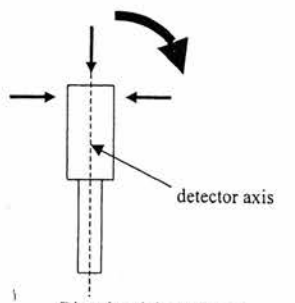

Directional dependence

Fig. 4. Orientation of detectors for measurements of symmetry and directional dependence. The solid arrows indicate the directions of rotation around the axis of the detector (symmetry) and around the end of the detector axis (directional dependence).

two axes. The use of inferior arcs in a treatment plan would require the investigation of directional dependence beyond the 0–180° gantry limits. However, as this would require the use of a spherical phantom and as inferior arcs are not used in this department, to avoid the potential for collision, these gantry angles were not measured.

For both symmetry and directional dependence, exposures of 100 MU were used for all detectors other than the SFD. The small signal to noise ratio of the SFD necessitated the use of exposures of 500 MU.

2.7. Correction factors

Correction factors (CFs) were calculated as the inverse of the directional dependence. These were curve fitted on Origin version 6 (Microcal Software Inc, MA, USA). CFs for all possible combinations of gantry (θ) and floor (α) angle. CF (θ ,α), were calculated by defining an effective angle (γ) as:

$$\gamma = \theta \sin \alpha$$

These CFs were then integrated over the appropriate gantry arc, to obtain one CF for each beam.

2.8. Calibration

Each detector was initially calibrated against the IC following the procedures and using factors traceable to the IPSM (1990) Code of practice [9] and the UK primary standards (NPL). Although the standard calibration conditions used in this department are fixed FSD, the stereotactic detectors were calibrated under isocentric conditions, which are the conditions under which the relative outputs were measured. This resulted in the following reference conditions:

10×10 cm^2 field size
5 cm deep
100 cm FAD
water equivalent phantom (WT1)

A CAL factor was obtained for each detector, defined as follows:

$$\mathrm{CAL} = \frac{R(\mathrm{IC}) \times \mathrm{Fx}' \times TP}{R(\mathrm{detector})}$$

where R is the reading on the electrometer for the appropriate detector, Fx′ is the traceable departmental calibration factor for the IC and electrometer to convert its reading to dose in water and TP is the temperature and pressure correction.

CAL factors were also obtained in a 5×5 cm^2 field to investigate conditions nearer the stereotactic situation. In addition, relative output factors for a 5×5 cm^2 field (100 cm FAD, 5 cm deep) were measured with each detector.

2.9. Calculation of dose

The calculated, or planned dose on XKnife, was calculated as:

$$D_c = \mathrm{MU} \times \psi$$

The measured dose for each detector was obtained from:

$$\mathrm{Dm} = R \times \mathrm{CAL} \times \mathrm{CF}(\gamma) \times \mathrm{OP}(\times TP)$$

where OP is the routine output correction for the machine on the day of measurement. TP is only used for IC measurements.

2.10. Single arcs

Single field rotations at position A were planned with the couch at 0° and gantry rotations of 20–120° and 240–340°. Exposures of 200 MU were delivered and the dose to the isocentre calculated and then measured. These single arcs were used to verify the methodology.

2.11. Plans

Generally, this department's approach is to use four to five arcs for a patient's treatment, with angles selected both to avoid sensitive structures and to shape the dose distribution. Inferior arcs are not used to avoid the potential problem of a collision between the couch and gantry. For the verification measurements, a plan for each collimator size was designed to include a variety of typical arcs and couch positions, with the isocentre at position B. MUs were calculated to give 17.5 Gy to the 90% dose region, which is the prescription used for single fraction treatments of arteriovenous malformations (AVMs).

To test the validity of the method for isocentres of different depths, plans were also calculated at position C, the off-axis position. The plan parameters for each situation are shown in Table 2.

2.12. Radiation isocentre

The position of the radiation isocentre with respect to the position of the lasers was determined using the Wintson Lutz test [18] for the four principal gantry angles (0°, 90°, 180°, 270°). The centre of the measurement volume for each detector was placed at the mean position of the radiation isocentre, averaged over all arcs, for each individual plan.

2.13. Uncertainties

In all experiments (symmetry, directional dependence, plans etc), measurements were carried out on at least three separate occasions. The mean, standard deviation (SD) and coefficient of variation (CV) were calculated. The CV is taken to be a measure of the reproducibility. The uncertainties in the calculated dose arise from the input data to the planning system. The uncertainties in the measured dose are a combination of the uncertainties in the electrometer read-

Table 2
Basic plan parameters for plans with isocentre positions at (a) B and (b) C, for both the 40 and 12.5 mm collimators[a]

Beam	Couch	Gantry start	Gantry end	Mean depth (mm)	40 mm collimator MU	12.5 mm collimator MU
(a)						
1	15	20	120	80	848	972
2	345	240	340	80	848	972
3	60	50	90	80	339	388
4	300	240	300	80	509	584
(b)						
1	15	20	120	65.5	793	901
2	345	240	340	41	717	797
3	60	50	90	42.6	288	321
4	300	240	300	35.4	421	465

[a] The MU to deliver 1945 cGy to the isocentre, in each case, are shown.

ing, detector calibration, calculation of correction factors and phantom and detector positional uncertainties. In each case, the overall uncertainty (1 SD) was calculated as the root mean square of their constituent parts.

3. Results

3.1. Symmetry

The symmetry of each detector is shown in Fig. 5. All detectors, other than the ion chamber, exhibit some degree of asymmetry. The diamond and the EFD show asymmetry of up to approximately 1%, the PFD and the SFD show up to approximately 1.5 and 3.5%, respectively. The reproducibility (CV) of each detector, other than the SFD, was 0.2%. The SFD reproducibility was 2%. The comparison of rotating gantry angle and fixed detector with fixed gantry and rotating detector showed differences close to the general reproducibility.

When the detector was moved by 1 mm in the superior–inferior direction (using the spacer), in the 40 mm collimator, there was no change in signal. However, when the test was carried out in the 12.5 mm collimator for comparison, the signal increased by less than 1% when the detector was moved 1 mm inferiorly at gantry 0° and by almost 2% at gantry 180°.

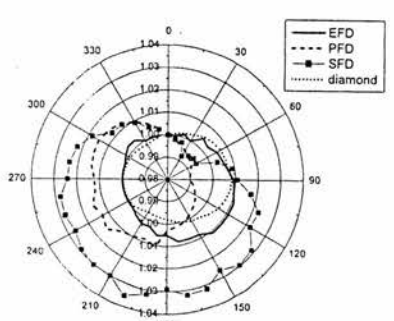

Fig. 5. Graph of symmetry against gantry angle for couch at 0°, for each detector . Values normalised to the response at gantry 0°.

3.2. Directional dependence

Fig. 6 shows the directional dependence of each detector, averaged across the two main axes and made symmetrical. The results for the SFD, EFD and PFD follow a parabolic shape with minimum responses of 93, 87 and 80%, respectively, at gantry 0 and 180°. The results are normalised to gantry 90°. The reproducibility is better than 0.5% for the EFD, and the measurements across the two axes are the same. Although the reproducibility of the PFD is also within 0.5%, the maximum difference between axes is ±2%. The reproducibility of the SFD measurements is 0.2%, but the difference between the two axes is +3 to −1%. In addition, there is a maximum of 2% difference between each half of the curve (0–90° and 90–180°).

Both the diamond and the ion chamber show a very small

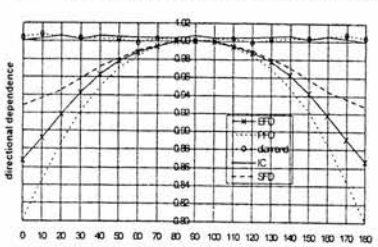

Fig. 6. Graph of directional dependence against gantry angle for couch at 90° and gantry between 0 and 180°. Values normalised to the response at the calibration orientation for each detector.

Table 3
An example table of CFs for the EFD, for combinations of gantry (θ) and couch angle (α) (these are used to account for directional dependence)

		Gantry									
		0	10	20	30	40	50	60	70	80	90
	0	1.155	1.155	1.155	1.155	1.155	1.155	1.155	1.155	1.155	1.155
	10	1.155	1.148	1.141	1.135	1.129	1.123	1.117	1.111	1.106	1.100
	20	1.155	1.142	1.129	1.118	1.107	1.096	1.086	1.077	1.068	1.060
	30	1.155	1.136	1.119	1.102	1.088	1.074	1.062	1.051	1.041	1.032
Couch	40	1.155	1.131	1.109	1.090	1.072	1.057	1.043	1.032	1.022	1.014
angle	50	1.155	1.126	1.101	1.079	1.060	1.044	1.030	1.019	1.011	1.005
	60	1.155	1.123	1.095	1.072	1.051	1.035	1.021	1.011	1.005	1.001
	70	1.155	1.121	1.091	1.066	1.045	1.029	1.016	1.007	1.002	1.000
	80	1.155	1.119	1.088	1.081	1.042	1.025	1.013	1.005	1.001	1.000
	90	1.155	1.119	1.088	1.062	1.041	1.024	1.012	1.004	1.000	1.001

amount of directional dependence of less than 1%. Both the detectors show an increase in response when irradiated normal to their calibration orientation. Note that the ion chamber results are normalised to gantry 0° whereas all the others are normalised to gantry 90°. This is due to the 90° difference in conventional orientation. The reproducibility of these results is better than 0.5% for both detectors and the measurements across the two axes are the same. The difference between the origin fitted values for directional dependence and the mean measured values was less than 0.3% for each detector.

3.3. Correction factors

Table 3 shows an example of a CF table calculated for the EFD for couch and gantry angles between 0 and 90°. Similar tables were calculated for all combinations of couch and gantry angle and for all detectors.

3.4. Calibration factors

Table 4 shows CAL values averaged over five sets of measurements of each detector against the IC in both a 10×10 cm^2 field and a 5×5 cm^2 field. The reproducibility of all measurements is approximately 0.5%. The differences between the calibrations in a 5×5 cm^2 and those in a 10×10 cm^2 field are very small for all detectors other than the SFD where the difference is 1.2%.

Table 5 shows the results for the ratio of a 5×5 cm^2 field to a 10×10 cm^2 field (100 cm FAD, 5 cm deep), for each detector, again measured on five separate occasions over a 5-day period. The reproducibility is within 0.2%. There are only small differences between the results for each detector and the results for the IC, other than for the SFD, which is 1.1% lower than the IC.

Calibrations carried out 2 months prior to the ones shown differed from the current ones by between 10 and 20% for each of the diodes. During this period, the PFD and EFD had been subject to a cumulative dose of approximately 200 Gy and the SFD to approximately 1000 Gy.

3.5. Uncertainties

The overall uncertainty estimated for the calculated dose is between 0.3 and 0.6% (1 SD), being larger for the smaller collimators. The uncertainty in the measured dose is estimated (at 1 SD) for each detector individually and found to be typically 0.5% for the IC and the diamond, 0.7% for the EFD, 1.3% for the PFD and 2.2% for the SFD. These figures should be applied to all of the following results. The SFD was not used for any dose measurements due to the large uncertainty associated with it.

3.6. Single arcs

Table 6 shows the results for rotations at position A for a 40 mm collimator for all detectors other than the SFD and for a 12.5 mm collimator for all detectors other than the SFD and IC. As the signal on the detectors increased by 1–2% in the 12.5 mm collimator when the 1 mm spacer was added, the extra spacer was used in both collimators. The CV is less than 0.5%. The difference between the calcu-

Table 4
Comparison of calibration factors (CAL values) for each detector in a small (5×5 cm^2) and a large (10×10 cm^2) field[a]

Detector	10×10	Coefficient of variation	5×5	Coefficient of variation	Difference
IC			1.0000		0.0
PFD	0.0243	0.5	0.0242	0.5	−0.2
EFD	0.0367	0.6	0.0369	0.5	0.4
SFD	0.3968	0.2	0.4016	0.2	1.2
Diamond	0.0925	0.4	0.0928	0.4	0.3

[a] All measurements were made on five separate occasions and the coefficient of variation (CV), as a % of the mean value, obtained.

Table 5
Comparison of a relative output ($5 \times 5\ cm^2/10 \times 10\ cm^2$, 100 cm FAD, 5 cm deep) measured with each detector and compared against the IC[a]

Detector	Relative factor	Coefficient of variation	Compared to IC
IC	0.934	0.2	0.0
PFD	0.937	0.0	0.3
EFD	0.930	0.1	−0.4
SFD	0.923	0.0	−1.1
Diamond	0.931	0.1	−0.2

[a] All measurements were made on five separate occasions and the coefficient of variation (CV), as a % of the mean value, obtained.

lated dose (D_c) and the measured dose (D_m) is between 0 and 1.1% for the 40 mm collimator and 0.3 and 3.1% for the 12.5 mm collimator, the largest differences being for the PFD. There is a difference between measurements at one side of the phantom (D_{m1}) compared with the other (D_{m2}), of the order of 0.5% for the EFD and PTW, 1% for the diamond and 2% for the PFD.

3.7. Plans

Table 7 shows the results for both collimators. The CV is better than 1% for all of the results. The best results in the 40 mm collimator are for the IC and the diamond. The differences between D_c and D_m are less than 0.5% for the total dose to the isocentre and all but one of the beams. The differences for the EFD are a little higher, with all differences falling within 1% for all beams other than beam 2, which is within 1.5%. The largest differences are for the PFD where everything lies within 2.5% for all beams other than beam 1 which is within 3.5%.

In the 12.5 mm collimator plan, the results for the EFD and the diamond are comparable with those for the 40 mm collimator which suggests that the positioning of the detector within the 12.5 mm collimator is good. The diamond again shows the smallest differences, with all measurements within 0.5%. The PFD again shows the largest differences although the results for individual beams appear to be slightly better than for the 40 mm collimator. Measurements were also made with the 1 mm extra spacer and no difference was found for either collimator size.

Table 8 shows the results for the off-axis plan at position C, with both collimators. Only one single measurement has been made at this position to date. The results are comparable with those at position B in the 40 mm collimator; the IC and the diamond show the best results with all differences better than, or around 0.5%. The differences for the EFD are less than or around 1.5%. The PFD again shows the highest differences, but with a maximum difference of 2.2% for the 12.5 mm collimator plan. The 12.5 mm collimator results for the PFD and the EFD are comparable with the 40 mm collimator, but for the diamond they are slightly higher.

In all of the above plans there was no change in signal with the addition of the 1 mm spacer.

4. Discussion

4.1. Symmetry

The comparison of the rotating gantry and fixed detector with the fixed gantry and rotating detector showed that the asymmetry was a result of the detector only and not due to phantom asymmetry or linac dose variation with gantry angle. For solid-state detectors, the effective centre of the measurement volume is usually assumed to lie on the CAX of the detector. The results in Fig. 5 show clearly that this is not the case. Small amounts of asymmetry displayed by the EFD, PFD and diamond may not be significant for measurements in routine X-ray beams. However, they may present a problem when trying to align the centre of the detector with the centre of the beam to measure OARs and PDDs in very small fields.

It is interesting to note that the asymmetry does have a line of approximate symmetry about it. As a result, each detector was rotated around its axis to try to align the line of symmetry with the beam CAX for gantry 0°. It is apparent from Fig. 5 that this has not quite been achieved. This is

Table 6
Comparison of the measured dose (D_{m1}, D_{m2}) against the calculated dose (D_c) for single arcs at position A, with a (a) 40 mm collimator and a (b) 12.5 mm collimator[a]

Detector	20–120°				240–340°			Compared to D_{m1} %
	D_c	D_{m1}	CV	Difference %	D_{m2}	CV	Difference %	
(a)								
EFD	152.8	153.3	0.3	0.3	152.5	0.5	−0.2	−0.5
PFD	152.8	151.6	0.3	−0.8	154.5	0.2	1.1	1.9
IC	152.8	153.1	0.2	0.2	152.6	0.3	−0.2	−0.3
Diamond	152.8	154.5	0.4	1.1	152.8	0.1	0.0	−1.1
(b)								
EFD	133.2	134.4	0.3	0.9	133.6	0.4	0.3	−0.5
PFD	133.2	134.7	0.5	1.1	137.3	0.3	3.1	1.9
Diamond	133.2	134.7	0.3	1.1	133.9	0.2	0.6	−0.6

[a] All measurements were made on three separate occasions and the coefficient of variation (CV), as a % of the mean value, obtained.

Table 7
Comparison of the difference between the measured dose and the calculated dose for plans at position B, with a (a) 40 mm collimator and a (b) 12.5 mm collimator[a]

Beam	% EFD difference	Coefficient of variation	% PFD difference	Coefficient of variation	% Diamond difference	Coefficient of variation	% PTW difference	Coefficient of variation
(a)								
1	−0.6	0.9	−3.3	0.4	0.3	0.6	−0.1	0.4
2	−1.4	1.0	−2.2	0.5	−0.7	0.9	−0.4	0.4
3	0.0	0.7	−1.8	0.7	0.2	0.3	0.4	0.4
4	−0.4	0.9	−1.8	0.7	−0.2	0.3	−0.2	0.2
Total	−0.8	0.9	−2.4	0.5	−0.2	0.0	−0.1	0.3
(b)								
1	−0.7	0.7	−2.3	0.9	0.2	0.3		
2	−1.2	0.9	−0.6	0.3	0.1	0.2		
3	0.7	0.8	−0.2	0.5	0.1	0.3		
4	0.7	0.6	0.7	0.6	0.1	0.3		
Total	−0.4	0.8	−0.9	0.5	0.1	0.3		

[a] All measurements were made on three separate occasions and the coefficient of variation (CV), as a % of the mean value, obtained.

because it is difficult to physically turn the diodes by small amounts simply because the cable tends to pull in a particular direction. To improve the alignment, a rigid fixing system could be used.

According to the manufacturer, the results are not surprising. In the case of the EFD, the materials surrounding the chip may not be uniform and the chip itself may not lie at the exact centre of the encapsulation. In addition, there are electrical connections and other features of design and construction that are not necessarily cylindrically symmetric. The same is true of the PFD but with the additional problem that the high-density material used for energy compensation may not be spatially uniform. Positioning the chip at the centre of the SFD, perfectly level, is also much more difficult in the SFD, which accounts for its larger asymmetry. The fact that the SFD measurements are the least reproducible may in part be due to the small signal to noise ratio and also because small differences in position between measurement sessions will lead to large differences in symmetry.

According to the manufacturer, the diamonds are naturally grown and therefore unlikely to be symmetrical. The percentage asymmetry for each detector was converted to a percentage change in TMR and then to a depth in water. This corresponded to a shift in the effective point of measurement of each detector away from the geometric centre by 1.2 mm (EFD), 2.7 mm (PFD), 1.1 mm (diamond) and 4.2 mm (SFD). However, this is not a true measure of effective point shift because asymmetry in response can also be caused by other factors, as briefly discussed above.

The increase in signal in the 12.5 mm collimator indicates that the effective point of measurement was not in fact placed at the radiation isocentre. The use of an average radiation isocentre position, rather than individual ones for each gantry angle, will cause more of a problem in the small collimator.

4.2. Directional dependence

Directional dependence is an inherent property of diodes and the results for the diodes are to be expected. Rikner and Grusell [15] quote the maximum directional dependence as 95% for the EFD and 85% for the PFD, both at 8 MV at 5 cm deep in a narrow beam. The measurements here show more directional dependence than that quoted, in particular for the EFD. However, because the directional dependence follows a parabolic shape, the expected values for any combination of couch and gantry angle can be predicted. The difference in directional dependence across the two axes is caused mainly by the asymmetry of the detectors. These differences correspond to the values of asymmetry at the corresponding positions, but with some differences due to the different set-ups for the measurement of the two parameters; symmetry is measured at position A and directional

Table 8
Comparison of the difference between the measured dose and the calculated dose for plans at position C, with a (a) 40 mm collimator and a (b) 12.5 mm collimator (measurements were made on only one occasion)

Beam	% EFD difference	% PFD difference	% Diamond difference	% PTW difference
(a)				
1	−0.8	−2.2	−0.4	−0.4
2	−0.7	−2.2	−0.6	−0.2
3	1.6	0.5	0.2	1.0
4	0.4	0.2	−0.3	−0.2
Total	−0.2	−1.4	−0.4	−0.1
(b)				
1	−1.3	−2.1	−1.1	
2	−1.0	−2.1	−1.1	
3	1.8	1.5	−0.3	
4	0.4	1.3	−1.3	
Total	−0.5	−0.9	−1.0	

dependence is measured at position B. All of these will lead to uncertainties associated with the CFs.

Averaging of the results for the SFD will lead to much larger uncertainties. It would therefore be more appropriate to calculate CFs in 3D for the SFD. Although this is possible, it seems unnecessary if the SFD offers no advantages over the other detectors.

The diamond exhibits a small amount of directional dependence whereby the response increases by 1% when it is irradiated with its long axis perpendicular to the beam. The IC also has an increase in response of around 1% when irradiated with its long axis parallel to the beam, possibly due to the shift in the effective point of measurement from one orientation to the other.

4.3. Correction factors

A table of correction factors is sufficient for simple calculations, but a mathematical model could be used instead.

4.4. Calibration factors

The differences between the calibrations in the 5×5 cm^2 field and the 10×10 cm^2 field are interesting. Although the differences for most of the detectors are small, they are reproducible and only the SFD displays a significant difference. From the results for the $5 \times 5/10 \times 10$ ratio, it appears that the SFD significantly underestimates the dose in a small field. Although each of the other detectors displays only a very small difference of the order of the experimental uncertainty, the differences are reproducible and consistent with other work [11] suggesting that these are real effects. However, it would appear that the SFD is the worst detector for measuring the output in a small field. This is in conflict with the manufacturer's recommendations.

Although the reproducibility of the calibrations over the period of 5 days is very good, during this period the detectors were only used for the calibrations. Over the 2 months period prior to these calibrations, the EFD and PFD were used extensively in commissioning and although the SFD had not been used for commissioning, it had also been subject to a high dose in the investigation of symmetry and directional dependence. However, the cumulative dose of 200 Gy to the EFD and PFD is less than the recommended re-calibration limit for patient diodes and the percentage decrease in calibration is much higher than expected [4]. As a result, CAL values were always measured for each detector against the IC, in a 5×5 cm^2 field, immediately prior to measurements in phantom.

4.5. Uncertainties

To have confidence in measurements to verify the dose to the isocentre, it is important that the uncertainty is minimised. The detectors with minimum uncertainty were the IC, diamond and the EFD, which suggests that these are the optimum detectors to use.

Positioning uncertainties in the verification process are comparable with the treatment process. For example, errors introduced by the CT slice thickness can lead to uncertainties of position of ± 1 mm [19]. Although the treatment process includes errors introduced by the patient, phantom measurements introduce other uncertainties. The absolute depth of the effective point has uncertainty associated with it, quoted as ± 0.15 mm for the diode. In addition, each sleeve is drilled with an uncertainty of approximately ± 0.1 mm. These uncertainties were minimised during the symmetry and directional dependence measurements by finding the position of the maximum signal. This implies coincidence of the effective point and the radiation isocentre.

4.6. Single arcs

The reproducibility for all measurements is very good. The differences between the expected and measured doses for these single fields give some indication of the errors introduced both by rotational fields and by averaging the directional dependence over the two axes. The IC is the only symmetrical detector and the consistent difference of -0.3% from one side is an indication of asymmetry in the set-up of the phantom, or in the phantom itself. The differences from one side to the other for the other detectors are consistent with their measured asymmetry.

The 1–2% difference in dose caused by a 1 mm positional error is due to the high dose gradient. The width of the 99% region in the 12.5 mm collimator is approximately 1.5 mm [11] and the width of the 100% is <0.5 mm.

From previous unpublished work, the relative output measured for each detector in a 12.5 mm collimator can be normalised to that for the diamond. The differences are indicative of the field size effect exhibited by diodes in these small fields. From the results in Table 6, the ratio of the measured dose in the 12.5 mm collimator to the 40 mm collimator, can be normalised to the ratio for the diamond. This same field size effect is seen. This implies that a field size correction could be applied to the diode results, accounting for changes in response due to the varying contribution of scatter. These corrections are less than 1% for the EFD and SFD and up to 2% for the PFD. These variations due to scatter results will form part of a future publication on scatter in small fields. Use of these corrections would improve the results.

4.7. Plans

The correspondence of the diamond and the EFD results with the IC in the 40 mm collimator, for position B, give confidence in the methodology. The diamond, with the least directional dependence of the solid-state detectors, is obviously the best detector to use in the smallest collimator, although the results for the EFD are still very good. Although the PFD has a larger error associated with it due to the larger asymmetry, the results are consistently low, suggesting a systematic error, which should be investigated further. For this reason, the PFD is not recommended for this type of work.

It is obvious that in the smallest collimator either the diamond or the EFD can be used to obtain accurate and reproducible results to within 1%. The fact that the 1 mm spacer made no difference to the signal on the detectors confirms that the width of the high dose region is increased through the use of multiple, rotational fields.

Plans at position C were carried out only once simply to verify that variations in depth and isocentre position did not affect the results. The results for all detectors are comparable with those at position B, showing that the method can be applied to plans at any position within the available channels in the phantom.

Field size corrections similar to those outlined for the single arcs could be applied to these results in the same way. Again, this would improve the correspondence between the measured and calculated doses.

4.8. Quality assurance

The technique has been incorporated into the department's quality assurance programme. As patient numbers are low (approximately 12 per year) the check is carried out only twice per year. If patient numbers increase, the frequency of the check will be increased.

For each check, the phantom is CT scanned and the images are transferred to XKnife where a typical plan is created for one collimator (a different collimator is selected on each occasion). For collimators ≥ 32.5 mm, the IC is used and for all other collimators, the diamond. Its calibration is verified against the IC at each measurement session. If the measured dose per beam differs from the calculated dose by >2% then all stereotactic treatments must be stopped until the differences are resolved. If the differences are between 1 and 2% then further investigations should be carried out, but stereotactic treatments can continue.

5. Conclusion

A simple, reproducible method of verifying the dose to the isocentre in two typical stereotactic plans, for a large (40 mm) and a small (12.5 mm) collimator has been developed. The symmetry and directional dependence of response for a range of detectors was investigated and correction factors calculated to account for them. The calibration of each detector was investigated over time and the recommendation made that diodes should be calibrated prior to each plan measurement. In addition, calibrations should be carried out in a 5×5 cm^2 field to be closer to the stereotactic situation. The asymmetry of the stereotactic diode and the fact that it underestimates the dose in a 5×5 cm^2 field make it unsuitable for this type of work. The 0.125 cm^3 ion chamber, the EFD and the diamond are the most accurate detectors to use in the 40 mm collimator. The electron diode and the diamond are the most accurate detectors in the 12.5 mm collimator. The PFD could possibly be used with a more accurate set-up. In all cases, the detectors must be positioned at the mean position of the radiation isocentre. The technique has been incorporated into the departmental quality assurance programme.

References

[1] Coffey CW, Sanders M, Cashon K, Miller R, Walsh J, Patel P. A tissue equivalent phantom for stereotactic radiosurgery localization and dose verification. Stereotact Funct Neurosurg 1993;61:130–141.
[2] Colombo F, Francescon P, Cora S, Cavedon C, Terrin G. A simple method to verify in vivo the accuracy of target coordinates in linear accelerator radiosurgery. Int J Radiat Oncol Biol Phys 1998;41:951–954.
[3] Duggan DM, Coffey CW. Use of a micro-ionization chamber and an anthropomorphic head phantom in a quality assurance program for stereotactic radiosurgery. Med Phys 1996;34:513–516.
[4] Essers M, Mijnheer B. In vivo dosimetry during external photon beam radiotherapy. Int J Radiat Oncol Biol Phys 1999;43:245–259.
[5] Gill SS, Thomas DGT, Warrington AP, Brada M. Relocatable frame for stereotactic external beam radiotherapy. Int J Radiat Oncol Biol Phys 1991;20:599–603.
[6] Guan TY, Almond PR, Park HC, Lindberg RD, Shields CB. Imaging of radiation dose for stereotactic radiosurgery. Med Dosim 1993;18:135–142.
[7] Hartmann GH, Bauer-Kirpes B, Serago CF, Lorenz WJ. Precision and accuracy of stereotactic convergent beam irradiations from a linear accelerator. Int J Radiat Oncol Biol Phys 1993;28:481–492.
[8] Heydarian M, Hoban PW, Beckham WA, Borchardt IM, Beddoe AH. Evaluation of a PTW diamond detector for electron beam measurements. Phys Med Biol 1993;38:1035–1042.
[9] IPSM code of practice for high-energy photon therapy dosimetry based on the NPL absorbed dose calibration service. Phys Med Biol 1990;35:1355–1360.
[10] Kortmann RD, Becker G, Perelmouter J, Buchgeister M, Meisner C, Bamberg M. Geometric accuracy of field alignment in fractionated stereotactic conformal radiotherapy of brain tumors. Int J Radiat Oncol Biol Phys 1999;43:921–926.
[11] McKerracher C, Thwaites DI. Assessment of new small-field detectors against standard field detectors for practical stereotactic beam data acquisition. Phys Med Biol 1999;44:2143–2160.
[12] Mendenhall WM, Friedman WA, Buatti JM, Bova FJ. Preliminary results of linear accelerator radiosurgery for acoustic schwannomas. J Neurosurg 1996;85:1013–1019.
[13] Miller RC, Foote RL, Coffey RJ, et al. Decrease in cranial nerve complications after radiosurgery for acoustic neuromas: a prospective study of dose and volume. Int J Radiat Oncol Biol Phys 1999;43:305–311.
[14] Perks JR, Rosenberg I, Warrington AP. Dose quality assurance for stereotactic radiotherapy treatments. Phys Med Biol 1999;44:N209–N215.
[15] Rickner G, Grussell E. Selective shielding of a p-Si detector for quality independence. Acta Radiol Oncol 1985;24:65–69.
[16] Simonova G, Liscak R, Novotny Jr J, Novotny J. Solitary brain metastases treated with the Leksell gamma knife: prognostic factors for patients. Radiother Oncol 2000;57:207–213.
[17] Westermark M, Arndt J, Nilsson B, Brahme A. Comparative dosimetry in narrow high-energy photon beams. Phys Med Biol 2000;45:685–702.
[18] Winston KR, Lutz W. Linear accelerator as a neurosurgical tool for stereotactic radiosurgery. Neurosurgery 1988;22:454–464.
[19] Yeung D, Palta J, Fontanesi J, Kun L. Systematic analysis of errors in target localization and treatment delivery in stereotactic radiosurgery (SRS). Int J Radiat Oncol Biol Phys 1993;28:493–498.

References

Adams E J, Suter B L, Warrington A P, Black P, Saran F and Brada M (2001) Design and implementation of a system for treating paediatric patients with stereotactically-guided conformal radiotherapy *Radiotherapy and Oncology* 60: 289-297

Alder J R and Cox R S (1995) Preliminary experience with the Cyberknife: Image Guided Stereoractic Radiosurgery *Radiosurgery* 317-326 (Karger)

Alderson S W, Lanzl L H, Rollins M and Spira J (1962) An instrumented phantom system for analog computation of treatment plans *British Journal of Radiology* 87: 185-195

Allahverdi M. (1998) Accuracy in Radiotherapy. PhD thesis, University of Edinburgh.

Allahverdi M, Nisbet A and Thwaites D I (1999) An evaluation of epoxy resin phantom materials for megavoltage photon dosimetry *Physics in Medicine and Biology* 44: 1125-1132

Allahverdi M and Thwaites D I (1999) Head and phantom scatter factors for simple and complex irradiation situations *Proc 5th Biennial ESTRO meeting on Physics for Clinical Radiotherapy, Gottingen* S22

Almond P R and Horton J L (2000) Radiotherapy Physics in Practice. *Planning and Acceptance Testing of Megavoltage Therapy Installations* Chapter 2: 6-30 (Oxford University Press)

Andreo P and Brahme A (1986) Stopping power data for high energy photon beams *Physics in Medicine and Biology* 31: 839-858

Arcovito G, Piermattei A, D'Abramo G and Bassi F A (1985) Dose measurements and calculations of small radiation fields for 9-MV x rays *Medical Physics* 12: 779-784

Ashburn J R, Al-Otoomi A, Sowards K, Tamimi M M and Meigooni A S (2001) Investigation of the new highly sensitive Gafchromic HS and XR films *Medical Physics* 28: 1244

Beddar A S, Mackie T R and Attix F H (1992) Water-equivalent plastic scintillation detectors for high-energy beam dosimetry: II. Properties and measurements *Physics in Medicine and Biology* 37: 1901-1913

----- (1992) Water-equivalent plastic scintillation detectors for high-energy beam dosimetry: I. Physical characteristics and theoretical considerations *Physics in Medicine and Biology* 37: 1883-1900

Beddar A S, Mason D J and O'Brien P F (1994) Absorbed dose perturbation caused by diodes for small field photon dosimetry *Medical Physics* 21: 1075-1079

Betti O O and Derechinsky Y E (1982) Irradiations stereotaxiques multifaisceaux *Neurochirurgie* 28: 55-56

Bjarngard B E, Tsai J-S and Rice R K1990 Doses on the central axes of narrow 6-MV x-ray beams *Medical Physics* 17: 794-799

Bomford C K (2003) Walter and Miller's Textbook of Radiotherapy. *Section 3: Megavoltage Beam Generators*. 162-183 (Churchill Livingstone)

Bortfeld T R, Kahler D L, Waldron T J and Boyer A L (1994) X-ray field compensation with multileaf collimators *International Journal of Radiation Oncology Biology and Physics* 28: 723-730

Bourland J D and McCollough C H (1994) Static field conformal stereotactic radiosurgery: physical techniques *International Journal of Radiation Oncology Biology and Physics* 28: 471-479

Bova F J, Buatti J M, Friedman W A, Mendiondo O A, Yang C-C and Liu C (1997) The university of Florida frameless high-precision stereotactic radiotherapy system *International Journal of Radiation Oncology Biology and Physics* 38: 875-882

Brahme A, Chavaudra J, Landberg T, McCullough E C, Nussling F and Rawlinson J A et al1988 Accuracy requirements and quality assurance of external beam therapy with photons and electrons *Acta Oncologica* 27: 1-26

Burgemeister E A (1981) Dosimetry with a diamond operating as a resistor *Physics in Medicine and Biology* 26: 269-275

Burns J E, Pritchard D H and Knight R T (1992) Peak scatter factors for Co-60 gamma-radiation *Physics in Medicine and Biology* 37: 2309-2318

Burns J E (1996) Conversion of PDD for photon beams from one SSD to another and calculations of TAR, TMR and TPR *The British Journal of Radiology* Supplement 25: 153-157

----- (1996) Caesium-137 gamma-ray beams *The British Journal of Radiology* Supplement 25: 39-45

Cardinale R M, Benedict S H, Wu Q, Zwicker R D, Gaballa H E and Mohan R (1998) A comparison of three stereotactic radiotherapy techniques; arcs vs. noncoplanar fixed fields vs. intensity modulation *International Journal of Radiation Oncology Biology and Physics* 42: 431-436

Carol M, Grant W H, Bleier A R, Kania A A, Targovnik H S, Butler E B and Woo S W (1996) The field matching problem as it applies to the peacock three dimensional conformal system for intensity modulation *International Journal of Radiation Oncology Biology and Physics* 34: 183-187

Chan M F and Ayyangar K M (1995) Confirmation of target localization and dosimetry for 3D conformal radiotherapy treatment planning by MR imaging of a ferrous sulfate gel head phantom *Medical Physics* 22: 1171-1175

Cheng C-W and Das I J (1996) Dosimetry of high energy photon and electron beams with CEA films *Medical Physics* 23: 1225-1232

Chetty I J and Charland P M (2002) Investigation of Kodak extended range (EDR) film for megavoltage photon beam dosimetry *Physics in Medicine and Biology* 47: 3629-3641

Chierego G, Francescon P, Colombo F and Pozza F (1993) From radiotherapy to stereotactic radiosurgery: physical and dosimetrical considerations *Radiotherapy and Oncology* 29: 214-218

Coffey C W, Sanders M, Cashon K, Miller R, Walsh J and Patel P (1993) A tissue equivalent phantom for stereotactic radiosurgery localization and dose verification *Stereotactic and Functional Neurosurgery* 61: 130-141

Colombo F, Benedetti A, Pozza F, Avanzo R C, Marchetti C, Chierego G and Zanardo A (1985) External stereotactic irradiation by linear accelerator *Neurosurgery* 16: 154-160

Convery D J and Rosenbloom M E (1992) The generation of intensity-modulated fields for conformal radiotherapy by dynamic collimation *Physics in Medicine and Biology* 37: 1359-1374

Corn B W, Andrews D W, Silverman C L, Rosenwasser R, Buchheit W and Glass J (1996) Detailed initial analysis of the treatment of cranial chordoma with fractionated stereotactic irradiation *Radiation Oncology Investigations* 4: 17-22

Cosgrove V P, Jahn U, Pfaender M, Bauer S, Budach V and Wurm R E (1999) Commissioning of a micro multi-leaf collimator and planning system for stereotactic radiosurgery *Radiotherapy and Oncology* 50: 325-336

Cosgrove V P, Murphy P S, McJury M, Adams E J, Warrington A P, Leach M O and Webb S (2000) The reprodicibility of polyacrylamide gel dosimetry applied to stereotactic conformal radiotherapy *Physics in Medicine and Biology* 45: 1195-1210

Das I and Cheng C (2001) Dosimetric characteristics of new Gafchromic-HS film *Medical Physics* 28: 1244

Das I J, Downes M B, Corn B W, Curran W J, Werner-Wasik M and Andrews D W (1996) Characteristics of a dedicated linear accelerator-based stereotactic radiosurgery-radiotherapy unit *Radiotherapy and Oncology* 38: 61-68

Dasu A, Lofroth P and Wickman G (1998) Liquid ionization chamber measurements of dose distributions in small 6MV photon beams *Physics in Medicine and Biology* 43: 21-36

Dawson D J, Hartmann G H and Akinradewo A C (1984) Analysis of physical parameters associated with the measurement of high-energy x-ray penumbra *Medical Physics* 11: 491-497

Dawson D J, Scroe N J and Hoya J D (1986) penumbral measurements in water for high-energy x rays *Medical Physics* 13: 101-104

Day M J and Aird E G A (1996) The equivalent field method for dose determinations in rectangular fields *The British Journal of Radiology* Supplement 25: 138-151

Duggan D M and C W Coffey (1996) Use of a micro-ionization chamber and an anthropomorphic head phantom in a quality assurance program for stereotactic radiosurgery *Medical Physics* 34: 513-516

Dutreix A, Bjarngard B E, Bridier A, Mijnheer B, Shaw J E, and Svensson H (1997) Monitor Unit Calculation for High Energy Photon Beams *ESTRO booklet No. 3* (Garant Publishers N.V.)

Dutreix J, Dutreix A and Tubiana M (1964) Electronic equilibrium and transition stages *Physics in Medicine and Biology* 10 177-190

Ertl A, Zehetmayer M, Schoggl A, Kindl P and Hartl R (1997) Dosimetry studies with TLDs for stereotactic radiation techniques for intraocular tumours *Physics in Medicine and Biology* 42: 2137-2145

Essers M and Mijnheer B (1999) In Vivo dosimetry during external photon beam radiotherapy *International Journal of Radiation Oncology Biology and Physics* 43: 245-259

Fairclough-Tompa L, Larsen T and Jaywant S M (2001) Immobilization in stereotactic radiotherapy: the head and neck localiser frame *Medical Dosimetry* 26: 267-273

Fan C J, Devanna W G, Leybovich L B, Kurup R G, Hopkins B J, Melian E, Anderson D and Glasgow G P (1997) Dosimetry of very-small (5-10mm) and small (12.5-40mm) diameter cones and dose verification for radiosurgery with 6MV x-ray beams *Stereotactic and Functional Neurosurgery* 67: 183-197

Flickinger J C (2002) What is the optimal dose and fractionation for stereotactic irradiation of acoustic neuromas? *International Journal of Radiation Oncology Biology and Physics* 54: 311-312

Francescon P, Cora S, Cavedon C, Scalchi P and Reccanello S (1998) Use of a new type of radiochromic film, a new parallel-plate micro-chamber, MOSFETs and TLD 800 microcubes in the dosimetry of small beams *Medical Physics* 25: 503-511

Friedman W A, Bova F J and Mendenhall W M (1995) Linear accelerator radiosurgery for arteriovenous malformations: the relationship of size to outcome *Journal of Neurosurgery* 82: 180-189

Fuss M, Debus J, Lohr F, Huber P, Rhein B, Engenhart-Cabillic R and Wannenmacher M (2000) Conventionally fractionated stereotactic radiotherapy (FSRT) for acoustic neuromas *International Journal of Radiation Oncology Biology and Physics* 48: 1381-1387

Gager L D, Wright A E and Almond A E (1977) Silicon diode detectors used in radiological physics measurements. Part I: Development of an energy compensating shield *Medical Physics* 4 49: 4-498

Galloway and Maclunas (1990) Stereotactic surgery *Critical reviews in biomedical engineering* 18: 181-205

Gerbi B J and Khan F M (1990) Measurement of dose in the build-up region using fixed-separation plane-parallel ionization chambers *Medical Physics* 17: 17-26

Gibbs F A, Buechler D, Leavitt D and Moeller J H (1992) Measurement of mechanical accuracy of isocenter in conventional linear-accelerator-based radopsurgery *International Journal of Radiation Oncology Biology and Physics* 25: 117-122

Gill S S, Thomas D G T, Warrington A P and Brada M (1991) Relocatable frame for stereotactic external beam radiotherapy *International Journal of Radiation Oncology Biology and Physics* 20: 599-603

Gillies B A, O'Brien P F, McVittie R, McParland C and Easton H (1993) Engineering modifications for dynamic stereotactically assisted radiotherapy *Medical Physics* 20: 1491-1495

Gladstone D J and Chin L M (1991) Automated data collection and analysis system for MOSFET radiation detectors *Medical Physics* 18: 542-548

Gotoh S, Ochi M, Hayashi N, Matsushima S, Uchida T, Obata S, Minami K, Hayashi K, Matsuo T, Iwanaga M, Yasunaga A and Shibata S (1996) Narrow photon beam dosimetry for linear accelerator radiosurgery *Radiotherapy and Oncology* 41: 221-224

Grebe G, Pfaender M, Roll M and Luedemann L (2001) Dynamic arc radiosurgery and radiotherapy: commissioning and verification of dose distributions *International Journal of Radiation Oncology Biology and Physics* 49: 1451-1460

Greene D and Williams P C (1993) X-rays: 2-43MV. *The British Journal of Radiology* Supplement 17: 61-96

Guan T Y, Almond P R, Park H C, Lindberg R D and Shields CB (1993) Imaging of radiation dose for stereotactic radiosurgery *Medical Dosimetry* 18: 135-142

Haider T K and El-Khatib E E (1994) Measurements of phantom scatter factors for small field sizes in high energy x rays *Medical Physics* 21: 663-666

Hampshire A and Walton L (2003) Gamma Knife Stereotactic Radiosurgery *Scope* 12: 9-14 (York, IPEM)

Hartmann G H, Schlegel W, Sturm V, Kober B, Pastyr O and Lorenz W J (1985) Cerebral radiation surgery using moving field irradiation at a linear accelerator facility *International Journal of Radiation Oncology Biology and Physics* 11: 1185-1192

Hartmann G H, Bauer-Kirpes B, Serago C F and Lorenz W J (1993) Precision and accuracy of stereotactic convergent beam irradiations from a linear accelerator *International Journal of Radiation Oncology Biology and Physics* 28: 481-492

Haryanto F, Fippel M, Laub W, Dohm O and Nusslin F (2002) Investigation of photon beam output factors for conformal radiation therapy - Monte Carlo simulations and measurements *Physics in Medicine and Biology* 47: N133-N143

Haworth A and Perry A M (1993) Data acquisition for linac based stereotactic radiosurgery *Australasian Physical and Engineering Sciences in Medicine* 16: 49-56

Heifetz M D, Wexler M and Thompson R (1984) Single-beam radiotherapy knife: a practical theoretical model *Journal of Neurosurgery* 60: 814-818

Heydarian M, Hoban P W, Beckham W A, Borchardt I M and Beddoe A H1993 Evaluation of a PTW diamond detector for electron beam measurements *Physics in Medicine and Biology* 38: 1035-1042

Heydarian M, Hoban P W and Beddoe A H (1996) A comparison of dosimetry techniques in stereotactic radiosurgery *Physics in Medicine and Biology* 41: 93-110

Higgins P D, Sibata C H, Siskind L and Sohn J W (1995) Deconvolution of detector size effect for small field measurement *Medical Physics* 22: 1663-1666

Hoban P W, Heydarian M, Beckham W A and Beddoe A H (1994) Dose rate dependence of a PTW diamond detector in the dosimetry of a 6MV photon beam *Physics in Medicine and Biology* 39: 1219-1229

Holt J G, Laughlin J S and Moroney J P (1970) The extension of the concept of tissue-air-ratios (TAR) to high-energy x-ray beams *Radiology* 96: 437-446

Horsley V and Clarke R H (1908) The structure and functions of the cerebellum examined by a new method *Brain* 31: 45

Houdek P V, VanBuren J M and Fayos J V (1983) Dosimetry of small radiation fields for 10-MV x rays *Medical Physics* 10: 333-336

ICRU (International Commission on Radiation Units and Measurements) (1976) Determination of absorbed dose in a patient irradiated by beams of x and gamma rays in radiotherapy procedures *ICRU Report 24* (Bethesda MD: ICRU)

ICRU (International Commission on Radiation Units and Measurements) (1987) Use of computers in external beam radiotherapy procedures with high-energy photons and electrons *ICRU Report 42* (Bethesda MD: ICRU)

IEC (International Electrotechnical Commission) (1989) Medical electrical equipment - medical electron accelerators - guidelines for functional performance characteristics *IEC 976*

IPEM (Institute of Physics and engineering in Medicine) (1999) Physics aspects of quality control in radiotherapy *Report 81* (York: IPEM)

IPSM (Institute of Physical Sciences in Medicine) (1990) Code of Practice for high-energy photon therapy dosimetry based on the NPL absorbed dose calibration service *Physics in Medicine and Biology* 35: 1355-1360

Jones D, Christopherson D A, Washington J T, Hafermann M D, Rieke J W, Travaglini J J and Vermeulen S S (1993) A frameless method for stereotactic radiotherapy *The British Journal of Radiology* 66: 1142-1150

Jursinic P A and Thomadsen B R (1999) Measurement of head-scatter factors with cylindrical build-up caps and columnar miniphantoms *Medical Physics* 26: 512-517

Karger C P, Jakel O, Debus J, Kuhn S and Hartmann G H (2001) Three-dimensional accuracy and interfractional reproducibility of patient fixation and positioning using a stereotactic head mask system *International Journal of Radiation Oncology Biology and Physics* 49: 1493-1594

Karlsson M G, Karlsson M, Sjogren R and Svensson H (1997) Semi-conductor detectors in output factor measurements *Radiotherapy and Oncology* 42: 293-296

Kase K R and Svensson G K Head scatter for several linear accelerators (4-18MV) (1986) *Medical Physics* 13: 530-1019

Khan F M (1994) The Physics of Radiation Therapy. *Chapter 4: 45-70 Clinical Radiation Generators.* (Baltimore, Williams and Wilkins)

Khan F M (1994) The Physics of Radiation Therapy. *Chapter 8: 131-175 Measurement of Absorbed Dose* (Baltimore, Williams and Wilkins)

Khan F M (1994) The physics of radiation therapy. *Chapter 10: 200-225 A system of dosimetric calculations* (Baltimore, Williams and Wilkins)

Khan F M, Gibbons J P and Roback D M (1996) Collimator (head) scatter at extended distances in linear accelerator-generated photon beams *International Journal of Radiation Oncology Biology and Physics* 35: 605-608

Kubsad S S, Mackie T R, Gehring M A, Misisco D J, Paliwal B R, Mehta M P and Kinsella T J (1990) Monte Carlo and convolution dosimetry for stereotactic radiosurgery *International Journal of Radiation Oncology Biology and Physics* 19: 1027-1035

Lam K L and Ten Haken R K (1996) In phantom determination of collimator scatter factor *Medical Physics* 23: 1207-1212

Larson D A, Bova F, Eisert D, Kline R, Loeffler J, Lutz W, Mehta M and Palta J (1993) Current radiosurgery practice: results of an ASRO survey *International Journal of Radiation Oncology Biology and Physics* 28: 523-526

Laub W U and Wong T (2003) The volume effect of detectors in the dosimetry of small fields used in IMRT *Medical Physics* 30: 341-347

Lax I, Blomgren H, Näslund I and Svanström R (1994) Stereotactic radiotherapy of malignancies in the abdomen *Acta Oncologica* 33: 677-683

Lederman G, Wertheim S, Lowry J, Rashid H, Silverman P, Qian G-X, Lombardi E and Wronski M (1998) Acoustic neuromas treated by fractionated stereotactic radiotherapy *Radiosurgery* 2: 25-30

Lee H-R, Pankuch M and Chu J C (2002) Evaluation and characterization of parallel plate microchamber's functionalities in small beam dosimetry *Medical Physics* 29: 2489-2496

Li A X, Soubra M, Szanto J and Gerig L H (1995) Lateral electron equilibrium and electronic contamination in measurements of head-scatter factors using miniphantoms and brass caps *Medical Physics* 22: 1167-1170

Lunsford L D, Flickinger J C, Lindner G and Maitz A (1989) Stereotactic Radiosurgery of the Brain Using the First United States 201 Cobalt-60 Source Gamma Knife *Neurosurgery* 24: 151-159

Mackie T R, Scrimger J W and Battista J J (1985) A convolution method of calculating dose for 15-MV x-rays *Medical Physics* 12: 188-196

Mackie T R, Holmes T, Swetdloff S, Reckwerdt P, Deasy J O, Yang J, Paliwal B and Kinsella T (1993) Tomotherapy: a new concept for the delivery of dynamic conformal radiotherapy *Medical Physics* 20: 1709-1719

Martens C, De Wagter C and De Neve W (2000) The value of the PinPoint ion chamber for characterization of small field segments used in intensity-modulated radiotherapy *Physics in Medicine and Biology* 45: 2519-2530

Maryanski M J, Ibbott G S, Eastman P, Schultz R J and Gore J C (1996) Radiation therapy dosimetry using magnetic resonance imaging of polymer gels *Medical Physics* 23 699-705

McKenzie A (1996) Cobalt-60 gamma-ray beams *The British Journal of Radiology* Supplement 25: 46-61

McKerracher C and Thwaites D I (1999) Assessment of new small-field detectors against standard field detectors for practical stereotactic beam data acquisition *Physics in Medicine and Biology* 44: 2143-2160

-----(2002) Verification of the dose to the isocentre in stereotactic plans *Radiotherapy and Oncology* 64: 97-107

McLaughlin W L, Soares C G, Sayeg J A, McCullough E C, Kline R W, Wu A and Maitz A H (1994) The use of a radiochromic detector for the determination of stereotactic radiosurgery dose characteristics *Medical Physics* 21: 379-388

McNee S G, Rampling R, Dale A J and Gregor A (1998) An Audit of 3D Treatment Planning Facilities and Practice in the UK *Clinical Oncology* 10: 18-23

Mijnheer B, Batterman J J and Wambersie A1987 What degree of accuracy is required and can be achieved in photon and neutron therapy? *Radiotherapy and Oncology* 8: 237-252

Mitsumori M, Shrieve D C, Alexander E III, Kaiser U B, Richardson G E, Black P McL and Loeffler J S (1998) Initial clinical results of linac-based stereotactic radiosurgery and stereotactic radiotherapy for piuitary adenomas *International Journal of Radiation Oncology Biology and Physics* 42: 473-580

Mobit P N and Sandison G A (1999) An EGS4 Monte Carlo examination of the response of a PTW-diamond radiation detector in megavoltage electron beams *Medical Physics* 26: 839-844

Mohan R and Chui C-S (1985) Validity of the concept of separating primary and scatter dose *Medical Physics* 12: 726-730

Mohan R, Chui C and Lidofsky L1986 Differential pencil beam dose computation model for photons *Medical Physics* 13: 64-73

NCS (Netherlands Commission on Radiation Dosimetry) (1998) Recommendations for the determination and use of scatter correction factors of megavoltage photon beams: measurement and use of collimator and phantom scatter correction factors of arbitrarily shaped fields with a symmetrical collimator setting *Report 12* NCS

Nelson W R, Hirayama H, and Rogers D W O (1985) The EGS4 Code System *Report SLAC-265* (Stanford; SLAC)

Niroomand-Rad A, Blackwell C R, Coursey B M, Gall K P, Galvin J M, McLaughlin W L, Meigooni A S, Nath R, Rodgers J E and Soares C G (1995) Radiochromic film dosimetry: Recommendations of AAPM Radiation Therapy Committee Task Group 55 *Medical Physics* 25: 2093-2115

Nizin P and Kase K (1988) A method of measuring the primary dose component in high-energy photon beams *Medical Physics* 15: 683-685

Norrgard F S E, Sipila P M, Kulmala J A J and Minn H R I (1998) Dose characteristics of in-house-built collimators for stereotactic radiotherapy with a linear accelerator *Physics in Medicine and Biology* 43: 1545-1556

O'Brien P F and Fung A (1994) Measured spatialaccuracy for linac-based radiosurgery *Medical Physics* 21: 1145-1147

O'Connor J E (1984) The density scaling theorem applied to lateral electronic equilibrium *Medical Physics* 11: 678-680

Ondra S L, Troupp H, George E D and Schwab K (1990) The natural history of symptomatic arteriovenous malformations of the brain: a 24-year follow-up assessment *Journal of Neurosurgery* 73: 387-391

Paskalev K, Seuntjens J P, and Podgorsak E B (2002) Dosimetry of ultra small photon fields *AAPM Symposium Proceeding No. 13: Recent Developments in Accurate Radiation Dosimetry* 298-318 (Madison, AAPM)

Perks J R, Rosenberg I and Warrington A P (1999) Dose quality assurance for stereotactic radiotherapy treatments *Physics in Medicine and Biology* 44: N209-N215

Perks J R, Jalali R, Cosgrove V P, Adams E J, Shepherd S F, Warrington A P and Brada M (1999) Optimization of stereotactically-guided conformal treatment planning of sellar and parasellar tumors based on normal brain dose volume histograms *International Journal of Radiation Oncology Biology and Physics* 45: 507-513

Planskoy B (1980) Evaluation of diamond radiation dosemeters *Physics in Medicine and Biology* 25: 519-532

Podgorsak E B, Olivier A, Pla, Lefebvre P-Y and Hazel J (1988) Dynamic stereotactic radiosurgery *International Journal of Radiation Oncology Biology and Physics* 14 115-126

Podgorsak E B (1992) Physics for radiosurgery with linear accelerators *Neurosurgery Clinics of North America* 3 9-34

Pollock B E, Lunsford L D, Kondziolka D, Flickinger J C, Bissonette D J, Kelsey S F and Jannetta P J (1995) Outcome analysis of acoustic neuroma management: a comparison of microsurgery and stereotactic radiosurgery *Neurosurgery* 36 215-427

Proimos B (1960) Synchronous field shaping in rotational megavolt therapy *Radiology* 74 753-757

Ramani R, Lightstone A W, Mason D L D and O'Brien P F (1994) The use of radiochromic film in treatment verification of dynamic stereotactic radiosurgery *Medical Physics* 21 389-392

Ramani R, Ketko M G, O'Brien P F and Schwartz M L (1995) A QA phantom for dynamic stereotactic radiosurgery: quantitative measurements *Medical Physics* 22 1343-1346

Ramani R, Russell S and O'Brien P (1997) Clinical dosimetry using MOSFETS *International Journal of Radiation Oncology Biology and Physics* 37 959-964

Ravindran B P, Fairclough L and Jaywant S M (2001) Phantom dosimetry for conformal stereotactic radiotherapy with a head and neck localizer frame *Physics in Medicine and Biology* 46 1975-1984

Rice R K, Hansen J L, Svensson G K and Siddon R L (1987) Measurements of dose distributions in small beams of 6MV x-rays *Physics in Medicine and Biology* 32 1087-1099

Rikner G (1985) Characteristics of a selectively shielded p-Si detector in Co-60 and 8 and 16MV roentgen radiation *Acta Radiologica Oncology* 24 205-208

Rikner G and Grussell E (1985) Selective shielding of a p-Si detector for quality independence *Acta Radiologica Oncology* 24 65-69

Robar J L (2000) A practical technique for verification of three-dimensional conformal dose distributions in stereotactic radiosurgery *Medical Physics* 27 978-987

Rogers D W O, Faddegon B A, Ding G X, Ma C-M and We J (1995) BEAM: A Monte Carlo code to simulate radiotherapy treatment units *Medical Physics* 22 503-524

Rustgi S N (1995) Evaluation of the dosimetric characteristics of a diamond detector for photon beam measurements *Medical Physics* 22 567-570

Sanchez-Doblado F, Andreo P, Capote R, Leal A, Perucha M, Arrans R, Nunez L, Mainegra E, Lagares J I and Carrasco E (2003) Ionisation chamber dosimetry of small photon fields: a Monte Carlo study on stopping-power ratios for radiosurgery and IMRT beams *Physics in Medicine and Biology* 48 1-19

Sanders M, Sayeg J, Coffey C, Patel P and Walsh J (1992) Beam profile analysis using GafChromic films *Stereotactic and Functional Neurosurgery* 61 124-129

Saylor M C, Tamargo T T, McLaughlin W L, Khan H M, Lewis D F and Schenfele R D (1988) A thin film recording medium for use in food irradiation *Radiation Physics Chemistry* 31 529-536-

Schlegel W, Pastyr O, Bortfeld T, Becker G, Schad L, Gademann G and Lorenz W J (1992) Computer systems and mechanical tools for stereotactically guided conformation therapy with linear accelerators *International Journal of Radiation Oncology Biology and Physics* 24 781-787

Scott T W, Beach J L and Mendiondo O A (1997) A precision repeat localization head frame for fractionated stereotactic radiotherapy *Medical Dosimetry* 22 5-8

Serago C F, Houdek P V, Hartmann G H, Saini D S, Serago M E and Kaydee A (1992) Tissue maximum ratios (and other parameters) of small circular 4, 6, 10, 15 and 24 MV x-ray beams for radiosurgery *Physics in Medicine and Biology* 37 1943-1956

Sibata C H, Mota H C, Beddar A S, Higgins P D and Shin K H (1991) Influence of detector size in photon beam profile measurements *Physics in Medicine and Biology* 36 621-631

Sixel K E and Podgorsak E B (1993) Build up region of high-energy x-ray beams in radiosurgery *Medical Physics* 20 761-764

Smith C W (1996) Orthovoltage x-ray beams (0.5mm-4.0mm Cu HVL) *The British Journal of Radiology* Supplement 25 24-38

Soldberg T D, Boedeker K L, Fogg R, Selch M T and Deschesne K M (2001) Dynamic arc radiosurgery field shaping: a comparison with static conformal and noncoplanar cicular arcs *International Journal of Radiation Oncology Biology and Physics* 49 1481-1491

Somigliana A, Cattaneo G M, Fiorino C, Borelli S, del Vecchio A, Zonca G, Pignoli E, Loi G, Calandrino R and Marchesini R (1999) Dosimetry of Gamma Knife and linac-based radiosurgery using radiochromic and diode detectors *Physics in Medicine and Biology* 44 887-897

Sontag M R and Cunningham J R (1978) The equivalent tissue-air ratio method for making absorbed dose calculations in a heterogeneous medium *Radiology* 129 787-794

Sperduto P W, Scott C, Andrews D, Schell M C, Flanders A, Werner-Wasik M, Demas W, Ryu J K, Gaspar L E , Bahary J, Souhami L, Rotman M and Curran W J (2002) Stereotactic radiosurgery with whole brain radiation therapy improves survival in patients with brain

metastases: report of radiation therapy oncology group phase III study 95-08 *International Journal of Radiation Oncology Biology and Physics* 54 3

Stevens M A, Turner J R, Hugtenburg R P and Butler P H (1996) High-resolution dosimetry using radiochromic film and a document scanner *Physics in Medicine and Biology* 41 2357-2365

Storchi P and van Gasteren J J M (1996) A table of phantom scatter factors of photon beams as a function of quality index and field size *Physics in Medicine and Biology* 41 563 -571

Suchowerska N, Hoban P W, Butson M, Davison A and Metcalfe P (2001) Directional dependence in film dosimetry: radiographic and radiochromic film *Physics in Medicine and Biology* 46 1391-1397

Theodorou K, Kappas C and Tsokas C (1998) A new non-invasive and relocatable immobilization frame for fractionated stereotactic radiotherapy *Radiotherapy and Oncology* 47 313-317

Theodorou K. (1999) Development of a prototype stereotactic radiotherapy-radiosurgery unit. PhD Thesis, University of Patras.

Thwaites D I, Williams J R, Aird E G, Klevenhagen S C and Williams P C (1992) A dosimetric intercomparison of megavoltage photon beams in UK radiotherapy centres. *Physics in Medicine and Biology* 37 445-461

Thwaites D I (1996) External audit in radiotherapy dosimetry. *Radiation Incidents in Hospitals* 21-28 (London, BIR)

Thwaites D I and Allahverdi M (1997) The use of a semianatomical phantom in interdepartmental dosimetry audit *Medical and Biological Engineering and Computing* 35 998-998

Thwaites D I, Powley S, and Allahverdi M (2003). The UK dosimetry audit network. *Proc Int Symp Standards and Codes of practice in Medical Radiation Dosimetry* (Vienna, IAEA).

Tokuuye K, Akine Y, Sumi M, Kagami Y, Murayama S, Nakayama H, Ikeda H, Tanaka M, Shibui S and Nomura K (1998) Fractionated stereotactic radiotherapy of small intracranial malignancies *International Journal of Radiation Oncology Biology and Physics* 42 989-994

Touboul E, Halabi A A, Buffat L, Merienne L, Huart J, Schlienger M, Lefkopoulos D, Mammar H, Missir O, Meder J-F, Laurent A and Housset M (1998) Single-fraction stereotactic radiotherapy: a dose-response analysis of arteriovenous malformation obliteration *International Journal of Radiation Oncology Biology and Physics* 41 855-861

Treuer H, Hoevels M, Luyken K, Gierich A, Kocher M, Muller R-P and Sturm V (2000) On isocentre adjustment and quality control in linear accelerator based radiosurgery with cisrcular collimators and room lasers *Physics in Medicine and Biology* 45 2331-2342

Tsai J-S, Buck B A, Svensson G K, Alexander E, Cheng C-W, Mannarino E G and Loeffler J (1991) Quality assurance in stereotactic radiosurgery using a standard linear accelerator *International Journal of Radiation Oncology Biology and Physics* 21 737-748

Tsai J-S, Curran B H, Sternick E S and Engler M J (1996) Use of a 1 mm collimator to test the accuracy of stereotactic radiotherapy *International Journal of Radiation Oncology Biology and Physics* 35 579-586

Vahc Y W, Chung W K, Park K R, Lee J Y, Lee Y H, Kwon O and Kim S (2001) The properties of ultramicrocylindrical ionization chamber for small field used in stereotactic radiosurgery *Medical Physics* 28 303-309

van Battum L J, Essers M and Storchi P (2002) Conversion of measured percentage depth dose to tissue maximum ratio values in stereotactic radiotherapy *Physics in Medicine and Biology* 47 3289-3300

Van Dam J, Leunens G and Dutreix A (1990) Correlation between temperature and dose rate dependence of semiconductor response; influence of accumulated dose *Radiotherapy and Oncology* 19 345-351

van Gasteren J J M, Heukelom S, van Kleffens H J, van der Laarse R , Venselaar J L M and Westermann C F (1991) The determination of phantom and collimator scatter components of the output of megavoltage photon beams: measurement of the collimator scatter part with a beam-coaxial narrow cylindrical phantom *Radiotherapy and Oncology* 20 250-257

Vatnitsky S and Jarvinen H1993 Application of a natural diamond detector for the measurement of relative dose distributions in radiotherapy *Physics in Medicine and Biology* 38: 173-184

Verellen D, Linthout N, Bel A, Soete G, Van den Berge D, D'Haens J and Storme G (1999) Assessment of the uncertainties in dose delivery of a commercial system for linac-based stereotactic radiosurgery *International Journal of Radiation Oncology Biology and Physics* 44 421-433

Verhaegen F, Das I J and Palmans H (1998) Monte Carlo dosimetry study of a 6MV stereotactic radiosurgery unit *Physics in Medicine and Biology* 43 2755 -2768

Verhaegen F (2001) A practical and theoretical course in radiotherapy physics Chapter 26: *Introduction to Monte Carlo methods* Joint Department of Physics, Royal Marsden Hospital, London.

Walton L, Bomford C K and Ramsden D (1987) The Sheffield stereotactic radiosurgery unit: physical characteristics and principles of operation *The British Journal of Radiology* 60 897-906

Wang X, Spirou S, LoSasso T, Stein J, Chui C-S and Mohan R (1996) Dosimetric verification of intensity-modulated fields *Medical Physics* 23 317-327

Warrington A P, Laing R W and Brada M (1994) Quality Assurance in fractionated stereotactic radiotherapy *Radiotherapy and Oncology* 30 239-246

Warrington A P (2003) Stereotactic Radiotherapy *Scope* 12 14-19 (York, IPEM)

Webb S (1993) The Physics of three-dimensional radiation therapy *Chapter 5: Conformal radiotherapy with a multileaf collimator* 218-241 (Bristol, IOP)

Weber L, Nilsson P and Ahnesjo A (1997) Build-up cap materials for measurement of photon head-scatter factors *Physics in Medicine and Biology* 42 1875-1886

Westermark M, Arndt J, Nilsson B and Brahme A (2000) Comparative dosimetry in narrow high-energy photon beams *Physics in Medicine and Biology* 45 685-702

Wickman G, Johansson B, Bahar-Gogani J and Holmstrom T (1998) Liquid ionisation chambers for absorbed dose measurements in water at low dose rates and intermediate photon energies *Medical Physics* 25 900-907

Wilkins D, Li X A, Cygler J and Gerig L (1997) The effect of dose rate dependence of p-type silicon detectors on linac relative dosimetry *Medical Physics* 24 879-881

Williamson J F, Khan F M and Sharma S C (1981) Film dosimetry of megavoltage photon beams: A practical method of isodensity-to-isodose curve conversion *Medical Physics* 8 94-98

Winston K R and Lutz W (1988) Linear accelerator as a neurosurgical tool for stereotactic radiosurgery *Neurosurgery* 22 454-464

Wulf J, Hadinger U, Oppitz U, Olshausen B and Flentje M (2000) Sterotactic radiotherapy of extracranial targets: CT-simulation and accuracy of treatment in the stereotactic body frame *Radiotherapy and Oncology* 57 225-236

Yeung D, Palta J, Fontanesi J and Kun L (1993) Systematic analysis of errors in target localization and treatment delivery in stereotactic radiosurgery (SRS) *International Journal of Radiation Oncology Biology and Physics* 28 493-498

Yin F-F, Zhu J, Yan H, Gaun H, Hammoud R, Ryu S and Kim J H (2002) Dosimetric characteristics of Novalis shaped beam surgery unit *Medical Physics* 29 1729-1738

Zhu T C and Bjarngard B E (1994) The head scatter factor for small field sizes *Medical Physics* 21 65-68

Zhu X R, Allen J J, Shi J and Simon W E (2000) Total scatter factors and tissue maximum ratios for small radiosurgery fields: Comparison of diode detectors, a parallel-plate ion chamber, and radiographic film *Medical Physics* 27 472-